DTIC FILE COPY

LARGE DISPLACEMENT AND ROTATIONAL
FORMULATION FOR LAMINATED CYLINDRICAL
SHELLS INCLUDING PARABOLIC
TRANSVERSE SHEAR

DISSERTATION

Scott T. Dennis
Captain, USAF
AFIT/DS/AA/88-1

DEPARTMENT OF THE AIR FORCE

AIR UNIVERSITY

AIR FORCE INSTITUTE OF TECHNOLOGY

Wright-Patterson Air Force Base, Ohio

88 6 23 055

LARGE DISPLACEMENT AND ROTATIONAL
FORMULATION FOR LAMINATED CYLINDRICAL
SHELLS INCLUDING PARABOLIC
TRANSVERSE SHEAR

DISSERTATION

Scott T. Dennis
Captain, USAF
AFIT/DS/AA/88-1

DTIC
SELECTED
JUN 2 3 1988

H

LARGE DISPLACEMENT AND ROTATIONAL FORMULATION

FOR   LAMINATED CYLINDRICAL SHELLS INCLUDING

PARABOLIC TRANSVERSE SHEAR

DISSERTATION

Presented to the Faculty of the School of Engineering

of the Air Force Institute of Technology

Air University

In Partial Fulfillment of the

Requirements for the Degree of

Doctor of Philosophy

Scott T. Dennis

Captain, USAF

May 1988

LARGE DISPLACEMENT AND ROTATIONAL FORMULATION

FOR LAMINATED CYLINDRICAL SHELLS INCLUDING

PARABOLIC TRANSVERSE SHEAR

Scott T. Dennis, B.S., S.M.

Captain, USAF

Approved:

Chairman _____ 13 May 1988

_____ 13 May 1988

_____ 13 May 1988

_____ 13 May 1988

_____ 13 May 1988

Accepted:

J.S. Przemieniecki 19 May 1988

Dean, School of Engineering

Acknowledgements

Thanks go to my committee chairman, Dr. Anthony Palazotto, for his interest, guidance, and time. Thank you Dr. Peter Torvik, Dr. Narendra Khot, and Dr. John Jones for also serving on the committee and Major Paul Copp for acting as the Dean's Representative. Additionally, the Cyber computer support provided by Dr. Khot is appreciated. Thanks also go to Dr. George Sendeckyi and AFOSR for providing travel support so that research results could be presented at both the 20th Midwestern Mechanics and the 29th AIAA SDM conferences. Finally, I thank my wife, Donna, and children, Sara and Timmy, for the numerous sacrifices made during this endeavor.

DTIC
COPY
INSPECTED
4

Accession For

NTIS GRA&I

A-1

Table of Contents

List of Figures

viii

x

List of Tables

List of Symbols

Chapter III

$\bar{r}$	position vector
x_i	Cartesian coordinates
$\bar{i}_i$	Cartesian basis vectors
y_i	curvilinear coordinates
$\bar{a}_i$	curvilinear basis vectors
ds	length of infinitesimal line segment
g_{ij}	elements of metric tensor
γ_{ij}	elements of Green's strain tensor
ε_{ij}	elements of physical strains
h_i	scale factors
u_i	displacement components
ξ_α	surface coordinates, shell midsurface coordinates
$a_{\alpha\beta}$	elements of surface metric tensor
$b_{\alpha\beta}$	elements of curvature tensor
$\bar{n}$	surface normal vector
C_α	surface curvatures
R_α	surface radii of curvature
$\bar{R}$	shell position vector
h	shell thickness
ζ	transverse shell coordinate
α_γ	square roots of surface metric elements
σ_{ij}	elements of 2nd Piola-Kirchhoff stress tensor
F_k	prescribed surface tractions
W^*	strain energy density
a_{ijkl}	elements of the elasticity tensor
Π_p	potential energy

σ_I, ε_I	contracted notation stress, strain
C_{IJ}	elasticity constants
ψ_α	bending rotations
$\phi_\alpha, \gamma_\alpha, \theta_\alpha$	degrees of freedom in kinematics
β_α	transverse shear rotations
$E_1, E_2,$ $G_{12}, G_{23},$ G_{13}, υ_{12}	orthotropic engineering elastic constants
Q_{IJ}	reduced stiffnesses
$\underline{\varepsilon}^\circ_i, \varkappa^I_J$	strain components of Eqn (3.47)
$\varepsilon^\circ_i, \varkappa_{ip}$	strain components of Eqn (3.49), (3.50)
k	$-4/3h^2$
Φ	ply orientation angle
x, s, ζ	cylindrical shell coordinates
c	$1/R$
u_i	energy terms of Eqn (3.62)
$\overline{Q}_{IJ}$	transformed reduced stiffnesses
Ω	shell middle surface
$A_{ij} - T_{ij}$	elasticity arrays of Eqn (3.63)
$A_{mn} - F_{mn}$	elasticity arrays of Eqn (3.65)
U, U_1, U_2	internal strain energy
V	energy of applied external forces

Chapter IV

K, N_1, N_2	stiffness arrays
q	nodal degrees of freedom vector
R	applied nodal loading vector
$F(q)$	equilibrium equations

Δq	small increment of nodal displacement
K_T	tangent stiffness matrix
$_JL_i$	linear strain definition arrays, Eqn (4.7)
$_JH_i$	nonlinear strain definition arrays, Eqn (4.7)
d	displacement gradient vector
$\tilde{K},\tilde{N}_1,\tilde{N}_2$	stiffness arrays of Eqn (4.9)
C_{ij}	generic stiffness elements
$_JS_m$	linear strain definition arrays, Eqn (4.16)
$\hat{K},\hat{N}_1,\hat{N}_2$	stiffness arrays, Eqn (4.15)
$\mathcal{D}$	array of shape functions and their derivatives
$\mathcal{H}_k$	Hermitian shape function arrays
$\mathcal{N}_k$	linear Lagrangian shape functions
ξ,η	natural coordinates
J	Jacobian matrix
Γ	inverse of Jacobian matrix
Q_k	quadratic Lagrangian shape functions
$u,v,w,$ $w,_1,w,_2,$ ψ_1,ψ_2	nodal degrees of freedom
W_i	integration weighting functions
λ_{cr}	buckling load
$\tilde{v}$	eigenvector
d_1,d_2	displacement gradient vectors, Eqn (4.42)

Chapter V

E,υ	isotropic engineering elastic constants
$q_o,q(x,s)$	applied transverse pressure

D	flexural rigidity
$\bar{w}, \bar{\sigma}_{I}, \zeta, \bar{u}, \bar{p}, \bar{q}, S = L/h$	
	nondimensionalized quantities
L	plate strip, shell length
a,b	plate or shell planform dimensions
w_c	center transverse displacement
δ, b, θ	shell geometry terms, see Figure 5.15
P	point load
λ_{VK}	buckling parameter based on von Karman equations
λ_{FNL}	buckling parameter based on large rotation assumptions
Z	Batdorf parameter
M	cylindrical panel parameter
c	extensibility factor
X,Y	global coordinates for arch
s'	circumferential coordinate of arch
P_t	total axial load on cylindrical panels

Abstract

A two dimensional geometrically nonlinear shell theory applicable to arbitrary geometries that can be described by orthogonal curvilinear coordinates and encompassing large displacements and rotations for small strain situations has been developed. Additionally, the theory includes a parabolic transverse shear stress distribution through the shell thickness. Two curved 28 and 36 degree of freedom finite elements are defined based on specialization of the theory to cylindrical coordinates. The computer program includes algorithms for linear, 'fully linearized' linear bifurcation, and nonlinear problems. Post collapse nonlinear solutions are found through a displacement incrementation scheme. The code provides solutions to the intermediate nonlinear von Karman flat plate and Donnell cylindrical shell equations in addition to the large displacement and rotational formulation.

Flat plate and cylindrical shell solutions do not shear lock based upon exact elemental integrations. Transverse shear deformation was found to be significant for linear thick pinched cylinders and clamped pressure vessels. Orthotropic pressure vessels where the longitudinal stiffness is greater than the circumferential experience much more transverse shear deformation than do those where the circumferential stiffness is greater than the longitudinal. Middle surface inextensibility is often assumed in the closed form solutions used for comparison

with the present approach. The consequences of this
assumption is examined for both linear and nonlinear
problems. The present formulation is applied to axially
compressed quasi-isotropic cylindrical panels. Due to the
high degree of displacement coupling resulting from the
large displacement/rotation assumptions, collapse loads are
predicted without including numerical geometric
imperfections that some formulations require to 'trigger'
the nonlinear response. Analytical results of axially
compressed panels that have large (>10% of planform area)
centered square cutouts were compared to experimental data.
The present approach very accurately predicts both global
and localized panel response.

LARGE DISPLACEMENT AND ROTATIONAL FORMULATION FOR LAMINATED CYLINDRICAL SHELLS INCLUDING PARABOLIC TRANSVERSE SHEAR

I. Introduction

Advanced composite materials, so named due to their high strength and stiffness to weight ratios, are seeing widespread use in many diverse industries. One of these is the aerospace industry where complex shell configurations are common structural elements. Structural elements consisting of composite materials offer unique advantages over those made of traditional isotropic materials in that properties can be tailored to meet specific design goals. Optimization of properties through tailoring can reduce the overall weight of a structure since stiffness and strength are designed only where they are required. A lower weight structure translates into higher performance.

Caution must be exercized, however, since optimized structural systems are often more susceptable to instabilities. Accurate modelling of the load-displacement behavior or equilibrium paths of structural elements would greatly aid the designer in predicting a structure's load carrying capacity and therefore, preventing instabilities.

Many situations in mechanics allow for simplifying assumptions to help the analyst in getting timely and accurate results. For many structural systems considered, it may be important to study geometric nonlinearity only.

1

For these cases, the elements that comprise the system experience only small material straining under load but may catastrophically fail due to their geometric configuration. It turns out that a wide class of structural systems can be accurately represented based on nonlinear geometrical, small strain, and linear elastic material behavior.

Within this class of problems, more simplifications to the geometric nonlinearity may or may not be warranted. Stability solutions for some situations within this class can be based solely on a simple linear bifurcation buckling analysis. Beams and flat plates are common structural elements that can be accurately analyzed to a large degree using the bifurcation approach. For post-buckling behavior, however, solution of the nonlinear equations that result from a collapse analysis is required. The equilibrium behavior of most shell structures can only be accurately represented through a collapse analysis.

In a nonlinear equilibrium path analysis, many of the nonlinear displacement terms may be considered negligible depending, of course, on the specific situation. An accurate load-displacement characterization of a flat plate is based on the von Karman equations where many nonlinear rotational terms have been discarded as negligible. This characterization gives an accurate representation for plate deflections that are many times the plate thickness. Similar assumptions for shell elements result in Donnell and Sanders type equations. These formulations are typically

valid for so called intermediate nonlinearity or theories that allow only moderate rotations. These theories, when used in a finite element formulation, have been shown to be inadequate in describing the collapse behavior of orthotropic cylindrical panels with large cutouts (1,2). The intermediate nonlinear theory as applied to that specific finite element formulation of those references can not capture the large local rotations near the cutout edges.

Laminated plates and shells also have an additional complication that must be considered. Because of potentially large directional variations of stiffness properties in these structures due to tailoring, three dimensional effects can become very important. Whereas classical two dimensional assumptions may be valid for an identical shell structure consisting of isotropic materials, they may lead to gross inaccuracies for an orthotropic construction.

The general class of problems that include large displacements and rotations, small strains, linearly elastic material behavior, and transverse shear deformation is addressed in this dissertation. Unfortunately, analytical closed form solutions, especially for shell geometries, are very limited in scope and cannot include all of the desired features. Hence, the finite element numerical approach is chosen as the solution technique used in this research.

Cylindrical shells are a common shell configuration in aerospace structural applications. They are the simplest

3

shell structure to analyze yet have many of the characteristics of more generally shaped shell geometries. Cylindrical shells with circular and rectangular cutouts are also important structural elements in the aerospace industry. As already alluded to, better tools are required to model their load-displacement behavior.

Based on the above, this dissertation addresses the area of orthotropic cylindrical shells including the following:

1. geometric nonlinearity with large displacements and rotations,

2. linear elastic behavior of laminated anisotropic materials,

3. cylindrical shells and panels and flat plates,

4. parabolic transverse distribution of shear stress,

5. the finite element method.

The above items taken together, especially the parabolic transverse shear and general geometric nonlinearity have resulted in many unique contributions to this field.

Previous related work is first briefly reviewed in Chapter II. In this chapter, overviews are presented first on various shell theories then on finite element applications of these theories. Chapter III presents the theoretical aspects of this research applicable to arbitrary shell geometries that can be described by orthogonal curvilinear coordinates. Following that, the finite element solution technique is formulated in Chapter IV for

4

cylindrical shell structures where flat plates and straight and curved beams are special cases. The numerical solution procedure is then applied to many problems. Unique contributions resulting from linear, bifurcation, and collapse analyses are presented in Chapter V.

II. <u>Literature Review</u>

Previous work related to this research is presented from two broad areas. First, both linear and nonlinear approaches to analyzing shell structures are briefly discussed. Theories are typically first applied to flat plates since they can be considered special and simplified shells. Consequently, many references are cited on flat plate analysis. In a similar vein, theories are often first developed for isotropic constructions before extending them such that more general material laws apply. The second half of the literature review discusses finite element numerical solutions to these plate and shell approaches. Again, linear and nonlinear, isotropic and laminated anisotropic solutions are cited. Numerical collapse analyses based on finite element discretizations require the solution of simultaneous nonlinear algebraic equations. Special techniques are required such that desired information on the structure's equilibrium path is properly extracted from these equat ons. Therefore, an overview is also given within the finite element area on some general categories of solution algorithms for nonlinear equations. The flow of both parts loosely follows what occurred historically.

<u>Shell</u> <u>Theories</u>

The shell structural element is thin by definition. Simplifications can therefore be made to the general equations of elasticity exploiting this thinness. Alternatively, an oriented continuum approach develops a

special theory of thin bodies independent of the classical equations of elasticity. One such oriented continuum approach is Cosserat surface theory where the behavior of the shell is described by the behavior of a surface made up of points, each assigned a triad of deformable vectors called directors. The directors give each point displacement as well as rotational degrees of freedom. Stress and strain quantities in the transverse, i.e., in the direction of the thin dimension, are taken into account. Discussions of the Cosserat surface in shell theory can be found in (3,4,5).

Many shell approaches are derived from the equations of elasticity. In reality, the behavior under load of the top and bottom surfaces of a shell can be very different. However, since the shell is assumed to be thin, the inplane stresses become dominant and we can describe, in an approximate manner, the behavior of the shell based solely on the behavior of a datum surface. In this way, a two dimensional (2-D) theory is used to approximate three dimensional (3-D) phenomena. The classical linear approach, known as Love shell theory (6) is based on the following assumptions: 1) the shell is thin, 2) the displacements and rotations are small, 3) normals to the shell datum surface before deformation remain normal after deformation, and 4) transverse normal stress is negligible. These assumptions lead to a thin shell theory that can be viewed as an extension to Kirchhoff flat plate theory and is often

7

called Kirchhoff-Love shell theory.

The third assumption prohibits transverse shear strains from being written in terms of displacements, effectively neglecting them, although the transverse shear stresses must be included in the equilibrium equations. Since the shell is thin, it is assumed to be in an approximate state of plane stress, i.e., the transverse normal stress is assumed to be negligibly small. Additionally, due to the thinness of the shell, the effects of the normal transverse strain are often neglected in the kinematics compared to the effects of the inplane strains, i.e., the length of a normal to the datum surface is often assumed to remain constant throughout deformation. The normal transverse strain can generally be included in the analysis through the constitutive relations. In deriving the equilibrium equations, statically equivalent forces and moments acting on the datum surface are defined by integrating stresses through the thickness. In this way, the 3-D shell behavior is completely described using a 2-D approximation (6,7,8,9,10). Elegant representations of Love shell theory can be derived strictly via definitions from surface theory without reference to 3-D relationships (7,8,10).

The strain displacement relations that include nonlinear displacement terms are used to represent large displacements and rotations of differential elements of the shell. Neglecting the nonlinear terms that represent inplane rotations is an example of the intermediate

nonlinear theories often used in stability analysis (11-19).
Neglecting the transverse rotational nonlinear terms as well
will result in a linear Love type shell theory. These
successive approximations to the shell strain displacement
relations are discussed in the papers by Librescu (19) and
Sanders (20).

An inconsistency in the original Love theory exists
since nonzero strains result from rigid body motion. It was
this inconsistency that perhaps urged many investigators to
develop slightly different shell theories. Many shell
theories based more or less on Love's assumptions have been
developed, each different since each neglects or
approximates small terms differently. Sanders (21)
redefined the force and moment resultants in such a way that
the rigid body strain anomaly disappeared. Flugge, Lure',
and Byrne (9) suspended the thin shell assumption resulting
in a theory with a less restrictive requirement on the
thinness of the shell. That theory also eliminated the
rigid body strain anomaly. Koiter (22,23) discusses the
significance of the approximations of Love theory and based
on an order magnitude study, states that refinements cannot
be consistently made without also including transverse
deformation effects. Other prominent related theories
include those of Novozhilov (24) and Vlasov (25).

Many theories simplify the Love theory by applying it
to specific shell geometries using both nonlinear and linear
strain displacement relations. Donnell (26) applied Love

9

theory to shallow cylindrical shells. Morley (27) extended the limits of Donnell theory. Reissner (9) applied the Donnell assumptions to a shallow spherical shell. The Donnell-Mushtari-Vlasov equations (12) result when the Donnell assumptions are applied to a shallow shell of arbitrary geometry.

Cheng (28,29) has developed an exact linear theory for circular cylindrical shells based on Love assumptions. By retaining all small terms that other theories in varying degrees neglect, the usual eighth order operator in the governing equilibrium equation of the transverse displacement can be separated into two complex conjugate operators of only fourth order thereby reducing the solution complexity.

The above theories all apply to a shell so thin that all transverse deformation effects, i.e., transverse stresses and strains, can be neglected. As the shell becomes thicker relative to its inplane dimensions, these transverse effects become more pronounced, especially the transverse shear deformations (22,23,30). The first theories that represented the transverse shear deformations relaxed the assumption on the deformed normals of the shell datum surface. Now the normal is permitted to rotate such that plane sections originally perpendicular to the datum surface remain planar but are no longer perpendicular as a result of the deformation. The shell strain displacement relations are derived from kinematics and the 3-D strain

10

displacement relations written in terms of arbitrary orthogonal curvilinear coordinates. The transverse shear is represented by including independent degrees of freedom in the kinematics. The shell is still fully described by the behavior of the datum surface and therefore these approaches represent 2-D theories (31).

The shell kinematics introduced by Bassett as discussed in (32), express the displacements as an infinite power series in the thickness parameter or coordinate. However, as seen in (32), subsequent approximations by Bassett resulted in neglecting the transverse shear and normal stresses. Hildebrand, Reissner, and Thompson (32) introduced truncated Bassett kinematics to analyze thin elastic orthotropic shells and the importance of the transverse stresses and strains. Naghdi (33) applied similar truncated series representations for general thin isotropic elastic shells. Hildebrand, et al, found that the effects of the second order displacement terms on the transverse shear deformation were negligible. Additionally, terms in the transverse displacement that resulted in nonzero transverse normal strains were found to be negligible. Reissner used these kinematics to analyze plates (34) and then sandwich shells (35). Mindlin similarly included rotatory inertia terms in the dynamic analysis of plates (36).

The above first order shear theories result from the so called Reissner-Mindlin (RM) kinematics and do not satisfy

11

the transverse shear boundary conditions on the top and bottom surfaces of the shell or plate since a constant shear angle through the thickness is assumed, i.e., plane sections remain plane. Because of this, the theories based on these kinematics usually require shear correction factors for equilibrium considerations.

Levinson (37), Murthy (38), and Reddy (31) have developed theories that include cubic terms in the inplane displacement kinematics. Satisfying zero transverse shear stress on the top and bottom surfaces of the shell results in a parabolic shear strain distribution through the thickness, thus agreeing more closely with linear elasticity. The number of variables in the kinematics is equal to that in the RM theory, but shear correction factors are not required. Bhimaraddi (39) has applied the parabolic shear strain distribution to analyze the linear vibrational behavior of isotropic cylindrical shells.

The preceding discussion applied primarily to shells made of isotropic materials. Hildebrand, et al (32) were the first to apply shell equations to an orthotropic material. Ambartsumyan (40) wrote an entire text on the subject based on Love theory with some discussion of transverse stresses. Vlasov devotes a chapter of his text to orthotropic shell theory (25). New texts by Reddy (31) and Vinson and Sierakowski (41) discuss anisotropic laminated shell structures including various transverse shear deformation treatments.

The simplifying assumption of laminated anisotropy is often used in applying a 2-D theory to plates and shells consisting of layers of composite materials (31). In this approach, the individual properties of the composite constituents, the fibers and the matrix, are 'smeared' and thus each lamina is treated as an orthotropic material. Additionally, laminated anisotropy assumes perfect bonding between layers, i.e., the interply adhesive has infinitesimal thickness but infinite stiffness. This approach leads to classical laminated plate theory (CLPT) and the references by Jones (42) and Ashton and Whitney (43) are thorough presentations thereof. CLPT relies on the Kirchhoff-Love assumption on the datum surface normals; however, both references point out that transverse shear deformation is more significant in laminated anisotropic structures over similar isotropic constructions.

Dong, Pister, and Taylor (44) develop small displacement Love theory similar to that of Ambartsumyan for the bending analysis of thin anisotropic plates and shells. These are specialized to give linear Donnell equations for anisotropic cylindrical shells. Bert (45) used Vlasov shell theory to formulate a linear laminated shell theory similar to CLPT.

Yang, Norris, and Stavsky (46) generalized the Reissner-Mindlin theory, i.e., first order transverse shear treatments, to laminated anisotropic plates. Whitney and Pagano (47) were the first to apply it to composite plate

13

analysis. Reddy (48) has applied Reissner-Mindlin theory to linear anisotropic shell structures of constant principal and twist curvatures. Noor (49) applies RM theory to examine the stability of laminated plates. The buckling of laminated cylindrical shells was studied by Hirano (50), Stavsky and Friedland (51), and Greenberg and Stavsky (52). Thick composite plate closed form solutions are reported by Reddy and Chao (53).

Reddy (31,54) has extended the cubic kinematical approach to analyze laminated anisotropic plates and he and Soldatos have applied them to solve several linear static and buckling problems (54-58). Additionally, Soldatos applies the parabolic shear theory to examine the stability of unsymmetrically laminated cylindrical panels (59,60). The parabolic shear theory is also assumed in a study of the linear behavior of laminated shells by Reddy and Liu (61).

Pagano (62-65) and Srinivas and Rao (66) have developed some exact solutions of 3-D elasticity equations governing composite plates that have been used to validate these theories. They conclude that CLPT gives fairly good approximations for both the displacements and stresses if the plate is thin. Thinness, as defined for layered composite plates, not only considers length to thickness ratios but also the degree of anisotropy. Transverse stresses are calculated from the equilibrium equations and the CLPT inplane stresses. Higher order shear theories do not give much better transverse stress results but

14

displacements show a marked improvement over CLPT for the thicker plates. Transverse stresses are calculated best from equilibrium instead of from the constitutive relations (42). Ren (67) similarly solves 3-D elasticity equations for a laminated cylindrical shell in cylindrical bending.

All of the above approaches can include various degrees of nonlinearity in the strain displacement relations in representing the displacements and rotations. For example, Reddy and Chandrashekhara (68) solve both cylindrical and spherical laminated shell cases assuming RM transverse shear and an intermediate nonlinearity. However, there are few such analytical closed form solutions for shell geometries, especially those that govern nonlinear behavior. Consequently, numerical solutions become necessary and specifically, the finite element method application to shell and plate theories is discussed next.

Finite Element Shell Applications

General 3-D elements could be used to model shell structures. However, since a shell is characterized by the dimension in the thickness direction being smaller than the inplane dimensions, numerical ill conditioning results. Additionally, use of 3-D elements would involve many degrees of freedom (dof) that may not be necessary. Consequently, elements that are specifically designed for shell structures are developed with flat plates considered a special case.

There are three approaches to applying finite element methods to shell structures; 1) the shell structure is

15

facetted with flat elements, 2) 2-D shell theory or Love theory is used to develop a curved shell element, and 3) curved shell elements are formed by degenerating the 3-D strain displacement relations (69). Method 1 was first suggested 25 years ago and new developments continue (69,70). This approach must contend with discontinuous bending moments between elements and achieves convergence only for fine meshes.

Method 2 has generally only been applied to solving linear problems; indeed, its acceptance has been hindered due to the absence of a general nonlinear shell theory. An early development of a linear cylindrical shell element is due to Bogner, Fox, and Schmit (71). Later, Yang (72) extended this work to shell geometries of constant principal and twist curvatures. Both elements are rectangular, based on linear Love shell theory, and apply only to isotropic materials. A more recent application of method 2 (and method 1) is found in the paper by Idelson (73) where the modelling of deep shell structures with flat, shallow, and deep shell elements is discussed. He found that flat elements can give better results in modelling the deep shell structures than do simple shallow shell elements. Indeed, the shallow shell elements can give totally erroneous results for some cases.

Method 3 is perhaps the most popular approach and first appeared in the form of the Ahmad element (74). In elements of this type, transverse displacements and rotations are

treated independently and hence are well suited to Reissner-Mindlin shear deformation theories. These elements can resemble 3-D elements in that they may have nodes on the top and bottom surfaces of the shell element. Other variations have nodes only on a datum surface. In both cases, however, normal stress is assumed to be zero consistent with most shell theories. The Ahmad element, at first, seemed to be ideal due to its simplicity and generality. However, as is now well known, it develops serious shear 'locking' problems as the shell becomes thinner. For the thin shell, the mesh of Ahmad elements can lock at a solution much stiffer than the classical result. This is a direct consequence of the approximations used in representing the displacement within an element. Consequently, this method is generally used with some means to remedy the locking phenomenon.

Shear locking generally occurs in plate and shell finite elements that have been formulated based on degenerated 3-D strain displacement relations and RM shear theories. Because of the constant transverse shear assumed through the shell thickness, these type of elements have independent displacement and rotational degrees of freedom. Consequently, there is no Kirchhoff-Love assumption placed on the rotations of the normals and the transverse shear does not vanish when the element is subjected to a constant bending moment. Furthermore, the shear stiffness dominates as the element thickness gets small due to lower order

17

displacement interpolations. Zienkiewicz, Taylor, and Too (75) introduced reduced or selective integration as a means to alleviate the shear locking phenomenon in these type of elements. If nonexact, i.e. reduced, numerical integration is used to evaluate the transverse shear stiffness integrals, the shear deformation is actually better represented since many of the incorrect shear terms present in the elemental formulation are not included in the integration (76). However, as the element gets even thinner, the locking problem once again becomes pronounced. Despite that, use of the reduced integration technique has become almost automatic for the degenerated type elements.

Reference (69) presents some alternative elements successfully applied to both thick and thin plates and shells. Due to a higher number of dof per element these elements do not lock as easily but may develop other problems in the form of spurious mechanisms. Kui, Liu, and Zienkiewicz (77) apply a displacement finite element method to analyze thin shells using an Ahmad type element. Discrete Kirchhoff-Love constraints are imposed within the element to lessen locking effects. This concept was first proposed by Wempner (78) who noticed that only the simple polynomial displacement approximations resulted in elements that shear locked. rockman (79) also uses this approach in developing a shell element that can undergo large displacements and rotations. Park and Stanley (80) avoid shear locking by redefining the shape functions present in

the strain displacement relations that contain generalized displacements and derivatives of displacements such that consistent approximations result.

Application of material anisotropy in finite elements naturally occurred first with plates before shells. Pryor and Barker (81) developed a linear flat element based on laminated anisotropic plate theory including RM shear deformations. The transverse shear stresses were determined from the three dimensional equations of elasticity. To better model the deformed normal of the plate, they suggest a more general approach where each layer of the laminate has rotational degrees of freedom. In this way, transverse stress continuity at each laminate boundary can be satisfied.

This idea has been applied using linear theory and the Ahmad element by several investigators (82). Recently, Palazotto and Witt (83) extended the approach to a geometrically nonlinear shell formulation and applied it to flat plates. Hinrichsen and Palazotto (82) used a cubic spline function to represent the transverse displacements of a flat plate and found that while giving a higher order approximation to displacements, the equations were simplified over the work of (83) which essentially used a quadratic spline.

Linear static, stability, and vibration analyses of laminated plates and shells with transverse shear deformation were performed by Noor and Mathers (84). Two

19

finite element formulations, mixed and displacement, are compared. Reddy (85) analyzed the nonlinear transient behavior of composite plates including RM transverse shear.

According to Reddy (86), very little work has been done in geometrically nonlinear anisotropic shell finite element analysis, at least before 1981. An early work by Schmit and Monforton (87) formulates an anisotropic cylindrical shell element that allows intermediate geometric nonlinearities. More recently, Leissa (88) compiled a comprehensive review of composite flat plate and shell panel bifurcation and post buckling analyses. Stolarski et al (89) present a simple triangular shell element formulation that includes intermediate nonlinearity. Some other recent papers by Noor and Peters (90), Meroueh (91), and Surana (92,93) can be cited. Noor and Peters analyzed nonlinear anisotropic cylindrical panels using a Hu-Washizu mixed shallow shell finite element approach that includes transverse shear deformation to determine global approximation modes, and then applies a Rayleigh-Ritz technique to determine the amplitudes of the modes. The effect of the degree of anisotropy was studied. Meroueh develops a general nonlinear plate and shell element based on a displacement model that includes third order terms in the thickness parameter thereby including transverse shear deformation. This paper deals primarily with structural systems with loadings and materials that are only adequately modelled considering large strains and nonlinear stress strain

20

relations. Surana has developed, in a series of papers-two of which are referenced here, a geometrically nonlinear approach that allow elements to undergo both large displacements and rotations between two successive load increments. This is done by retaining the nonlinear trigonometric terms in the displacement functions that relate the nodes on the top and bottom surfaces of the element. Typically, these terms have been linearized by other investigators, see (70,74).

Recently, capabilities have been added to the family of flat elements of the STAGS finite element code developed by Lockheed Corporation. The code's purpose is to solve buckling and collapse problems in structural mechanics. The improvements use an updated Lagrangian approach that allows large rotations for small strain situations (94). Analyses done by Tisler (1) and Knight and Starnes (2) have shown that the elements with intermediate geometric nonlinear capability, i.e., not including this new approach, cannot adequately describe the nonlinear behavior of anisotropic cylindrical panels with large cutouts.

Use of higher order kinematics to represent the displacements through the thickness may reduce the shear locking in finite element formulations that was discussed earlier. Putcha and Reddy (95) used cubic kinematics in formulating a mixed element for nonlinear anisotropic plate analysis. For many of the cases examined, the element did not lock as its thickness was decreased even using exact

integration.

Resulting from the finite element discretization are simultaneous nonlinear equations that are typically solved via a direct iteration or Newton-Raphson method. Thorough overviews of solution techniques can be found in Stricklin and Haisler (96), Bathe and Cimento (97), Riks (98), and Waszczszyn (99). Bergan (100) states that a successful nonlinear analysis depends on the solution algorithm being reliable and efficient. The direct iteration is generally not used because it is not reliable since it often diverges, and the Newton-Raphson, without modifications, is not used because it is inefficient and sometimes unreliable. All of the solution techniques presented here use the Newton-Raphson approach in some way. The original Newton-Raphson method uses linearized incremental equations but convergence is not guaranteed for all cases and thus, this method can become unreliable. A form of the Newton-Raphson method that is guaranteed to converge increments many small load steps instead of only a single increment in reaching a target load. To make this approach more efficient, the tangent stiffness matrix need not be updated with each iteration. This form is called the modified Newton-Raphson method. In this case, more equilibrium iterations per increment will usually be required but the stiffness or coefficient matrix will not be refactorized nearly as often.

The incremental/iterative type solution schemes as discussed above are used in most general purpose finite

element codes. They have three major disadvantages: 1) the load step size must somehow be predetermined and it usually remains fixed throughout the total solution procedure, 2) the above solution procedures can not trace the nonlinear response beyond critical or limit points, i.e., a point of the equilibrium path where the coefficient matrix is singular, and 3) the updating of the coefficient matrix is inefficient (101). A general description of several solution techniques that improve on these drawbacks follows.

The current stiffness parameter, S_p, can be used to address the first two disadvantages. The current stiffness parameter, due to Bergan (100) can detect an imminent limit point since it approaches zero as the limit point is approached. The equilibrium iterations can then be suppressed until the limit point is passed. Since S_p is a measure of incremental stiffness or curvature it can also be used to vary the load increment. Smaller load increments can be automatically imposed as the magnitude of S_p gets smaller. The stiffness parameter has been used successfully in this context in (83,100).

Another incremental/iterative method that can be used to successfully pass through a limit point is the displacement control method (101,102,103). In the displacement control method, one component of displacement is prescribed and the corresponding load becomes the unknown. Rearranging the equations to reflect the changed

23

dependent and independent variables results in an unsymmetric and unbanded coefficient matrix. Techniques are then invoked such that the resulting unbanded unsymmetric system is solved in an efficient manner. As a result of the variables being rearranged, the coefficient matrix is no longer singular at the limit point and hence, solutions are possible. In this way, the displacement control method can be used in conjunction with the stiffness parameter. Since the impending limit point can be detected, the displacement control method is invoked at some point beforehand. The displacement control method can be used for the total solution process also but may fail at other points on the equilibrium path (98).

Generalizations of the above Newton-Raphson load and displacement control techniques are the arc length or continuation approaches. Instead of acting along hyperplanes of constant load or displacement, iteration acts along arbitrarily shaped 'constraint surfaces'. The Riks/Wempner (104-106) approach uses a constraint equation that limits the load step thus defining an arc length. The solutions for each iteration follow a path, i.e., along a constraint surface, that is normal to the fixed length tangent defined by the load constraint. Crisfield (107-109) develops a circular constraint surface solution technique. Other types of constraint surfaces have been developed and are discussed by Padovan and Moscarello in (110). Reference (110) also discusses an approach where the constraint

surface can change with each iteration.

Another type of solution method addresses the third drawback of the standard methods by using better ways to update the coefficient matrix of the nonlinear equations. These algorithms, which attempt to minimize a functional, usually the potential energy for the static case, are widely used in the structural optimization field (111).

The general strategy is to find a search direction and then perform a unidimensional minimization along that search line. Ways to determine the search direction vector and perform the unidimensional search differentiate the various algorithms. A brief overview is found in (108) and more detailed accounts in (97,112). Two of these types of algorithms are the conjugate direction and quasi-Newton. The conjugate direction search algorithm finds a new search direction partly based on previous search directions. This dramatically improves convergence over those methods that do not consider information from previous search directions. Quasi-Newton or variable metric methods offer improvements over the conjugate direction method since an array carries previous search information instead of only a scalar as in the latter. This array is an approximation to the inverse of the stiffness matrix. Examples of different quasi-Newton methods are the Davidon-Fletcher-Powell (DFP) and the Broyden-Fletcher-Goldfarb-Shanno (BFGS) methods. The BFGS method updates the coefficient matrix using a matrix of rank two. For this reason, the BFGS update can be thought of as

in between the modified Newton-Raphson (no update) and the traditional Newton-Raphson (full rank update) and explains why these approaches are termed "quasi-Newton". Crisfield (109) describes how to combine the line search methods with a constraint surface technique.

Based on the preceding discussions of over one hundred references, much work has been accomplished in the analysis of composite shell and flat plate structures. Not nearly as much attention has been placed on studying their nonlinear response, however. The research effort to be described presently will focus on nonlinear composite shell behavior. Although the theory is two dimensional, the very important influence of transverse shear deformation is included in the approach.

III. Theoretical Approach

Once again, the purpose of this research effort is to develop better tools to predict the nonlinear load-displacement or equilibrium response of shell structures. Certain simplifications are required in order to reduce the scope of the problem. Only geometrical nonlinearity is considered and for most engineering materials this would also imply a small strain assumption. Additionally, only cylindrical shells and flat plates are analyzed, although the assumptions will allow for arbitrary shell geometries described by orthogonal coordinates. Since we will limit ourselves to orthogonal systems, the notions of covariance, contravariance, Christoffel symbols, etc. commonly seen in the study of curvilinear coordinates, are not needed. The theory presented encompasses large displacements and rotations, elastic laminated anisotropic material behavior, and parabolic transverse shear stress distribution through the thickness. While leading into the theory, many ideas from the literature review are recalled and expanded upon. First though, some general relationships and definitions to be used in developing the theory are introduced.

General Relationships

In describing the response of a solid body under load, nonlinearities are present in the general case. The governing equations are the strain displacement relations,

27

the equations of equilibrium, and the constitutive laws. Nonlinearities due solely to geometrical considerations are found in the first and second sets of governing equations and nonlinearities due solely to physical or material considerations are found in the third set of equations. The geometrical nonlinearities can be a result of large strains, rotations, and displacements of the fibers of a differential volume element that has undergone a transformation from some original configuration. Material nonlinearities are a result of straining beyond the limit of proportionality usually caused by large strains. Beyond this limit, the stress strain relationship is nonlinear and a special case is the material that has been strained beyond its yield point and plastic flow results. It therefore appears that nonlinearity is of two general types, geometrical and material, and each is treated independently. In this regard, Novozhilov (113) categorizes four basic problems in the theory of elasticity:

1. geometrically/materially linear

2. materially nonlinear

3. geometrically nonlinear

4. geometrically/materially nonlinear

Of course, all problems can be treated as in 4 above, however; usually specific situations will allow some simplifying assumptions. The most drastic simplification occurs in 1 above. The governing equations are the

classical linear equations of elasticity. Strain, displacements, rotations, etc., are all assumed to be small quantities. If the rotations and displacements of the transformation are small but the strains of the body are such that the proportional limit of the material is exceeded and a nonlinear stress strain relationship is required then only material nonlinearity is considered. If the rotations and displacements are large but the strains are small such that a linear material law can apply, then only geometrical nonlinearity is considered. A wide class of problems can be solved considering only geometrical nonlinearity, and it is this class of problems that are considered in the present research. (113)

A convenient way to represent governing relationships in solid mechanics is in terms of the original configuration, i.e., prior to deformation. These types of formulations are termed Lagrangian and this viewpoint will be adhered to in the following. In Lagrangian formulations, the Green's strain tensor and its energy conjugate, the Second Piola-Kirchhoff stress tensor are used to define the internal strain energy of the body (113-115).

In what follows, the general expressions of the three dimensional strain displacement relations are derived, surface quantities are defined, and the total potential energy and constitutive laws are developed. These relationships represent the theoretical foundation from

29

which the nonlinear shell theory of the present work is built.

Strain Displacement in Curvilinear Coordinates

Although shell theory can be based entirely on surface definitions, transverse effects, i.e., in the direction of the surface normal, are then not easily included (7,8,10). One way to define strain displacement relations that can easily incorporate three dimensionality (3-D) is to specialize the general 3-D strain displacement relations expressed in arbitrary orthogonal curvilinear coordinates. These are derived in several elasticity texts, see (6) for example. To introduce nomenclature and ideas to be used later, a brief description of the derivation follows.

Consider the point M of Figure 3.1 that is located in 3-D space by the position vector, $\bar{r}$. The point M has Cartesian coordinates, x_i, as shown in Eqn (3.1).

$$\bar{r} = x_i \, \bar{i}_i \qquad i=1,2,3 \qquad\qquad (3.1)$$

where,

x_i = Cartesian coordinates

$\bar{i}_i$ = Cartesian basis vectors

A summation convention on repeated indices applies unless otherwise stated, and barred quantities refer to vectors.

We can also represent point M with curvilinear coordinates y_i. The Cartesian coordinates are related to

30

the curvilinear coordinates through transformations of the form shown in Eqn (3.2).
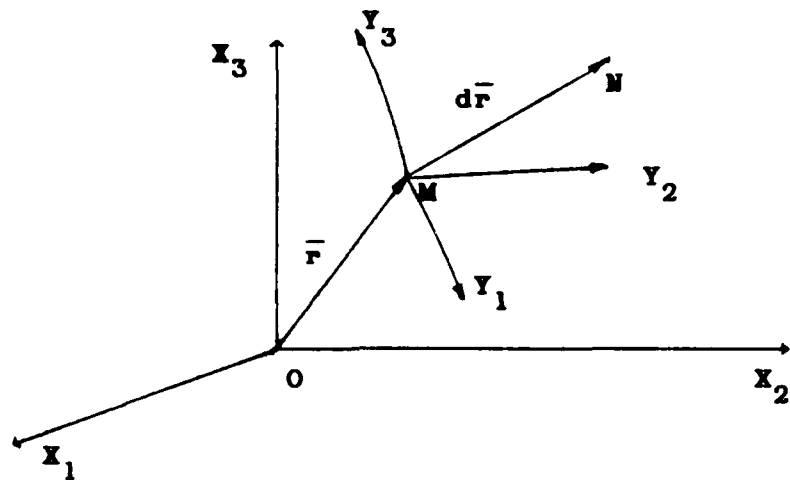
FIGURE 3.1. Point M Located in 3 Space by Position Vector $\bar{r}$. Vector $d\bar{r}$ has Length ds.

$$x_i = x_i(y_1,y_2,y_3) = x_i(y_j)$$

$$y_i = y_i(x_1,x_2,x_3) = y_i(x_j)$$

(3.2)

Basis vectors, $\bar{a}_i$, of the curvilinear system are found by taking the differential of the position vector, $\bar{r}$. From Eqn (3.1),

$$d\bar{r} = dx_i\bar{i}_i$$

(3.3)

The length, ds, of the infinitesimal line segment MN (see vector $d\bar{r}$ of Figure 3.1) is then given by,

$$(ds)^2 = d\bar{r} \cdot d\bar{r}$$

(3.4)

The length ds is independent of coordinate system and

31

therefore from Eqn (3.2),

$$d\bar{r} = \bar{a}_1 dy_1 + \bar{a}_2 dy_2 + \bar{a}_3 dy_3 \qquad (3.5)$$

where,

$$\bar{a}_i \equiv \frac{\partial \bar{r}}{\partial y_i} = \bar{r}_{,i}$$

A curvilinear basis vector, $\bar{a}_i$, is tangent to the Y_i coordinate line. From Eqns (3.4) and (3.5) we can write,

$$(ds)^2 = (\bar{a}_i \cdot \bar{a}_j) dy_i dy_j = g_{ij} dy_i dy_j \qquad (3.6)$$

where,

$$g_{ij} \equiv \bar{a}_i \cdot \bar{a}_j$$

The elements of g_{ij} form a symmetric tensor called the metric that links the two coordinate systems X_i and Y_i through the invariant property of length. The Y_i coordinate system is called orthogonal if its metric is diagonal, i.e., when $g_{ij} = 0$ for $i \neq j$. This is assumed from this point on.

Next, consider the infinitesimal line segment, MN, of length ds now embedded in a differential volume element, see Figure 3.2. This differential volume is linearly transformed, i.e., deformed, to a new configuration where the line segment is now of length ds^*, and whose transformed coordinate system has a metric G_{ij}. As a result of deformation, the line segment MN of Figure 3.2 moves to M^*N^* represented by the displacement vector, $\bar{u}$. By subtracting

the original and deformed squared lengths of the line segment, the Green's strain tensor, γ_{ij}, is defined as shown in Eqn (3.7).

$$(ds^*)^2 - (ds)^2 = 2\gamma_{ij}dy_i dy_j \qquad (3.7)$$

Previously defined quantities then give,

$$2\gamma_{ij} = G_{ij} - g_{ij} = \bar{a}_i \cdot \bar{u},_j + \bar{a}_j \cdot \bar{u},_i + \bar{u},_i \cdot \bar{u},_j \qquad (3.8)$$

The physical strains, ε_{ij}, are then found from,

$$\varepsilon_{ij} = \frac{\gamma_{ij}}{h_i h_j} \qquad (3.9)$$

In Eqn (3.9), the h_i are called scale factors and are defined by $g_{ii} = h_i^2$ (no sum) and the γ_{ij} are shown in Eqn (3.10) where the u_i are the coordinates of the displacement vector, $\bar{u}$. In the general large strain case, the ε_{ii} (no sum) are related to the elongations of the fibers of the differential volume element and the ε_{ij} ($i \neq j$) are related to the shears, i.e., the difference from ninety degrees originally perpendicular fibers are oriented after deformation. For the case of small strains ($\varepsilon < .04$, Ref (115)), the ε_{ii} (no sum) are the elongations and the ε_{ij} ($i \neq j$) are the shears. That is to say, for large strains, the ε_{ij} do not have physical meanings; but for small strains, the ε_{ij} have the engineering definitions. The elongations and shears are identically zero for rigid body displacements and rotations of the body under loading (115).

33

In this way, there are no theoretical limitations on the magnitudes of displacement and rotation elements of the body can undergo (113).

Stein (116) represents geometric nonlinearity alternatively by expanding the exact large strain expressions into Taylor series. The manner in which he truncates these series gives small strain representations that are slightly different than those shown in Eqn (3.10).
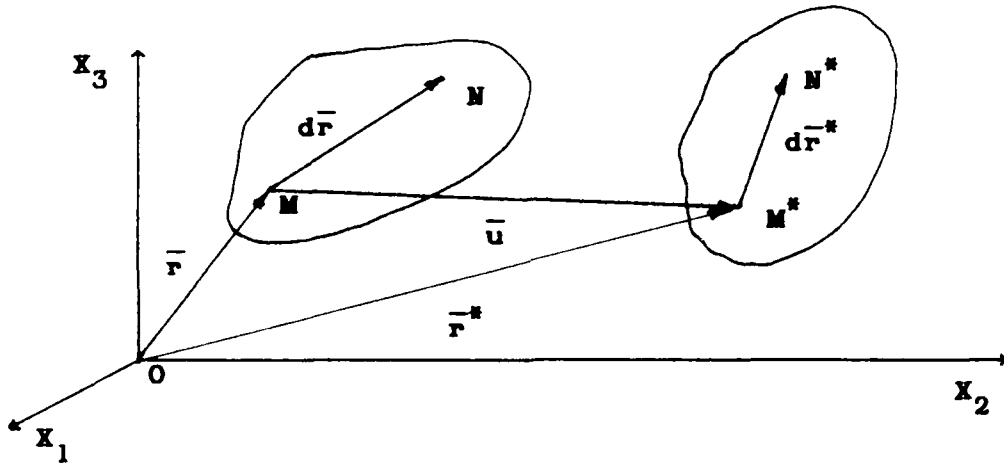
FIGURE 3.2. Segment MN Deforms to M*N* Through Displacement Vector $\bar{u}$.

$$\gamma_{11} = h_1\frac{\partial u_1}{\partial y_1} + \frac{h_1 u_2}{h_2}\frac{\partial h_1}{\partial y_2} + \frac{h_1 u_3}{h_3}\frac{\partial h_1}{\partial y_3}$$
$$+ \frac{1}{2}\left(\frac{\partial u_1}{\partial y_1} + \frac{u_2}{h_2}\frac{\partial h_1}{\partial y_2} + \frac{u_3}{h_3}\frac{\partial h_1}{\partial y_3}\right)^2$$
$$+ \frac{1}{2}\left(\frac{\partial u_2}{\partial y_1} - \frac{u_1}{h_2}\frac{\partial h_1}{\partial y_2}\right)^2 + \frac{1}{2}\left(\frac{\partial u_3}{\partial y_1} - \frac{u_1}{h_3}\frac{\partial h_1}{\partial y_3}\right)^2$$

$$\gamma_{22} = h_2\frac{\partial u_2}{\partial y_2} + \frac{h_2 u_3}{h_3}\frac{\partial h_2}{\partial y_3} + \frac{h_2 u_1}{h_1}\frac{\partial h_2}{\partial y_1}$$
$$+ \frac{1}{2}\left(\frac{\partial u_2}{\partial y_2} + \frac{u_3}{h_3}\frac{\partial h_2}{\partial y_3} + \frac{u_1}{h_1}\frac{\partial h_2}{\partial y_1}\right)^2$$
$$+ \frac{1}{2}\left(\frac{\partial u_3}{\partial y_2} - \frac{u_2}{h_3}\frac{\partial h_2}{\partial y_3}\right)^2 + \frac{1}{2}\left(\frac{\partial u_1}{\partial y_2} - \frac{u_2}{h_1}\frac{\partial h_2}{\partial y_1}\right)^2$$

$$\gamma_{33} = h_3\frac{\partial u_3}{\partial y_3} + \frac{h_3 u_1}{h_1}\frac{\partial h_3}{\partial y_1} + \frac{h_3 u_2}{h_2}\frac{\partial h_3}{\partial y_2}$$
$$+ \frac{1}{2}\left(\frac{\partial u_3}{\partial y_3} + \frac{u_1}{h_1}\frac{\partial h_3}{\partial y_1} + \frac{u_2}{h_2}\frac{\partial h_3}{\partial y_2}\right)^2$$
$$+ \frac{1}{2}\left(\frac{\partial u_1}{\partial y_3} - \frac{u_3}{h_1}\frac{\partial h_3}{\partial y_1}\right)^2 + \frac{1}{2}\left(\frac{\partial u_2}{\partial y_3} - \frac{u_3}{h_2}\frac{\partial h_3}{\partial y_2}\right)^2$$

$$\gamma_{12} = \frac{1}{2}\left(h_1\frac{\partial u_1}{\partial y_2} + h_2\frac{\partial u_2}{\partial y_1} - u_2\frac{\partial h_2}{\partial y_1} - u_1\frac{\partial h_1}{\partial y_2}\right)$$
$$+ \frac{1}{2}\left(\frac{\partial u_1}{\partial y_2} - \frac{u_2}{h_1}\frac{\partial h_2}{\partial y_1}\right)\left(\frac{\partial u_1}{\partial y_1} + \frac{u_2}{h_2}\frac{\partial h_1}{\partial y_2} + \frac{u_3}{h_3}\frac{\partial h_1}{\partial y_3}\right)$$
$$+ \frac{1}{2}\left(\frac{\partial u_2}{\partial y_1} - \frac{u_1}{h_2}\frac{\partial h_1}{\partial y_2}\right)\left(\frac{\partial u_2}{\partial y_2} + \frac{u_1}{h_1}\frac{\partial h_2}{\partial y_1} + \frac{u_3}{h_3}\frac{\partial h_2}{\partial y_3}\right) \qquad (3.10)$$
$$+ \frac{1}{2}\left(\frac{\partial u_3}{\partial y_1} - \frac{u_1}{h_3}\frac{\partial h_1}{\partial y_3}\right)\left(\frac{\partial u_3}{\partial y_2} - \frac{u_2}{h_3}\frac{\partial h_2}{\partial y_3}\right)$$

$$\gamma_{13} = \frac{1}{2}\left(h_3\frac{\partial u_3}{\partial y_1} + h_1\frac{\partial u_1}{\partial y_3} - u_1\frac{\partial h_1}{\partial y_3} - u_3\frac{\partial h_3}{\partial y_1}\right)$$
$$+ \frac{1}{2}\left(\frac{\partial u_1}{\partial y_3} - \frac{u_3}{h_1}\frac{\partial h_3}{\partial y_1}\right)\left(\frac{\partial u_1}{\partial y_1} + \frac{u_3}{h_3}\frac{\partial h_1}{\partial y_3} + \frac{u_2}{h_2}\frac{\partial h_1}{\partial y_2}\right)$$
$$+ \frac{1}{2}\left(\frac{\partial u_3}{\partial y_1} - \frac{u_1}{h_3}\frac{\partial h_1}{\partial y_3}\right)\left(\frac{\partial u_3}{\partial y_3} + \frac{u_1}{h_1}\frac{\partial h_3}{\partial y_1} + \frac{u_2}{h_2}\frac{\partial h_3}{\partial y_2}\right)$$
$$+ \frac{1}{2}\left(\frac{\partial u_2}{\partial y_1} - \frac{u_1}{h_2}\frac{\partial h_1}{\partial y_2}\right)\left(\frac{\partial u_2}{\partial y_3} - \frac{u_3}{h_2}\frac{\partial h_3}{\partial y_2}\right)$$

$$\gamma_{23} = \frac{1}{2}\left(h_3\frac{\partial u_3}{\partial y_2} + h_2\frac{\partial u_2}{\partial y_3} - u_2\frac{\partial h_2}{\partial y_3} - u_3\frac{\partial h_3}{\partial y_2}\right)$$
$$+ \frac{1}{2}\left(\frac{\partial u_2}{\partial y_3} - \frac{u_3}{h_2}\frac{\partial h_3}{\partial y_2}\right)\left(\frac{\partial u_2}{\partial y_2} + \frac{u_3}{h_3}\frac{\partial h_2}{\partial y_3} + \frac{u_1}{h_1}\frac{\partial h_2}{\partial y_1}\right)$$
$$+ \frac{1}{2}\left(\frac{\partial u_3}{\partial y_2} - \frac{u_2}{h_3}\frac{\partial h_2}{\partial y_3}\right)\left(\frac{\partial u_3}{\partial y_3} + \frac{u_2}{h_2}\frac{\partial h_3}{\partial y_2} + \frac{u_1}{h_1}\frac{\partial h_3}{\partial y_1}\right)$$
$$+ \frac{1}{2}\left(\frac{\partial u_1}{\partial y_2} - \frac{u_2}{h_1}\frac{\partial h_2}{\partial y_1}\right)\left(\frac{\partial u_1}{\partial y_3} - \frac{u_3}{h_1}\frac{\partial h_3}{\partial y_1}\right)$$

Surface/Shell Geometrical Definitions

The strain displacement relations for a shell can not be expressed until the geometrical scale factor quantities (the h_i's) of Eqn (3.10) are defined. Ideas from surface theory are introduced to this end. In Figure 3.3 consider a point on a smooth surface that is located in three dimensional space by a position vector, $\bar{r}$, directed from an arbitrarily placed origin of a Cartesian coordinate system. As before, $\bar{r}$ has Cartesian coordinates, x_i.

$$\bar{r} = x_i \bar{i}_i \qquad i=1,2,3 \qquad (3.11)$$

Any point on the surface can also be represented by curvilinear coordinates, ζ_1 and ζ_2. The two sets of coordinates, once again, are related through transformations of the form in Eqn (3.12).

$$x_i = x_i(\zeta_1, \zeta_2) = x_i(\zeta_\alpha) \qquad (3.12)$$

The usual convention of lower case Latin subscripts taking on values 1,2, and 3 and Greek subscripts 1 and 2 applies. Parametric curves or coordinate lines are formed on the surface by fixing ζ_1 or ζ_2 and allowing the other to vary.

The basis vectors, $\bar{a}_1$ and $\bar{a}_2$, of the surface form a two dimensional space tangent to the surface at every point and are found as in the 3-D case by taking the differential of the position vector, $\bar{r}$,

$$d\bar{r} = \bar{r}_{,1}d\zeta_1 + \bar{r}_{,2}d\zeta_2 \qquad (3.13)$$

36

and then define,

$$\bar{a}_1 = \bar{r},_1 = x_{i,1}\bar{i}_i$$

$$\bar{a}_2 = \bar{r},_2 = x_{i,2}\bar{i}_i$$

(3.14)

where, now, $(\ )_{,\alpha}$ refers to differentiation with respect to the two curvilinear coordinates, ζ_α.
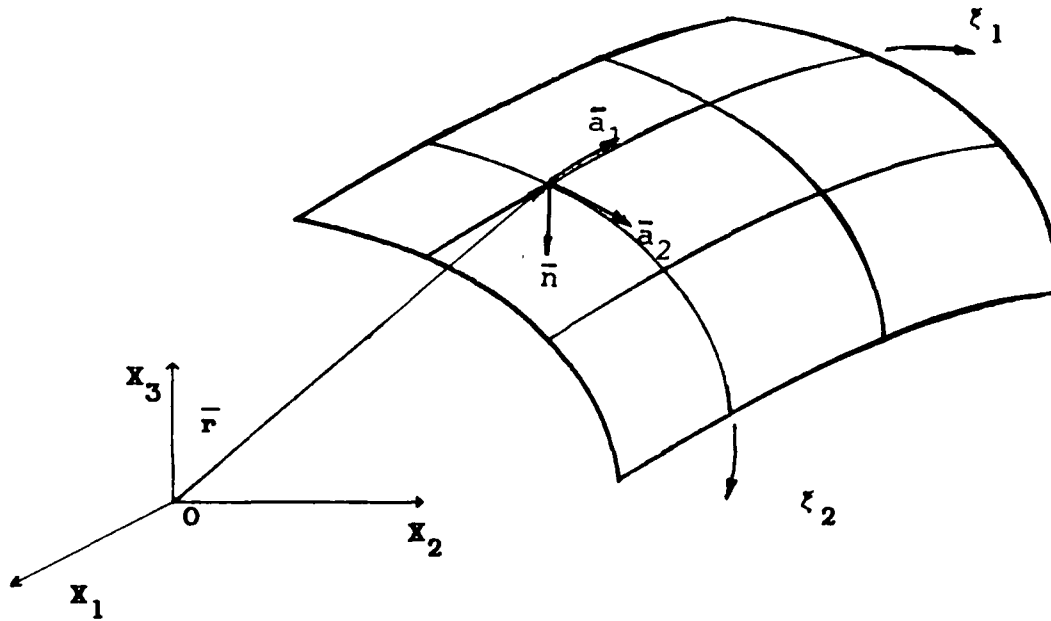
FIGURE 3.3. Position Vector $\bar{r}$ Locates Arbitrary Point on Surface.

A measure of length on the surface is given by the first fundamental form,

$$(ds)^2 = d\bar{r} \cdot d\bar{r} = a_{11}(d\zeta_1)^2 + 2a_{12}d\zeta_1 d\zeta_2 + a_{22}(d\zeta_2)^2$$

(3.15)

The $a_{\alpha\beta}$ are elements of a symmetric tensor called the surface metric defined analogously to the 3-D metric.

The unit surface normal, $\bar{n}$, is defined from the cross product of the basis vectors, and a measure of the curvature of the surface is given by the second fundamental form,

$$-d\bar{n} \cdot d\bar{r} = b_{11}(d\zeta_1)^2 + 2b_{12}d\zeta_1 d\zeta_2 + b_{22}(d\zeta_2)^2 \qquad (3.16)$$

The $b_{\alpha\beta}$ are elements of another symmetric tensor called the curvature tensor and are formed from the dot products of the surface normal and the second derivatives of the position vector,

$$b_{\alpha\beta} = \bar{n} \cdot \bar{r}_{,\alpha\beta} = n_i x_{i,\alpha\beta} \qquad (3.17)$$

where n_i are the coordinates of the surface normal.

For the special case where parametric lines are lines of curvature, i.e., orthogonal coordinates, the metric and curvature tensors become diagonal, i.e., $a_{12} = a_{21} = b_{12} = b_{21} = 0$. As in the 3-D relationships, assume orthogonality in what follows.

The curvature of a normal section is given by the ratio of the two fundamental forms, Eqns (3.15) and (3.16), and from that the two principal curvatures of the surface at each point are found. That is, the curvatures of the surface, C_α, in the direction of the lines of curvature are given by,

$$C_1 = b_{11}/a_{11} = 1/R_1$$

$$C_2 = b_{22}/a_{22} = 1/R_2 \qquad (3.18)$$

where R_α are the radii of curvature of the surface.

The surface just described will represent the shell's datum or reference surface. Next, assume that a description of the behavior of the datum surface is sufficient to describe the behavior of the entire shell. This assumption is a consequence of the inherent "thinness" of the shell to reduce its dimensionality and will be examined fully in a later section. Given this assumption, the behavior of the datum surface must be connected to points of the shell not on the datum surface. This is done by adding to the geometrical description a third parameter, ζ, that varies along the surface normal, See Figure 3.4. The position vector, $\bar{R}$, to an arbitrary point of the <u>shell</u> can now be given by

$$\bar{R}(\zeta_1,\zeta_2,\zeta) = \bar{r}(\zeta_1,\zeta_2) + \zeta\bar{n}(\zeta_1,\zeta_2) \qquad (3.19)$$

The first fundamental form for shell then is found from

$$(ds)^2 = d\bar{R} \cdot d\bar{R}$$

$$= a_{11}(1-\zeta/R_1)^2(d\zeta_1)^2 + a_{22}(1-\zeta/R_2)^2(d\zeta_2)^2 + d\zeta^2$$

$$(3.20)$$

and the scale factors for the shell to be used in Eqn (3.10) in expressing the shell strain displacement relations are defined from Eqn (3.20),

$$h_1 = \alpha_1(1 - \zeta/R_1) \; , \; h_2 = \alpha_2(1 - \zeta/R_2) \; , \; h_3 = 1 \qquad (3.21)$$

where $\alpha_\gamma^2 = a_{\gamma\gamma}$ (no sum).

Details of the above can be found in (6).
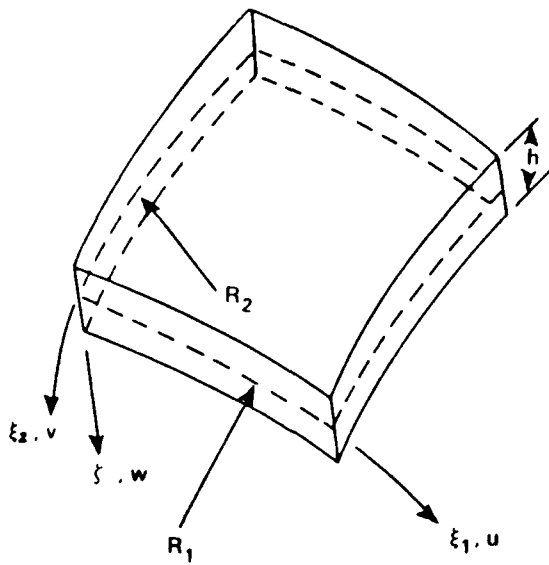
FIGURE 3.4. Surface and Shell Coordinate System.

Virtual Work, Generalized Hooke's Law, Potential Energy

For a body of volume V in equilibrium with prescribed forces on a part of its surface, S_1, and prescribed geometric boundary conditions on the remaining surface, S_2, that has undergone an infinitesimal virtual displacement, $\delta\bar{u}$, we have,

$$\int_V (\sigma_{ij}\delta\varepsilon_{ij} - P_k\delta u_k)\, dV - \int_{S_1} F_k\delta u_k\, dS = 0 \qquad (3.22)$$

where,

σ_{ij} are elements of the 2nd Piola-Kirchhoff stress tensor, i,j=1,2,3

ε_{ij} are defined in Eqn (3.9),

P_k are components of prescribed body forces,

F_k are components of prescribed surface tractions.

Next, assume for a conservative system, there exists a strain energy density function, W^*, such that,

$$\frac{\partial W^*}{\partial \varepsilon_{ij}} = \sigma_{ij} \tag{3.23}$$

Furthermore, assume that there exists a relationship between stress and strain and that the strains are small. In this case, we have a generalized Hooke's law as shown in Eqn (3.24).

$$\sigma_{ij} = a_{ijkl} \, \varepsilon_{kl} \tag{3.24}$$

where a_{ijkl} are constants of the elasticity tensor.
Therefore from Eqns (3.23) and (3.24), the strain energy density becomes,

$$W^* = \frac{1}{2} a_{ijkl} \, \varepsilon_{ij} \, \varepsilon_{kl} \tag{3.25}$$

Eqn (3.25) shows that the strain energy density is a positive definite function of the strains (114). Using Eqn (3.25), the virtual work expression of Eqn (3.22), can be rewritten as shown below,

$$\delta \int_V W^*(u_i) \; dV - \int_{S_1} F_i \; \delta u_i \; dS = 0 \tag{3.26}$$

where the body forces have been eliminated.

Now, assuming that the applied external forces are conservative, we have the principle of stationary potential energy,

$$\delta \Pi_p = 0 \tag{3.27a}$$

41

where, if the forces vary neither in magnitude nor direction during virtual displacements,

$$\Pi_p = \int_V W^*(u_i) \ dV - \int_{S_1} F_i \ u_i dS \qquad (3.27b)$$

In Eqn (3.27), the strain energy density is written in terms of the displacement components by using Eqns (3.25) and (3.9). The integrals are taken over the original, undeformed volume and surfaces consistent with the Lagrangian viewpoint. Additionally, the array of elasticity constants of Eqn (3.24) are defined with respect to the original configuration.

In this research, materials that obey certain constitutive laws are considered. Specifically, these materials consist of unidirectional fibers embedded in a matrix as shown in Figure 3.5, where the small element contains a single fiber parallel to the 1 axis. We can assume that this material is transversely isotropic with respect to planes parallel to the 2-3 plane (117). In this case, Eqn (3.24) becomes,

$$\begin{Bmatrix} \sigma_1 \\ \sigma_2 \\ \sigma_3 \\ \sigma_4 \\ \sigma_5 \\ \sigma_6 \end{Bmatrix} = \begin{bmatrix} C_{11} & C_{12} & C_{13} & 0 & 0 & 0 \\ C_{12} & C_{22} & C_{23} & 0 & 0 & 0 \\ C_{13} & C_{23} & C_{33} & 0 & 0 & 0 \\ 0 & 0 & 0 & C_{44} & 0 & 0 \\ 0 & 0 & 0 & 0 & C_{55} & 0 \\ 0 & 0 & 0 & 0 & 0 & C_{66} \end{bmatrix} \begin{Bmatrix} \varepsilon_1 \\ \varepsilon_2 \\ \varepsilon_3 \\ \varepsilon_4 \\ \varepsilon_5 \\ \varepsilon_6 \end{Bmatrix} \qquad (3.28)$$

where contracted notation is introduced, i.e.,

$$\sigma_i = \sigma_{ii} \ (\text{no sum}) \qquad \varepsilon_i = \varepsilon_{ii} \ (\text{no sum})$$

$$\sigma_4 = \sigma_{23} \qquad\qquad\quad \varepsilon_4 = 2\varepsilon_{23}$$

$$\sigma_5 = \sigma_{13} \qquad\qquad\quad \varepsilon_5 = 2\varepsilon_{13}$$

$$\sigma_6 = \sigma_{12} \qquad\qquad\quad \varepsilon_6 = 2\varepsilon_{12}$$
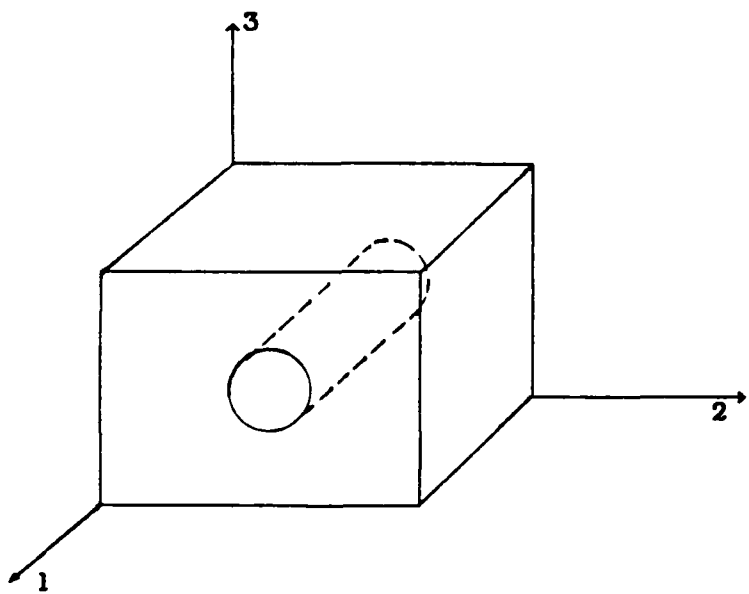
FIGURE 3.5. Small Element of Transverse Isotropic Material Characterized by Unidirectional Fibers Embedded in a Matrix.

43

Transverse isotropy assumes $E_2 = E_3$ and $\nu_{12} = \nu_{13}$ and the C_{ij} written in terms of engineering constants become,

$$C_{11} = E_1 \frac{1 - \nu_{23}^2}{\Delta} \quad , \quad C_{12} = C_{13} = E_1 \nu_{21} \frac{1 + \nu_{23}}{\Delta} \quad ,$$

$$C_{33} = C_{22} = E_2 \frac{1 - \nu_{12}\nu_{21}}{\Delta} \quad , \tag{3.29}$$

$$C_{23} = E_2 \frac{\nu_{23} + \nu_{12}\nu_{21}}{\Delta} \quad , \quad C_{44} = G_{23} , \; C_{66} = G_{12} , \; C_{55} = G_{13}$$

$$\Delta = 1 - 2\nu_{12}\nu_{21} - \nu_{23}^2 - 2\nu_{12}\nu_{21}\nu_{23}$$

All of the necessary tools have been introduced for a Lagrangian displacement based energy approach to solve elastic geometrically nonlinear shell problems. To develop shell strain displacement relations, first identify the general 3-D curvilinear coordinates y_1, y_2, and y_3 of Eqns (3.9) and (3.10) with the shell coordinates, ξ_1, ξ_2, and ζ. Then, by defining kinematics that relate the middle surface displacements to the continuum displacements of the shell, strain displacement relations are written, and finally, the total potential energy expressed in terms of displacement using Eqns (3.9), (3.10), and (3.28) is extremized with respect to displacement resulting in the equilibrium equations. The definition of the kinematics for these types of formulations is obviously very important. The assumptions that will eventually lead to general shell

kinematics and a potential energy expression are next discussed.

Basic Assumptions and Approach

A shell, by definition, is characterized by one dimension, the thickness, being smaller than the planform dimensions. Consequently, we exploit this characteristic and describe generally three dimensional phenomena using a two dimensional theory. As discussed by Koiter (22,23) and John (30), Love's shell theory is a consistently approximated approach where all transverse stresses are neglected as small. Koiter points out, based on an order of magnitude study, that any refinements to Love's approximations are meaningless unless transverse stresses are considered in the refined theory.

Transversely loaded thicker shells or those consisting of orthotropic layers generally deflect more than that predicted by Love theories. This increased deflection is due primarily to transverse shear deformation (30). A goal in the present research then, is to include the important 3-D effects yet at the same time, consider them from a 2-D standpoint for simplicity. In a generally nonlinear study this reduction in dimension is crucial.

A 2-D shell approach can begin by assuming displacements as power series in the thickness or transverse coordinate, ζ. In this way, the 3-D behavior of the shell is fully described by the 2-D behavior of the middle surface

45

since all variables are functions only of the coordinates ζ_1 and ζ_2. Bassett (32) first described a shell's displacements as infinite power series as shown in Eqn (3.30).

$$u_i = u_i^\circ + \zeta u_i^{\circ\prime} + \frac{1}{2} \zeta^2 u_i^{\circ\prime\prime} + \ldots \qquad (3.30)$$

where,

$$u_i^\circ = U_i^\circ (\xi_\alpha, 0)$$

$$u_i^{\circ\prime} = \frac{\partial U_i^\circ}{\partial \zeta} \bigg|_{\zeta=0}$$

These kinematics give nonzero transverse strains from Eqns (3.9) and (3.10), yet subsequent approximations by Bassett effectively neglected them as small.

Hildebrand, Reissner, and Thompson (HRT) (32) and Nagdhi (33) examined similar kinematics in an effort to judge the relative importance of the terms leading to transverse strains. They truncated the series in Eqn (3.30) after the second order terms. Next, if a plane stress approximation is made ($\sigma_3 \cong 0$), ε_3 can be found via the constitutive relations of Eqn (3.28), and then the transverse displacement, u_3, is determined through integration. HRT conclude that the resulting linear and quadratic ζ terms present in u_3 are small and can be neglected. This leads to an inconsistency since now, both ε_3 and σ_3 are zero. This inconsistency is widely accepted, however. Since we first state that $\sigma_3 \cong 0$, there is not a

nonzero $\sigma_3\varepsilon_3$ potential energy contribution. Additionally, ε_3 is not completely neglected, it is included in Π_p through ε_1 and ε_2 and the constitutive relations of Eqns (3.28) and (3.36). This procedure approximately corrects the inconsistency (114).

Resulting from these types of studies are the so called Reissner Mindlin (RM) theories based on kinematics as shown in Eqn (3.31).

$$u_1 = u(1 - \zeta/R_1) + \zeta\psi_1 \qquad (3.31)$$
$$u_2 = v(1 - \zeta/R_2) + \zeta\psi_2$$
$$u_3 = w$$

where the five degrees of freedom (dof), u, v, w, ψ_α, $(\alpha=1,2)$, are functions of the inplane coordinates, ζ_α. These theories relax the Kirchhoff-Love hypothesis requiring normals to the midplane remaining normal throughout deformation. By including the additional two dof, ψ_α instead of the $w_{,\alpha}$ found in Love theories, the normals are free to rotate such that after deformation they are generally no longer normal to the midplane. This type of deformation implies a constant transverse shear rotation through the thickness, and consequently shear correction factors are required for equilibrium (11). Plate and shell solutions based on Eqn (3.31) show significant improvements over Love theories for situations when transverse shear deformation is important. However, numerical shear locking occurs when finite element formulations based on RM theories

47

are applied to thin plate bending problems, for example. This serious drawback is due to the dominance of shear terms over the bending terms in the energy expression as the plate becomes thin, and resulting solutions are much too stiff.

In an effort to avoid the shear locking phenomenon but also to include transverse shear deformation, consider the truncated power series for the displacements shown in Eqn (3.32), where each dof u_i°, ψ_i, θ_i, and ϕ_i are functions only of ξ_α.

$$u_i = u_i^\circ + \zeta \psi_i + \zeta^2 \theta_i + \zeta^3 \phi_i \qquad (3.32)$$

Next, assume that the transverse shear stresses vanish on the top and bottom surfaces of the shell. For material behavior as in Eqn (3.28), this implies the transverse strains vanish on these surfaces also. For example, a flat plate ($R_\alpha = \infty$, see Figure 3.4) of thickness h, gives,

$$\varepsilon_5 \Big|_{\zeta = \pm \frac{h}{2}} = \frac{\partial u_1}{\partial \zeta} + \frac{\partial u_3}{\partial \xi_1} \qquad (3.33)$$

$$= \left[\psi_1 + 2\zeta \theta_1 + 3\zeta^2 \phi_1 + u_{3,1}^\circ + \zeta \psi_{3,1} + \zeta^2 \theta_{3,1} \right. $$
$$\left. + \zeta^3 \phi_{3,1} \right] \Big|_{\zeta = \pm \frac{h}{2}} = 0$$

For Eqn (3.33) to hold true for both the top and bottom surfaces of the plate, $\theta_1 = \psi_3 = \phi_3 = 0$. Based on HRT conclusions, one should also neglect the $\zeta^2 \theta_3$ term in u_3 as

48

small compared to the only other remaining term, u_3°. After solving for ϕ_1 in (3.33), we see that the transverse shear expression is parabolic, i.e.,

$$\varepsilon_5 = \left[1 - \frac{4\zeta^2}{3h^2} \right] (\psi_1 + u_{3,1}^{\circ}) \qquad (3.34)$$

A similar exercise can be applied to ε_4.

The resulting flat plate kinematics are shown in Eqn (3.35) where the u_i° have been replaced by u, v, and w. These kinematics have been applied to numerous linear plate bending, buckling and vibration problems by Reddy (54,57,58,95) and others (37,38). Note that these kinematics have the same number of dof as do the kinematics of Reissner-Mindlin theories. Finite element formulations based on this approach apparently do not shear lock for some formulations and also do not require shear correction factors (54,58).

Parabolic transverse shear distributions can also be achieved from the kinematics of Eqn (3.32) by setting $\theta_1 = \theta_2 = \phi_1 = \phi_2 = \psi_3 = 0$. This approach gives a nonzero ε_3 and results reported by Kwon and Akin (118) indicate that their plate element based upon a mixed finite element formulation also does not shear lock for those linear problems analyzed. An excellent discussion of flat plate kinematics of varying complexity for both 2-D and 3-D analyses is due to Lo, Christensen, and Wu (119).

$$u_1 = u + \zeta \psi_1 - \frac{4}{3h^2} \zeta^3 (\psi_1 + w,_1)$$

$$u_2 = v + \zeta \psi_2 - \frac{4}{3h^2} \zeta^3 (\psi_2 + w,_2) \qquad (3.35)$$

$$u_3 = w$$

Although ε_3 is identically zero in a linear analysis when calculated from the kinematics of Eqn (3.35), we can still include it through the constitutive relations thus approximately eliminating the inconsistency of $\sigma_3 = \varepsilon_3 = 0$ (114). Similar to the analysis done by HRT, assume that the shell is in an approximate state of plane stress, i.e., $\sigma_3 = 0$. Therefore, from Eqn (3.28),

$$\varepsilon_3 = - \frac{C_{13}}{C_{33}} \varepsilon_1 - \frac{C_{23}}{C_{33}} \varepsilon_2 \qquad (3.36)$$

Eqns (3.28) and (3.36) then give in material axes, i.e., with the fibers aligned as in Figure 3.5, where ε_3 has been eliminated,

$$\begin{Bmatrix} \sigma_1 \\ \sigma_2 \\ \sigma_6 \\ \sigma_4 \\ \sigma_5 \end{Bmatrix} = \begin{bmatrix} Q_{11} & Q_{12} & 0 & 0 & 0 \\ Q_{12} & Q_{22} & 0 & 0 & 0 \\ 0 & 0 & Q_{66} & 0 & 0 \\ 0 & 0 & 0 & Q_{44} & 0 \\ 0 & 0 & 0 & 0 & Q_{55} \end{bmatrix} \begin{Bmatrix} \varepsilon_1 \\ \varepsilon_2 \\ \varepsilon_6 \\ \varepsilon_4 \\ \varepsilon_5 \end{Bmatrix} \qquad (3.37)$$

where $Q_{ij} = C_{ij} - \dfrac{C_{13} C_{j3}}{C_{33}}$.

For transverse isotropy, it is easily shown that,

$$Q_{11} = E_1/\Delta, \quad Q_{12} = \nu_{21}E_2/\Delta, \quad Q_{22} = E_2/\Delta \qquad (3.38)$$

$$Q_{66} = G_{12}, \quad Q_{44} = G_{23}, \quad Q_{55} = G_{13}$$

where $\Delta = 1 - \nu_{12}\nu_{21}$.

We have assumed that the transverse shear stress effects are greater than the transverse normal stress effects since we have included the former yet generally neglected the latter. This is consistent with previous findings. Koiter (22,23) and John (30) point out that the magnitudes of the transverse stresses are as shown in Eqn (3.39).

$$\sigma_4, \ \sigma_5 = \text{Order} \ [\ E\varepsilon\Theta \ ], \qquad (3.39)$$

$$\sigma_3 = \text{Order} \ [\ E\varepsilon\Theta^2 \ ]$$

where $\Theta = \max \left[\dfrac{h}{D}, \ \sqrt{h/R}, \ \sqrt{\varepsilon} \right]$ and D is the distance from the point on the middle surface under consideration to the edge of the shell, and R is the smallest principal radius of curvature of the undeformed middle surface. From Eqn (3.39), σ_3 is generally small in comparison to σ_4 and σ_5 for thin plates and shells.

If the point under consideration is far enough away

from the shell boundary, D is of the same order as the shell length, L. Additionally, assuming small strains, Koiter (22) further points out that the transverse normal stress is in general h/R times the bending stresses whereas the transverse shear stresses are of order h/L times the bending stresses. We can then consider cases where σ_3 is much smaller than σ_4 or σ_5 for L/R small compared to unity (61).

$$\frac{\sigma_3}{\sigma_4} = \frac{(h/R)\sigma_1}{(h/L)\sigma_1} = \frac{L}{R} << 1. \qquad (3.40)$$

For a transversely loaded flat plate, according to the preceding discussion, the transverse normal stress is of order h/L times the transverse shear stresses. Therefore, σ_3 is generally always small compared to σ_4 and σ_5 except near the plate edges, i.e., for small D. Examining the 3-D elasticity solutions for flat plates (Pagano (62)) and cylindrical shells (Ren (67)) in cylindrical bending, the above relationships between stresses are seen to hold true.

Based on the preceding discussion, the following assumptions are reiterated. The shell is thin, and therefore, assume it is in an approximate state of plane stress, i.e., $\sigma_3 \cong 0$. The transverse shear stresses, σ_4 and σ_5, are parabolic functions through the thickness and vanish on the top and bottom surfaces. The transverse normal strain, ε_3, is approximately zero. This implies that

normals to the midsurface of the shell cannot change length.

One additional assumption simplifies the nonlinear strain displacement relations. Once again, since the shell is thin, inplane stresses and strains generally dominate its behavior with the transverse quantities having a less important influence. Therefore, we make the following simplifying assumption. Represent the inplane strains, ε_1, ε_2, and ε_6 as shown in Eqns (3.9) and (3.10) retaining all terms. However, represent the transverse shear strains, ε_4 and ε_5, using only the linear displacement terms of Eqns (3.9) and (3.10) for simplicity. Therefore, because the shell is thin, consider the nonlinear strain displacement terms as higher order for the transverse strains. Exact ε_1, ε_2, and ε_6 and linear ε_4 and ε_5 (recall ε_3 has been eliminated through the $\sigma_3 = 0$ assumption) results in the following limits for the magnitudes of rotation. If ε_4 or ε_5 are negligible compared to ε_1, ε_2, and ε_6, i.e. the classical case, then we have a large rotation theory since exact strain displacement relations are assumed for the important strains. However, if ε_4 or ε_5 are not negligible compared to the inplane strains, then the allowable rotations are limited to some degree. Librescu (19) shows that nonlinear (not exact!) inplane strains with linear transverse shear strains define a consistent moderate rotation theory. Therefore, the present approach will always accurately follow rotations greater than what the

53

moderate theories permit depending on the importance of the transverse shears for the specific application.

Nonlinear inplane strains, linear transverse shear strains, and zero transverse normal strain (the latter determined from the kinematics) will result in an incompatible strain field through the shell thickness. Examination of the compatibility equations reveals that only the equation involving inplane strains exclusively, is satisfied, as is expected since the inplane strains are determined correctly from the kinematics via Eqn (3.10). The other five compatibility equations involve the transverse strains and hence cannot be satisfied since these strains are not defined by Eqn (3.10) since subsequent approximations are made. However, for situations where some of the rotational terms are small, i.e., intermediate nonlinearity, these compatibility equations are better approximated. For the linear case, i.e., small rotations and displacements, all six compatibility equations are satisfied.

Therefore, for the general large rotation and displacement case, we cannot expect to accurately represent through the thickness stresses and displacements. However, through the use of the nonlinear Green's strain and higher order kinematics, we can expect to accurately represent the load displacement behavior of the midplane of the shell as it experiences large rotations. This will give better

54

predictions of the collapse and post buckling behavior of shells where large rotations and displacements occur.

As previously mentioned, shear correction factors are not required with these kinematics as in those that represent constant shear through the thickness. Additionally, shear locking of the finite element formulation as the thickness decreases is expected to be alleviated using these kinematics. Evidence of the latter is found in the compatibility relations. Comparison of these equations for a flat plate based on the present approach, Eqn (3.35), with those that result from using the Reissner-Mindlin kinematics of Eqn (3.31), reveals the presence of shear terms in the former that reduce to zero as the plate thickness decreases. Shear terms that reduce to zero are not present in the Reissner-Mindlin compatibility equations. The avoidance of the numerical difficulties of shear locking and the use of shear correction factors is the primary reason in the present research for using the higher order kinematics over the simpler ones that give constant transverse shear representations.

Kinematics

Based on the preceding development, consider the following kinematics for the arbitrary shell described by orthogonal curvilinear coordinates, referring back to Figure 3.4 for conventions.

$$u_1(\zeta_1, \zeta_2, \zeta) = u(1 - \zeta/R_1) + \zeta\psi_1 + \zeta^2\phi_1 + \zeta^3\gamma_1 + \zeta^4\theta_1$$

$$u_2(\zeta_1, \zeta_2, \zeta) = v(1 - \zeta/R_2) + \zeta\psi_2 + \zeta^2\phi_2 + \zeta^3\gamma_2 + \zeta^4\theta_2$$

$$u_3(\zeta_1, \zeta_2) = w \qquad\qquad (3.41)$$

where,

u, v, w, ψ_α, ϕ_α, γ_α, and θ_α, are functions of ζ_1 and ζ_2.

ψ_α are rotations of the normals and,

ϕ_α, γ_α, θ_α, are functions to be determined such that σ_4 and σ_5 vanish on the top and bottom surfaces of the shell.

The assumed displacements of Eqn (3.41) are slightly more involved than those introduced for flat plates in Eqn (3.32). For a plate, only third order terms in the thickness parameter, ζ, were necessary to give the desired parabolic transverse stress distribution. Shell structures, due to their curved surfaces, however, have coupling between displacements that plates do not and the fourth order terms become necessary. Also, the $(1 - \zeta/R_\alpha)$ expressions found in the first terms of the power series representing the displacements are not found in similar series for flat plate analysis. These additional terms simplify the algebra and the final form for the shell kinematics. The kinematics will ultimately closely resemble the plate kinematics that have been used in the literature and shown in Eqn (3.35). Additionally, Reddy (61) arrives at identical general shell

56

kinematics as derived here but uses a different approach.

Keeping only linear displacement terms from Eqn (3.9), (3.10), and (3.21), the transverse shear strains become,

$$\varepsilon_4 = \frac{1}{h_2} (u_{3,2} + h_2 u_{2,3} - u_2 h_{2,3})$$

$$\varepsilon_5 = \frac{1}{h_1} (u_{3,1} + h_1 u_{1,3} - u_1 h_{1,3}) \tag{3.42}$$

where,

( )$_{,\alpha}$ ($\alpha=1,2$) refers to differentiation with respect to ζ_α as before, and,

( )$_{,3}$ refers to differentiation with respect to ζ.

Using Eqn (3.41) in (3.42a) and assuming zero transverse shear stress, and therefore, strain, on the shell boundaries similar to that developed earlier for the flat plate gives,

$$\phi_2 = 0,$$

$$\theta_2 = \frac{\gamma_2}{2R_2}, \tag{3.43}$$

$$\left[1 - \underline{\frac{h^2}{8R_2^2}}\right] \gamma_2 \approx \gamma_2 = \frac{-4}{3h^2} (\psi_2 + \frac{w_{,2}}{\alpha_2})$$

where h is the shell thickness.

Assume, for the moment, that we have a fairly thick shell, i.e., let $R_2 = 5h$. In this case, the underlined term in Eqn (3.43) is only .005 and therefore can be neglected compared to 1 as indicated. Furthermore, we can neglect the fourth

57

order term (θ_2) of Eqns (3.41) and (3.43) since it is only 1/20 of the third order term. A similar exercise is applied to ε_5.

Eqn (3.43) in (3.41) then gives for the general shell kinematics,

$$u_1(\zeta_1,\zeta_2,\zeta) = u(1 - \frac{\zeta}{R_1}) + \zeta\psi_1 + \zeta^3 k(\psi_1 + \frac{w,_1}{\alpha_1})$$

$$u_2(\zeta_1,\zeta_2,\zeta) = v(1 - \frac{\zeta}{R_2}) + \zeta\psi_2 + \zeta^3 k(\psi_2 + \frac{w,_2}{\alpha_2})$$

$$u_3(\zeta_1,\zeta_2) = w \tag{3.44}$$

where, $k = \frac{-4}{3h^2}$.

For a flat plate, $\zeta/R_\alpha = 0$ and $\alpha_\gamma = 1$ and Eqn (3.44) reduces to Eqn (3.35). The sign convention for rotational terms of Eqn (3.44) is shown for a flat plate for simplicity in Figure 3.6. For small rotations, the slope of the elastic curve, $w,_1$, is approximately equal to the total rotation of the elastic curve. The $w,_1$ are positive as shown since a positive slope is indicated. The rotations, ψ_1 and β_1, are negative as shown in the top diagram since these quantities follow the right hand rule as defined by the kinematics of Eqn (3.44). Additionally, the rotation of the normal, ψ_1, and the shear rotation, β_1, combine to give the total rotation, $w,_1$. The shear rotational term

corresponds to the cubic term of the kinematics, see Eqn (3.44). Figure 3.7 shows the independent relationship of ψ_1 and β_1. The first diagram shows a rotation of the normal, associated with bending, and no shear deformation i.e., the normal to the midplane remains normal after deformation. The second diagram shows only shear deformation, no bending, i.e., the normal to the midplane is no longer normal after deformation. Similar arguments can be used in describing $w_{,2}$, ψ_2, and β_2 see Figures 4.3 and 4.4 only in this case the kinematics define these rotations by a left hand rule.

For larger rotations, the slope $w_{,1}$ cannot represent the rotation of the elastic curve as accurately. However, the relationships between the bending, shear, and total rotations will still apply for these size rotations. In this way, the shell model becomes too stiff compared to reality since the shear rotations, i.e., the transverse shear strains, are overestimated due to letting $w_{,1}$ equal the rotation of the elastic curve instead of the correct tangent of the rotation. The error depends on the magnitudes of the shear rotations as was discussed earlier.
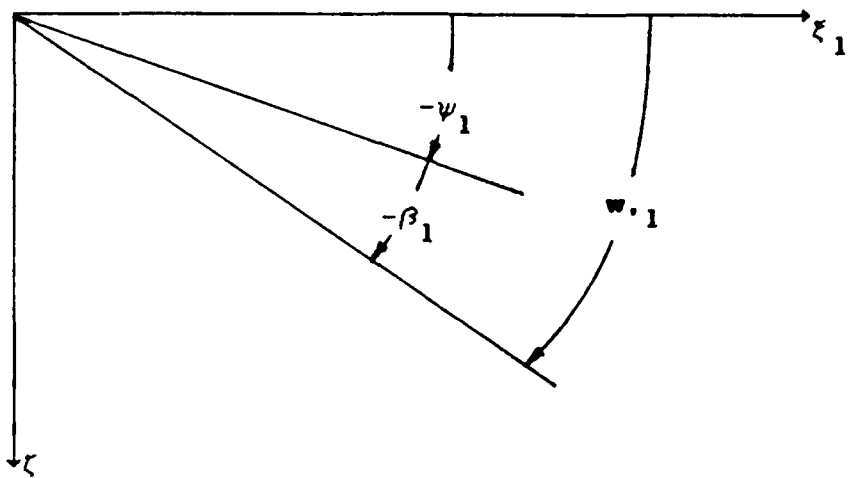
$$w,_1 = -\psi_1 - \beta_1$$

$$w,_1 + \psi_1 = -\beta_1$$
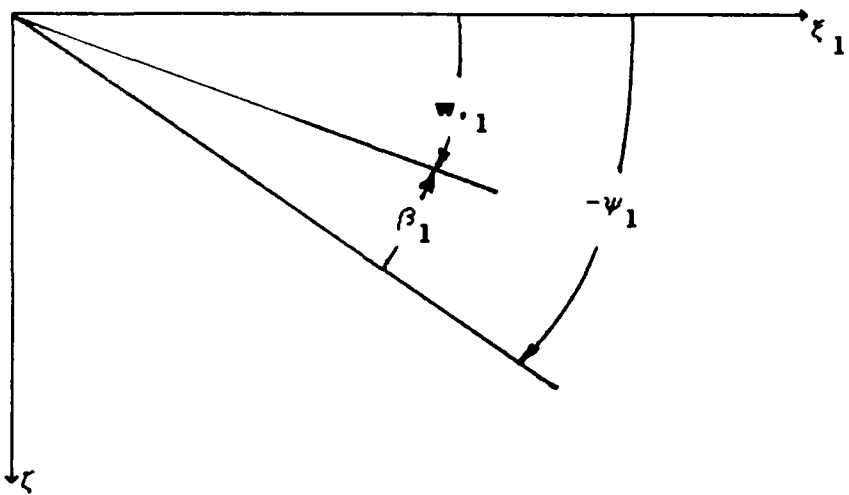
$$w,_1 = -\psi_1 + \beta_1$$

$$w,_1 + \psi_1 = \beta_1$$

FIGURE 3.6. Sign Convention of Rotational Quantities Where ψ and β Always Combine to Give the Slope of Elastic Curve. Note arrowhead on β_1 shows opposite sense in each diagram.

60
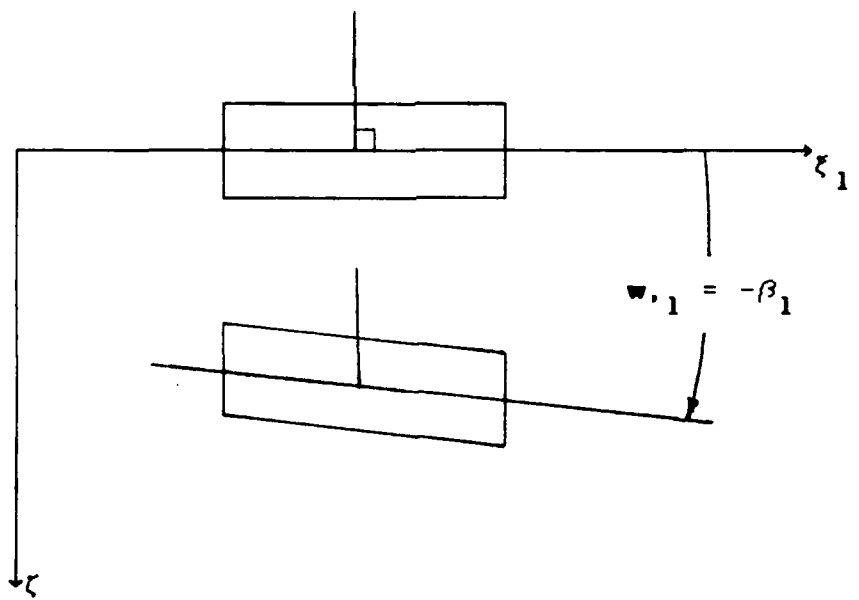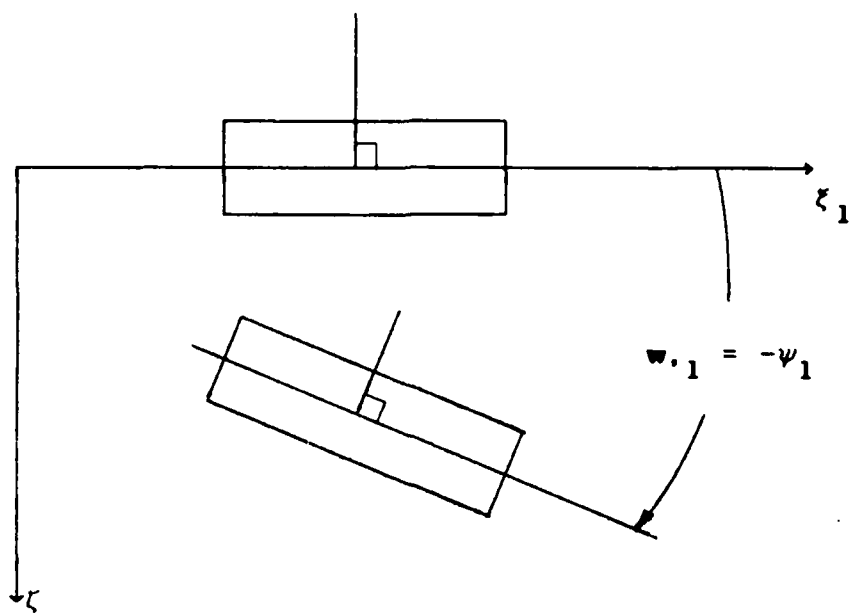
FIGURE 3.7.   Independent Quantities ψ_1 and β_1.

Shell Strain Displacement Relations

The transverse shear strain, ε_4, is now found from Eqns (3.42) and (3.44) giving,

$$\varepsilon_4 = \frac{1}{h_2} (w_{,2} + \alpha_2 \psi_2) \left[1 - \frac{4\zeta^2}{h^2} + \underline{\frac{8\zeta^3}{3h^2 R_2}} \right] \qquad (3.45)$$

Once again, assume that $R_2 = 5h$ and consider points of the shell at the extreme outside fibers, i.e., at $\zeta = h/2$. In this case the underlined term of Eqn (3.45) is 1/15 of the next largest term and therefore, we neglect it. A similar exercise is appled to ε_5 giving for the transverse shear strains,

$$\varepsilon_4 = \frac{1}{h_2} (w_{,2} + \alpha_2 \psi_2) \left[1 - \frac{4\zeta^2}{h^2} \right]$$

$$\qquad (3.46)$$

$$\varepsilon_5 = \frac{1}{h_1} (w_{,1} + \alpha_1 \psi_1) \left[1 - \frac{4\zeta^2}{h^2} \right]$$

The general strain displacement relations of Eqns (3.9) and (3.10) with the kinematics of Eqn (3.44) will give the inplane shell strain displacement relations. These expressions can then be specialized for a shell geometry of interest by defining the scale factors, h_i, using Eqn (3.21).

Substituting Eqn (3.44) into Eqns (3.9) and (3.10) and carrying out the indicated differentiation yields for the

inplane strain displacement equations,

$$\varepsilon_1 = \varepsilon_{11} = \frac{\gamma_{11}}{h_1^2} = \underline{\varepsilon}_1^\circ + \zeta \varkappa_1^1 + \zeta^2 \varkappa_1^2 + \zeta^3 \varkappa_1^3 + \zeta^4 \varkappa_1^4 + \zeta^6 \varkappa_1^6$$

$$\varepsilon_2 = \varepsilon_{22} = \frac{\gamma_{22}}{h_2^2} = \underline{\varepsilon}_2^\circ + \zeta \varkappa_2^1 + \zeta^2 \varkappa_2^2 + \zeta^3 \varkappa_2^3 + \zeta^4 \varkappa_2^4 + \zeta^6 \varkappa_2^6$$

$$\varepsilon_6 = 2\varepsilon_{12} = \frac{2\gamma_{12}}{h_1 h_2} = \underline{\varepsilon}_6^\circ + \zeta \varkappa_6^1 + \zeta^2 \varkappa_6^2 + \zeta^3 \varkappa_6^3 + \zeta^4 \varkappa_6^4 + \zeta^6 \varkappa_6^6$$

$$(3.47)$$

where,

the $\underline{\varepsilon}_J^\circ$ and $\varkappa_J^I$ terms ($J=1,2,6$, $I=1,2,3,4,6$) are functions of the displacements and the scale factors, and can be found in Appendix A for the arbitrary shell,

the superscripts on $\varkappa_J^I$ are not exponents, they are individual strain components that correspond to the power of ζ that multiplies it, and

the subscripts on $\varkappa_J^I$ indicate the strain, ε_1, ε_2, or ε_6 that these components correspond.

The $\underline{\varepsilon}_J^\circ$ and $\varkappa_J^I$ terms of Eqn (3.47) are dependent on the transverse coordinate, ζ, through the scale factors terms and their derivatives. In developing the 2-D theory, it will be convenient to define the strains such that the terms multiplying the ζ's in the power series are functions only of the inplane parameters, ζ_1 and ζ_2. To this end, typical scale factor expressions can be expanded into binomial

63

series as shown below,

$$\frac{1}{1 - \dfrac{\zeta}{R_\alpha}} = 1 + \frac{\zeta}{R_\alpha} + \frac{\zeta^2}{R_\alpha^2(1-\zeta/R_\alpha)} \qquad (3.48)$$

$$\frac{1}{\left(1 - \dfrac{\zeta}{R_1}\right)\left(1 - \dfrac{\zeta}{R_2}\right)} = 1 + \zeta\left(\frac{1}{R_1} + \frac{1}{R_2}\right) + \text{rem}$$

For the thick shell case where $R_\alpha=5h$ and $\zeta=h/2$, the first two terms on the right hand sides for each expression in Eqn (3.48) represent 99% and 97%, respectively, of the total on the left hand sides. Consequently, series expansions as in Eqn (3.48) and similar expansions are truncated after the first order ζ terms, and substituted into Eqn (3.47) resulting in,

$$\varepsilon_i = \varepsilon_i^\circ + \zeta^p \varkappa_{ip}, \qquad i=1,2,6 \qquad (3.49)$$
$$p=\text{sum } 1 \text{ to } 7$$

where, ε_i° and $\varkappa_{11}$ through $\varkappa_{17}$ are shown in Appendix A as well as the truncated series for each scale factor expression. Note that the convention on i (and j) has been changed so that instead of taking on values 1,2, or 3, they now represent the values 1,2, and 6. This will always be the case from this point on.

The first subscript of $\varkappa_{ip}$ refers to the strain component 1,2, or, 6 and the second subscript refers to the power of ζ it multiplies. The $\varepsilon_i^\bullet$ and the $\varkappa_{11}$ through $\varkappa_{17}$

64

terms now consist of displacement expressions that are dependent only on the surface parameters ζ_1 and ζ_2.

The scale factor terms of the transverse shear strains (See Eqn 3.46) are expanded into similar series but in this case, are truncated after the constant term. This is consistent with previous thin shell assumptions where transverse effects are treated in a relatively simpler fashion than are the inplane quantities. Eqn (3.46) is then rewritten as,

$$\varepsilon_m = \varepsilon_m^\circ + \zeta^2 \, \varkappa_{m2},\tag{3.50}$$

where,

m = 4,5

$\varepsilon_4^\circ = w_{,2}/\alpha_2 + \psi_2, \quad \varepsilon_5^\circ = w_{,1}/\alpha_1 + \psi_1,$ and,

$\varkappa_{42} = 3k\varepsilon_4^\circ, \quad \varkappa_{52} = 3k\varepsilon_5^\circ, \quad k = -4/3h^2$

The strain displacement relations of Eqns (3.49) and (3.50) can be specialized to cylindrically shaped shells and flat plates. For typical cylindrical coordinates, let x be the longitudinal coordinate and Θ be the circumferential coordinate, see Figure 3.8. In this case, the surface's first fundamental form becomes,

$$(ds)^2 = (dx)^2 + R^2(d\Theta)^2\tag{3.51}$$

and therefore, $\alpha_1 = 1$, and $R_1 = \infty$, $R_2 = \alpha_2 = R$.

65
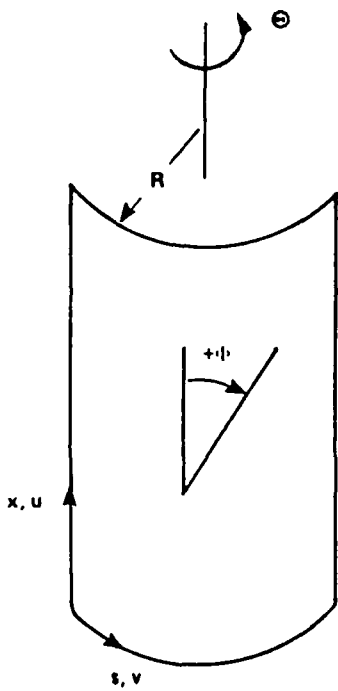
FIGURE 3.8.   Cylindrical Shell Coordinate x-Θ and x-s
Systems, Ply Orientation Angle, Φ, Convention.

A more convenient form for finite element formulation
is to replace the Θ coordinate with the circumferential
coordinate, s, also shown in Figure 3.8.   The strain
displacement relations that result from substitutions of the
parameters of Eqn (3.51) into Eqn (3.44) are easily
converted to x-s coordinates by,

$$\frac{\partial}{\partial \Theta} = R \frac{\partial}{\partial s} \tag{3.52}$$

Alternatively, Eqns (3.49) and (3.50) are specialized
directly to x-s coordinates using $\alpha_1 = \alpha_2 = 1$, $R_1 = \infty$, $R_2 = R$.   The

resulting strain displacement relations are shown in Eqns (3.53-56) where $c=1/R$ and $k=-4/3h^2$.

The flat plate strain displacement relations can be found from Eqn (3.49) with $\alpha_\gamma=1$ and $R_\gamma=\infty$ or from Eqns (3.53-55) with $c = 1/R = 0$.

$$\varepsilon_1 = \varepsilon_1^\circ + \zeta^p \varkappa_{1p}. \tag{3.53}$$

$$\varepsilon_1^\circ = u_{,1} + 1/2(u_{,1}^2 + v_{,1}^2 + w_{,1}^2) \tag{a}$$

$$\varkappa_{11} = \psi_{1,1} - v_{,1}^2 c^2 + \psi_{1,1}u_{,1} + \psi_{2,1}v_{,1} \tag{b}$$

$$\varkappa_{12} = v_{,1}^2 c^2/2 - \psi_{2,1}v_{,1}c + 1/2(\psi_{1,1}^2 + \psi_{2,1}^2) \tag{c}$$

$$\varkappa_{13} = k(w_{,11} + \psi_{1,1}) + u_{,1}k(w_{,11} + \psi_{1,1}) + v_{,1}k(w_{,21} + \psi_{2,1}) \tag{d}$$

$$\varkappa_{14} = -v_{,1}kc(w_{,21} + \psi_{2,1}) + \psi_{1,1}k(w_{,11} + \psi_{1,1})$$
$$+ \psi_{2,1}k(w_{,21} + \psi_{2,1}) \tag{e}$$

$$\varkappa_{15} = 0 \tag{f}$$

$$\varkappa_{16} = (k/2)^2 (w_{,11}^2 + 2w_{,11}\psi_{1,1} + \psi_{1,1}^2 + w_{,21}^2$$
$$+ 2w_{,21}\psi_{2,1} + \psi_{2,1}^2) \tag{g}$$

$$\varkappa_{17} = 0 \tag{h}$$

$$\varepsilon_2 = \varepsilon_2^\circ + \zeta^p \varkappa_{2p}. \tag{3.54}$$

$$\varepsilon_2^\circ = v_{,2} - wc + 1/2(v_{,2}^2 + w_{,2}^2 + u_{,2}^2 + v^2c^2 + w^2c^2)$$

$$+ vw_{,2}c - v_{,2}wc \tag{a}$$

$$\varkappa_{21} = \psi_{2,2} - wc^2 + u_{,2}^2c + w_{,2}^2c + w^2c^3 - c^2(v_{,2}w - vw_{,2})$$

$$+ v\psi_2 c^2 + v_{,2}\psi_{2,2} + u_{,2}\psi_{1,2} - c(\psi_{2,2}w - \psi_2 w_{,2}) \tag{b}$$

$$\varkappa_{22} = \psi_{2,2}c + 1/2(\psi_{2,2}^2 + \psi_{1,2}^2 + \psi_2^2c^2) + 2\psi_{1,2}u_{,2}c +$$

$$+ v\psi_2 c^3 - 2c^2(\psi_{2,2}w - \psi_2 w_{,2}) + \psi_{2,2}v_{,2}c \tag{c}$$

$$\varkappa_{23} = k(w_{,22} + \psi_{2,2}) + c(\psi_{2,2}^2 + \psi_{1,2}^2) + ku_{,2}(w_{,12} + \psi_{1,2})$$

$$+ \psi_2^2 c^3 + kv_{,2}(w_{,22} + \psi_{2,2}) + vkc^2(w_{,2} + \psi_2)$$

$$- wkc(w_{,22} + \psi_{2,2}) + w_{,2}kc(w_{,2} + \psi_2) \tag{d}$$

$$\varkappa_{24} = kc(w_{,22} + \psi_{2,2}) + 2u_{,2}kc(w_{,12} + \psi_{1,2})$$

$$+ vkc^3(w_{,2} + \psi_2) + 2kc^2(-ww_{,22} - w\psi_{2,2} + w_{,2}^2 + w_{,2}\psi_2)$$

$$+ k\psi_{2,2}(w_{,22} + \psi_{2,2}) + \psi_{1,2}k(w_{,12} + \psi_{1,2})$$

$$+ \psi_2 kc^2(w_{,2} + \psi_2) + v_{,2}kc(w_{,22} + \psi_{2,2}) \tag{e}$$

$$\varkappa_{25} = 2kc\left[\psi_{2,2}(w_{,22} + \psi_{2,2}) + \psi_{1,2}(w_{,12} + \psi_{1,2})\right.$$

$$\left. + \psi_2 c^2(w_{,2} + \psi_2)\right] \tag{f}$$

$$\varkappa_{26} = (k^2/2)\left[w_{,22}^2 + 2w_{,22}\psi_{2,2} + \psi_{2,2}^2 + w_{,12}^2 + 2w_{,12}\psi_{1,2}\right.$$

$$\left. + \psi_{1,2}^2 + c^2(w_{,2}^2 + 2w_{,2}\psi_2 + \psi_2^2)\right] \tag{g}$$

$$\varkappa_{27} = k^2c\left[(w_{,22} + \psi_{2,2})^2 + (w_{,12} + \psi_{1,2})^2 + c^2(w_{,2} + \psi_2)^2\right]$$

$$\tag{h}$$

$$\varepsilon_6 = \varepsilon_6^\circ + \zeta^p \varkappa_{6p}. \tag{3.55}$$

$$\varepsilon_6^\circ = u_{,2} + v_{,1} + u_{,1}u_{,2} + v_{,1}v_{,2} + w_{,1}w_{,2} + c(vw_{,1} - v_{,1}w)$$

$$\varkappa_{61} = c(u_{,2} - v_{,1}) + \psi_{1,2} + \psi_{2,1} + u_{,1}\psi_{1,2} + \psi_{1,1}u_{,2}$$

$$c(u_{,1}u_{,2} - v_{,1}v_{,2} + w_{,1}w_{,2} - w\psi_{2,1} + w_{,1}\psi_2) + v_{,1}\psi_{2,2}$$

$$+ v_{,2}\psi_{2,1} \tag{b}$$

$$\varkappa_{62} = c(\psi_{1,2} + u_{,1}\psi_{1,2} + u_{,2}\psi_{1,1} - cw\psi_{2,1} + cw_{,1}\psi_2)$$

$$+ \psi_{1,1}\psi_{1,2} + \psi_{2,1}\psi_{2,2} \tag{c}$$

$$\varkappa_{63} = 2kw_{,12} + k\psi_{1,2} + k\psi_{2,1} + ku_{,2}(w_{,11} + \psi_{1,1})$$

$$+ ku_{,1}(w_{,12} + \psi_{1,2}) + kv_{,1}(w_{,22} + \psi_{2,2})$$

$$+ kcw_{,1}(w_{,2} + \psi_2) - kcw(w_{,12} + \psi_{2,1})$$

$$+ c(\psi_{1,1}\psi_{1,2} + \psi_{2,1}\psi_{2,2}) + kv_{,2}(w_{,12} + \psi_{2,1}) \tag{d}$$

$$\varkappa_{64} = kc(w_{,12} + \psi_{1,2}) + kcu_{,2}(w_{,11} + \psi_{1,1})$$

$$+ \psi_{2,1}(w_{,22} + \psi_{2,2}) - kc^2(ww_{,12} + w\psi_{2,1} - w_{,1}w_{,2}$$

$$- w_{,1}\psi_2) + k(\psi_{1,1}w_{,12} + 2\psi_{1,1}\psi_{1,2} + \psi_{1,2}w_{,11})$$

$$+ \psi_{2,2}(w_{,12} + \psi_{2,1}) + kcu_{,1}(w_{,12} + \psi_{1,2}) \tag{e}$$

$$\varkappa_{65} = kc(\psi_{1,1}w_{,12} + \psi_{1,2}w_{,11} + \psi_{2,1}w_{,22} + \psi_{2,2}w_{,12}$$

$$+ 2\psi_{1,1}\psi_{1,2} + 2\psi_{2,1}\psi_{2,2}) \tag{f}$$

$$\varkappa_{66} = k^2\Big[(w_{,11} + \psi_{1,1})(w_{,12} + \psi_{1,2}) + (w_{,12} + \psi_{2,1})(w_{,22} + \psi_{2,2})\Big]$$

$$\varkappa_{67} = k^2c\Big[(w_{,11} + \psi_{1,1})(w_{,12} + \psi_{1,2}) + (w_{,12} + \psi_{2,1})(w_{,22} + \psi_{2,2})\Big]$$

$$\varepsilon_4 = (w,_2 + \psi_2) + \zeta^2 3k(w,_2 + \psi_2) \qquad (3.56)$$

$$\varepsilon_5 = (w,_1 + \psi_1) + \zeta^2 3k(w,_1 + \psi_1)$$

Shell Potential Energy

Consider a shell that is constructed of layers of the transversely isotropic material described by Eqn (3.37). Generally, the fibers of the kth individual layer or ply are oriented at an angle, Φ, as shown in Figure 3.8. Therefore, the constitutive relations of Eqn (3.37) for that ply must be transformed into shell coordinates resulting in Eqn (3.57).

$$\begin{Bmatrix} \sigma_1 \\ \sigma_2 \\ \sigma_6 \end{Bmatrix}^k = \begin{bmatrix} \bar{Q}_{11} & \bar{Q}_{12} & \bar{Q}_{16} \\ & \bar{Q}_{22} & \bar{Q}_{26} \\ & & \bar{Q}_{66} \end{bmatrix}^k \begin{Bmatrix} \varepsilon_1 \\ \varepsilon_2 \\ \varepsilon_6 \end{Bmatrix}, \qquad (3.57)$$

$$\begin{Bmatrix} \sigma_4 \\ \sigma_5 \end{Bmatrix}^k = \begin{bmatrix} \bar{Q}_{44} & \bar{Q}_{45} \\ & \bar{Q}_{55} \end{bmatrix}^k \begin{Bmatrix} \varepsilon_4 \\ \varepsilon_5 \end{Bmatrix}$$

where, the $\bar{Q}_{ij}$ (i,j=1,2,6) and $\bar{Q}_{mn}$ (m,n=4,5) are elements of symmetric arrays of transformed stiffnesses for the kth ply and σ_i, ε_i, σ_m, and ε_m are measured with respect to shell coordinates ζ_α and ζ (42).

Next, from Eqn (3.27), let

$$\Pi_p = U + V \qquad (3.58)$$

where,

70

U is the internal strain energy, and

V is the work done by the external forces.

Eqns (3.57),(3.58), (3.49), and (3.50) then give for the internal strain energy of the arbitrary shell,

$$U_1 = \frac{1}{2} \int_{\Omega} \int_{h} \left[\overline{Q}_{11}(\varepsilon_1^\circ + \zeta^P \varkappa_{1p})^2 + \overline{Q}_{22}(\varepsilon_2^\circ + \zeta^P \varkappa_{2p})^2 \right.$$

$$+ 2\overline{Q}_{12}(\varepsilon_1^\circ + \zeta^P \varkappa_{1p})(\varepsilon_2^\circ + \zeta^r \varkappa_{2r}) + \overline{Q}_{66}(\varepsilon_6^\circ + \zeta^P \varkappa_{6p})^2$$

$$+ 2\overline{Q}_{16}(\varepsilon_1^\circ + \zeta^P \varkappa_{1p})(\varepsilon_6^\circ + \zeta^r \varkappa_{6r})$$

$$\left. + 2\overline{Q}_{26}(\varepsilon_2^\circ + \zeta^P \varkappa_{2p})(\varepsilon_6^\circ + \zeta^r \varkappa_{6r}) \right] d\zeta d\Omega \ ,$$

$$(3.59a)$$

$$U_2 = \frac{1}{2} \int_{\Omega} \int_{h} \left[\overline{Q}_{44}(\varepsilon_4^\circ + \zeta^2 \varkappa_{42})^2 + \overline{Q}_{55}(\varepsilon_5^\circ + \zeta^2 \varkappa_{52})^2 \right.$$

$$\left. + 2\overline{Q}_{45}(\varepsilon_4^\circ + \zeta^2 \varkappa_{42})(\varepsilon_5^\circ + \zeta^2 \varkappa_{52}) \right] d\zeta d\Omega$$

$$(3.59b)$$

where,

$U = U_1 + U_2$, $p,r = 1,2,3,4,5,6,7$,

$\overline{Q}_{IJ}$ generally vary as a function of ζ since a laminate is constructed of plies with different *fiber* orientations, and,

Ω represents the shell middle surface.

Manipulations of Eqn (3.59) are facilitated if the following quantities are defined. From Eqn (3.49), let

71

$$\gamma = \gamma^\circ + \mathcal{K}\,\mathcal{Z} \qquad\qquad (3.60)$$

where,

$$\gamma = \begin{Bmatrix} \varepsilon_1 \\ \varepsilon_2 \\ \varepsilon_6 \end{Bmatrix} , \quad \gamma^\circ = \begin{Bmatrix} \varepsilon_1^\circ \\ \varepsilon_2^\circ \\ \varepsilon_6^\circ \end{Bmatrix} , \quad \mathcal{K} = \begin{bmatrix} \varkappa_{11} & \varkappa_{12} & \cdots & \varkappa_{17} \\ \varkappa_{21} & \varkappa_{22} & \cdots & \varkappa_{27} \\ \varkappa_{61} & \varkappa_{62} & \cdots & \varkappa_{67} \end{bmatrix} , \quad \mathcal{Z} = \begin{Bmatrix} \zeta \\ \zeta^2 \\ \vdots \\ \zeta^7 \end{Bmatrix}$$

Using Eqn (3.60) in Eqn (3.59a),

$$U_1 = \frac{1}{2} \int_\Omega \int_h (Q\,\gamma)^T \gamma \, d\zeta d\Omega \qquad\qquad (3.61)$$

where,

$$Q = \begin{bmatrix} \overline{Q}_{11} & \overline{Q}_{12} & \overline{Q}_{16} \\ & \overline{Q}_{22} & \overline{Q}_{26} \\ & & \overline{Q}_{66} \end{bmatrix}^k$$

Then, Eqn (3.61) is concisely written in terms of an area integral representing the shell midsurface as shown in Eqn (3.62) where the ζ dependence has been integrated by defining a series of elasticity arrays.

$$U_1 = \frac{1}{2} \int_\Omega (u_1 + u_2 + u_3)\, d\Omega \qquad\qquad (3.62)$$

where,

72

$$u_1 = \int_h \pmb{\gamma}^{\cdot T} Q \, \pmb{\gamma}^{\cdot} \, d\zeta = \int_h \epsilon_j^{\cdot} \, \epsilon_i^{\cdot} \, \bar{Q}_{ij} \, d\zeta$$

$$= \epsilon_j^{\cdot} \, \epsilon_i^{\cdot} \, A_{ij} \tag{a}$$

$$u_2 = \int_h 2\pmb{\gamma}^{\circ T} Q \, \varkappa \, z \, d\zeta = \int_h 2\epsilon_j^{\circ} \, \bar{Q}_{ij} \varkappa_{ip} \, \zeta^P \, d\zeta$$

$$= 2\epsilon_j^{\circ} (\varkappa_{11} B_{ij} + \varkappa_{12} D_{ij} + \varkappa_{13} E_{ij} + \varkappa_{14} F_{ij} +$$
$$\varkappa_{15} G_{ij} + \varkappa_{16} H_{ij} + \varkappa_{17} I_{ij}) \tag{b}$$

$$u_3 = \int_h z^T (\varkappa^T Q \, \varkappa) \, z \, d\zeta = \int_h \varkappa_{jp} \, \varkappa_{ir} \, \bar{Q}_{ij} \, \zeta^{P+r} \, d\zeta$$

$$= \varkappa_{j1} \varkappa_{11} D_{ij} + 2 \, \varkappa_{j1} \varkappa_{12} E_{ij} + (2 \, \varkappa_{j1} \varkappa_{13} + \varkappa_{j2} \varkappa_{12}) F_{ij}$$

$$+ 2(\varkappa_{j1} \varkappa_{14} + \varkappa_{j2} \varkappa_{13}) G_{ij} + (2 \, \varkappa_{j1} \varkappa_{15} + 2\varkappa_{j2} \varkappa_{14}) H_{ij}$$

$$+ 2(\varkappa_{j1} \varkappa_{16} + \varkappa_{j2} \varkappa_{15} + \varkappa_{j3} \varkappa_{14}) I_{ij} + (2 \, \varkappa_{j1} \varkappa_{17} +$$

$$2 \, \varkappa_{j2} \varkappa_{16} + 2\varkappa_{j3} \varkappa_{15} + \varkappa_{j4} \varkappa_{14}) J_{ij} +$$

$$2(\varkappa_{j2} \varkappa_{17} + \varkappa_{j3} \varkappa_{16} + \varkappa_{j4} \varkappa_{15}) K_{ij} + (2 \, \varkappa_{j3} \varkappa_{17} +$$

$$2 \, \varkappa_{j4} \varkappa_{16} + \varkappa_{j5} \varkappa_{15}) L_{ij} + 2(\varkappa_{j4} \varkappa_{17} + \varkappa_{j5} \varkappa_{16}) P_{ij}$$

$$+ (2 \, \varkappa_{j5} \varkappa_{17} + \varkappa_{j6} \varkappa_{16}) R_{ij} + 2\varkappa_{j6} \varkappa_{17} S_{ij} + \varkappa_{j7} \varkappa_{17} T_{ij}$$

$$\tag{c}$$

where $i,j = 1,2,6$ and $p,r = 1,2,3,4,5,6,7$

73

In the above expressions, many elasticity arrays have been introduced and are defined by,

$$[A_{ij}, B_{ij}, D_{ij}, E_{ij}, F_{ij}, G_{ij}, H_{ij}, I_{ij}, J_{ij}, K_{ij},$$

$$L_{ij}, P_{ij}, R_{ij}, S_{ij}, T_{ij}] =$$

$$\int_h \bar{Q}_{ij} [1, \zeta, \zeta^2, \zeta^3, \zeta^4, \zeta^5, \zeta^6, \zeta^7, \zeta^8, \zeta^9, \zeta^{10}, \zeta^{11}, \zeta^{12}, \zeta^{13}, \zeta^{14}] \, d\zeta$$

(3.63)

where $i, j = 1, 2,$ and 6.

A similar manipulation is performed on Eqn (3.59b) for the shear terms, giving,

$$U_2 = \frac{1}{2} \int_\Omega (\, \varepsilon_m^\circ \varepsilon_n^\circ \, A_{mn} + 2\varepsilon_n^\circ \varkappa_{m2} \, D_{mn} + \varkappa_{n2} \varkappa_{m2} \, F_{mn} \,) \, d\Omega$$

and,   (3.64)

$$[A_{mn}, D_{mn}, F_{mn}] = \int_h \bar{Q}_{mn} [\, 1, \zeta^2, \zeta^4] \, d\zeta$$ (3.65)

where $m, n = 4, 5$.

Primarily due to the assumed nonlinearity, many new elasticity arrays are shown above. A cursory examination would lead one to believe that many orders of magnitude in ζ separate the A_{ij} elasticity terms from terms of the higher order elasticity arrays. This is true, of course, given the definitions in Eqn (3.63). However, further examination reveals that the energy terms that contain the higher order elasticity constants also are multiplied by powers of $k = -4/3h^2$. Because of the squared shell thickness term in

74

the denominator of k, the energy terms are not many orders of magnitude apart. For example, the D_{ij}, F_{ij}, and H_{ij} *energy* *terms* are all the *same* order of magnitude in h or ζ despite the definitions of the *arrays* given in Eqn (3.63).

In a general geometrically nonlinear analysis, the energy due to the externally applied loads contains nonlinear displacement terms. These arise when, because of large rotations, the applied loading develops higher order coupling components in coordinate directions where no loading originally existed. As discussed by Brush and Almroth (12), these higher order terms give potential energy contributions that are negligibly small for the cases of intermediate nonlinearity. However, the large rotational case generally must account for them. An alternative approach that will achieve the required coupling is to prescribe displacements, not loads. In a large displacement/rotation situation, if the loading is actually a prescription of displacement, the higher order nonlinear loading terms need not be included (since applied loading is zero). This is the approach taken here.

Laminated shell constructions that have symmetric ply stacking sequences about the middle surface are governed by much simpler expressions. For symmetric laminates, the elasticity arrays of Eqn (3.63) that are associated with odd powers of ζ (B_{ij}, E_{ij}, G_{ij}...S_{ij}) are identically zero. Effectively one half of the energy terms then will vanish.
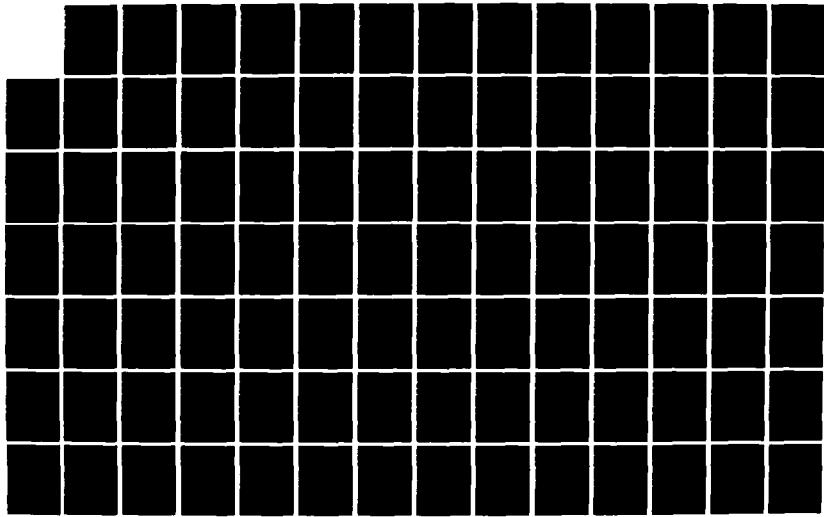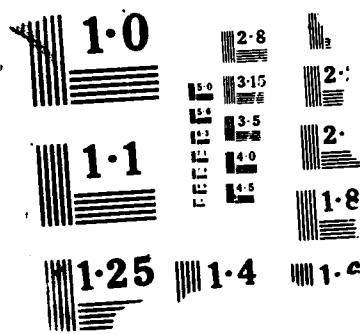
Because this represents such a major simplification to this approach, solutions are calculated only for isotropic and symmetric laminates. The finite element formulation of the next chapter includes the energy that contains the terms of the elasticity arrays for the unsymmetric laminates; the computer code based on the finite element formulation, however, does not.

With the above in mind, Eqn (3.58) with Eqns (3.62), (3.64), and (3.53-56) give the total potential energy of the cylindrical shell. This expression is then extremized with respect to the displacements giving the equilibrium equations. Solving these nonlinear coupled partial differential equations is the topic of the next chapter.

A final comment concerns the magnitudes of rotation the present approach will allow differential elements to undergo accurately. The author expects increased accuracy for rotations beyond those valid in the intermediate nonlinear theories. This is because all of the nonlinear displacement terms of Green's strain tensor for the inplane strains of the shell have been retained. The intermediate theories only retain the nonlinear displacement terms in the transverse displacement, w, as a result of assuming that the rotations are small compared to unity (113). This results in nonlinear terms in the extensional A_{ij} terms only, see Appendix B. In contrast, the present approach includes nonlinear A_{ij} energy terms as well as nonlinear terms in D_{ij}

through T_{ij} due to nonlinearity in the curvature terms of Eqn (3.49). The limit on the magnitude of rotation is unknown since it is problem dependent. However, the linear assumption used in defining the transverse shear strains has a direct limiting impact, as was previously discussed.

IV. <u>Finite Element Solution</u>

If the variation of the total potential energy expression just derived in the previous chapter were carried through, the result would be five coupled nonlinear partial differential equations representing equilibrium. A powerful numerical technique that can be used to solve these equations is the finite element method. In this approach, the continuum displacements of the equilibrium equations are approximated through interpolation functions and the values of displacement at discrete points within the domain and on the boundary of the shell. The mesh of the discrete or nodal points define individual elements where the approximate energy of each element is summed giving the total potential energy. The variation of Π_p of the discretized domain then gives coupled nonlinear algebraic equations where the unknowns are the discrete values of displacement called nodal displacements.

In a generally nonlinear analysis, these equations are not usually solved directly, but instead, are linearized and solved by incremental/iterative methods. The linearized equations are found by effectively carrying out an additional differentiation of Π_p with respect to the displacements. These two differentiations of Π_p, i.e., the first variation and the linearization, could be accomplished term by term. Alternatively, the manipulations that follow can give a relatively convenient form for Π_p such that these

derivatives are straight forward to accomplish. This can all be done independent of the specific finite element definition. The specific elemental definition depends on the approximations used for each unique displacement term present in the strain displacement relations. These terms form the displacement gradient vector and only some are distinct elemental degrees of freedom. In what follows, the element independent formulation is first presented, then two element types are defined. Following the complete representation of the total potential energy in finite element casting, the algorithms for linear, linear bifurcation, and nonlinear solutions are presented. Finally, some comments on the coupling characteristics of the displacements for both shells and flat plates are given.

Element Independent Formulation

The result of the finite element discretization of the 2-D shell domain gives the potential energy Π_p as shown in the general expression of Eqn (4.1). The end result of this section is the derivation of Eqn (4.1) from Eqns (3.58), (3.62), and (3.64) such that important conditions, to be discussed subsequently, are met.

$$\Pi_p = \frac{q^T}{2} \left[K + \frac{N_1}{3} + \frac{N_2}{6} \right] q - q^T R \tag{4.1}$$

where,

q is a column array of displacements at the discrete points, the nodal displacements,

R is a column array of loads at the discrete points, the nodal loads,

K is an array of constant stiffness coefficients,

N_1 is an array of stiffness coefficients that are linear in displacement,

N_2 is an array of stiffness coefficients that are quadratic in displacement.

Carrying out the variation of Eqn (4.1) gives the equilibrium equations, F, as shown in Eqns (4.2) and (4.3). In Eqn (4.2) note that the stiffness arrays K, N_1, and N_2 of Eqn (4.1) are duplicated as a result of carrying out the variation of Eqn (4.1). This is one of the conditions alluded to above.

$$\delta \Pi_p = \delta q^T \left[\left\{ K + \frac{N_1}{2} + \frac{N_2}{3} \right\} q - R \right] = 0 \qquad (4.2)$$

$$= \delta q^T \, F(q) = 0$$

Then for arbitrary and independent δq,

$$F(q) = 0 \qquad (4.3)$$

Eqn (4.3) represents nonlinear algebraic equations in the nodal degrees of freedom (dof) q. Solutions to Eqn (4.3) can be found iteratively through the linearized incremental equations. These are derived by expanding Eqn (4.3) into a Taylor series as shown below where the higher order terms have been neglected since Δq is assumed to be small.

$$F(q + \Delta q) = F(q) + \frac{\partial F}{\partial q} \Delta q + \ldots = 0 \qquad (4.4)$$

Rearranging Eqn (4.4) and letting $K_T = K + N_1 + N_2$ gives Eqn (4.6) where, once again, the stiffness arrays K, N_1, and N_2 are duplicated as a result of taking the partial derivatives of F. This is another of the required conditions in deriving Eqn (4.1).

$$\frac{\partial F}{\partial q} \Delta q = -F(q) \qquad (4.5)$$

$$[K + N_1 + N_2] \Delta q = -F(q)$$

$$K_T \Delta q = -F(q) \qquad (4.6)$$

where K_T is called the tangent stiffness matrix.

Eqn (4.6) gives solutions in an iterative manner via a Newton-Raphson technique. The current values of the elements of q are substituted into N_1 and N_2 resulting in an array of constants for K_T. The set of linear equations are then solved for Δq, which is then added to q giving the updated nodal displacements. Assuming the solution is not yet converged, the right hand side (RHS) of Eqn (4.6) is nonzero. Iteration continues until F becomes arbitrarily small signifying equilibrium has been satisfied.

The preceding general development assumed a certain formalism in the definitions of K, N_1, and N_2 such that these terms repeated themselves in the first variation of Π_p

and again in the Taylor series expansion that gave the incremental equations. We therefore seek definitions of K, N_1, and N_2 such that if the potential energy is given by Eqn (4.1), then its variation is given by Eqn (4.2) and the incremental equations by Eqn (4.6). Ensuring this formalism will greatly decrease the number of algebraic manipulations since once K, N_1, and N_2 are formed in the Π_p expression of Eqn (4.1), the variation and linearization are then very straight forward. Additionally, fewer programming lines are needed since the same arrays are present in both the equilibrium and incremental equations and hence need be calculated only once in solving Eqn (4.6).

Rajasekaran and Murray (120) outline a procedure that will give the desired repetition and also symmetry of the three components, K, N_1, and N_2, that comprise K_T. Some modifications are required in the present case. We start by dividing <u>each</u> strain component of Eqns (3.53-55) into linear and nonlinear parts as shown in Eqn (4.7).

$$\varepsilon_i^{\circ} = {_o}L_i^T \, d \; + \; \frac{1}{2} \, d^T \, {_o}H_i \, d \qquad (4.7)$$

$$\varkappa_{ip} = {_p}L_i^T \, d \; + \; \frac{1}{2} \, d^T \, {_p}H_i \, d$$

where,

$_JL_i$ $(J = 0,1,2,....,7)$ are column arrays, $_JH_i$ are symmetric matrices,

d is the displacement gradient vector,

$i = 1,2,6$ and $p=1$ to 7, as before,

82

$_p L_i$ for p=5,6,7 contain all zeroes.

The $_j L_i$ and $_j H_i$ arrays contain constants and the displacement gradient vector contains the unique displacement terms that define the strain components in Eqns (3.53-56). Although there are 17 unique displacement terms in Eqns (3.53-56), one additional term, u, is included for generality since any other shell geometry other than cylindrical would have this term represented in the strain displacement relations also. The vector, d, then is an 18x1 array as shown in Eqn (4.8). As will be seen later, it is the way the elements of d are approximated that defines the specific element type and therefore, the element definition can be done independent of the development of this section. Each of the 15 $_j L_i$ 18x1 column arrays and 24 $_j H_i$ 18x18 matrices for a cylindrical shell are shown in Appendix C, where equivalent flat plate arrays are found by letting 1/R = 0.

$$d^T = \left\{ u \; u_{,1} \; u_{,2} \; v \; v_{,1} \; v_{,2} \; w \; w_{,1} \; w_{,2} \; w_{,11} \; w_{,22} \; w_{,12} \right.$$
$$\left. \psi_1 \; \psi_{1,1} \; \psi_{1,2} \; \psi_2 \; \psi_{2,1} \; \psi_{2,2} \right\}$$

(4.8)

Next, Eqn (4.7) is substituted into the internal strain energy of Eqn (3.62) giving for the inplane energy expression, i.e., those energy terms due to ε_1, ε_2, and ε_6.

$$U_1 = \frac{1}{2} \int_\Omega d^T \left[\tilde{K} + \tilde{N}_1 + \frac{1}{4} \tilde{N}_2 \right] d \; d\Omega \qquad (4.9)$$

where,

$$\tilde{K} = \underline{A_{ij}\,{}_oL_{io}L_j^T} + 2B_{ij}\,{}_oL_{i1}L_j^T + D_{ij}(2\,{}_oL_{i2}L_j^T + {}_1L_{i1}L_j^T)$$
$$+ E_{ij}(2\,{}_oL_{i3}L_j^T + 2\,{}_1L_{i2}L_j^T) + F_{ij}(2\,{}_oL_{i4}L_j^T + 2\,{}_1L_{i3}L_j^T$$
$$+ {}_2L_{i2}L_j^T) + G_{ij}(2\,{}_1L_{i4}L_j^T + 2\,{}_2L_{i3}L_j^T) + H_{ij}(2\,{}_2L_{i4}L_j^T$$
$$+ {}_3L_{i3}L_j^T) + 2I_{ij}\,{}_3L_{i4}L_j^T + J_{ij}\,{}_4L_{i4}L_j^T$$

$$(4.9a)$$

$$\tilde{N}_1 = A_{ij}\,{}_oL_i d^T\,{}_oH_j + B_{ij}({}_oL_i d^T\,{}_1H_j + {}_1L_i d^T\,{}_oH_j) + D_{ij}({}_oL_i d^T\,{}_2H_j$$
$$+ {}_2L_i d^T\,{}_oH_j + {}_1L_i d^T\,{}_1H_j) + E_{ij}({}_oL_i d^T\,{}_3H_j + {}_3L_i d^T\,{}_oH_j$$
$$+ {}_1L_i d^T\,{}_2H_j + {}_2L_i d^T\,{}_1H_j) + F_{ij}({}_oL_i d^T\,{}_4H_j + {}_4L_i d^T\,{}_oH_j$$
$$+ {}_1L_i d^T\,{}_3H_j + {}_3L_i d^T\,{}_1H_j + {}_2L_i d^T\,{}_2H_j) + G_{ij}({}_oL_i d^T\,{}_5H_j$$
$$+ {}_1L_i d^T\,{}_4H_j + {}_2L_i d^T\,{}_3H_j + {}_4L_i d^T\,{}_1H_j + {}_3L_i d^T\,{}_2H_j)$$
$$+ H_{ij}({}_oL_i d^T\,{}_6H_j + {}_1L_i d^T\,{}_5H_j + {}_2L_i d^T\,{}_4H_j + {}_3L_i d^T\,{}_3H_j$$
$$+ {}_4L_i d^T\,{}_2H_j) + I_{ij}({}_oL_i d^T\,{}_7H_j + {}_1L_i d^T\,{}_6H_j + {}_2L_i d^T\,{}_5H_j$$
$$+ {}_3L_i d^T\,{}_4H_j + {}_4L_i d^T\,{}_3H_j) + J_{ij}({}_1L_i d^T\,{}_7H_j + {}_2L_i d^T\,{}_6H_j$$
$$+ {}_3L_i d^T\,{}_5H_j + {}_4L_i d^T\,{}_4H_j) + K_{ij}({}_2L_i d^T\,{}_7H_j + {}_3L_i d^T\,{}_6H_j$$
$$+ {}_4L_i d^T\,{}_5H_j) + L_{ij}({}_3L_i d^T\,{}_7H_j + {}_4L_i d^T\,{}_4H_j) + P_{ij}\,{}_4L_i d^T\,{}_7H_j$$

$$(4.9b)$$

84

$$\tilde{N}_2 = A_{ij}\,{}_0H_i dd^T{}_0H_j + B_{ij}\,{}_0H_i dd^T{}_1H_j + D_{ij}({}_0H_i dd^T{}_2H_j$$

$$+ {}_1H_i dd^T{}_1H_j) + E_{ij}({}_0H_i dd^T{}_3H_j + 2{}_1H_i dd^T{}_2H_j) + F_{ij}({}_0H_i dd^T{}_4H_j$$

$$+ 2{}_1H_i dd^T{}_3H_j + {}_2H_i dd^T{}_2H_j) + G_{ij}({}_0H_i dd^T{}_5H_j + 2{}_1H_i dd^T{}_4H_j$$

$$+ 2{}_2H_i dd^T{}_3H_j) + H_{ij}({}_0H_i dd^T{}_6H_j + 2{}_1H_i dd^T{}_5H_j + 2{}_2H_i dd^T{}_4H_j$$

$$+ {}_3H_i dd^T{}_3H_j) + I_{ij}({}_0H_i dd^T{}_7H_j + 2{}_1H_i dd^T{}_6H_j + 2{}_2H_i dd^T{}_5H_j$$

$$+ 2{}_3H_i dd^T{}_4H_j) + J_{ij}(2{}_1H_i dd^T{}_7H_j + 2{}_2H_i dd^T{}_6H_j + 2{}_3H_i dd^T{}_5H_j$$

$$+ {}_4H_i dd^T{}_4H_j) + K_{ij}(2{}_2H_i dd^T{}_7H_j + 2{}_3H_i dd^T{}_6H_j + 2{}_4H_i dd^T{}_5H_j)$$

$$+ L_{ij}(2{}_3H_i dd^T{}_7H_j + 2{}_4H_i dd^T{}_6H_j + {}_5H_i dd^T{}_5H_j)$$

$$+ P_{ij}(2{}_4H_i dd^T{}_7H_j + 2{}_5H_i dd^T{}_6H_j) + R_{ij}(2{}_5H_i dd^T{}_7H_j$$

$$+ {}_6H_i dd^T{}_6H_j) + S_{ij}2{}_6H_i dd^T{}_7H_j + T_{ij}{}_7H_i dd^T{}_7H_j$$

$$(4.9c)$$

In the above, each term of $\tilde{K}$, $\tilde{N}_1$, and $\tilde{N}_2$ represents nine terms due to the summation convention on i and j. Eqn (4.9d) shows this using the underlined term of $\tilde{K}$ from Eqn (4.9a) as an example. Each of these nine terms results in an 18x18 array. Eqn (4.9e) show one representative term from $\tilde{N}_1$; Eqn (4.9f) shows one representative term from $\tilde{N}_2$. These equations point out that each term contains an 18x18 array that is premultiplied by a scalar elasticity element, A_{11} in the examples shown.

$$A_{ij} \begin{bmatrix} {_o}L_i & {_o}L_j^T \end{bmatrix} = A_{11}\,{_o}L_1\,{_o}L_1^T + A_{12}\,{_o}L_1\,{_o}L_2^T + A_{16}\,{_o}L_1\,{_o}L_6^T$$
$$\text{1x1} \qquad \text{18x1} \quad \text{1x18}$$
$$+ A_{12}\,{_o}L_2\,{_o}L_1^T + A_{22}\,{_o}L_2\,{_o}L_2^T + A_{26}\,{_o}L_2\,{_o}L_6^T$$
$$+ A_{16}\,{_o}L_6\,{_o}L_1^T + A_{26}\,{_o}L_6\,{_o}L_2^T + A_{66}\,{_o}L_6\,{_o}L_6^T$$

$$(4.9d)$$

$$A_{11} \begin{bmatrix} {_o}L_1 & d^T & {_o}H_1 \end{bmatrix} \tag{4.9e}$$
$$\text{1x1} \quad \text{18x1} \quad \text{1x18} \quad \text{18x18}$$

$$A_{11} \begin{bmatrix} {_o}H_1 & d & d^T & {_o}H_1 \end{bmatrix} \tag{4.9f}$$
$$\text{1x1} \quad \text{18x18} \quad \text{18x1} \quad \text{1x18} \quad \text{18x18}$$

With the exception of only a few terms of $\tilde{K}$, the desired formalism of Eqns (4.1), (4.2), and (4.6) will **not** be exhibited using the terms as defined in Eqns (4.9). That is, if the first variation were carried through on Eqn (4.9) with the $\tilde{K}$, $\tilde{N}_1$, and $\tilde{N}_2$ as defined in Eqns (4.9a-f), totally new terms would result. Similarly, the formation of the linearized incremental/iterative equations would result in still different terms. To avoid these tedious manipulations, we seek equivalent energy forms for $\tilde{K}$, $\tilde{N}_1$, and $\tilde{N}_2$ such that these terms are present in the three expressions for Π_p, $F(q)$, and K_T, i.e., Eqns (4.1), (4.2), and (4.6).

We can easily show the undesirable terms that result from carrying through the variation of the terms of Eqns (4.9a-c). Using the second energy term from Eqn (4.9b) as

an example, the variation is given in Eqn (4.10).

$$\delta\left\{ \frac{1}{2} \int_\Omega d^T B_{ij} \, _oL_i d^T \, _1H_j d \; d\Omega \right\} = \frac{1}{2} \int_\Omega B_{ij} \left\{ \delta d^T \, _oL_i d^T \, _1H_j d \right.$$

$$\left. + d^T \, _oL_i \delta d^T \, _1H_j d + d^T \, _oL_i d^T \, _1H_j \delta d \right\} \; d\Omega$$

$$(4.10)$$

Using $B_{ij}=B_{ji}$, and since all $L^T d = d^T L$ and $d^T H d$ terms are scalars and thus can be transposed or moved freely, the right hand side (RHS) can be rewritten as shown below and we see that the forms of the original term of Eqn (4.10) and its first variation of Eqn (4.11) are not the same.

$$\text{RHS} = \frac{1}{2} \int_\Omega B_{ij} \; \delta d^T \left\{ _oL_i d^T \, _1H_j + 2 \, _1H_j d \, _oL_i^T \right\} d \; d\Omega \qquad (4.11)$$

Each of the energy terms of $\tilde{N}_i$ are of the form shown on the left hand side (LHS) of Eqn (4.12) and thus the example of Eqn (4.10) and (4.11) is representative. As suggested by Ref (120), if each of these terms is replaced by terms of the form found on the RHS of Eqn (4.12), the desired repeating formalism of Eqns (4.1), (4.2), and (4.6) will apply.

$$\frac{1}{2} \int_\Omega d^T C_{ij} \, _pL_i \; d^T \, _rH_j d \; d\Omega =$$

$$\frac{1}{6} \int_\Omega d^T C_{ij} \left[_pL_i \; d^T \, _rH_j + d^T \, _pL_i \, _rH_j + \, _rH_i \; d \, _pL_j^T \right] d \; d\Omega$$

$$(4.12)$$

where,

C_{ij} refers to the elements from any of the elasticity arrays, A_{ij} to T_{ij},

$p,r = 0$ to 7 and $i,j=1,2,6$ as before.

Therefore, using the same term from $\tilde{M}_1$ as before, i.e., the LHS of Eqn (4.10) with the Eqn (4.12) substitution, the first variation is as shown in Eqn (4.13). It is stressed that this term is representative of all the $\tilde{M}_i$ terms of Eqn (4.9b).

$$\delta \left\{ \frac{1}{6} \int_\Omega d^T B_{ij} \left[{}_oL_i \, d^T \, {}_1H_j + d^T \, {}_oL_i \, {}_1H_j + {}_1H_i \, d \, {}_oL_j^T \right] d \; d\Omega \right\}$$

$$= \frac{1}{6} \int_\Omega B_{ij} \left\{ \left(\delta d^T {}_oL_i d^T {}_1H_j d + d^T {}_oL_i \delta d^T {}_1H_j d + d^T {}_oL_i d^T {}_1H_j \delta d \right) \right.$$

$$+ \left(\delta d^T d^T {}_oL_{i1} H_j d + d^T \delta d^T {}_oL_{i1} H_j d + d^T d^T {}_oL_{i1} H_j \delta d \right)$$

$$+ \left. \left(\delta d^T {}_1H_i d {}_oL_j^T \, d + d^T {}_1H_i \delta d {}_oL_j^T d + d^T {}_1H_i d {}_oL_j^T \, \delta d \right) \right\} \; d\Omega$$

$$= \frac{1}{6} \int_\Omega B_{ij} \; \delta d^T \left[3 {}_oL_i d^T {}_1H_j + 3 d^T {}_oL_{i1} H_j + 3 {}_1H_i d {}_oL_j^T \right] d \; d\Omega$$

$$(4.13)$$

Therefore, a comparison of the terms in the first and final lines of Eqn (4.13) show that the LHS gives a repeating form on the RHS. The final result of Eqn (4.13) is expanded into unabridged form in Eqn (4.13a). In a similar fashion, we can show that the derivation of the linearized incremental/iterative equations (Eqn (4.6)) also results in

88

similar repeating forms.

$$\frac{1}{6} \int_\Omega \left\{ B_{11} \, \delta d^T \left[3_o L_1 d^T_{1} H_1 + 3 d^T_{o} L_{11} H_1 + 3_1 H_1 d_o L_1^T \right] d \right.$$

$$+ B_{12} \, \delta d^T \left[3_o L_1 d^T_{1} H_2 + 3 d^T_{o} L_{11} H_2 + 3_1 H_1 d_o L_2^T \right] d$$

$$+ \ldots$$

$$\left. + B_{66} \, \delta d^T \left[3_o L_6 d^T_{1} H_6 + 3 d^T_{o} L_{61} H_6 + 3_1 H_6 d_o L_6^T \right] d \right\} \, d\Omega$$

$$(4.13a)$$

Unfortunately, the suggested forms for $\tilde{K}$ and $\tilde{N}_2$ as given by (120) such that Eqns (4.1), (4.2), and (4.6) are applicable, only partially apply here due to the complexity of the present strain displacement relations. Those forms of (120) suggest representations that do give the desired repetition, however. Each of the terms of the $\tilde{K}$ and $\tilde{N}_2$ arrays are of the general forms of the LHS of Eqn (4.14). In Eqn (4.14), two forms for both $\tilde{K}$ and $\tilde{N}_2$ are shown. With the C_{ij} once again referring to elements from any of the elasticity arrays, the LHS are those energy terms from Eqn (4.9), that do not repeat in deriving the equilibrium and the linearized incremental/iterative equations. If each is replaced by the corresponding RHS of Eqn (4.14) then the formalism of Eqns (4.1), (4.2), and (4.6) is easily shown similarly to the $\tilde{N}_1$ example of Eqns (4.12) and (4.13). The first substitution shown in Eqn (4.14) for each of the arrays $\tilde{K}$ and $\tilde{N}_2$ are taken from Ref (120) and the second

substitutions are unique generalizations thereof.

From $\tilde{\underline{K}}$:

$$\frac{1}{2} \int_{\Omega} d^T C_{ij} \, {}_pL_i \, {}_pL_j^T \, d \, d\Omega \quad \text{(no sum on p)} = \text{no change}$$

$$\frac{1}{2} \int_{\Omega} d^T \, 2C_{ij} \, {}_pL_i \, {}_rL_j^T \, d \, d\Omega =$$

$$\frac{1}{2} \int_{\Omega} d^T C_{ij} \left[{}_pL_i \, {}_rL_j^T + {}_rL_i \, {}_pL_j^T \right] d \, d\Omega$$

From $\tilde{\underline{N}}_2$:

$$\frac{1}{8} \int_{\Omega} d^T C_{ij} \, {}_pH_i dd^T \, {}_pH_j \, d \, d\Omega = \frac{1}{12} \int_{\Omega} d^T C_{ij} \left[{}_pH_i dd^T {}_pH_j \right.$$

$$\left. + \frac{1}{2} d^T {}_pH_j d_pH_i \right] d \, d\Omega \qquad \text{(no sum on p)}$$

$$\frac{1}{8} \int_{\Omega} d^T C_{ij} \, {}_rH_i dd^T {}_pH_j \, d \, d\Omega = \frac{1}{8} \int_{\Omega} \frac{d^T}{3} C_{ij} \left[{}_rH_i dd^T {}_pH_j \right.$$

$$\left. + \frac{1}{2} d^T {}_rH_i d_pH_j + {}_pH_i dd^T {}_rH_j + \frac{1}{2} d^T {}_pH_i d_rH_j \right] d \, d\Omega$$

$$(4.14)$$

Based on Eqns (4.12) and (4.14), Eqn (4.9) can now be rewritten as in Eqn (4.15).

$$U_1 = \frac{1}{2} \int_\Omega d^T \left[\tilde{K} + \tilde{N}_1 + \frac{1}{4} \tilde{N}_2 \right] d \, d\Omega$$

$$= \frac{1}{2} \int_\Omega d^T \left[\hat{K} + \frac{\hat{N}_1}{3} + \frac{\hat{N}_2}{6} \right] d \, d\Omega \qquad (4.15)$$

where the elements of the arrays $\hat{K}$, $\hat{N}_1$, and $\hat{N}_2$ are found from $\tilde{K}$, $\tilde{N}_1$, and $\tilde{N}_2$ by making the aforementioned substitutions of Eqns (4.12) and (4.14).

The shear energy terms of Eqns (3.64) and (3.56) are handled in a totally analogous manner only much more simply since transverse shear strains are linear in displacement and hence all ${}_J H_m$ terms are zero arrays and therefore not included. Analogous to Eqn (4.7), the transverse shear strains of Eqn (3.56) are written below in Eqn (4.16).

$$\varepsilon_m^{\bullet} = {}_0 S_m^T \, d \qquad (4.16)$$

$$\varkappa_{2m} = {}_2 S_m^T \, d$$

The 4 ${}_J S_m$ (J=0,2, m=4,5) 18x1 column arrays are shown in Appendix C for a cylinder. Due to the assumed linearity of these strains, additional energy terms from the transverse shear terms are only given for $\tilde{K}$ of Eqn (4.9). These additional terms are found from Eqns (3.64) and (4.16) and are shown below in Eqn (4.17). The equivalent repeating forms that are added to $\hat{K}$ of Eqn (4.15) are found via Eqn (4.14) as with the inplane energy terms only using the ${}_J S_m$ arrays instead of the ${}_J L_1$ arrays.

91

$$A_{mn} \circ S_m \circ S_n^T + 2D_{mn} \circ S_m \cdot S_n^T + F_{mn} \cdot S_m \cdot S_n^T \qquad (4.17)$$

where m,n = 4,5 as before.

The final step in reaching the goal of this section, i.e., the derivation of Eqn (4.1), is the actual discretization of the shell domain. We approximate the continuum displacements by interpolation functions (also called shape functions) and the nodal displacements in Eqn (4.18).

$$u = \mathcal{N}\, q \qquad (4.18)$$

where,

u is the vector of continuum displacements,

$\mathcal{N}$ is an array of interpolation or shape functions,

q are the nodal values of displacements as before.

Next, the displacement gradient vector, d, is approximated from Eqn (4.18) as shown in Eqn (4.19).

$$d = \mathcal{D}\, q \qquad (4.19)$$

where $\mathcal{D}$ is the array of shape functions and their derivatives and is defined for specific elements in the next section. Substituting Eqn (4.19) into the final expression of Eqn (4.15) including the transverse shear terms, then finally gives Eqn (4.1) for the potential energy.

$$\Pi_p = \frac{q^T}{2} \left[K + \frac{N_1}{3} + \frac{N_2}{6} \right] q - q^T R \qquad (4.1)$$

where we can now identify,

92

$$K = \int_{\Omega} \mathcal{D}^T \hat{K} \, \mathcal{D} \, d\Omega$$

$$N_1 = \int_{\Omega} \mathcal{D}^T \hat{N}_1 \, \mathcal{D} \, d\Omega \qquad\qquad (4.20)$$

$$N_2 = \int_{\Omega} \mathcal{D}^T \hat{N}_2 \, \mathcal{D} \, d\Omega$$

Note that N_1 and N_2 are actually functions of the elements of d not q (see Eqn (4.14)) so that in practice, Eqn (4.19) is employed prior to Eqn (4.6) in the solution process. The terms of Eqns (4.1), (4.2), (4.6), and (4.20) are now defined, except for the details of $\mathcal{D}$. The elements of $\mathcal{D}$ are defined according to a specific elemental definition and will be developed in the next section.

The element independent arrays, $\hat{K}$, $\hat{N}_1$, and $\hat{N}_2$ are formed based on literally hundreds of 18x1, 18x18, and 1x18 symbolic matrix multiplications, see Eqn (4.9) with Eqns (4.12) and (4.14) substitutions, where the $_pL_i$ and $_pH_i$ arrays are shown in Appendix C for cylindrical shells. These multiplications are impractical to carry out by hand unless major simplifications, i.e., the elimination of 'small' terms in the strain displacement relations, are effected. Referencing Eqns (3.53-55) will show that identifying 'small' terms is difficult for the large displacement/rotation case. Alternatively, the symbolic manipulator code, MACSYMA, can accomplish these multiplications with relative ease without eliminating any

93

terms. Furthermore, once expressions have been calculated for the entries of $\hat{K}$, $\hat{N}_1$, and $\hat{N}_2$, MACSYMA can convert these to Fortran statements. Since these arrays are independent of element definition, subroutines are very easily implemented that calculate the entries of $\hat{K}$, $\hat{N}_1$, and $\hat{N}_2$ where elemental information is included separately through $\mathcal{D}$. The MACSYMA commands used to form the entries of the arrays $\hat{K}$, $\hat{N}_1$, and $\hat{N}_2$ are shown in Appendix D.

Since errors in this aspect of the finite element coding can be easily overlooked, straight forward von Karman plate and Donnell cylindrical shell relationships were included as solution options in the code. Although the parabolic transverse shear stress distribution is still assumed, the resulting strain components, as shown in Appendix B, are relatively simple and the formation of the arrays $\hat{K}$, $\hat{N}_1$, and $\hat{N}_2$ for these cases was accomplished by hand. During validation of the nonlinear finite element algorithms then, simple von Karman and Donnell solutions are first generated and compared to published results that are typically based on similar assumptions on the nonlinearity.

In the finite element solution procedure, the stiffness of each element is calculated individually and added into a global stiffness array. In this way the result of Eqn (4.1) and (4.20) equivalently represents the potential energy of an individual element, where the total Π_p is found by summing the energies from each element. Although the

94

relationships of Eqn (4.18) and (4.19) imply that the quantities u, N, and D are global, i.e., pertain to the entire shell domain, in practice, they are actually defined on an elemental level. The method of approximating the elements of d in Eqn (4.19) is what actually defines the specific element. Two elements are presented next.

28 and 36 Degree of Freedom Curved Elements

The displacement or compatible finite element approach as used here, is formulated based on the total potential energy, Π_p. The continuum displacements are approximated by the discrete values of displacement at the nodes and interpolation functions leading to simultaneous algebraic equations in the unknowns, the nodal displacements. If the assumed displacement functions are chosen such that several requirements are met then the exact answers are approached as the discretization mesh is refined (121). Furthermore, if these requirements are met, the finite element solution will always give a result that is too stiff compared to the exact result and therefore, monotonic convergence can be observed as the mesh is refined. These requirements are as follows:

1) continuous displacement within an element,

2) the element must be able to represent constant strain,

3) rigid body modes are present in the assumed displacements,

4) compatibility exists between elements, i.e., there are

no gaps or overlaps, and

5) the element should not have preferred directions, i.e., it should be geometrically invariant; this is not a requirement, but certainly desired.

Many problems in structural mechanics are governed by second order differential equations. This is a result of only first order derivatives of the field variables present in Π_p. Satisfaction of the above requirements is easily carried out in these cases using Lagrangian interpolation functions since only C^0 continuity, i.e., continuity of the displacement dof themselves not any of their derivatives, is required for compatibility between elements. However, classical plate bending for example, is governed by fourth order differential equations since second order derivatives of the transverse displacement, w, appear in Π_p. As is discussed in detail in Refs (31,70,121,122), the presence of the second derivatives of the transverse displacement in the Π_p functional requires C^1 continuity for interelement compatibility, i.e., the first derivatives of w, in addition to w, must be continuous between elements, for requirement 4 to be satisfied. It is not difficult to construct Hermitian interpolation functions that meet the above requirements for the case of 1-D Euler beam elements when w and its first derivative, $w_{,1}$, are the nodal degrees of freedom. Hermitian interpolation gives the required continuity of w and $w_{,1}$ between elements. However, the natural extension to

96

2-D Kirchhoff plates where w and its two first derivatives, $w_{,1}$ and $w_{,2}$, serve as nodal dof, does not meet the fourth requirement in that the normal slope of w is not continuous between elements and the resulting formulation is called nonconforming. The C^1 characteristic led to the development in the 60's and early 70's of numerous conforming and nonconforming Kirchhoff plate bending elements.

Some displacement formulations are purposely incompatible or nonconforming since the resulting element is softened and the overly stiff solution of a compatible model is offset. These formulations converge as the mesh is refined only if the element passes the patch test (121,123). The patch test is a numerical test of element validity and involves satisfaction of requirements 2 and 4 above for an infinitely refined mesh.

Another way to view this is explained by Almroth and Brogan (124). In the finite element assembly process, the summation of the energy of the individual elements into the total Π_p leaves out the work done by forces on the element boundaries. For conforming elements, i.e., those that satisfy all requirements previously mentioned, this work vanishes because contributions of adjacent elements cancel one another. However, the work done by these forces and the discontinuity of displacement is neglected in nonconforming elements. If this work that has been neglected approaches zero as the mesh size approaches infinity, then the correct

97

solution can be attained.

Nonconforming elements are perfectly acceptable and converge to correct answers if the above holds true. There exists, then, a trade off between simplicity and compatibility. Typical displacement based conforming elements for C^1 analysis are complex. Nonconforming elements are relatively simple but are not compatible.

The 12 dof Adini-Clough-Melosh (ACM) plate element has three dof, w, $w_{,1}$ and $w_{,2}$, at each corner node and is one such nonconforming element as just discussed. It performs well when the plate domain is discretized into rectangular elements. In the case of general quadrilateral shapes, however, the normal slope and w are incompatible and this element cannot pass the patch test (122). Bogner, et al (122) formulated a 16 dof element with the same dof per node as above but with the second derivative, $w_{,12}$, included as a nodal dof as well. This element is compatible only for a rectangularly shaped element. Compatible generally shaped quadrilateral plate bending elements have been formed based on dividing the area into four triangular subregions. This approach results in a compatible formulation that does not have the numerous dof that would result without defining the subregions. An example is the approach used by Fraeijs De Veubeke (125) where the dof are w and its two first derivatives for the element's corner nodes and the normal derivative for midside nodes.

Other plate bending elements, or equivalently, elements that would require C^1 continuity if based on Π_p, have been derived using alternative variational functionals (31,70,95,126,127). Assumed stress models are based on the complementary energy, Π_c; assumed displacement and stress are used in the mixed models based on Reissner's functional, Π_R; and, several hybrid approaches, where displacement or stress is assumed in the element interior and/or on the boundary, can be based on either Π_c or Π_p. These alternative approaches generally do not have the stringent requirements on the continuity of the assumed variables as does the displacement model, but often require many more dof per element. Also, there is apparently some question as to the existence of a valid functional based upon Π_c in geometrically nonlinear elasticity (128).

The Ahmad element for plate and shell bending problems based on Reissner-Mindlin shear theory and the Π_p functional does not have the continuity problems associated with Kirchhoff elements since the nodal displacement and the nodal rotations are treated independently and only C° continuity is required for compatibility. However, this element suffers from the shear locking phenomenon when thinner plates and shells are analyzed as was discussed earlier.

Reddy et al (58,95) have analyzed linear plate bending problems using the parabolic transverse shear distribution

based on both displacement and mixed variational approaches. The displacement approach uses Lagrangian bilinear interpolation for u, v, ψ_1, and ψ_2 and nonconforming Hermitian interpolation for w, $w_{,1}$ and $w_{,2}$. The mixed approach uses in separate analyses, bilinear and biquadratic interpolation for all displacement and force dof. Both elements performed well in duplicating known exact solutions. However, the mixed element experienced shear locking when the bilinear interpolation was used and hence, the mixed approach was eliminated from consideration early in the present research.

In many ways, the present theory is an extension to the linear plate problems studied by Reddy. The potential energy expression for the shell of the present research requires C° continuity for u, v, ψ_1, and ψ_2 and C^1 continuity for w. Based on Reddy's results, the simplest approach would be a curved shell element derived from Π_p with bilinear interpolation for u, v, ψ_1, and ψ_2 and Hermitian interpolation for w, $w_{,1}$, and $w_{,2}$ resulting in a 4 noded 28 dof rectangular element. Certainly in a nonlinear analysis such as this with its higher computational expense, the simplest element possible is preferred. Although a nonconforming element is proposed, the restriction of rectangularly shaped elements is not really a drawback since this fits conveniently with the orthogonal curvilinear coordinates that have been assumed from the start.

We begin the element definition by assuming the following incomplete 12 term quartic for the transverse displacement, w, of a cylindrical shell element with four corner nodes, see Figure 4.1.

$$w(x,s) = a_1 + a_2x + a_3s + a_4x^2 + a_5xs + a_6s^2 + a_7x^3 + a_8x^2s$$
$$+ a_9xs^2 + a_{10}s^3 + a_{11}x^3s + a_{12}xs^3 \qquad (4.21)$$

This assumed displacement for w results in a cubic along any edge of a rectangular domain that has local x-s coordinates as in Figure 4.1. Both w and the tangential derivative of w $(w,_t)$ are compatible along the edges of the element since they are determined from w and $w,_t$ at two endpoints. However, this leaves only the normal derivative of w $(w,_n)$ at each endpoint to define $w,_n$ along the edge and hence $w,_n$ is incompatible (122). Although an element with this function assumed for w is nonconforming, it will pass the patch test and therefore converges as the mesh is refined (122,123). However, monotonic convergence from a stiffer solution can no longer be expected as in an elemental formulation that satisfies all requirements. For generally shaped quadrilaterals, w becomes quartic along an edge and it as well as $w,_n$ are incompatible between elements. These elements pass a 'milder' form of the patch test and therefore, can be used. However, convergence is of a lower order and thus many elements are required (124).
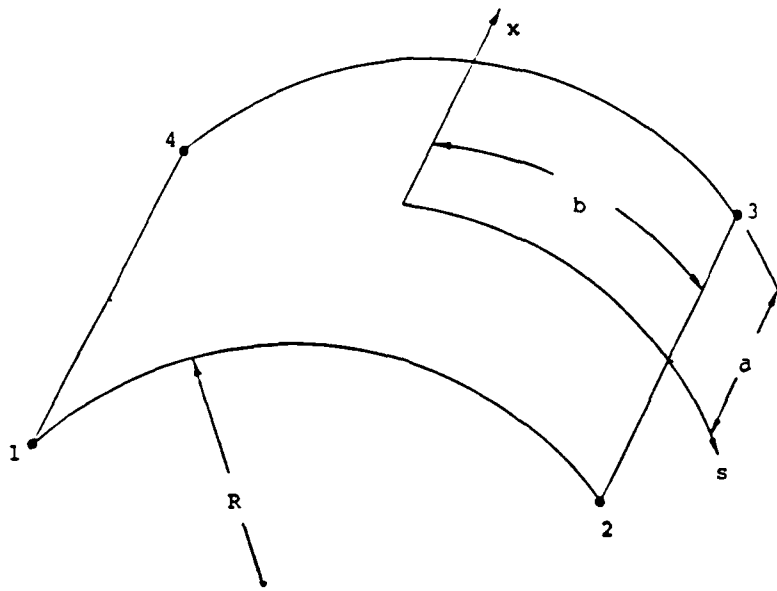
FIGURE 4.1. Rectangular Shell Element with Four Nodes, 2a x 2b Planform.

Assuming a rectangularly shaped element with side dimensions of 2a and 2b, as in Figure 4.1, Eqn (4.21) can be rewritten into the form of Eqn (4.18) for an individual element as shown in Eqn (4.22).

$$w(x,s) = \begin{bmatrix} \mathscr{K}_1 & \mathscr{K}_2 & \mathscr{K}_3 & \mathscr{K}_4 \end{bmatrix} \begin{Bmatrix} q_1 \\ q_2 \\ q_3 \\ q_4 \end{Bmatrix} \qquad (4.22)$$

where, for the kth node,

$$q_k^T = \{\ w\quad w,_1\quad w,_2\ \}_k \qquad (4.22a)$$

$\mathscr{K}_k$ are Hermitian shape functions shown below,

$$\mathscr{K}_k^T = \left\{ \begin{array}{c} \mathscr{K}_{k1} \\ \mathscr{K}_{k2} \\ \mathscr{K}_{k3} \end{array} \right\} = \left\{ \begin{array}{c} \dfrac{1}{8}(1+\zeta_k\zeta)(1+\eta_k\eta)(2+\zeta_k\zeta+\eta_k\eta-\zeta^2-\eta^2) \\[2ex] \dfrac{a}{8}\zeta_k(1+\zeta_k\zeta)^2(\zeta_k\zeta-1)(1+\eta_k\eta) \\[2ex] \dfrac{b}{8}\eta_k(1+\zeta_k\zeta)(\eta_k\eta-1)(1+\eta_k\eta)^2 \end{array} \right\}$$

(4.22b)

where the kth node has natural coordinates (ζ_k, η_k) and $\zeta = x/a$, $\eta = s/b$, see Figure 4.2.

Since only C^* continuity is required for displacement dof u, v, ψ_1, and ψ_2, we can use Lagrangian interpolation functions (121). The simplest approach would be to assume linear distributions of these displacements throughout the element domain. For this case, we approximate these displacements of the form of Eqn (4.18) for an individual element as shown in Eqn (4.23).

$$\left\{ \begin{array}{c} u \\ v \\ \psi_1 \\ \psi_2 \end{array} \right\} = \left[\begin{array}{cccc|c|cccc} \mathscr{N}_1 & 0 & 0 & 0 & \cdots & \mathscr{N}_4 & 0 & 0 & 0 \\ 0 & \mathscr{N}_1 & 0 & 0 & \cdots & 0 & \mathscr{N}_4 & 0 & 0 \\ 0 & 0 & \mathscr{N}_1 & 0 & \cdots & 0 & 0 & \mathscr{N}_4 & 0 \\ 0 & 0 & 0 & \mathscr{N}_1 & \cdots & 0 & 0 & 0 & \mathscr{N}_4 \end{array} \right] \left\{ \begin{array}{c} q_1 \\ \hline \vdots \\ \hline q_4 \end{array} \right\}$$

(4.23)

where, now for the kth node,

$$q_k^T = \{ \, u \; v \; \psi_1 \; \psi_2 \, \}_k \tag{4.23a}$$

$\mathscr{N}_k$ are Lagrangian shape functions shown below,

$$\mathscr{N}_k = \frac{1}{4}(1 + \zeta_k\zeta)(1 + \eta_k\eta) \tag{4.23b}$$

103
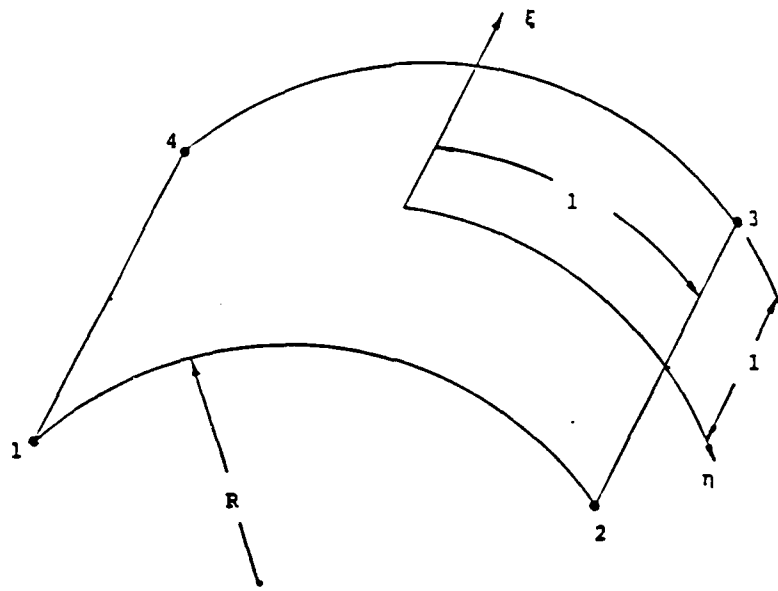
FIGURE 4.2. Rectangular Shell Element of Figure 4.1 in Natural Coordinates, $\zeta = x/a$ and $\eta = s/b$.

Combining the Hermitian approximations for w and its derivatives using Eqn (4.22) with the Lagrangian approximations for u, v, ψ_1, and ψ_2 using Eqn (4.23), the displacement gradient vector in natural coordinates can be given as shown below in Eqn (4.24).

$$
d(\zeta,\eta) \;=\; Dq \;=\;
\begin{bmatrix}
N_1 & 0 & 0 & \vdots & \ldots & \vdots & N_4 & 0 & 0 \\
0 & H_1 & 0 & \vdots & \ldots & \vdots & 0 & H_4 & 0 \\
0 & 0 & N_1 & \vdots & \ldots & \vdots & 0 & 0 & N_4
\end{bmatrix}
\begin{Bmatrix}
q_1 \\
\text{---} \\
\vdots \\
\text{---} \\
q_4
\end{Bmatrix}
\quad (4.24)
$$

where, finally, for the kth node

$$
q_k^T = (u \; v \; w \; w_{,1} \; w_{,2} \; \psi_1 \; \psi_2)_k \qquad (4.24a)
$$

104

$$
\mathbb{N}_k = \begin{bmatrix} \mathscr{N}_k & 0 \\ \mathscr{N}_{k,\zeta} & 0 \\ \mathscr{N}_{k,\eta} & 0 \\ 0 & \mathscr{N}_k \\ 0 & \mathscr{N}_{k,\zeta} \\ 0 & \mathscr{N}_{k,\eta} \end{bmatrix}
\qquad
\mathbb{H}_k = \begin{bmatrix} \mathscr{H}_{k1} & \mathscr{H}_{k2} & \mathscr{H}_{k3} \\ \mathscr{H}_{k1,\zeta} & \mathscr{H}_{k2,\zeta} & \mathscr{H}_{k3,\zeta} \\ \mathscr{H}_{k1,\eta} & \mathscr{H}_{k2,\eta} & \mathscr{H}_{k3,\eta} \\ \mathscr{H}_{k1,\zeta\zeta} & \mathscr{H}_{k2,\zeta\zeta} & \mathscr{H}_{k3,\zeta\zeta} \\ \mathscr{H}_{k1,\eta\eta} & \mathscr{H}_{k2,\eta\eta} & \mathscr{H}_{k3,\eta\eta} \\ \mathscr{H}_{k1,\eta\zeta} & \mathscr{H}_{k2,\eta\zeta} & \mathscr{H}_{k3,\eta\zeta} \end{bmatrix}
$$

(4.24b)

D = 18x28 array of shape functions and derivatives defined by $\mathbb{N}_k$ and $\mathbb{H}_k$ of above.

The displacement gradient vector in terms of elemental shell coordinates, x-s, of Figure 4.1, is found using the Jacobian matrix, J. For a rectangularly shaped element as in Figure 4.1, J is very straight forward to find. More generally, the derivation is as follows. Assume a generic function f(x,s) that represents any of the elements of d where x,s are functions of the natural coordinates, ζ, η. Since,

$$ f_{,\zeta} = f_{,x}\, x_{,\zeta} + f_{,s}\, s_{,\zeta} \qquad (4.25) $$

$$ f_{,\eta} = f_{,x}\, x_{,\eta} + f_{,s}\, s_{,\eta} $$

then,

$$
\begin{Bmatrix} f_{,x} \\ f_{,s} \end{Bmatrix} =
\begin{bmatrix} x_{,\zeta} & s_{,\zeta} \\ x_{,\eta} & s_{,\eta} \end{bmatrix}^{-1}
\begin{Bmatrix} f_{,\zeta} \\ f_{,\eta} \end{Bmatrix} =
\begin{bmatrix} \Gamma_{11} & \Gamma_{12} \\ \Gamma_{21} & \Gamma_{22} \end{bmatrix}
\begin{Bmatrix} f_{,\zeta} \\ f_{,\eta} \end{Bmatrix} \quad (4.26)
$$

Additionally, second derivative relationships are required for w dof, for example from Eqn (4.25),

$$f,_{\zeta\zeta} = (f,_x x,_\zeta),_\zeta + (f,_s s,_\zeta),_\zeta \tag{4.27}$$

$$= (f,_{xx} x,_\zeta + f,_{xs} s,_\zeta) x,_\zeta + f,_x x,_{\zeta\zeta}$$

$$+ (f,_{ss} s,_\zeta + f,_{xs} x,_\zeta) s,_\zeta + f,_s s,_{\zeta\zeta}$$

and therefore, using similar expressions for $f,_{\zeta\eta}$ and $f,_{\eta\eta}$,

$$
\begin{Bmatrix} f,_{xx} \\ f,_{ss} \\ f,_{xs} \end{Bmatrix}
=
\begin{bmatrix}
x,^2_\zeta & s,^2_\zeta & 2s,_\zeta x,_\zeta \\
x,^2_\eta & s,^2_\eta & 2s,_\eta x,_\eta \\
x,_\zeta x,_\eta & s,_\zeta s,_\eta & (s,_\zeta x,_\eta + x,_\zeta s,_\eta)
\end{bmatrix}^{-1}
\begin{bmatrix}
\begin{Bmatrix} f,_{\zeta\zeta} \\ f,_{\eta\eta} \\ f,_{\zeta\eta} \end{Bmatrix}
\end{bmatrix}
$$

$$
-
\begin{bmatrix}
x,_{\zeta\zeta} & s,_{\zeta\zeta} \\
x,_{\eta\eta} & s,_{\eta\eta} \\
x,_{\zeta\eta} & s,_{\zeta\eta}
\end{bmatrix}
\begin{bmatrix}
\Gamma_{11} & \Gamma_{12} \\
\Gamma_{21} & \Gamma_{22}
\end{bmatrix}
\begin{Bmatrix} f,_\zeta \\ f,_\eta \end{Bmatrix}
$$

$$\tag{4.28}$$

Rearranging Eqn (4.28) and combining terms into a 3x5 matrix, Λ, then gives,

$$
\begin{Bmatrix} f,_{xx} \\ f,_{ss} \\ f,_{xs} \end{Bmatrix}
\equiv
\begin{bmatrix} \Lambda \end{bmatrix}
\begin{Bmatrix} f,_\zeta \\ f,_\eta \\ f,_{\zeta\zeta} \\ f,_{\eta\eta} \\ f,_{\zeta\eta} \end{Bmatrix}
\tag{4.29}
$$

Finally, combining Eqns (4.26) and (4.29), the inverse of the Jacobian matrix, Γ, that relates d of the two coordinate systems of Figures 4.1 and 4.2 is given by the expressions in Eqn (4.30).

$$d(x,s) = \Gamma \, d(\zeta,\eta) \tag{4.30}$$

where,

$$\Gamma = \begin{bmatrix} \Gamma_1 & 0 & 0 \\ 0 & \Gamma_2 & 0 \\ 0 & 0 & \Gamma_1 \end{bmatrix} \qquad (4.30a)$$

and,

$$\Gamma_1 = \begin{bmatrix} 1 & 0 & 0 & 0 & 0 & 0 \\ 0 & \Gamma_{11} & \Gamma_{12} & 0 & 0 & 0 \\ 0 & \Gamma_{21} & \Gamma_{22} & 0 & 0 & 0 \\ 0 & 0 & 0 & 1 & 0 & 0 \\ 0 & 0 & 0 & 0 & \Gamma_{11} & \Gamma_{12} \\ 0 & 0 & 0 & 0 & \Gamma_{21} & \Gamma_{22} \end{bmatrix} , \qquad (4.30b)$$

$$\Gamma_2 = \begin{bmatrix} 1 & 0 & 0 & 0 & 0 & 0 \\ 0 & \Gamma_{11} & \Gamma_{12} & 0 & 0 & 0 \\ 0 & \Gamma_{21} & \Gamma_{22} & 0 & 0 & 0 \\ 0 & \Lambda_{11} & \Lambda_{12} & \Lambda_{13} & \Lambda_{14} & \Lambda_{15} \\ 0 & \Lambda_{21} & \Lambda_{22} & \Lambda_{23} & \Lambda_{24} & \Lambda_{25} \\ 0 & \Lambda_{31} & \Lambda_{32} & \Lambda_{33} & \Lambda_{34} & \Lambda_{35} \end{bmatrix} \qquad (4.30c)$$

For the rectangular element of Figures 4.1 and 4.2, $\Gamma_{11}=1/a$, $\Gamma_{22}=1/b$, $\Lambda_{13}=1/a^2$, $\Lambda_{24}=1/b^2$, and $\Lambda_{35}=1/ab$. The remaining entries of Γ (except the 1's) are zero.

The 28 dof element shown in Figure 4.3 is now completely defined and is summarized by Eqns (4.8), (4.24),

107

and (4.30), where Eqn (4.19) is now written as shown below.

$$d = \Gamma \, D \, q \qquad\qquad (4.31)$$

$$= \mathcal{D} \, q$$

where,

d = 18x1 (Eqn (4.8)),

Γ = 18x18 (Eqn (4.30)),

D = 18x28 (Eqn (4.24)), and,

q = 28x1 (Eqn (4.24)).
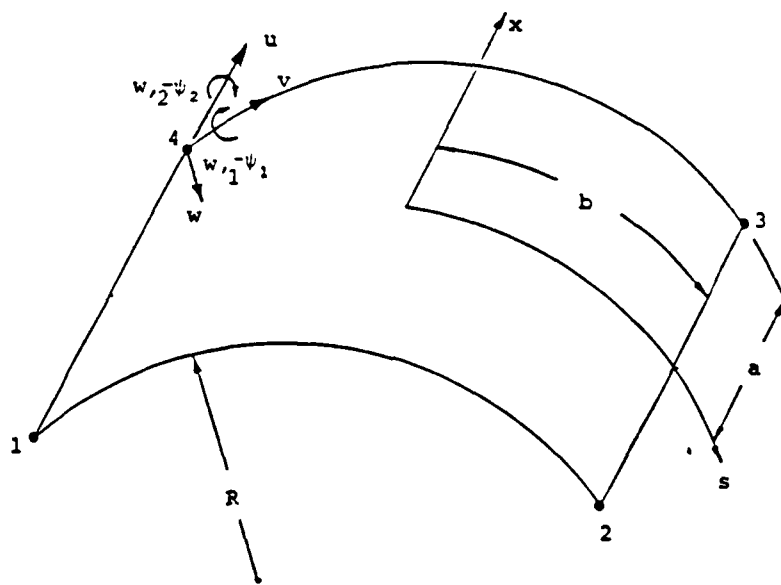
FIGURE 4.3.   28 dof Rectangular Shell Element.   Each Node has 7 dof, $q_k^T = \{u \; v \; w \; w_{,1} \; w_{,2} \; \psi_1 \; \psi_2\}_k$, k=1,2,3,4.

The inplane continuum displacement dof, u and v, are coupled to the transverse displacement dof to a much greater degree in the cylindrical shell compared to the flat plate due to the nonzero curvature in the circumferential

direction of the former. Indeed, in a linear analysis, u
and v are decoupled from the remaining dof for the flat
plate. Consequently, it is felt that linear approximations
for these variables, though quite adequate for the flat
plate, are much too crude for the shell, especially for
cases where membrane action is important. Therefore, the 28
dof element derived above can be extended to allow a
quadratic approximation for the inplane dof u and v. To
accomplish this, four additional nodes located at the
midsides of the rectangularly shaped element must be
included, see Figure 4.4. We can define the resulting 36
dof element, i.e., the 28 dof from before, and two
additional dof, u and v, at each of the midside nodes, by
appending to the 28 dof expressions. The equivalent
relationship of Eqn (4.24) for the 36 dof element is shown
in Eqn (4.32). In Eqn (4.32), quadratic Lagrangian shape
functions, Q_k, have replaced the linear N_k from before only
for the u and v dof. The additional 8 dof have been
appended to the end of the q array and therefore, q is now
36x1 and D is now 18x36. The displacement gradient vector,
d, in shell coordinates is found using the same inverse
Jacobian, Γ, as before, and therefore, Eqn (4.31) applies
for the 36 dof element as well but with the new D and q
arrays as defined below.

$$d(\zeta,\eta) \;=\; Dq \;=\; \begin{bmatrix} \Phi_1 & 0 & 0 & \bigl|\ldots\bigr| & \Phi_4 & 0 & 0 & \Phi_5 & \bigl|\ldots\bigr| & \Phi_8 \\ 0 & \mathbb{H}_1 & 0 & \bigl|\ldots\bigr| & 0 & \mathbb{H}_4 & 0 & 0 & \bigl|\ldots\bigr| & 0 \\ 0 & 0 & \mathbb{N}_1 & \bigl|\ldots\bigr| & 0 & 0 & \mathbb{N}_4 & 0 & \bigl|\ldots\bigr| & 0 \end{bmatrix} \begin{Bmatrix} q_1 \\ \vdots \\ q_4 \\ q_5 \\ \vdots \\ q_8 \end{Bmatrix}$$

where,   (4.32)

$$q_k^T = \{ u \; v \; w \; w,_1 \; w,_2 \; \psi_1 \; \psi_2 \}_k \; , \quad k=1,2,3,4$$

$$q_k^T = \{ u \; v \}_k \; , \quad k=5,6,7,8$$

$\mathbb{N}_k$, $\mathbb{H}_k$ as before in Eqn (4.24b)

$$\Phi_k = \begin{bmatrix} Q_k & 0 \\ Q_{k,\zeta} & 0 \\ Q_{k,\eta} & 0 \\ 0 & Q_k \\ 0 & Q_{k,\zeta} \\ 0 & Q_{k,\eta} \end{bmatrix} \; .$$

$$Q_k = \frac{1}{4}(1+\zeta_k\zeta)(1+\eta_k\eta)(\zeta_k\zeta+\eta_k\eta-1) \; , \quad k=1,2,3,4$$

$$Q_k = \frac{1}{2}(1-\zeta^2)(1+\eta_k\eta) \; , \quad k=6,8$$

$$Q_k = \frac{1}{2}(1-\eta^2)(1+\zeta_k\zeta) \; , \quad k=5,7$$

D= 18x36 array

q= 36x1 array

As has been stated, the shape function approximations assumed for w are nonconforming, i.e., the normal slope of w is incompatible between elements.   This incompatibility,

however, is not nearly as significant for this formulation as it is for simpler ones, e.g., Kirchhoff plate elements. The present case, we recall, includes parabolic transverse shear distribution through the thickness. The shear rotations, β_α, we found are equal to a combination of the derivatives of w, and the bending rotations, ψ_α, see Figures 3.6 and 3.7. For the limiting thin plate and shell situation, we would expect zero shear rotation and the incompatibility, in effect, disappears since $w,_\alpha = \psi_\alpha$ where ψ_α are compatible approximations. This is not true for Kirchhoff elements with nonconforming w approximations.
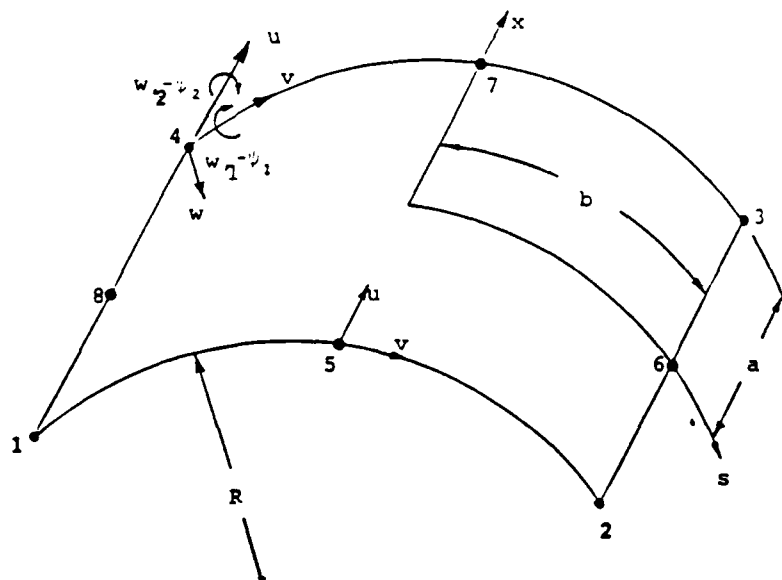
FIGURE 4.4. 36 dof Rectangular Shell Element. Corner Nodes have 7 dof, Midside Nodes have 2 dof.

Algorithms

We are now prepared to rewrite the linearized incremental/iterative relations that give the nonlinear solution using Eqns (4.20) and (4.6) where all quantities have now been defined. The integrals in Eqn (4.6) are, again, calculated for each individual element. Each element's contribution is assembled according to the elemental connectivity of the discretized domain into a global array. Therefore, Eqn (4.6) in practice is represented as in below.

$$\sum_{k=1}^{n} \left[\int_{\Omega_e} \mathcal{D}^T \left[\hat{K} + \hat{N}_1 + \hat{N}_2 \right] \mathcal{D} \, d\Omega_e \right]_k \Delta q = \qquad (4.33)$$

$$- \sum_{k=1}^{n} \left[\int_{\Omega_e} \mathcal{D}^T \left[\hat{K} + \frac{\hat{N}_1}{2} + \frac{\hat{N}_2}{3} \right] \mathcal{D} \, d\Omega_e \right]_k q \; + R$$

where,

Ω_e = 2-D domain of individual element

n = total number of elements in the mesh

$\Delta q, q$ = global column arrays of displacement that have been assembled from elemental Δq and q.

R = global load array with as many rows as the total number of dof, i.e., same dimension as the global q.

In Eqn (4.33), the $\mathcal{D}$ array refers to an individual element, as previously defined. The $\hat{K}$, $\hat{N}_1$, and $\hat{N}_2$ are independent of the specific element definition, but; the

112

latter two arrays are functions of the displacement gradient vector, d, that does define the element. The global load vector, R, can be determined in two ways. Loads can be lumped at the nodes after the elemental integrations and global assemblies have been accomplished, or, alternatively, an equivalent nodal loading scheme for each element can be used for distributed loadings. In the latter, the equivalent nodal loads are calculated on an elemental level using the same shape functions that approximate the elemental displacements. The procedures for both methods are straight forward and further explanation can be found in (121).

In both methods of above, only linear load terms have been considered in this research for simplicity as was discussed in Chapter III, i.e., R is an array of constants. The theoretically complete approach would be to include the higher order displacement dependent terms in R that result due to the large rotations of the differential volumes of the shell (114). As discussed in the theoretical development of Chapter III, incrementation of displacement instead of load in the large rotational cases will accomplish the same end. The fact that loading is applied only through prescribing displacements in the large rotational case is recognized as a restriction; but, the author believes it is worthwhile given the added complexity of including nonlinear loading expressions.

Solutions to Eqn (4.33) are found iteratively where convergence is achieved when the RHS becomes small, i.e., the equilibrium equations are nearly satisfied. The integrations of Eqn (4.33) are accomplished numerically using Gaussian quadrature in natural coordinates, ζ and η. Using one of the terms from the first summation of Eqn (4.33) as an example, we first transform using the Jacobian determinant to natural coordinates. Then, as shown in Eqn (4.34), the numerical integration is performed by a double summation of weighting factors multiplied by the integrand that has been evaluated at the Gaussian integration points. (121)

$$\int_{\Omega_e} \mathcal{D}^T \left[\hat{K} + \hat{M}_1 + \hat{M}_2 \right] \mathcal{D} \, d\Omega_e = \quad (4.34)$$

$$= \int_{-1}^{1} \int_{-1}^{1} \mathcal{D}^T \left[\hat{K} + \hat{M}_1 + \hat{M}_2 \right] \mathcal{D} \, \det J \, d\xi d\eta$$

$$= \sum_{i}^{m} \sum_{j}^{m} W_i \, W_j \, \phi \, (\xi_i, \eta_j)$$

where,

detJ = determinant of the Jacobian matrix,

$\phi = \mathcal{D}^T \left[\hat{K} + \hat{M}_1 + \hat{M}_2 \right] \mathcal{D}$ detJ, evaluated at Gauss integration points (ξ_i, η_j),

W_i, W_j = weighting factors.

The range on the indices i and j define the order of the

114

numerical integration. For an exact evaluation of the integral shown above, mxm quadrature is required for an integrand of polynomial degree 2m-1 as shown in (121).

Three different types of solution algorithms were incorporated into the finite element solution. Brief descriptions of linear, linear bifurcation, and nonlinear analyses follow. It is important to point out that the same set of subroutines and main program elements are used for all three algorithms. The difference among the three is that the simpler algorithms merely do not perform all of the calculations that the more complex algorithms require.

Linear Algorithm

The analysis of linear problems that have known published results is a very important initial step in the validation of a finite element code. These simple analyses not only can point out algorithmic errors, but also possible numerical problems, namely, shear locking. Since quantities such as displacement, rotations, etc., in a linear analysis are assumed to be small, the arrays N_1 and N_2 are eliminated and therefore are not calculated. Furthermore, since relationships are linear, the equilibrium equations of Eqns (4.2) and (4.3) are solved directly for q, i.e., the iterative solutions of Eqn (4.6) or (4.33) are not necessary.

Elemental integrations and global assembly are accomplished as previously stated but the above

115

simplifications allow the linear solution equivalent of Eqn (4.33) to be represented as in Eqn (4.35).

$$\sum_{k=1}^{n} \left[\int_{-1}^{1} \int_{-1}^{1} \mathcal{D}^T \, \hat{K} \, \mathcal{D} \, \det J \, d\xi d\eta \right]_k q = R \qquad (4.35)$$

where R can be found as previously discussed, and the integrals are evaluated numerically as in Eqn (4.34).

The assembly of the elemental stiffnesses into the global stiffness array is accomplished taking advantage of the bandedness and symmetry of the latter. In this way, the final size of the global array is minimized since many zeroes have been eliminated. Prescribed displacements are imposed after all of the elemental stiffnesses have been calculated and assembled. These displacement boundary conditions, which generally are nonzero, are applied by typically zeroing out the column and row of the global stiffness array that corresponds to the prescribed dof except for the diagonal position which is replaced by 1. The RHS is modified by adding the equivalent forces caused by the prescribed dof, except for the row corresponding to it. For this position, the prescribed displacement value is placed (129).

Next, the solution of the simultaneous equations is found by straight forward Gaussian elimination. The resulting global displacement vector can then be used to find the strains and then the stresses via previous

relationships. The stresses are calculated at the same Gauss points that were used in the elemental stiffness integrations. Since the calculated stresses are most accurate at these points, they are not extrapolated to the node points as is sometimes done (121).

The elemental stiffness integrands of Eqn (4.35) consist of polynomials of degree 6 at most since $\mathcal{D}$ and $\mathcal{D}^T$ each contain cubic polynomials due to the w interpolations. Consequently, exact integration requires a 4x4 point numerical scheme. It is possible to use a lower integration order while sacrificing only a small amount of accuracy. However, due to the generally inexpensive nature of these problems, 4x4 integration was used for all linear cases presented in the next chapter.

Recall that lower order transverse shear theories, e.g., Reissner-Mindlin (RM) theories, cannot accurately predict thin plate or shell behavior when elemental stiffnesses are integrated exactly since excessive transverse shear energy is stored. For these formulations, lower order integration of elemental stiffnesses is required for linear or quadratic Lagrangian elements to avoid numerical shear locking. The present research, however, assumes cubic interpolation for the transverse displacement, w. As developed using a simple beam element for illustration in Appendix E, the cubic w alleviates shear locking without the artifice of inexact integration.

Linear Bifurcation Algorithm

Our purpose in this research is primarily the study of the nonlinear behavior of flat plates and cylindrical shells. However, the quantities required for the nonlinear analysis are the same quantities that can be used in a linear bifurcation study, and therefore, the latter can be done without much additional effort. However, the primary purpose of the linear bifurcation analysis in this research is that it represents a relatively simple and inexpensive method to validate some of the assumed nonlinearity. In this way, the linear bifurcation analysis can be viewed as an intermediate step between the linear and nonlinear analyses.

Instability, as defined for solid bodies under load, is the phenomenon in which a small increase in load causes a disproportionately large increase in deformation. Therefore, since load and deformation are not proportional, instability is necessarily a nonlinear phenomenon. Linear bifurcation analysis is a mathematical idealization that can be used to find the load that causes instability (the critical load), without solving the much more involved nonlinear problem. In linear bifurcation analysis, instead, the critical load is found through an eigenvalue problem. The eigenvalue we seek corresponds to that load level that gives two adjacent orthogonal equilibrium configurations. Initially, we assume that the structure linearly follows the

primary, or prebuckled, path with increasing load. Eventually, a load is reached, i.e., the critical load, where the path bifurcates. The continuation of the primary path represents one equilibrium state and the adjacent equilibrium state is the secondary or buckled path.

This relatively simple procedure can be used to effectively approximate the critical load only in certain cases. The critical load for Euler columns and axially loaded flat plates can be found very accurately using the linear bifurcation technique. This is the case, for the most part, since the true nature of these structures exhibits little redistribution of stress or change in geometry prior to the rapid development of the instability. Analytically, the prebuckled shape of the flat plate remains flat; the deformation pattern of the secondary path is orthogonal to the prebuckled shape and is characterized by a sinusoidal transverse deformation pattern. In actual tests, the plate will not remain flat before instability due to eccentricities in the plate and loading geometry. However, most of the prebuckling deformation is inplane and the postbuckle is characterized by large transverse deformation.

A shell structure, on the other hand, generally does experience stress redistribution and geometry changes prior to instability and often linear bifurcation analyses of these structures is in significant error.

Stability of a structure in equilibrium can be

determined by examining the definiteness of the second variation of the total potential energy, $\delta^2 \Pi_p$. Since, for conservative systems, a local minimum for Π_p corresponds to a stable equilibrium configuration, the load that first gives a $\delta^2 \Pi_p$ that is not positive definite is the critical load. The derivation of the linearized incremental equations earlier in this chapter, in effect, gave $\delta^2 \Pi_p$. Consequently, a linear bifurcation analysis can proceed as follows. Eqn (4.6) is rewritten below in Eqn (4.36).

$$\left[K + N_1(q) + N_2(q^2) \right] \Delta q = K_T \Delta q = \Delta R \qquad (4.36)$$

where, the RHS represents the out of balance forces, $\Delta R = -F(q)$.

At the critical load level K_T is singular, indicating that a small (actually infinitesimal) increase in the load will cause a large (actually infinite) increase in deformation. In linear bifurcation theory, we assume that the structure behaves linearly up to this point and therefore, we can scale a reference load, R_{ref}, by a positive constant, λ, where the critical load, R_{cr}, is given by

$$R_{cr} = \lambda_{cr} R_{ref} \qquad (4.37)$$

The constant λ_{cr} can then be found via Eqn (4.38).

$$\left| K + \lambda_{cr} N_1(q_{ref}) + \lambda_{cr}^2 N_2(q_{ref}^2) \right| = 0 \qquad (4.38)$$

120

First, any reference load, R_{ref}, is chosen that is less than the bifurcation load. The linear problem is then solved for displacements, q_{ref}, via Eqn (4.35). After substituting q_{ref} into N_1 and N_2 via the displacement gradient vector, d, λ is gradually increased until the determinant of Eqn (4.38) equals zero. The λ that satisfies Eqn (4.38) is λ_{cr}. The buckled mode shape is the eigenvector that corresponds to the eigenvalue, λ_{cr}. The eigenvector, $\tilde{v}$, is calculated from Eqn (4.39). The components of $\tilde{v}$ can not be found explicitly since the coefficient matrix is singular. However, by prescribing one component of $\tilde{v}$, the remaining components are then solved for as a proportion of the prescribed component.

$$\left[K + \lambda_{cr} N_1(q_{ref}) + \lambda_{cr}^2 N_2(q_{ref}^2) \right] \tilde{v} = 0 \qquad (4.39)$$

In practice, Eqns (4.38) and (4.39) are simplified by neglecting the higher order terms found in the array, N_2, see Eqn (4.40). This approach is called the fully linearized approach and results in a standard generalized eigenvalue problem.

$$\left| K + \lambda_{cr} N_1(q_{ref}) \right| = 0 \qquad (4.40)$$

Note that the K and N_1 arrays of Eqns (4.38), (4.39) and (4.40) are _global_ stiffness arrays. That is, K is assembled once, q_{ref} is found, then we assemble the global $N_1(q_{ref})$

121

once. Therefore, after K and N_1 have been assembled, they

do not change. In solving Eqn (4.40) for λ_{cr}, λ is linearly

stepped and the sign of the determinant can be examined.

The actual algorithm will stop, due to the type of routine

used to find the determinant, any time the matrix $K+\lambda N_1$ is

not positive definite. However, this is in practice very

convenient since we never have to worry about finding a λ

that is not the primary eigenvalue. This is because for any

$\lambda > \lambda_{cr}$ where λ_{cr} is the primary eigenvalue, the matrix

$K+\lambda N_1$ will not be positive definite and the determinant

routine will return an error message to that effect.   In

these cases, the user now knows that the load, λR_{ref}, is

greater than the bifurcation load, and therefore, a smaller

R_{ref} is chosen and the algorithm of Eqn (4.40) is begun

again.

As studied by Chang and Chen (130), the fully

linearized bifurcation method which fits very well with our

finite element formulation, is not the same as the classical

bifurcation buckling analysis.   The classical buckling

approach, based on the so called B-notation approach

(70,131), formulates the initial stress matrix, K_σ, instead

of N_1. The initial stress matrix, also called the geometric

matrix, is a function of stress instead of displacement. In

this way, there is effectively less displacement coupling in

the classical approach. As the reference also points out,

since the fully linearized approach includes more of the

nonlinear displacement terms, it is more mathematically complete than is the classical approach. The classical approach applied to plates and shells typically includes only transverse degrees of freedom. Bifurcation is indicated by the load that first gives out of plane deformation. In this way, the buckled configuration is orthogonal to the prebuckled. However, the present approach allows both inplane and transverse deformation in the prebuckled and postbuckled configurations. Therefore, orthogonal deformation patterns can not be expected in the fully linearized approach.

Nonlinear Algorithm

The primary thrust of the present research is the nonlinear analysis. For these problems, Eqn (4.6), the linearized incremental/iterative equations are solved via a Newton-Raphson approach. As stated in the linear bifurcation algorithm description, the tangent stiffness matrix is singular at the critical load level signifying the onset of instability. This is a characteristic of the nonlinear collapse behavior as well. Knowledge of post collapse behavior, which cannot be derived via the straight forward bifurcation analysis just presented, can be important. Crisfield (107) gives the following example. Post collapse analysis of an individual component of a complete structure would tell of the former's load shedding characteristics. The load once carried by the collapsed

123

component would have to be redistributed to the other components of the complete structure.

Consequently, as discussed in the Literature Review Chapter, we need a solution algorithm that permits the traversing of limit points characterized by a singular K_T. Structures that exhibit the equilibrium path of Figure 4.5 have generally two types of limit points, given by points A and B. The structure that gives this response is usually restrained by simple supports at the boundary giving freedom of rotation there. The load is increased until point A on the curve is reached. At that time, the structure will violently snap through to an inverted configuration at point C where the load can once again be increased. The other type of limit point occurs in the unstable portion of the equilibrium curve of Figure 4.5 at point B, called a snap back point. Multiple degree of freedom systems typically have complex unstable equilibrium paths that can not be completely represented in only two dimensions and a general description is not attempted here, see Thompson and Hunt (132).

The algorithm adopted was a straight forward displacement control method. The displacements, not loads, are incremented and therefore the snap through limit points are easily traversed since the coefficient matrix is no longer singular at point A of Figure 4.5. However, snap back limit points may cause difficulties for the same

reasons as the snap through type do in the load incrementation approach. Both displacement and load control options are written into the finite element code.
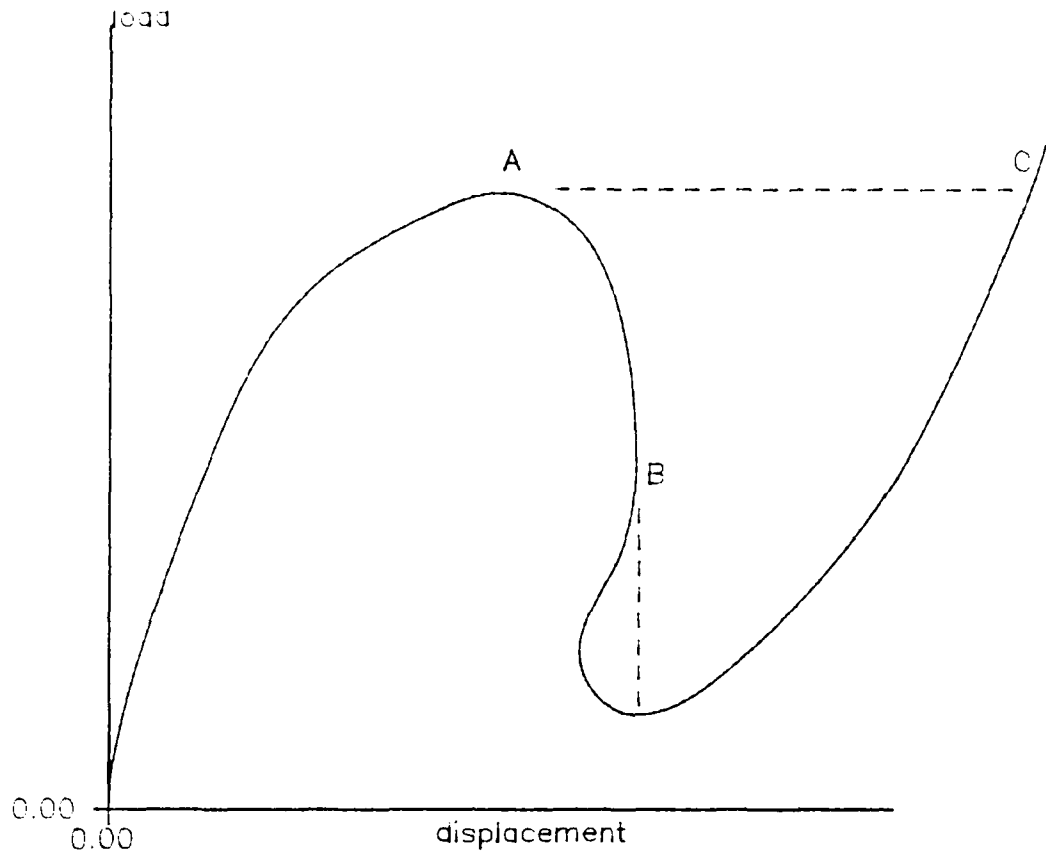
FIGURE 4.5. Equilibrium Path Showing Snap Through and Snap Back Limit Points.

In the nonlinear algorithm, the first iteration of the first increment is the linear solution, i.e., the N_1 and N_2 are not included. The displacement gradient vector is then calculated based on the linear displacement results. N_1 and N_2 are next evaluated and iteration continues until convergence is achieved. A global criterion, as shown in Eqn (4.41), was used to determine if a given increment of displacement or load has converged to a solution. In Eqn (4.41), the summations extend over the total number of degrees of freedom. A norm of displacement dof is calculated for each iteration and the norm of the previous iteration is subtracted from the norm of the present iteration. That result is then divided by the norm of the first iteration. When the resulting scalar is smaller than a user provided percentage tolerance, then convergence has been achieved.

$$\frac{\sqrt{\sum_i (q_i^r)^2} \quad - \quad \sqrt{\sum_i (q_i^{r-1})^2}}{\sqrt{\sum_i (q_i^1)^2}} \text{ X } 100\% \leq \text{TOL} \qquad (4.41)$$

where,

q_i^r, q_i^{r-1}, q_i^1 are the elements of q for the rth, $(r-1)^{th}$, and first iterations for a given increment,

TOL is a user defined percentage.

A final comment on the nonlinear algorithm concerns the

126

order of the numerical integration. The polynomials in the elemental stiffness integrands for this case are twelfth order at the most since $\mathcal{D}$ and $\mathcal{D}^T$ are cubic and N_2 contains up to sixth order polynomials due to w^2 terms. Consequently, we require a 7x7 point rule for exact integrations (121). Obviously, this makes the evaluation of elemental stiffnesses very expensive especially considering the iterative nature of the nonlinear problem.

Coupling Characteristics

As mentioned in the previous section referring to the linear bifurcation problem, the B-notation approach has less displacement coupling than does the N-notation approach. The B-notation approach uses force resultant terms in the initial stress matrix whereas the N-notation approach uses the displacement dependent matrix N_1. The same relative degree of displacement coupling holds true for the nonlinear algorithm as well since the same force resultant matrix, K_σ, is used in the nonlinear analysis in the B-notation approach (70,131). A significant consequence of this becomes clear in the next chapter where the present formulation yields collapse for an axially loaded symmetrically laminated cylindrical panel, but numerical transverse imperfections are required in the alternate approach to achieve a degree of coupling such that collapse occurs (16). Without the imperfections, the response of the shell is linear.

Despite the higher degree of displacement coupling that

exists in the present formulation as indicated for the shell above, one type of coupling for the flat plate case still can not be achieved. Although a transversely loaded flat plate correctly does not generate inplane displacements in the linear symmetric laminate case (because this is a 2-D theory, see Refs (62,119)), certainly it does in the nonlinear case. However, as the remainder of this chapter will show, an axially loaded flat plate, despite the high degree of displacement coupling, will <u>never</u> generate out of plane displacements for symmetrically arranged laminates.

The above cases for a flat plate are easily shown using the element independent arrays, $\hat{K}$, $\hat{N}_1$, and $\hat{N}_2$, developed earlier in this chapter. It is important to note the $\mathcal{D}$ array that defines the element in Eqn (4.33) for example, does not influence the coupling features between inplane and transverse displacements. Consequently, we can examine coupling characteristics through the elements of the displacement gradient vector, d, instead of the nodal dof vector, q. We first refine the definition for d of Eqn (4.8) by dividing d into two parts: d_1 corresponds to the six inplane displacement terms, and d_2 corresponds to the twelve transverse displacement terms, see Eqn (4.42).

$$d_1^T = (\ u\ u,_1\ u,_2\ v\ v,_1\ v,_2\ )$$

$$d_2^T = (\ w\ w,_1\ w,_2\ w,_{11}\ w,_{22}\ w,_{12}\ \psi_1\ \psi_{1,1}\ \psi_{1,2}\ \psi_2\ \psi_{2,1}\ \psi_{2,2}$$

(4.42)

We can examine coupling between d_1 and d_2 by

considering the nonlinear analyses of axially and transversely loaded flat plates. In an nonlinear analysis, recall that the initial iteration of the first increment is the solution of the linear problem. We know that in the linear problem the inplane and transverse dof are decoupled. That is, an axially loaded flat plate will generate nonzero d_1, but d_2 will be zero. Additionally, a transversely loaded flat plate gives a nonzero d_2, but d_1 equals zero. The above is true because there are no coupling entries in $\hat{K}$ between the elements of d_1 and d_2 if the plate is isotropic or consists of symmetrically stacked lamina. Figure 4.6 shows a schematic of the nonzero entries for the symmetric 18x18 $\hat{K}$ matrix and we can see the absence of coupling terms. In the Figure, x refers to a nonzero entry, blanks refer to zeroes. The entries of the upper 6x6 matrix are associated with the inplane displacement dof, i.e., d_1; the entries of the lower 12x12 matrix are associated with the transverse dof, i.e., d_2; and, the 6x12 matrix in the upper right corner contains the coupling entries.

Similar Figures are shown for the remaining two arrays, $\hat{N}_1$ and $\hat{N}_2$. There are two Figures for each of these where we assume that either $d_1=0$ or $d_2=0$ initially. For the case of $d_1=0$, we have a transversely loaded flat plate where the linear solution yields nonzero d_2 elements. For the case of $d_2=0$, we have an axially loaded flat plate where the linear solution yields nonzero d_1 elements. Given the above two

starting conditions, the nonzero terms in $\hat{N}_1$ and $\hat{N}_2$ are identified.

From Figure 4.7, we have only coupling terms present in $\hat{N}_1$ and Figure 4.9 shows the corresponding $\hat{N}_2$. Therefore, in the nonlinear analysis, a nonzero d_1 is generated by transverse loading. However, from Figures 4.8 and 4.10, we see that when d_1 is nonzero and d_2 is zero after the linear solution, i.e., the axially loaded flat plate, no coupling exists. Therefore, d_2 will remain zero for all subsequent iterations and increments. Although nonzero terms exist in these arrays that correspond to the transverse displacement, since the loading is identically zero except for loading corresponding to inplane dof, the trivial solution for the transverse dof results. Examination of similar arrays for the cylindrical shell reveals that coupling always exists, i.e., for axial or transverse loads, both d_1 and d_2 are nonzero.

FIGURE 4.6.   Element Independent Array $\hat{K}$ for Flat Plate.

FIGURE 4.7.   Element Independent Array $\hat{N}_1$ for Flat   Plate
where $d_1=0$, $d_2 \neq 0$.

131

$$\hat{N}_1 = \begin{bmatrix} & & & & & & & & & & & & & & & & & \\ & X & X & & X & X & & & & & & & & & & & & \\ & & X & & X & X & & & & & & & & & & & & \\ & & & & & & & & & & & & & & & & & \\ & & & & X & X & & & & & & & & & & & & \\ & & & & & X & & & & & & & & & & & & \\ \hline & & & & & & & & & & & & & & & & & \\ & & & & & & X & X & & & & & & & & & & \\ & & & & & & X & & & & & & & & & & & \\ & & & & & & & X & X & X & & X & X & & X & X & & \\ & & & & & & & X & X & & X & X & & X & X & & \\ & & & & & & & & X & & X & X & & X & X & & \\ & & & & & & & & & & & & & & & & & \\ & & & & & & & & & X & X & & X & X & & \\ & & & & & & & & & & X & & X & X & & \\ & & & & & & & & & & & & & & & & & \\ & & & & & & & & & & & X & X & & \\ & & & & & & & & & & & & X & \end{bmatrix}$$

FIGURE 4.8. Element Independent Array $\hat{N}_1$ for Flat Plate where $d_1 \neq 0$, $d_2 = 0$.

$$\hat{N}_2 = \begin{bmatrix} & & & & & & & & & & & & & & & & & \\ & X & X & & X & X & & & & & & & & & & & & \\ & & X & & X & X & & & & & & & & & & & & \\ & & & & & & & & & & & & & & & & & \\ & & & & X & X & & & & & & & & & & & & \\ & & & & & X & & & & & & & & & & & & \\ \hline & & & & & & & & & & & & & & & & & \\ & & & & & & X & X & X & X & X & & X & X & & X & X & \\ & & & & & & X & X & X & X & & X & X & & X & X & \\ & & & & & & X & X & X & & X & X & & X & X & \\ & & & & & & & X & X & & X & X & & X & X & \\ & & & & & & & & X & & X & X & & X & X & \\ & & & & & & & & & & & & & & & & & \\ & & & & & & & & & X & X & & X & X & \\ & & & & & & & & & & X & & X & X & \\ & & & & & & & & & & & & & & & & & \\ & & & & & & & & & & & X & X & \\ & & & & & & & & & & & & X & \end{bmatrix}$$

FIGURE 4.9. Element Independent Array $\hat{N}_2$ for Flat Plate where $d_1 = 0$, $d_2 \neq 0$.

$$
\hat{N}_2 =
\begin{array}{c|cccccc|cccccccccccc|}
 & 1 & 2 & 3 & 4 & 5 & 6 & 7 & 8 & 9 & 0 & 1 & 2 & 3 & 4 & 5 & 6 & 7 & 8 \\
1 & & & & & & & & & & & & & & & & & & \\
2 & & x & x & & x & x & & & & & & & & & & & & \\
3 & & & x & & x & x & & & & & & & & & & & & \\
4 & & & & & & & & & & & & & & & & & & \\
5 & & & & & x & x & & & & & & & & & & & & \\
6 & & & & & & x & & & & & & & & & & & & \\ \hline
7 & & & & & & & & & & & & & & & & & & \\
8 & & & & & & & x & x & & & & & & & & & & \\
9 & & & & & & & x & & & & & & & & & & & \\
0 & & & & & & & & & x & x & x & & x & x & & x & x & \\
1 & & & & & & & & & & x & x & & x & x & & x & x & \\
2 & & & & & & & & & & & x & & x & x & & x & x & \\
3 & & & & & & & & & & & & & & & & & & \\
4 & & & & & & & & & & & & & x & x & & x & x & \\
5 & & & & & & & & & & & & & & x & & x & x & \\
6 & & & & & & & & & & & & & & & & & & \\
7 & & & & & & & & & & & & & & & & x & x & \\
8 & & & & & & & & & & & & & & & & & x & \\
\end{array}
$$

FIGURE 4.10. Element Independent Array $\hat{N}_2$ for Flat Plate where $d_1 \neq 0$, $d_2 = 0$.

We have assumed linear relations for the loading vector, that is for simplicity, the loads have been assumed to be independent of the displacements.   Generally in a nonlinear analysis, the loads are functions of the displacements. We wish to determine whether the above problem concerning the axially loaded flat plate can be solved if the higher order loading terms are included. That is, perhaps the higher order loading terms that result from the large displacements and rotations will give nonzero entries in the load vector corresponding to the transverse dof, and hence, give nonzero transverse displacements.   The force relations that result from Cauchy's law for the general geometrically nonlinear problem are shown in Eqn

133

(4.43) for a flat plate where the second term leads to nonlinear loading terms (114).

$$F_i = P_i + P_j u_{i,j} \qquad (4.43)$$

where,

P_k are applied tractions,

u_k are continuum displacements

Using the assumed kinematics of Eqn (3.44) with $R_\gamma = \infty$, $\alpha_\gamma = 1$ in Eqn (4.43) we can examine the resulting terms for the special case of the axially loaded flat plate. For this situation, let $P_2 = P_3 = 0$ and let $P_1 = P$, i.e., the plate is subjected to a constant axial pressure in the x direction as shown in the Figure 4.11. From Eqn (3.26), let the work done by the pressure loading as a result of a virtual displacement be given by,

$$\int_{S_1} F_i \delta u_i dS_1 = \iint P \left[(1 + u_1{}_{,1}) \delta u_1 + u_2{}_{,1} \delta u_2 + w_{,1} \delta w \right] ds d\zeta$$

$$(4.44)$$

Using the kinematics of Eqn (3.44) in the above, the coupling terms that will give the desired effect integrate to zero and therefore, even considering the higher order loading terms, we cannot generate transverse displacements in an axially loaded flat plate. What is usually done is to assume an initial numerical geometric imperfection. By assuming a small transverse displacement pattern at the outset, d_2 is nonzero and the coupling will always be

134

present, see Figure 4.7.

Additional degrees of freedom in u_3 of Eqn (3.35) could be defined such that the desired coupling results.
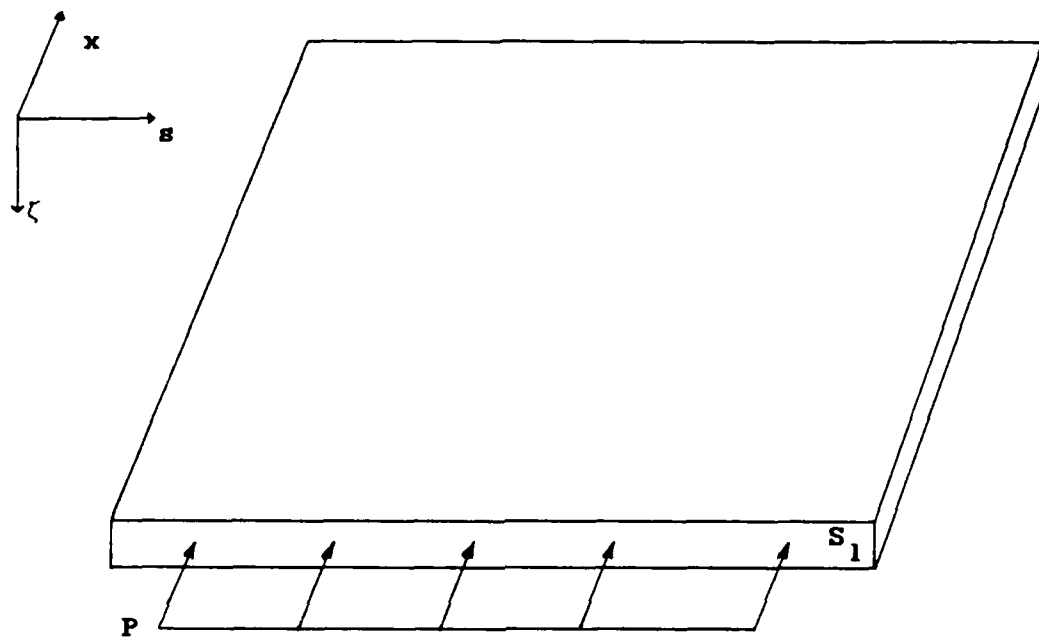
FIGURE 4.11. Flat Plate Loaded by Inplane Pressure, P, Along Surface S_1.

135

V.   Results and Discussion

Based on the theoretical development of Chapter II and
its subsequent finite element casting described in Chapter
III, many types of problems in structural mechanics can be
solved. Naturally, a new finite element code must be
validated versus many known solutions before new results can
be generated. Several well recognized problems, both linear
and nonlinear, flat plate and cylindrical shell, are tested
for this purpose. For each analysis type, i.e., linear,
linear bifurcation, and nonlinear, the validation examples
are presented first. New results were found for each of the
three types and these will generally follow the validation
examples. Unique contributions due to both the parabolic
shear representation and the large rotation and displacement
capability are discussed. It is stressed at this point that
only isotropic in addition to symmetrically arranged
laminated constructions are considered.   The theory was
formulated to consider unsymmetric laminates as well, but
the code was written only for the symmetric cases. This is
of immediate importance in the linear flat plate cases since
the inplane degrees of freedom (dof) are always decoupled
from the transverse dof.   Most of the results were
calculated on a Vax 11/785 or 8650 with double precision
arithmetic. The final nonlinear shell problem, because of
its size, was run on a Cyber 845 with virtual memory
capability.

136

Linear Flat Plate Analysis

Much effort was spent in solving the linear problems based on Eqn (4.35). It is these relatively simple problems that would first uncover typical numerical difficulties, i.e., locking, slow convergence, etc., as well as any coding or algorithmic errors. It was found that the 28 dof element performed very well for the linear flat plate case. No evidence of shear locking was exhibited, nor does convergence require an excessive number of elements compared to other studies. In this section, strictly validation problems were tested since the theory when simplified to a linear flat plate is very similar to that explored by others, primarily Reddy (31,54,57,58,95). Two examples of cylindrical bending and then four examples of rectangular plate bending are presented. One of the cylindrical bending solutions includes many through the thickness results. These results, when compared to 3-D solutions, illustrate some of the consequences of the 2-D assumptions that form the foundation of the present approach.

The simplest problems tested are the simply supported isotropic and orthotropic infinite plate strips subjected to uniform transverse pressure loading q_o, i.e., cylindrical bending, see Figure 5.1. The purpose of these first plate strip tests was initial verification of the code logic and therefore, limited results are shown. The isotropic material properties, the strip geometry, loading, and the

137

boundary conditions (b.c.) are shown in Eqn (5.1) and we see that this first test case represents a thin plate since $S=L/h=100$. The finite element results will be compared to a classical series solution for the center plate transverse displacement, w_c, taken from Szilard (133) and shown in Eqn (5.2).
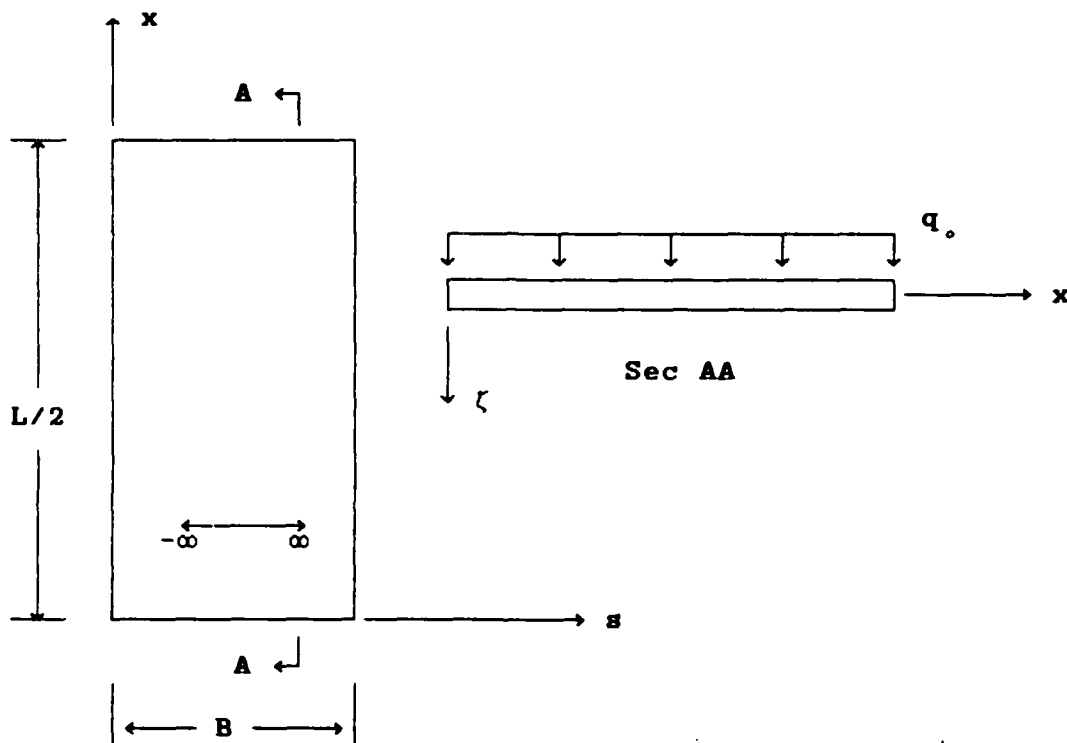
FIGURE 5.1. Plate Strip Model of Length, L/2, Width, B. Actual Strip is Infinite in s direction, Length, L in the x Direction.

$E = 3.e7$ psi   **b.c.**

$\nu = .25$ ● $x=0$:   symmetry, $w,_1=\psi_1=0$ (5.1)

$h = .1$ in $x=L/2$: $w=\psi_2=0$

$L = 10.$ in

$q_o = 1000.$ psi   ● $s=0,B$: $\psi_2=w,_2=0$

$$w_{max} = w_c = \frac{4q_o L^4}{\pi^5 D} \sum_m \frac{1}{m^5} \sin \frac{m\pi}{2} , \qquad m=1,3,5,\ldots \qquad (5.2)$$

where $D = \dfrac{Eh^3}{12(1-\nu^2)}$.

Three regular meshes, i.e., each element is the same size, were tested where the idealized width, B, was determined such that each element had an aspect ratio of one. Equivalent linear plane strain boundary conditions modelled the infinite width in the s direction. Symmetry conditions are indicated at x=0 since only one half of the strip length is modelled, see Figure 5.1. Simply supported edges imply freedom of the normal rotation by requiring that the normal moment be zero there. However, the present formulation does not have force dof in the elemental definition and therefore, the normal moment can not be set explicitly to zero; only geometrical simple supports can be satisfied. Although the present formulation does not define resultant force equilibrium relationships, we can approximately satisfy the zero moment condition using the moment definition from classical plate theory, i.e., $M_n=-D[w,_{11} + \nu w,_{22}]$. A displacement finite element formulation based on the classical theory can not satisfy the zero moment simple support condition either unless $w,_{11}$ and $w,_{22}$ are nodal dof. In the classical theory, the second

139

derivatives on w represent rates of change of rotations and thus may be replaced by first derivatives on ψ for the present theory, i.e., for illustration, let $M_n = -D[\psi_{1,1} + \nu\psi_{2,2}]$. If ψ_2 is set to zero along $x=L/2$, then $\psi_{2,2}$ also will equal zero. However, we can not guarantee that $\psi_{1,1}$ will equal zero by allowing ψ_1 freedom and therefore the normal moment along that edge will not be identically zero. The nonvanishing normal moment will affect the displacement calculations near boundary. However, the stress calculations are affected to a greater degree than are the displacements since they are secondary variables determined from the displacements and through the thickness stiffnesses. The inplane dof, u and v, do not play a role in these examples since they are decoupled from the transverse dof in the linear solutions and therefore no boundary conditions are stated for them.

The center plate transverse displacement results for the isotropic case, shown in Table 1, are very accurate even for the coarse mesh and show convergence to the Szilard result based on 100 terms.

Mesh (x X s)	w_c (FEM)	w_c (Szilard, 100 terms)
5x1	48.454	
10x1	48.747	
20x1	48.819	48.828

TABLE 1.   Simply Supported Isotropic Thin Cylindrical Bending Center Transverse Displacement, w_c (in.).

A similar orthotropic thin plate problem was tested where the material and geometrical properties are given in Eqn (5.3) and the boundary conditions in Eqn (5.1). The classical thin plate series solution for w_c is given by Hinrichsen (82) where Eqn (5.2) applies by letting the flexural rigidity, D, be given by Eqn (5.4). Again, the results as shown in Table 2, are very accurate and show no evidence of shear locking.

$$E_1 = 2.5e7 \text{ psi} \qquad\qquad (5.3)$$
$$E_2 = 1.e6 \text{ psi}$$
$$\nu_{12} = .25$$
$$G_{12} = G_{13} = .5e6 \text{ psi}$$
$$G_{23} = .2e6 \text{ psi}$$
$$h = .1 \text{ in}$$
$$L = 10. \text{ in}$$
$$q_o = 1000. \text{ psi}$$

$$D = \frac{Q_{11}h^3}{12}, \qquad\qquad Q_{11} = \frac{E_1^2}{E_1 - \nu_{12}^2 E_2} \qquad (5.4)$$

Mesh (x X s)	w_c (FEM)	w_c (Hinrichsen, 100 terms)
5x1	61.884	
10x1	62.258	
20x1	62.633	62.344

TABLE 2. Simply Supported Orthotropic Thin Cylindrical Bending Center Transverse Displacement, w_c (in.) .

More extensive results were obtained for simply

supported [0/0] and [0/90/0] laminate strips under the sinusoidal transverse pressure loading shown in Eqn (5.5). These two examples were analyzed based on the equations of 3-D elasticity by Pagano (62) and therefore represent excellent tests of the transverse shear deformation characteristic as well as the through the thickness axial displacement, $u_1(\zeta)$, and the two stresses, $\sigma_1(\zeta)$ and $\sigma_5(\zeta)$. These functions are calculated from the displacement dof and the kinematics for $u_1(\zeta)$ and the constitutive relations for $\sigma(\zeta)$. Using the properties of Eqn (5.3), except allowing the thickness to vary (all plies have equal thickness, h=total laminate thickness), the nondimensionalized center transverse displacement, $\bar{w}$, for a 20x1 regular mesh and various S=L/h are given in Table 3. Additionally, the same displacement results are plotted in Figures 5.2 and 5.3 versus the 3-D results obtained by Pagano thus illustrating the effect of transverse shear deformation as the laminates become thick in relation to the length. For both laminates, the classical laminated plate theory (CLPT) solution also reported by Pagano is given by $\bar{w}=.5$.

$$q = q_\circ \sin\left[\pi \frac{(x+L/2)}{L}\right] \tag{5.5}$$

$S=L/h$	$\overline{w}$ [0/0]	$\overline{w}$ [0/90/0]
100	.4939	.5133
50	.5012	.5243
20	.5522	.6012
10	.7333	.8738
5	1.442	1.934

TABLE 3. Finite Element [0/0] and [0/90/0] Nondimensionalized $\overline{w}=100E_2 h^3 w_c/q_o L^4$ Center Displacement.

As the plots show, the transverse shear deformation gives a much more flexible plate for the thick laminates compared to the classical thin strip bending. Additionally, note that even for the very thick strip where the length is only five times the thickness, the present 2-D theory gives excellent displacement agreement with the Pagano 3-D results.
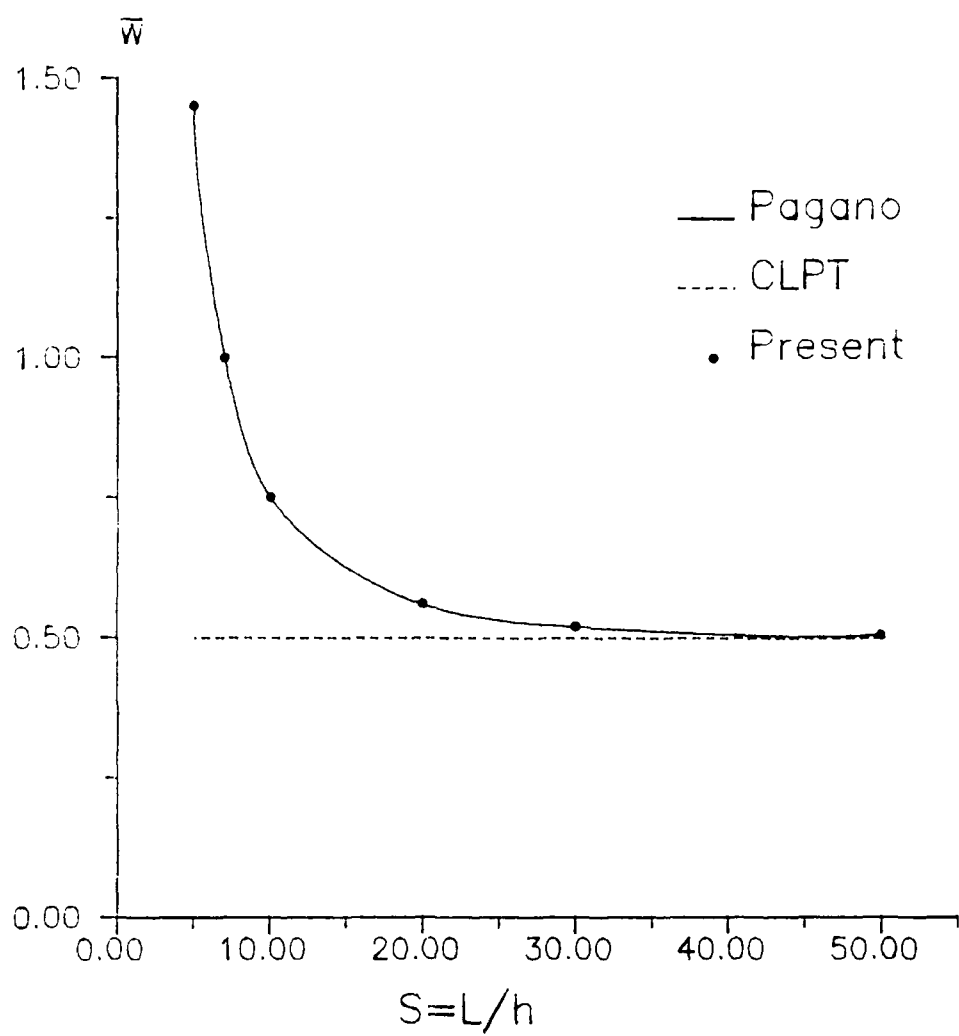
FIGURE 5.2. Nondimensionalized Center Displacement, $\bar{w}$ for Various S=L/h, [0/0] Plate Strip.

144
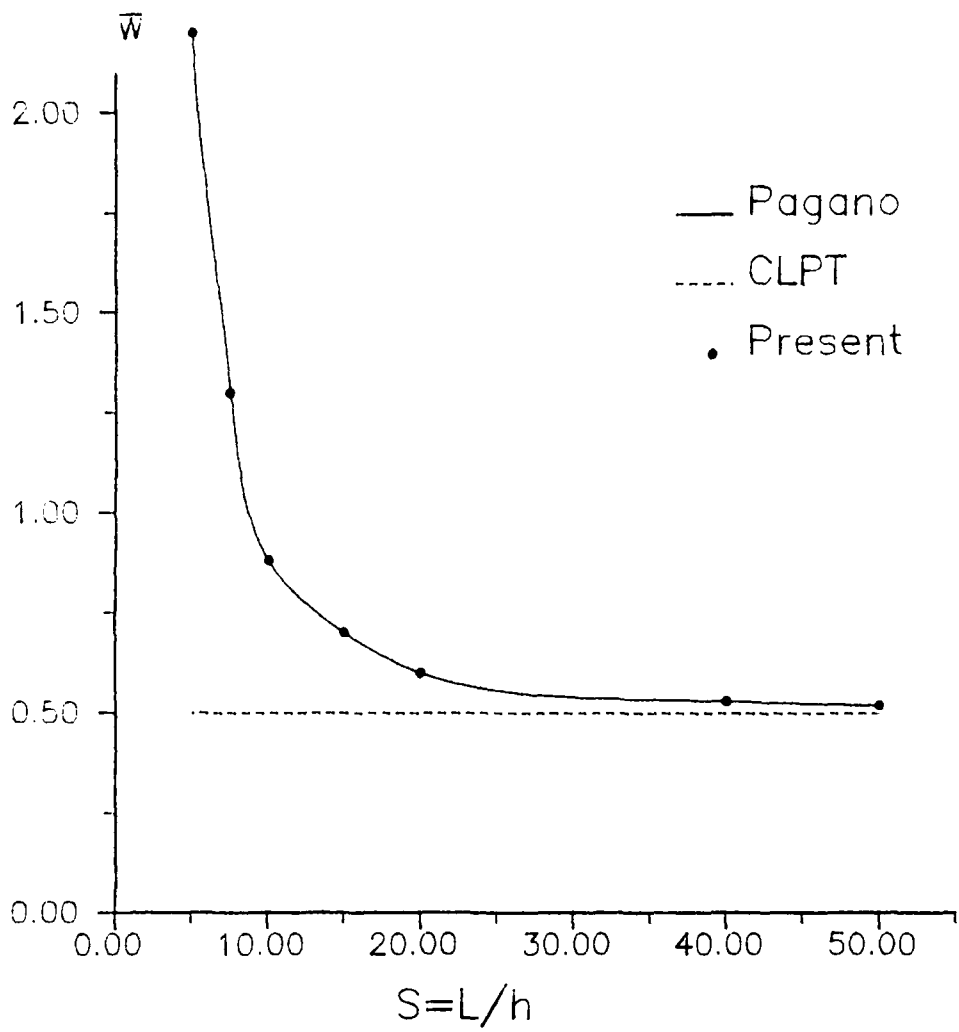
FIGURE 5.3. Nondimensionalized Center Displacement, $\bar{w}$ for Various S=L/h, [0/90/0] Plate Strip.

145

Through the thickness axial displacement and stress results were calculated for these cases as well and compared to the 3-D solutions. Nondimensionalized quantities are defined in Eqn (5.6) for the axial displacement and stresses based on the model geometry of Figure 5.1. That is, for any s coordinate, $\overline{\sigma}_1$ is taken from the center of the strip (x=0) and $\overline{u}$ and $\overline{\sigma}_5$ are taken from the strip boundary (x=L/2). For the [0/0] laminate, Figures 5.4 and 5.5 give stresses $\overline{\sigma}_1$ and $\overline{\sigma}_5$ for S=L/h=4 as a function of the transverse coordinate, ζ. Figure 5.6 gives $\overline{\sigma}_1$ for S=10. For the [0/90/0] laminate, Figures 5.7-5.9 give $\overline{u}$, $\overline{\sigma}_1$, and $\overline{\sigma}_5$ for S=4. Figures 5.10-5.12 give $\overline{u}$, $\overline{\sigma}_1$, and $\overline{\sigma}_5$ for S=10.

$$\overline{\sigma}_1 = \frac{\sigma_1(0,s,\zeta)}{q_o} \qquad \overline{\sigma}_5 = \frac{\sigma_5(L/2,s,\zeta)}{q_o} \qquad (5.6)$$

$$\overline{u} = \frac{E_2 u(L/2,s,\zeta)}{hq_o} \qquad \overline{\zeta} = \frac{\zeta}{h}$$

The results shown in the Figures are plotted versus the 3-D solutions and the results obtained from classical laminated plate theory (CLPT). The transverse stress, $\overline{\sigma}_5$, for CLPT is determined from the equilibrium equations and the CLPT axial displacement is a linear function of ζ. The Figures show that the present theory predicts the displacements and stresses for the unidirectional laminate [0/0] very well. For the [0/90/0] laminate, the normal stress, $\overline{\sigma}_1$, is very well represented and the axial

displacement, $\bar{u}$, fairly well represented, both usually falling between the 3-D and CLPT results. On the other hand, the transverse shear stress, $\bar{\sigma}_5$, is generally poorly predicted for the [0/90/0] laminate, see Figures 5.9 and 5.12. This is an expected result since the present theory does not attempt to satisfy equilibrium in the transverse direction. Pagano enforces continuity of the transverse stresses from ply to ply and therefore can satisfy equilibrium at the ply interfaces. It is well known that the transverse stresses can be found as a function of the transverse coordinate much more accurately from the 2-D shear theories by integrating the equilibrium equations, instead of solving via the constitutive relations (42). The former was not carried out here.

The transverse normal stress, σ_3, for the [0/90/0] laminate was calculated by Pagano based on the 3-D solution. For S=L/h=4, its maximum value ($\zeta=h/2$) is approximately .05 times the maximum σ_1 ($\zeta=h/2$). This is consistent with the general remarks made earlier based on Koiter (22,23) where we would expect σ_1 to be approximately 16 times σ_3 at their maximum values. Very slight deviations from an exactly antisymmetrical solution (with respect to ζ) for σ_1 and u are indicated by Pagano for the [0/90/0] laminate that become more pronounced as S approaches zero. They are only noticeable for S=4 and are not shown, see Ref (62). We can not get a solution in the present case that exhibits this

147

non-antisymmetric nature in σ_1 and u since we do not include σ_3. This is a 3-D effect that is a result of the varying σ_3 through the thickness and nonzero ε_3.

The preceding cylindrical bending examples lead to the following conclusions. Even for a very thick plate strip, the center plate transverse displacement for all cases very closely represents the 3-D result. For unidirectional laminates, the through the thickness functions of axial displacement, axial normal stress, and transverse shear stress are generally very accurate when compared to the 3-D values and usually fall between CLPT and 3-D results. For bidirectional laminates, the axial displacement and axial normal stress are fairly well represented, and again, fall between the CLPT and 3-D results. However, the transverse shear stress, calculated from the constitutive relations, is in error up to approximately 50% due to nonenforcement of transverse equilibrium. To a limited degree, the results illustrate the accuracy that might be expected in more complex problems. Except for $\overline{\sigma}_5$, we see that quantities calculated based on midsurface ($\zeta=0$) dof are generally accurately represented,. For the unidirectional laminates, all through the thickness behavior compares very well to the 3-D result.
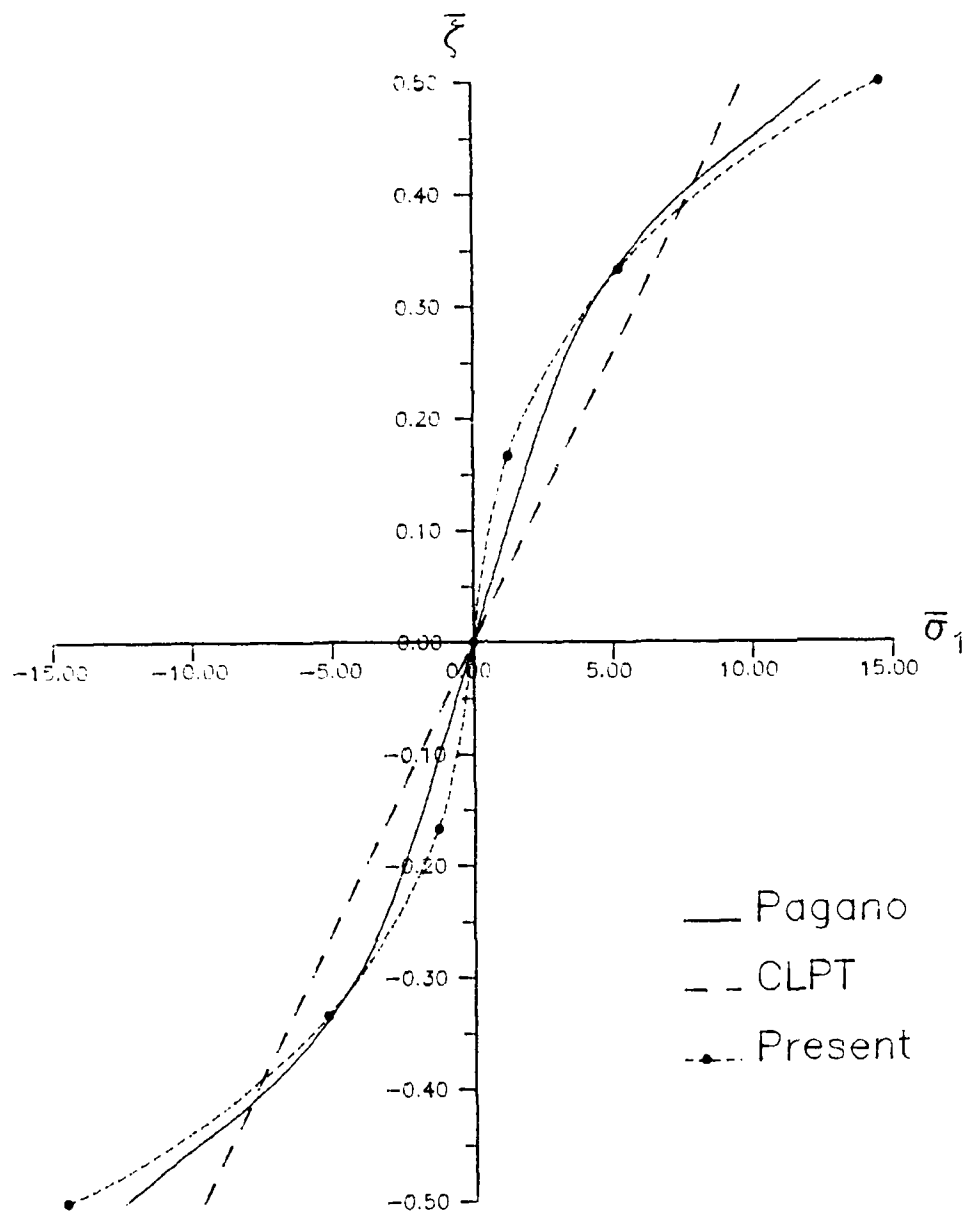
FIGURE 5.4. Nondimensionalized Stress, $\bar{\sigma}_1(\bar{\zeta})$ for [0/0] Plate Strip and S=L/h=4.

149
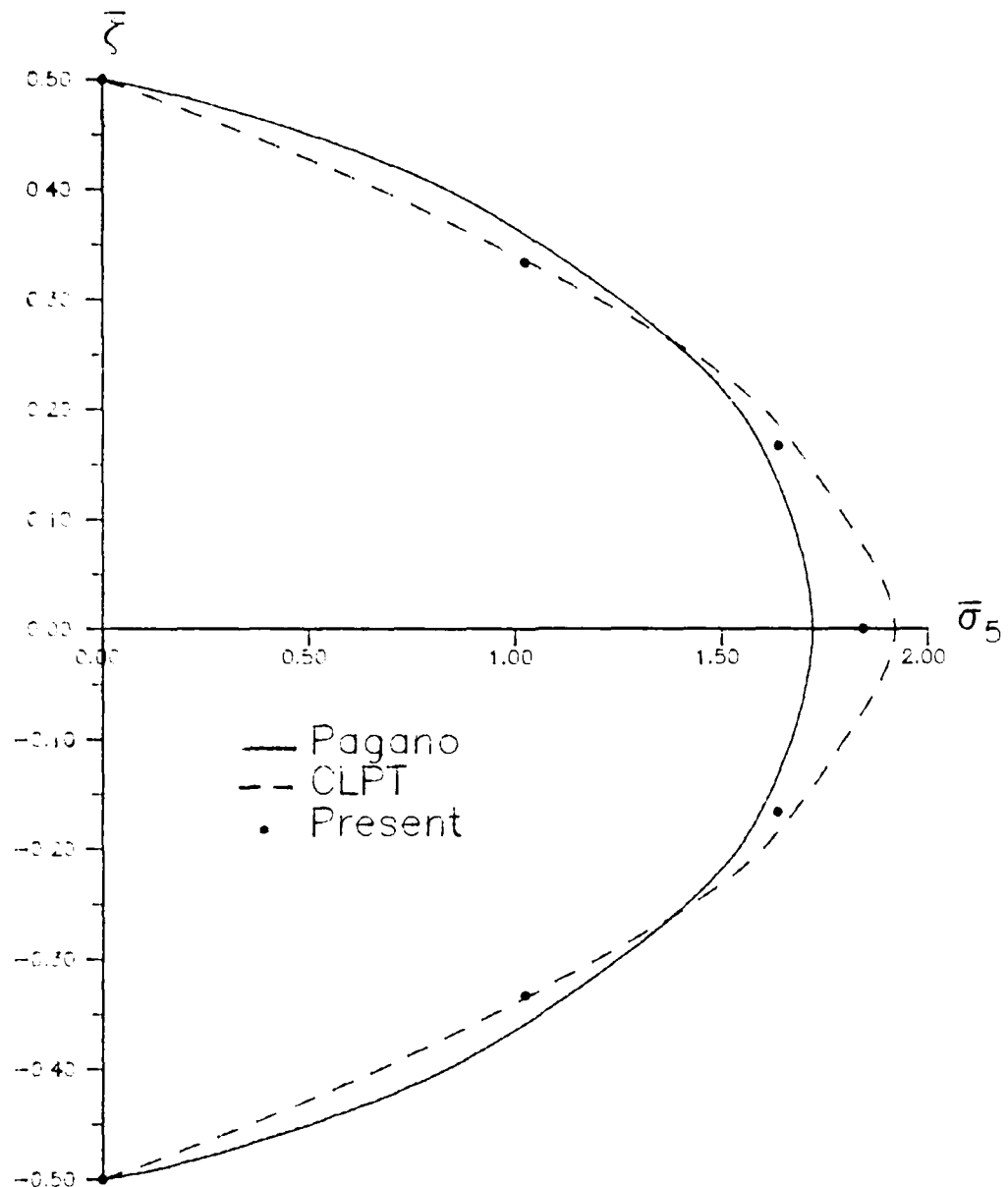
FIGURE 5.5. Nondimensionalized Stress, $\overline{\sigma}_5(\overline{\zeta})$ for [0/0] Plate Strip and S=L/h=4.
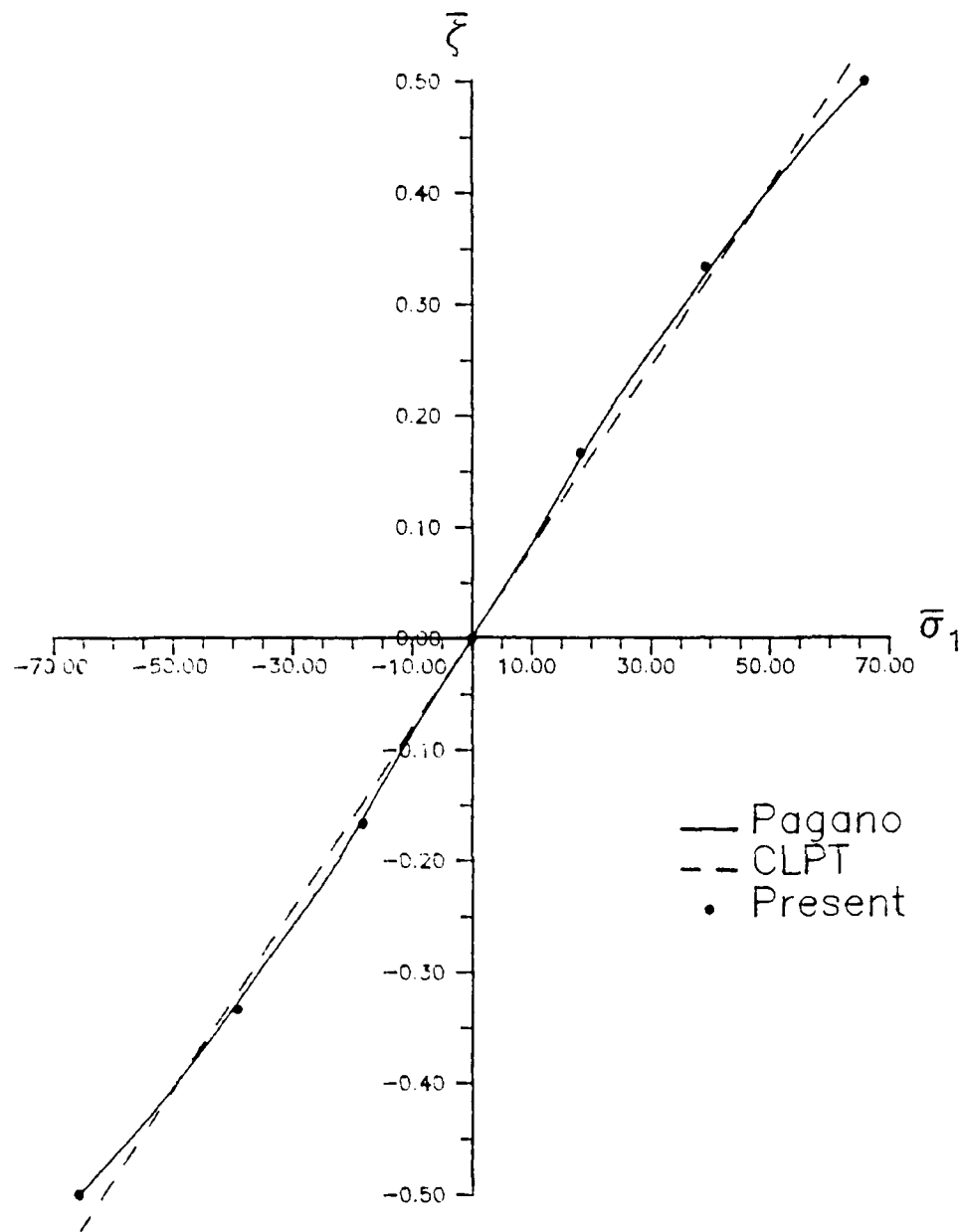
FIGURE 5.6. Nondimensionalized Stress, $\overline{\sigma}_5(\overline{\zeta})$ for [0/0] Plate Strip and S=L/h=10.

151
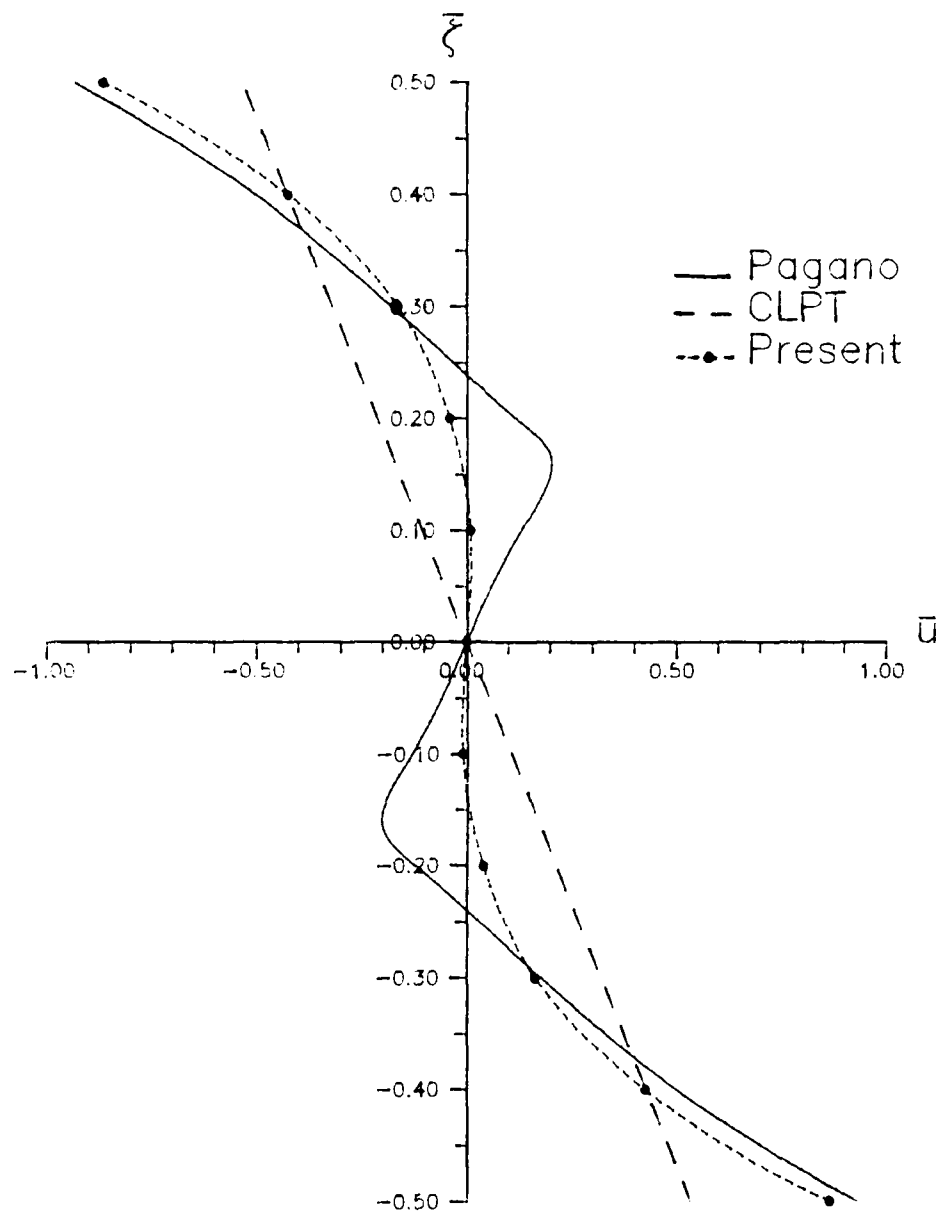
FIGURE 5.7. Nondimensionalized Axial Displacement, $\bar{u}(\bar{\zeta})$, for [0/90/0] Plate Strip and S=L/h=4.

152
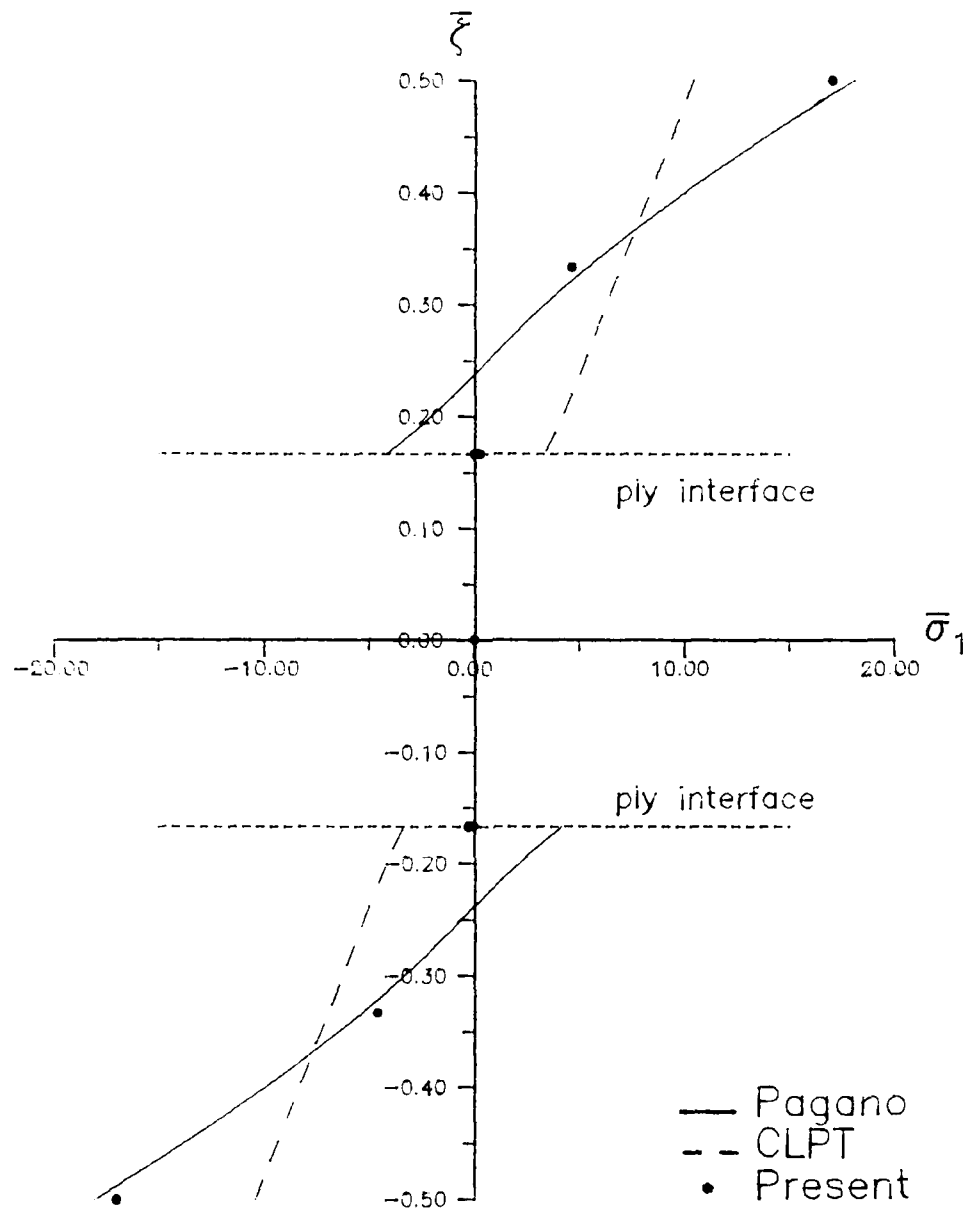
FIGURE 5.8. **Nondimensionalized Stress,** $\bar{\sigma}_1(\bar{\zeta})$, **for** [0/90/0] **Plate Strip and S=L/h=4.**
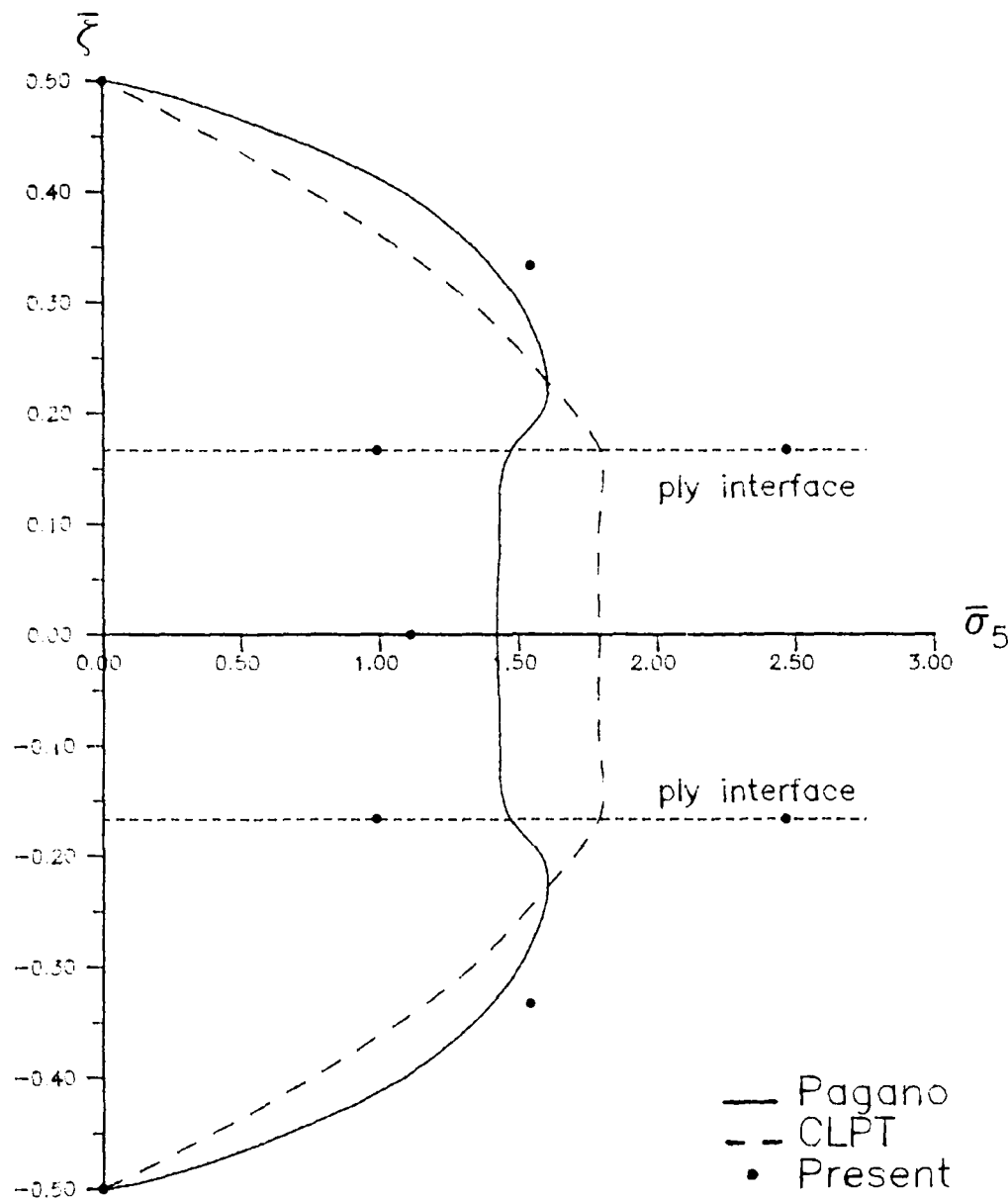
FIGURE 5.9. Nondimensionalized Stress, $\bar{\sigma}_5(\bar{\zeta})$, for [0/90/0] Plate Strip and S=L/h=4.

154
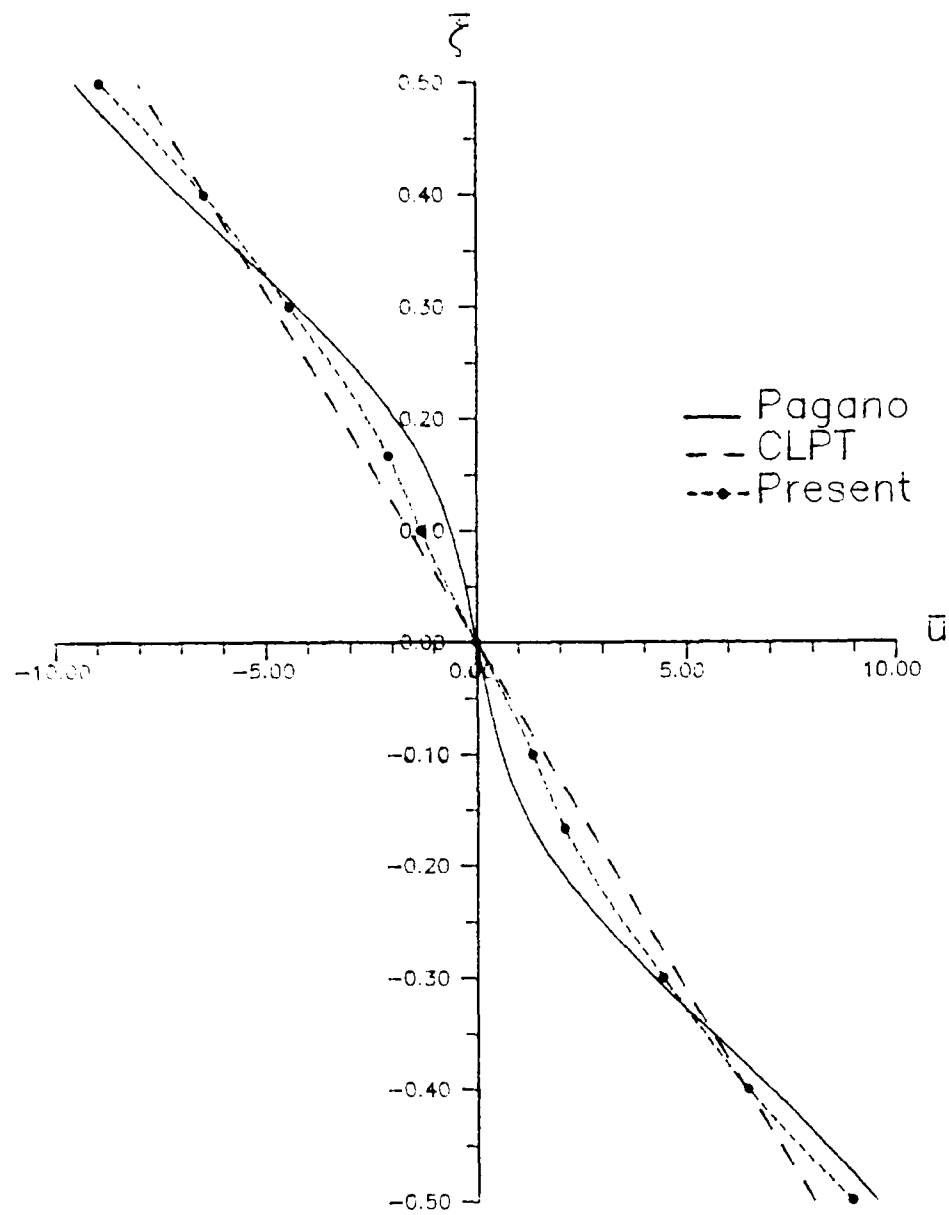
FIGURE 5.10. Nondimensionalized Axial Displacement, $\bar{u}(\bar{\zeta})$, for [0/90/0] Plate Strip and S=L/h=10.
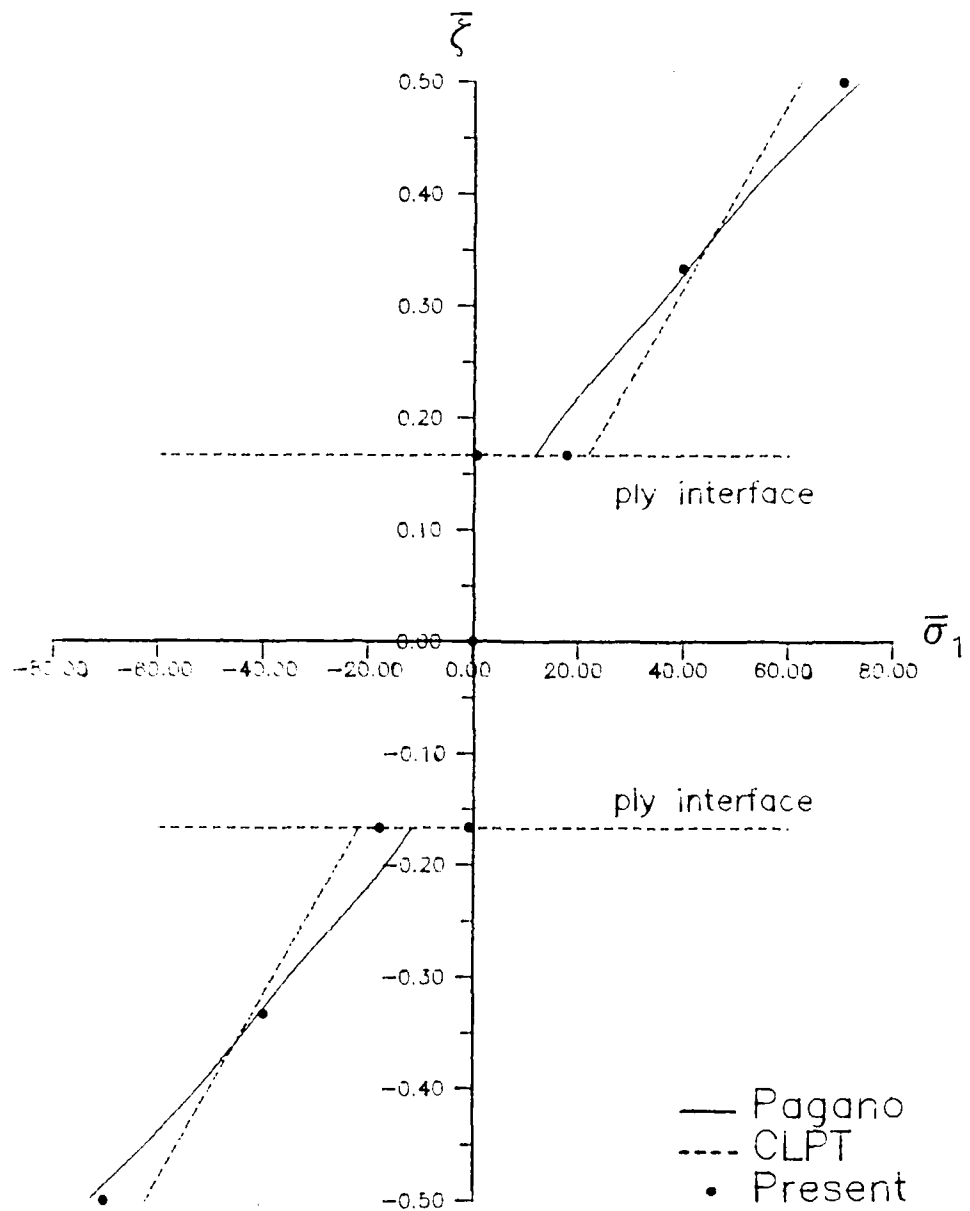
FIGURE 5.11. Nondimensionalized Stress, $\bar{\sigma}_1(\bar{\zeta})$, for [0/90/0] Plate Strip and S=L/h=10.

156
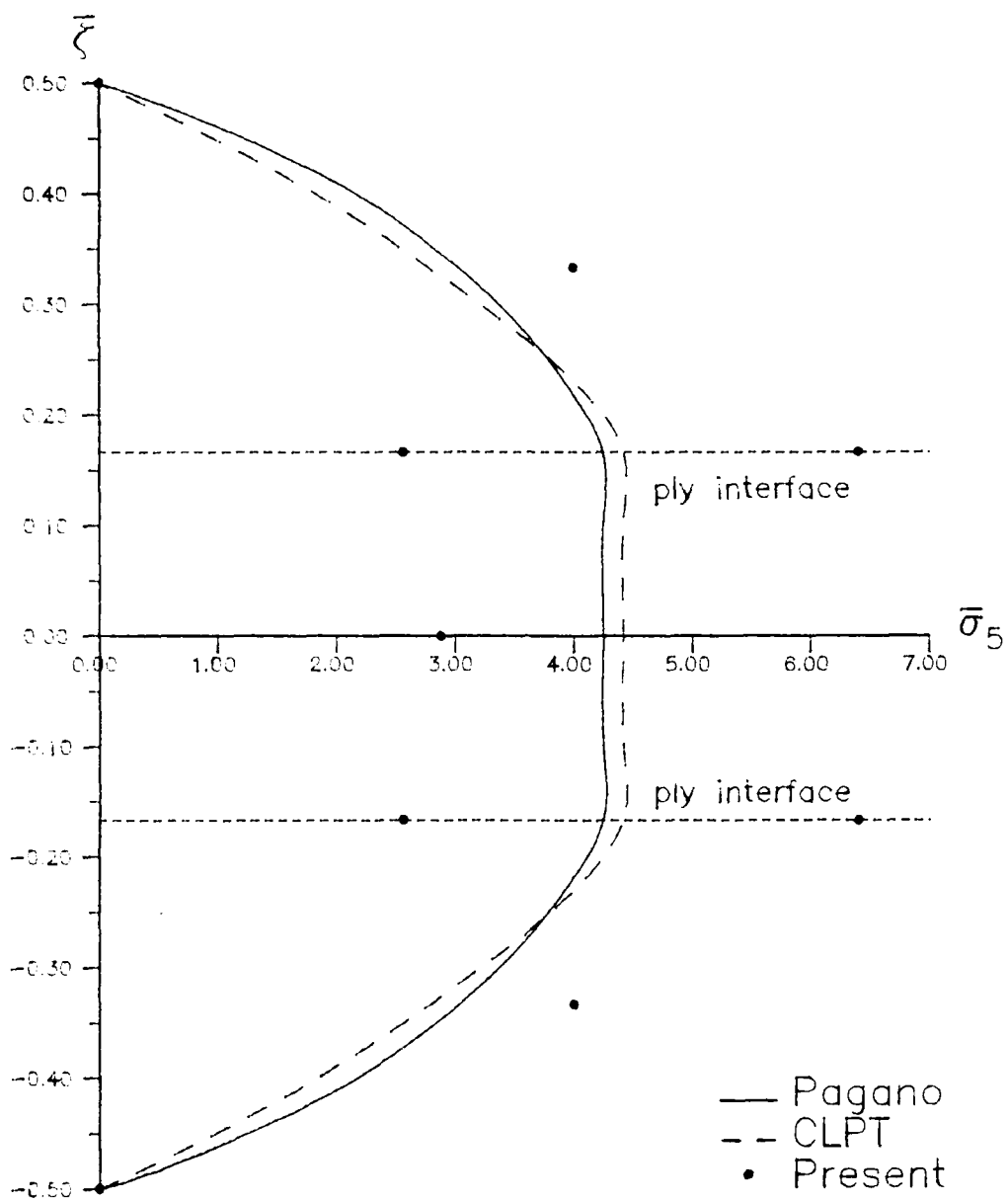
FIGURE 5.12. Nondimensionalized Stress, $\overline{\sigma}_5(\overline{\zeta})$, for [0/90/0] Plate Strip and S=L/h=10.

157

We next consider several transversely loaded finite dimensional plate bending solutions. Figure 5.13 shows the geometry for these cases, where in each only the upper right quarter of the plate is modelled due to symmetry. Although not shown in the results for every case, regular meshes of 4, 16, and 64 elements (2x2, 4x4, and 8x8) were tested for convergence. Additionally, stress results are shown for two cases, where mesh refinement near the plate boundary was required for accurate results.
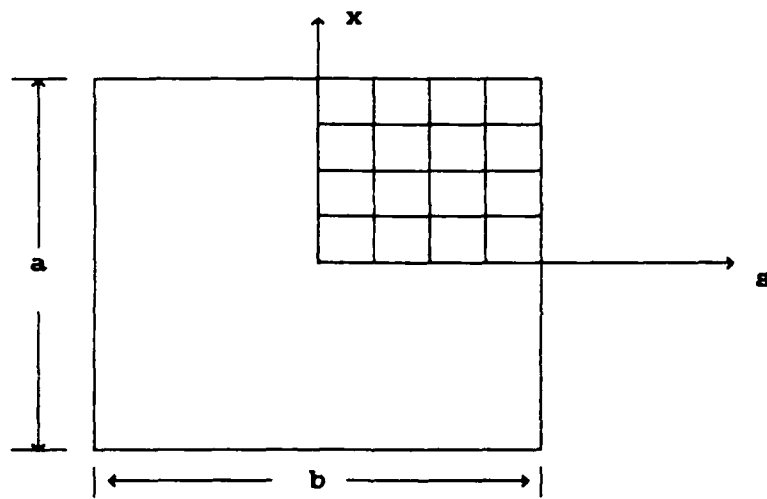
FIGURE 5.13. Rectangular Plate Geometry, Upper Quarter Discretized into 4x4 Regular Mesh.

The first solution presented is to a simply supported rectangular isotropic plate under uniform pressure loading. The material and geometrical properties and the boundary conditions are shown in Eqn (5.7). The simple supports are as described for the cylindrical bending examples, where again, the normal moment can not explicitly be set to zero.

158

$$E= 10.e6 \text{ psi}$$

$$\nu= .3$$

$$h= \text{thickness}$$

$$q_{o}= 10000. \text{ psi}$$

<u>b.c</u>

$\bullet x=a/2: \quad w=\psi_2=0.$

$x=0: \quad \text{symmetry, } w_{,1}=\psi_1=0$ (5.7)

$\bullet s=b/2: \quad w=\psi_1=0.$

$s=0: \quad \text{symmetry, } w_{,2}=\psi_2=0$

Tables 4 (a/b=1.0) and 5 (a/b=.5) show the nondimensionalized center transverse displacement, $\bar{w}=w_c h^3 E/q_o a^4$ ($w_c=w(0,0,\zeta)$), for the aforementioned 3 regular mesh arrangements for 3 values of S=a/h. Also shown are closed form Navier series solutions generated by Reddy (31) based on the parabolic transverse shear theory as well as the CLPT solutions. We see that the results are excellent and that the formulation accurately predicts both thick and thin plate transverse displacements. The results shown were found by exact integration of the elemental stiffness relations, i.e., reduced integration was not required and the formulation does not shear lock.

S=a/h	Mesh	$\bar{w}$ (FEM)	$\bar{w}$ (Reddy)
100	2x2	.02397	
	4x4	.04253	
	8x8	.04425	.0444
10	2x2	.04613	
	4x4	.04662	
	8x8	.04666	.0467
5	2x2	.05378	
	4x4	.05360	
	8x8	.05356	.0535
			CLPT=.0444

TABLE 4.   Transverse Displacement for Simply Supported
Square (a/b=1.0) Isotropic Plate Under Uniform Pressure.

S=a/h	Mesh	$\bar{w}$ (FEM)	$\bar{w}$ (Reddy)
100	2x2	.05020	
	4x4	.10530	
	8x8	.11030	.1106
10	2x2	.11300	
	4x4	.11408	
	8x8	.11419	.1142
5	2x2	.12594	
	4x4	.12505	
	8x8	.12486	.1248
			CLPT=.1106

TABLE 5.   Transverse Displacement for Simply Supported
Rectangular (a/b=.5) Isotropic Plate   Under   Transverse
Uniform Pressure.

160

A problem similar to the previous is a square orthotropic ([0]) plate subjected to uniform transverse pressure. The geometry and boundary conditions are the same as in the isotropic case and the orthotropic material properties are given in Eqn (5.8). Table 6 shows nondimensionalized center transverse displacements and nondimensionalized stress results for three thickness ratios where the nondimensionalization is given in Eqn (5.9).

$$
\begin{aligned}
E_1 &= 20.83e6 \text{ psi} \\
E_2 &= 10.94e6 \text{ psi} \\
\nu_{12} &= .44 \\
G_{12} &= 6.1e6 \text{ psi} \\
G_{13} &= 3.71e6 \text{ psi} \\
G_{23} &= 6.19e6 \text{ psi}
\end{aligned}
\tag{5.8}
$$

$$
\overline{w} = \frac{23.2e6 \; w_c}{q_o h}
$$

$$
\overline{\sigma}_1 = \frac{\sigma_1(0,0,h/2)}{q_o} \;, \quad \overline{\sigma}_5 = \frac{\sigma_5(a/2,0,0)}{q_o}
\tag{5.9}
$$

This problem has been solved by Reddy (31) via a series solution to the differential equations governing the 2-D parabolic shear theory and by Srinvas and Rao (66) based on 3-D elasticity. Similar to the plate strip example, the results even for the transverse shear stress, $\overline{\sigma}_5$, agree very well with the 3-D results. The Table shows $\overline{\sigma}_5$ results based on two mesh arrangements. All results are due to an 8x8 mesh, but some reflect stresses calculated from an irregular

8x8 mesh, see Figure 5.14. That is, the value of $\bar{\sigma}_5$ was desired from the plate coordinate (a/2,0). The value found based on a regular mesh as shown in Table 6 is generally inaccurate compared to Reddy and the 3-D result. In view of the inability of the present formulation to identically satisfy the zero normal moment condition along a simply supported edge as was previously discussed, mesh refinement near those edges was attempted. As can be seen, the stress results improve dramatically after mesh refinement, very accurately duplicating the published results.

		S=a/h		
		20	10	7.143
$\bar{w}$	FEM	10447.5	689.80	191.71
	Reddy	10450.0	689.5	191.6
	3-D	10443.	688.57	191.07
$\bar{\sigma}_1$	FEM	144.6	36.12	18.41
	Reddy	144.3	36.01	18.34
	3-D	144.31	36.021	18.346
$\bar{\sigma}_5$	FEM	8.657	5.067	3.703
	FEM *	10.77	5.27	3.792
	Reddy	10.85	5.382	3.805
	3-D	10.873	5.341	3.731

* Irregular mesh, refined near (a/2,0)

TABLE 6. Simply Supported Square [0] Laminate Under Uniform Transverse Pressure, 8x8 Mesh.
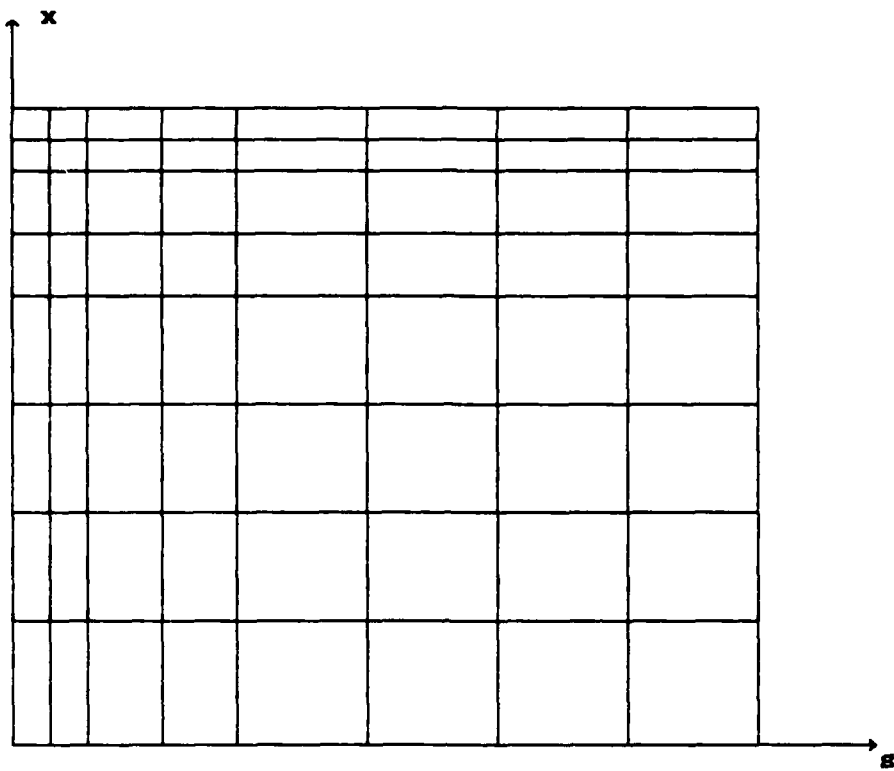
FIGURE 5.14. Rectangular Plate Geometry Irregular Mesh for Stress Calculation Near the Boundary.

Next, examine a simply supported [0/90/0] rectangular (a/b= 1/3) plate under sinusoidal transverse pressure, see Eqn (5.10). This problem has been solved using a Navier series by Reddy (31) based on the parabolic shear theory and by Pagano (64) based on 3-D elasticity and thus represents an excellent validation for a nonsquare bidirectional laminate. Eqn (5.11) shows the material properties and the center transverse displacement nondimensionalization. The results are shown in Table 7 where, again, various S=a/h values are shown exhibiting the shear deformation effect.

163

The results further confirm that the finite element linear flat plate algorithm is operating properly and that the parabolic transverse shear assumption gives excellent displacement comparison to the 3-D results, even for the very thick plate. The elemental equations are again always integrated exactly and do not shear lock.

$$q = q_o \sin \frac{\pi}{a} (x+a/2) \sin \frac{\pi}{b} (s+b/2) \qquad (5.10)$$

$E_1 = 37.5e6 \text{ psi}$

$E_2 = 1.5e6 \text{ psi}$ $\qquad (5.11)$

$G_{12} = G_{13} = .75e6 \text{ psi}$

$\nu_{12} = .25$ $\qquad \bar{w} = \dfrac{100 w_c h^3 E_2}{q_o a^4}$

$G_{23} = .3e6 \text{ psi}$

$q_o = 10000. \text{ psi}$

$a = 8. \text{ in}, \ b = 24. \text{ in}$

S=a/h	$\bar{w}$	Reddy	Pagano
4	2.6465	2.6411	2.82
10	.8638	.8622	.919
20	.5945	.5937	.610
100	.5066	.5070	.508
		CLPT = .503	

TABLE 7. Simply Supported Rectangular [0/90/0] Plate (a/b=1/3) Under Sinusoidal Transverse Pressure, 8x8 Mesh.

Additional stress results were generated for a [0/90/90/0] square simply supported, see Eqn (5.7), plate under sinusoidal pressure, see Eqn (5.10). The material and

geometrical properties are given in Eqn (5.11) with a=b=8. Nondimensionalized values of displacement and stresses as defined by Eqn (5.12) are shown in Table 8. Also shown are results obtained by Phan and Reddy (58) based on a closed form Navier series solution. In order to accurately predict the transverse shear stresses, $\bar{\sigma}_4$ and $\bar{\sigma}_5$, refinements to the mesh near the area of calculation were required similar to in the unidirectional case. Comparisons are again very good and the effect of the irregular mesh stress calculations is evident from the Table, see especially the $\bar{\sigma}_4$ and $\bar{\sigma}_5$ results for S=100.

$$\bar{w} = \frac{100 w_c h^3 E_2}{q_o a^4} \qquad \bar{\sigma}_1 = \frac{\sigma_1(0,0,h/2) \ h^2}{q_o a^2}, \quad \bar{\sigma}_5 = \frac{\sigma_5(a/2,0,0) \ h}{q_o a}$$

$$\bar{\sigma}_2 = \frac{\sigma_2(0,0,h/2) \ h^2}{q_o a^2}, \quad \bar{\sigma}_4 = \frac{\sigma_4(0,a/2,0) \ h}{q_o a} \qquad\qquad (5.12)$$

$$\bar{\sigma}_6 = \frac{\sigma_6(a/2,a/2,h/2) \ h^2}{q_o a^2}$$

$S=a/h$		$\bar{w}$	$\bar{\sigma}_1$	$\bar{\sigma}_2$	$-\bar{\sigma}_6$	$\bar{\sigma}_4$	$\bar{\sigma}_5$
10	FEM	.7169	.5499	.3868	.0253	.1376	.2598
	FEM*					.1453	.2611
	Navier	.7147	.5456	.3888	.0268	.1431	.2640
20	FEM	.5068	.5428	.3018	.0221	.09675	.2603
	FEM*					.1152	.2764
	Navier	.5060	.5393	.3043	.0228	.1234	.2824
100	FEM	.4295	.5282	.2652	.0209	-.2351	.0325
	FEM*					.0971	.2810
	Navier	.4343	.5387	.2708	.0213	.1117	.2897

* Irregular mesh, refined near area of calculation

TABLE 8. Simply Supported [0/90/90/0] Square Plate Under Sinusoidal Transverse Pressure, 8x8 Mesh.

The final linear flat plate example is a square clamped $[0/\pm45/90]_s$ laminate under both uniform and sinusoidal pressure loading. Closed form solutions are difficult for this problem due to the clamped boundary conditions and the presence of D_{16} and D_{26} terms in the equilibrium equations resulting from the ±45 plies. Phan and Reddy (58) use a similar displacement based finite element formulation and their results are compared to the present solutions in Table 9. The material and geometrical properties and boundary conditions are shown in Eqn (5.13). The clamped boundary conditions do allow some movement at the edges. The bending rotations, ψ_1 and ψ_2, are restrained thus the development of edge moments is allowed. However, since both of the derivatives of w are not set to zero, shear rotations at the boundary may develop. For example, w=0 along x=a/2. This

166

implies that $w_{,2}$ is also zero along that edge. However, since $w_{,1}$ is not set to zero and ψ_1 is, a shear rotation, $\beta_1 = w_{,1}$, will generally be present, see Figure 3.7.

The nondimensionalized (Eqn (5.11)) center transverse displacement for several values of $S = a/h$ compares very well with those published by Phan and Reddy. The results shown were generated using a 4x4 mesh for one quarter of the plate as did Phan; the latter also evaluated the elemental stiffnesses based on a lower integration order, and hence, their results are slightly more flexible than in the present case as is expected. The reference, as mentioned and duplicated here, assumes symmetry in their plate model. However, the presence of the D_{16} and D_{26} terms as a result of the ±45 degree plies gives bending-twisting coupling. This coupling should preclude the biaxial symmetry that is forced due to the boundary conditions. Further discussion of biaxial symmetry can be found in (88,134,135). Since validation of the code versus published results is the primary goal here, similar boundary conditions have been assumed.

$E_1 = 60.e6$ psi   <u>b.c.</u>

$E_2 = 1.5e6$ psi   @x=a/2: $w = \psi_1 = \psi_2 = 0$

$G_{13} = G_{12} = .9e6$ psi   x=0:   symmetry, $w_{,1} = \psi_1 = 0$

$\nu_{12} = .25$ @s=b/2: $w = \psi_1 = \psi_2 = 0$

$G_{23} = .75e6$ s=0:   symmetry, $w_{,2} = \psi_2 = 0$

$q_o = 10000.$

$a = b = 16.$ in   (5.13)

S=a/h	uniform load		sinusoidal load	
	$\bar{w}$	Phan	$\bar{w}$	Phan
100	.0947	.0960	.0690	.0699
50	.1094	.1108	.0787	.0798
20	.1848	.1864	.1280	.1292
10	.3871	.3890	.2601	.2615
4	1.4624	1.4648	.9759	.9772

TABLE 9. Clamped Square $[0/\pm45/90]_s$ Plate Under Uniform and Sinusoidal Pressure, 4x4 Mesh.

As the many examples above point out, the linear flat plate algorithm is giving very accurate displacement and stress results, for the most part. The formulation, due to its higher order approximations for w, does not shear lock, and therefore, the artifice of inexact integration to soften the element is not required. The cases presented show the effect of the formulation's inability to satisfy identically the zero normal moment boundary condition for a simply supported edge. After accounting for this shortcoming, very good midsurface displacement and stress solutions are attainable. By comparing the thick plate solutions to existing 3-D solutions, we see that, at least for the linear flat plate, the 2-D simplifying assumptions are well justified. In nearly every case, convergence was monotonic but showed no clear pattern converging from either a too stiff or a too flexible solution, see Tables 4 and 5. This

is a direct result of the nonconforming interpolations of the transverse displacement w.

Linear Cylindrical Shell Analysis

Several standard linear cylindrical shell problems were analyzed in an effort to validate the finite element solution for the curved elements. The first test case involves a clamped shallow shell where membrane action has little influence on the deformation and consequently, the simpler 28 dof element with linear inplane displacement approximations, performs well. However, as the examples that follow show, the 28 dof element proved inadequate for shell behavior governed by a greater amount of membrane deformation, and in these cases the 36 dof element with quadratic inplane displacement approximations is required. After validation of the curved 36 dof element, new linear shell results were generated considering the effects of transverse shear deformation. For all results presented in this section as in the previous, the elemental stiffnesses have been integrated exactly.

Consider an isotropic clamped shallow shell under a uniform radial pressure distribution as shown in Figure 5.15. This shell problem has been solved based on the classical Love assumption neglecting transverse stresses and on the shallow shell Donnell strain displacement assumptions by Brebbia and Connor (136). Only one quarter of the panel is modelled due to symmetry and the boundary conditions are

169

shown in Eqn (5.14). Note that for the shell structures, since the inplane dof are coupled with the transverse dof, boundary conditions are generally stated for u and v as well as the other displacements.

$$\bullet x=10: \quad u=v=w=w,_1=w,_2=\psi_1=\psi_2=0$$

$$x=0: \quad \text{symmetry, } u=w,_1=\psi_1=0$$

$$\bullet s=10: \quad u=v=w=w,_1=w,_2=\psi_1=\psi_2=0 \qquad (5.14)$$

$$s=0: \quad \text{symmetry, } v=w,_2=\psi_2=0$$

E=4.5e6psi
$\nu=.3$
$\theta=.1$ rad
R=100. in
h=.125 in
$q_o=.04$ psi
L=20. in
$\delta/b = .0496$
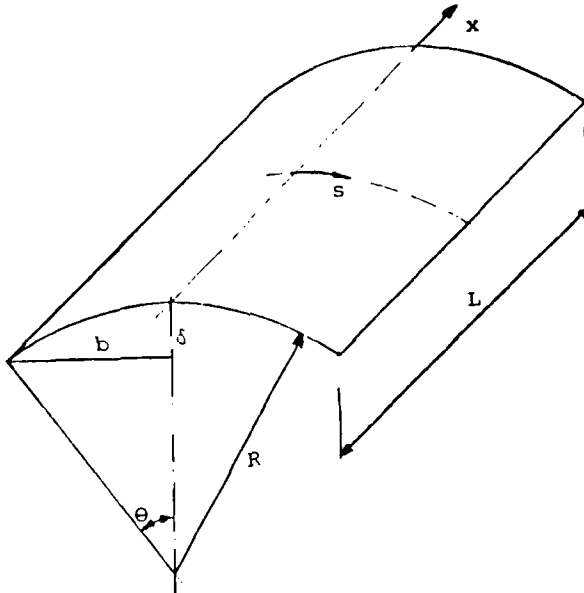
FIGURE 5.15. Isotropic Clamped Cylindrical Shell Under Uniform Radial Pressure.

For this shell geometry, the ratios L/h=160 and R/h=800 define a thin shell, and hence, since transverse shear deformation is probably minimal, results for the present case should compare well with the published results. Center transverse (radial) displacement calculated from three regular mesh arrangements are shown for both the 28 dof and

170

36 dof element formulations in Table 10. Examining the results, note that the 16 element (4x4) mesh is nearly converged, and that the convergence is not monotonic, i.e., the 4x4 mesh gives the largest values for displacement. In the linear flat plate problems, all convergence was monotonic although not always from a stiffer solution. Both the 28 and 36 dof meshes converge to comparable results to those of Brebbia and Connor.

This test case represents a relatively simple shell problem since due to the pressure loading, clamped boundary conditions, and shallow geometry ($\delta/b=.0496$), bending deformation is much greater than membrane deformation. Therefore, lower order approximations for the inplane displacement dof, u and v, are adequate since these displacements do not play a significant role.

Mesh	$\overset{w}{36}$ dof	$\overset{w}{28}$ dof
2x2	.004685	.004585
4x4	.01167	.01139
8x8	.01144	.01136
Brebbia and Connor		.011

TABLE 10. Transverse Center Displacement (in.) for Clamped Cylindrical Shell Under Radial Pressure.

A more challenging shell example is the barrell vault loaded by its own weight shown in Figure 5.16. This shell
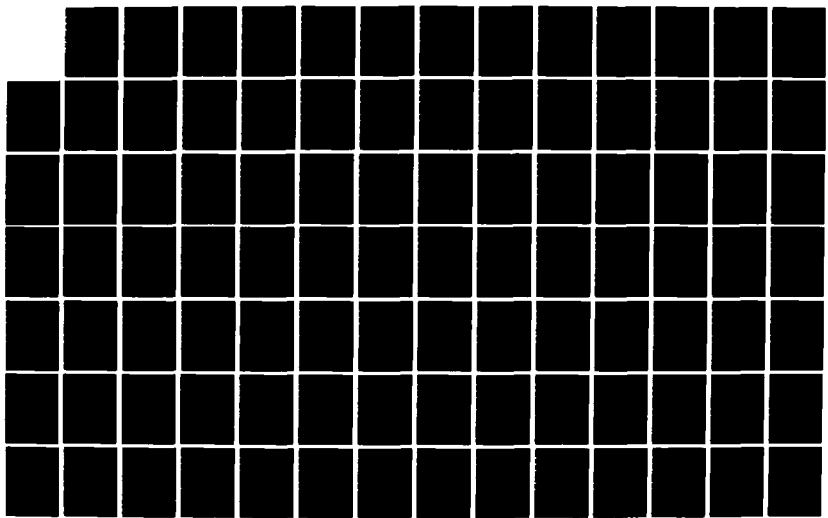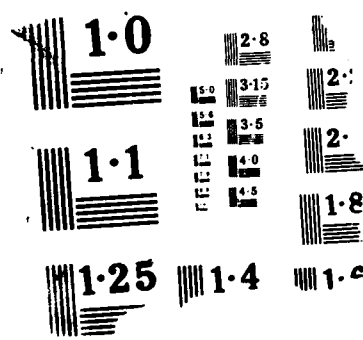
problem, a popular testcase, has a practical application in that it is a typical roofing component. Due to symmetry, only one quarter of the vault is discretized. The boundary conditions are given in Eqn (5.15) where the longitudinal edges are free and a diaphragm restrains the circumferential edges. The diaphragm restraint does not allow any movement in its own vertical plane. The loading in this case is always directed downward and therefore has components circumferentially as well as radially as opposed to the previous shell case where the pressure was directed only radially. For a flat plate, weight loads and radial pressure always acted in the same direction. The deadweight loading can be expressed in components, q_s and q_ζ, as shown in Eqn (5.16) for coordinate directions s and ζ respectively.

E=3.e6
ν=0.0
θ=.698 rad
R= 25.ft
h=.25 ft
q_o=.625 psi

L=50. ft

δ/b=.364
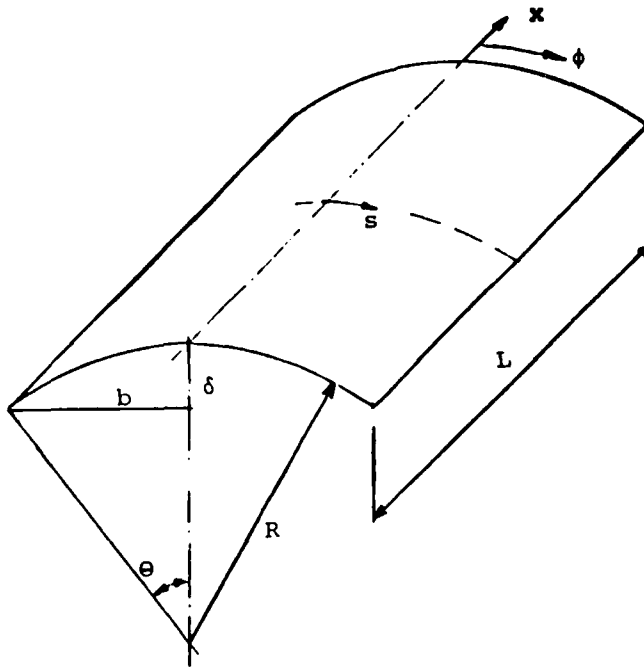
FIGURE 5.16. Isotropic Barrell Vault Under Its Own Weight.

$$\bullet x=25 \quad (\text{diaphragm}): \quad v=w=\psi_2=0 \qquad (5.15)$$

$$x=0: \quad \text{symmetry}, \quad u=w,_1=\psi_1=0$$

$$\bullet s=0: \quad \text{symmetry}, \quad v=w,_2=\psi_2=0$$

$$q_s = q_o \sin (s/R) \qquad (5.16)$$

$$q_\zeta = q_o \cos (s/R)$$

The ratios, L/h=200 and R/h=100, again define a thin shell and transverse shear deformation should be minimal. However, due to the longitudinal free boundary condition, partial inplane loading, and nonshallow geometry (δ/b=.364), membrane action should be more significant for this case than in the previous. Bending still is predominant due to

173

the diaphragm restrained edges. The transverse displacement results for two points of the shell are shown for various meshes in Table 11, where designation 'L' refers to the 28 dof element and 'Q' refers to the 36 dof element. The first displacement shown is the displacement of the crown or center of the vault and the second shown is the shell's maximum radial displacement taken from the center of the free edge. Also shown are published results taken from Scordelis and Lo (137).

An obvious observation is the overly stiff displacements predicted by the 28 dof element meshes. The more refined 8x12L mesh gives results that show the correct trend but are still very stiff. On the other hand, the 36 dof element with the quadratic approximations for u and v show much better comparisons even for the coarse 3x3Q mesh.

Mesh	w_{crown}	w_{max}
8x8L	.1462	.7774
8x12L	.02439	1.253
3x3Q	-.1808	2.537
6x6Q	-.5046	3.853
6x9Q	-.5238	3.921
Scordelis Lo	-.552	3.696

TABLE 11. Transverse Displacement Results (in.) for Barrell Vault.

174

Figure 5.17 shows radial displacement, w, as a function of circumferential angle, ϕ, at x=0. Figure 5.18 shows the inplane displacement, u, as a function of ϕ at x=25. These Figures further confirm the overly stiff predictions resulting from meshes of the 28 dof element. Also shown are results taken from Zienkiewicz (70) based on an isoparametric curved shell formulation.

A final comment on the barrell vault problem concerns the linear Donnell equations. These equations, formulated in Appendix B, were applied to the 36 dof element meshes of Table 11 and results for the transverse displacement were within 1% of those shown. This indicates that, although the Donnell equations are applicable only for shallow open shell cases, a finite element mesh of Donnell elements gives accurate results for a nonshallow barrell vault.
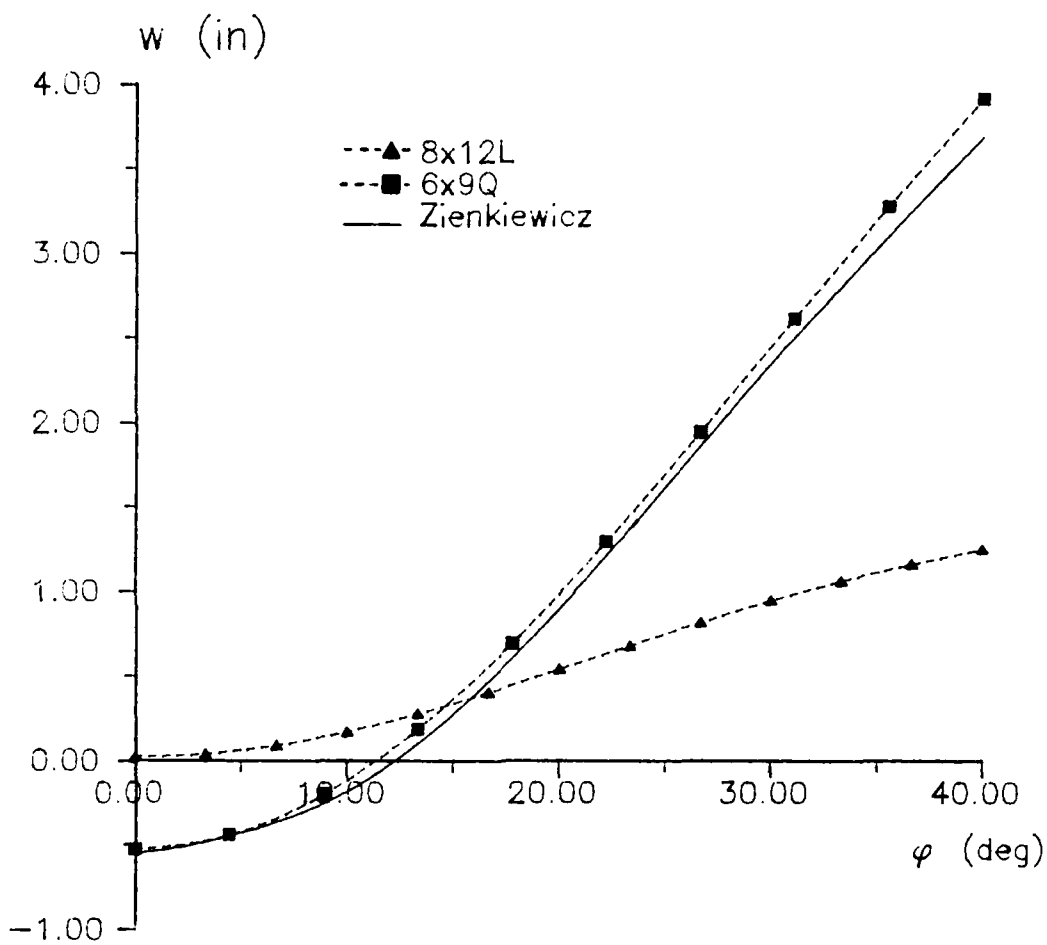
FIGURE 5.17. Radial Displacement, w, as a Function of Circumferential Angle, ϕ deg, (x=0).
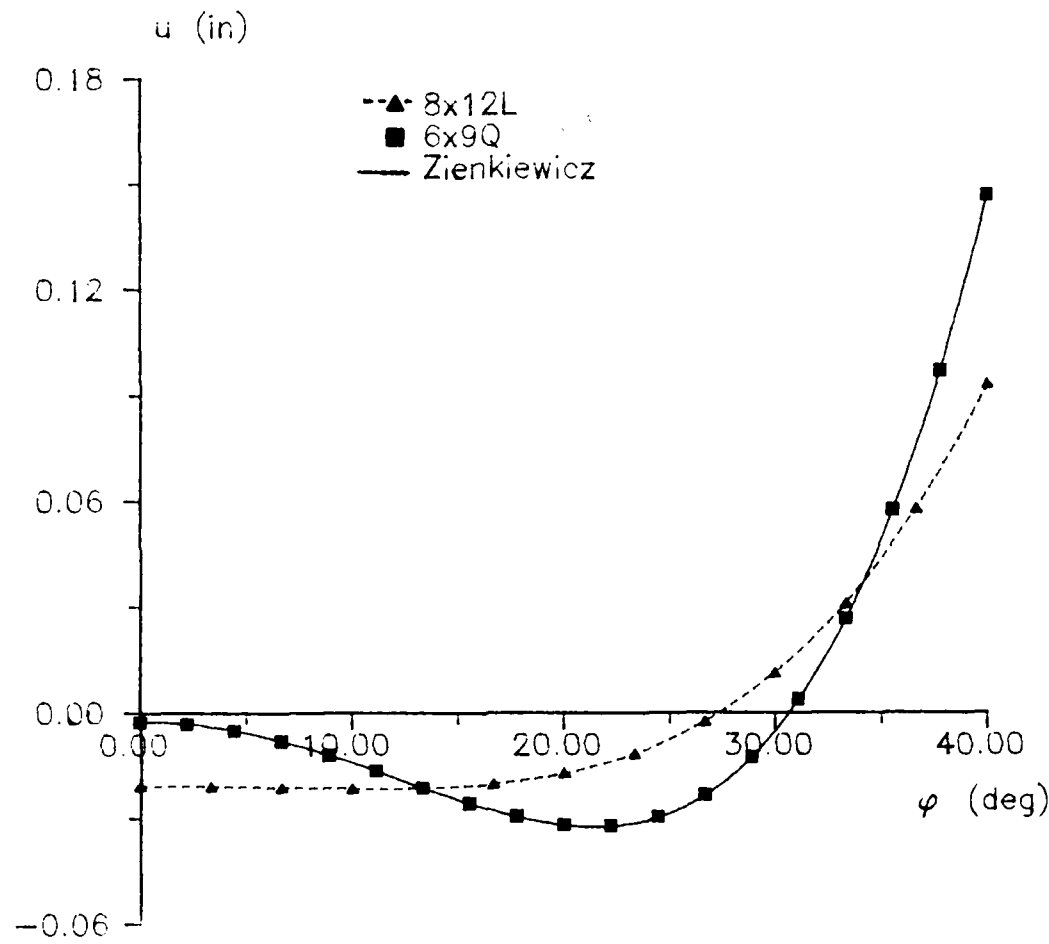
FIGURE 5.18. Inplane Displacement, u, as a Function of Circumferential Angle, ϕ deg, (x=25).

177

Another popular testcase is the pinched cylinder shown in Figure 5.19. The cylinder is acted upon by self equilibrating point loads, P. Due to symmetry, only one octant of the cylinder is discretized and the symmetry boundary conditions are given in Eqn (5.17). As in the previous problem, meshes of either the 28 or the 36 dof element were tested.

E=10.5e6 psi
ν=.3125
R=4.953 in
h=.094 in
P=100 lbs
L=10.35 in
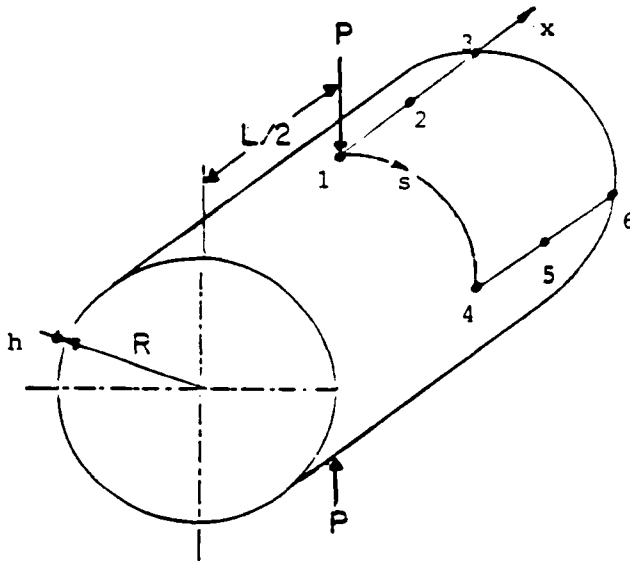
FIGURE 5.19. Isotropic Pinched Cylinder.

$$
\begin{aligned}
&\bullet x=0: \quad \text{symmetry, } u=w,_1=\psi_1=0 \\
&\bullet s=0,7.7802: \quad \text{symmetry, } v=w,_2=\psi_2=0
\end{aligned}
\qquad (5.17)
$$

The radial displacement, w, for six points (numbered 1-6 in Figure 5.19) is shown in Table 12. Also shown are results obtained by Brockman (79) using a penalty function finite element approach and the inextensible solution derived by Timoshenko (138). As is now known, the 28 dof element, designated by "L", can only be used to predict the

178

behavior of a cylindrical shell where membrane deformation is small. The pinched cylinder results show that the already very refined 4x16L mesh is still much too stiff. The 36 dof element meshes, again designated by a 'Q', show convergence to the results obtained by others. Because of rapidly changing bending stress circumferentially, refinements to the mesh were much more important in this coordinate direction than in the longitudinal direction.

Mesh	Point					
	1	2	3	4	5	6
4x16L	.02482					
4x3Q	.01405	.01337	.01337	-.01253	-.01256	-.01262
4x6Q	.07726	.07548	.07488	-.06939	-.06952	-.07005
4x9Q	.1016	.09907	.09815	-.09136	-.09143	-.09190
4x12Q	.1078	.1049	.1039	-.09680	-.09685	-.09732
*	.1074	.1040	.1031	-.0967	-.0968	-.0970
**	.1084	.1084	.1084	-.1000	-.1000	-.1000

TABLE 12. Isotropic Cylinder Transverse Displacement Results (in.). * Brockman, ** Timoshenko

Based on the three cylindrical shell testcases, we conclude that the 28 dof element is generally too stiff and should not be used to model the curved geometries. Additionally, the 36 dof element predicts the cylindrical shell response very well for the standard cases tested and therefore the linear shell algorithm is considered validated.

179

Similar to that done in the flat plate cases, a transverse shear deformation study was carried out on two cylindrical shell geometries. In these studies, only the shell thickness was varied, keeping the lengths and radii constant. In this way, a change in thickness would result not only in a change in $S=L/h$ as in the plate case, but also in the ratio R/h. A more complete parametric study would examine changes in all three parameters, h, L, and R.

Consider again the pinched isotropic cylinder of Figure 5.19. Using the 4x12Q mesh and the boundary conditions of Eqn (5.17), the transverse displacement, w, directly under the point load is determined for many shell thicknesses. These results are then normalized by dividing by the inextensible center displacement solution of Timoshenko, shown in Eqn (5.18) where D is the flexural rigidity. For various $S=L/h$ values, the ratios, $\bar{w}$, of the present transverse displacement to the Timoshenko value are shown in Table 13 and plotted in Figure 5.20. The results show that for small values of S, the finite element results are increasingly more flexible due to transverse shear deformation. Additionally, for large values of S, the finite element solution gives stiffer results compared to Timoshenko, i.e., $\bar{w}<1$. The inplane displacements, u and v, play a greater role in the deformation of the thinner shells, i.e., where S is large, since membrane behavior becomes more significant. Timoshenko's solution is based on

inextensibility, i.e., u and v are zero at the midsurface.

The answer to why the finite element results are increasingly stiffer than the inextensible results for larger S can be found by examining the classical cylindrical shell formulation that allows both bending and membrane deformation. Solutions to these differential equations for similar loadings, see Saada (6) for example, give the membrane contribution to the transverse displacement as a negative linear function of l/h. Therefore, membrane deformation is only important for small thickness and gives transverse displacements that are less than the inextensible solution. The negative linear function seen in Figure 5.20 for large S is due to membrane deformation. Due to the nature of the applied loading, the midsurface is in a state of tension, thus the stiffer solution. An additional conclusion of this study is important in later problems as well as in the present. Since u and v are always included in the shell formulation, solutions that assume an inextensible midsurface (where one does not actually exist) can not be duplicated.

$$w = \frac{.149 \ PR^3}{2DL} \qquad (5.18)$$

$S=L/h$	$\bar{w}$
320	.8300
280	.8649
240	.8981
180	.9441
140	.9722
110	.9930
80	1.016
55.05	1.043
27.53	1.108
13.76	1.241

TABLE 13. Center Transverse Displacement Normalized by Inextensible Solution for Pinched Cylinder.
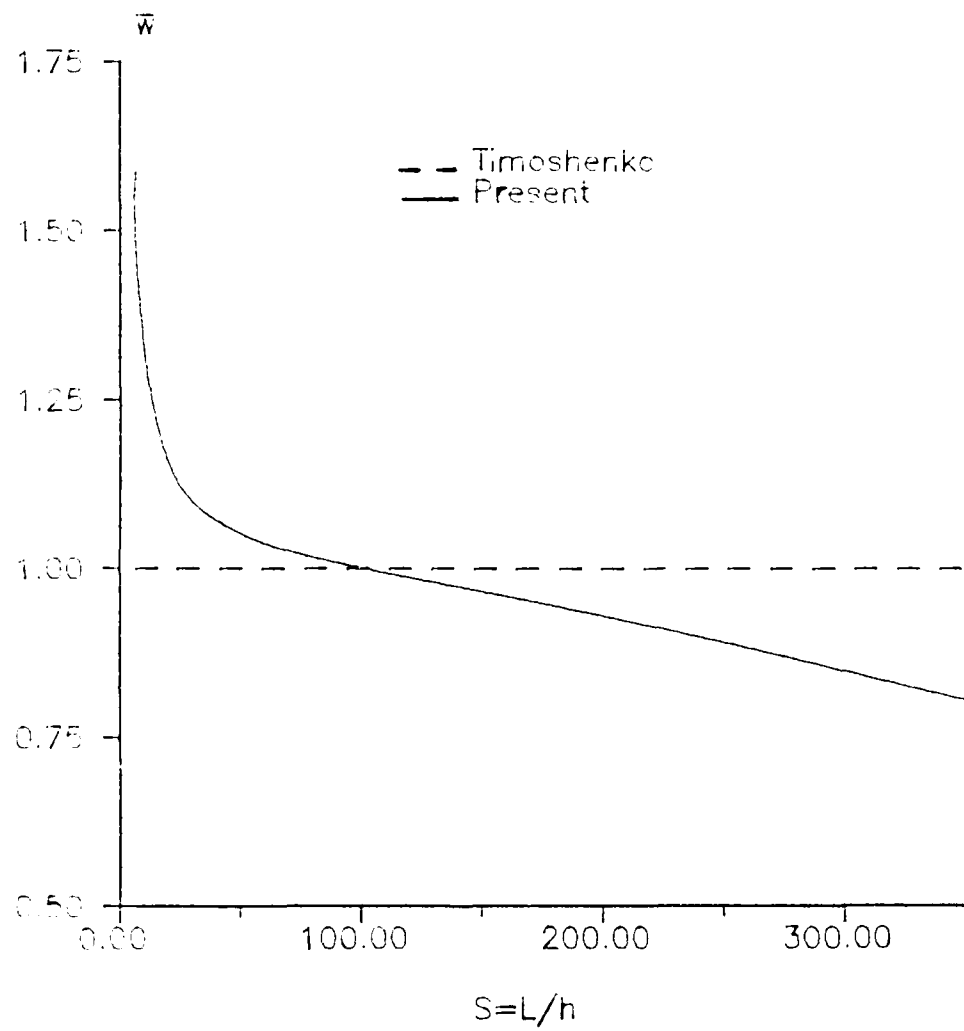
FIGURE 5.20. **Normalized Center Transverse Displacements for Pinched Cylinder.**

183

A similar analysis was also performed on a cylindrical pressure vessel restrained by rigid end plates, as shown in Figure 5.21. A convergence study determined that for this shell, refinements in the x-direction were required due to the large bending deformation near the rigid edges and little refinement circumferentially was necessary due to the axisymmetric nature of the geometry and loading. The transverse displacement results of the convergence study, based on one octant of the vessel and the boundary conditions of Eqn (5.19), are shown in Table 14 for several x-coordinates. These results are compared to the classical result taken from Kraus (9). As can be seen, accurate results require many elemental subdivisions along the longitudinal axis. For the point nearest the edge shown (x=27.5 in), the 12x4Q regular mesh does not compare as closely as may be desired; further refinement will accomplish this. Therefore, the shear study will only consider $0.0 \leq x \leq 22.50$ in. For these coordinates, the mesh gives very accurate results.

184

E=4.5e6 psi
ν=.3
L=60. in
R=30. in
q=-500. psi
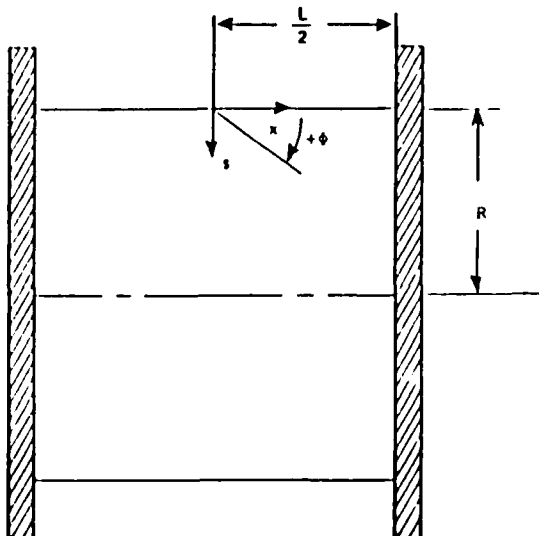
FIGURE 5.21. Cylindrical Pressure Vessel with Rigid End Plates.

| x (in.) | Mesh | | | classical |
	4x4Q 4x12Q	8x4Q 8x8Q	12x4Q	
0.	-2.0358	-2.0006	-2.0003	-2.0003
7.50	-1.9237	-1.9972	-1.9981	-1.9985
15.00	-2.2568	-2.0142	-2.0108	-2.0097
22.50	-1.4351	-2.0299	-2.0325	-2.0311
25.00	*	*	-1.5972	-1.6547
26.25	*	-0.9733	*	-1.2696
27.50	*	*	-0.6417	-0.7675
30.00	0.	0.	0.	0.

TABLE 14. Transverse Displacement (in.) Convergence for Isotropic Pressure Vessel Meshes. * no node at this coordinate.

$\bullet$x=30: $v=w=w,_1=w,_2=\psi_1=\psi_2=0$

  x=0:   symmetry, $u=w,_1=\psi_1=0$ (5.19)

$\bullet$s=0,47.124:   symmetry, $v=w,_2=\psi_2=0$

Next, for the isotropic case, vary the thickness, h, while keeping all other quantities constant. The displacement results are normalized by the classical

185

solution values from Kraus and are designated $\bar{w}$. The classical result is represented by $\bar{w}$. Figure 5.22 shows the influence of transverse shear deformation as S=L/h becomes small for three points along the x axis. The transverse shear deformation is larger for the point nearest the rigid end plate because significant bending occurs there. In contrast, at x=0, i.e., the center of the vessel, the deformation is almost totally due to membrane behavior and therefore the normalized transverse displacement does not differ much from the classical solution. Additionally, the pressure vessels with S=L/h values less than approximately 30, there exists a countershear point, i.e., a point along the x-axis where the transverse shear rotation angle, β_1, changes sign. Depending on where this point occurs and the magnitude of $\beta_1(x)$, the normalized displacement at x=0 may dip below 1.0. This means that the transverse shear deformation gives transverse displacements that are smaller than the classical values for some points along the longitudinal axis. The presence of a countershear point has not been discussed in the literature to the best of the author's knowledge. In contrast, the transverse shear effect in the flat plate always gave a shear rotation such that the displacements were greater than the classical result.

Additional displacement results were obtained for cylindrical laminates using the same geometry and boundary

conditions as in the isotropic vessel. The orthotropic material properties for these shells are shown in Eqn (5.20). The laminates studied are shown in Table 15 along with their effective stiffness quantities based on the material properties and ply orientation. The laminates are rank ordered in the Table according to longitudinal stiffness, E_x, where the quasi-isotropic laminate, $[-60/0/60]_s$, has the same effective stiffness in both the longitudinal and circumferential directions.

$$E_1 = 2.5e7 \text{ psi}$$
$$E_2 = 4.5e5 \text{ psi}$$
$$\nu_{12} = .25 \qquad (5.20)$$
$$G_{12} = G_{13} = .5e6 \text{ psi}$$
$$G_{23} = .2e6 \text{ psi}$$

Laminate	E_x(e7 psi)	E_s(e7 psi)	ν_{xs}	ν_{sx}
[0]	2.5000	0.04500	.2500	.0045
[0/90/0]	1.6834	0.86423	.01303	.006690
$[-60/0/60]_s$	0.89055	0.89055	.3071	.3071
[90/0/90]	0.86423	1.6834	.006690	.01303
[90]	0.04500	2.5000	.004500	.2500

TABLE 15. Effective Laminate Stiffness Based on Eqn (5.20) and Ply Orientation Angles.

Similar to the isotropic case, the finite element transverse displacement results for x=0, 15, and 22.5 in. were normalized by the classical solution result taken from Kraus (9) and are designated by $\bar{w}$. Kraus' solution is strictly based on a pressure vessel with orthotropic

187

material properties, i.e., where the material axes are alligned with the cylindrical axes. As will be seen, however, the nonunidirectional pressure vessel laminates, using the effective laminate stiffnesses of Table 15, are also governed by this solution for the thin shell case. Additionally, the behavior of the quasi-isotropic pressure vessel is influenced by the bending-twisting coupling terms due to nonzero D_{16} and D_{26}. However, Kraus' solution can not predict this coupling since it is based on unidirectional configurations, i.e., where D_{16} and D_{26} equal zero. The assumption of symmetry in the present case will eliminate the D_{16} and D_{26} influence in the finite element results and this coupling is therefore not included in either solution.

As Figure 5.23-5.27 show, the same trends are evident in the composite cases as was seen in the isotropic. The greatest $\bar{w}$ for small S=L/h occurs at the point nearest the rigid end plates. The smallest $\bar{w}$ occurs at the center of the vessel where the smallest amount of bending occurs. The laminates where the stiffness in the longitudinal direction (E_x) is relatively small (see Table 15) experienced the most pronounced effects of a countershear point. Indeed, for the most flexible, [90] of Figure 5.27, all points between x=0 and 15 gave smaller transverse displacement than the classical result for S≤15. For the point nearest the end plate, the greatest $\bar{w}$ occurs in the laminate with the

highest longitudinal stiffness, see Figure 5.28. For a given value of S, the greater E_x for a laminate, the greater $\bar{w}$. This means that for $E_x > E_s$, there is more transverse shear deformation. A comparison between the isotropic and quasi-isotropic vessels for x=22.5 in. is shown in Figure 5.29. Since both vessels have equal extensional stiffnesses in the circumferential and longitudinal directions, we conclude that the quasi-isotropic is influenced to a greater degree by the transverse shear deformation due to its material orthotropy, i.e., $E_1 \neq E_2$.

For values of longitudinal coordinate, x, near the center of the vessel, σ_1 is small and in these regions, a plane stress situation exists for the s-ζ planes. As given by Timoshenko (139) for the isotropic case, the transverse normal stress, σ_3, is approximately 20% of the hoop stress for S=L/h=10. For S=20, σ_3 is only 10% of σ_2. The point is, for the thicker pressure vessel, σ_3 can be significant. Indeed, near the clamped edge where σ_1 is large, we truly have a 3-D state of stress. Timoshenko's solution can also be used to examine the validity of assuming a constant w through the thickness. For S=20, the difference between the transverse displacement taken at the inner and outer surface is only 3%, at S=10, it is 7%. For the present example, then, the assumption of $w=w(\zeta)$ is very good even for the very thick shell.
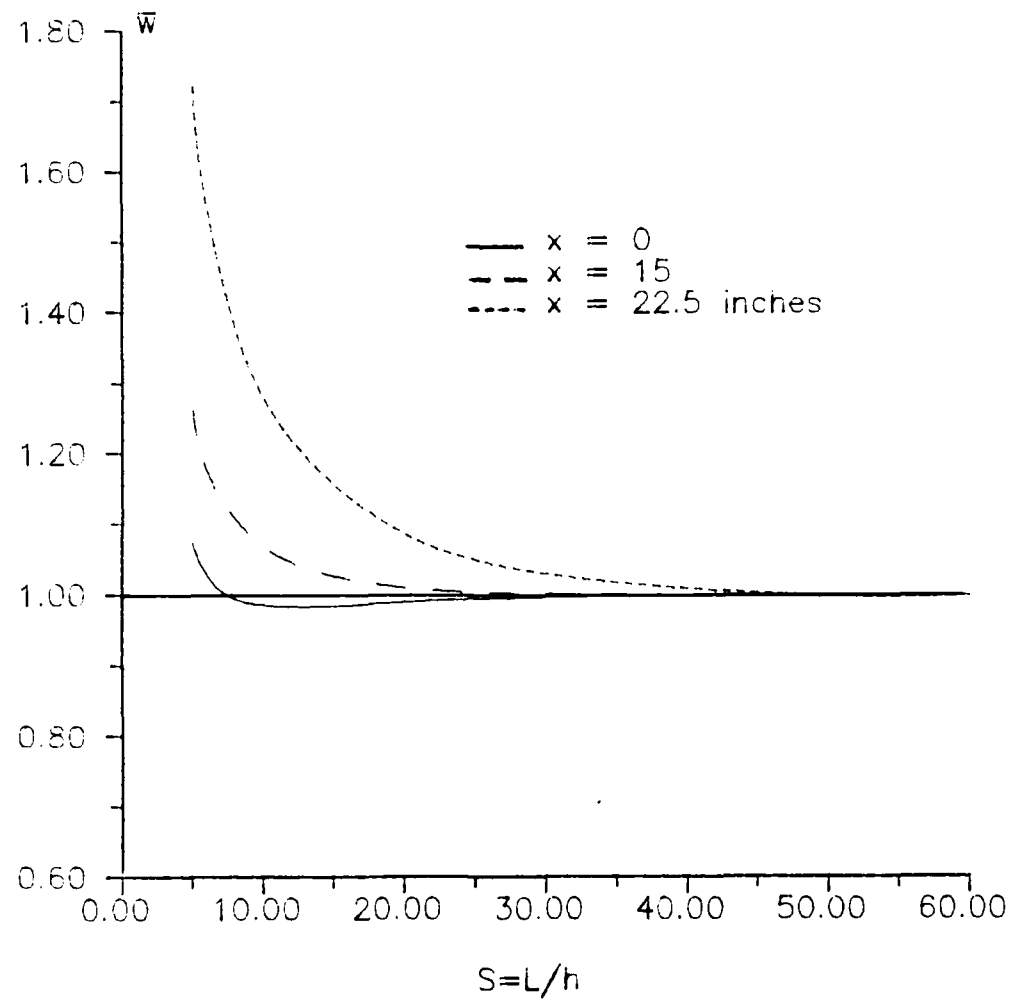
FIGURE 5.22. Isotropic Pressure Vessel Normalized Transverse Displacement.

190
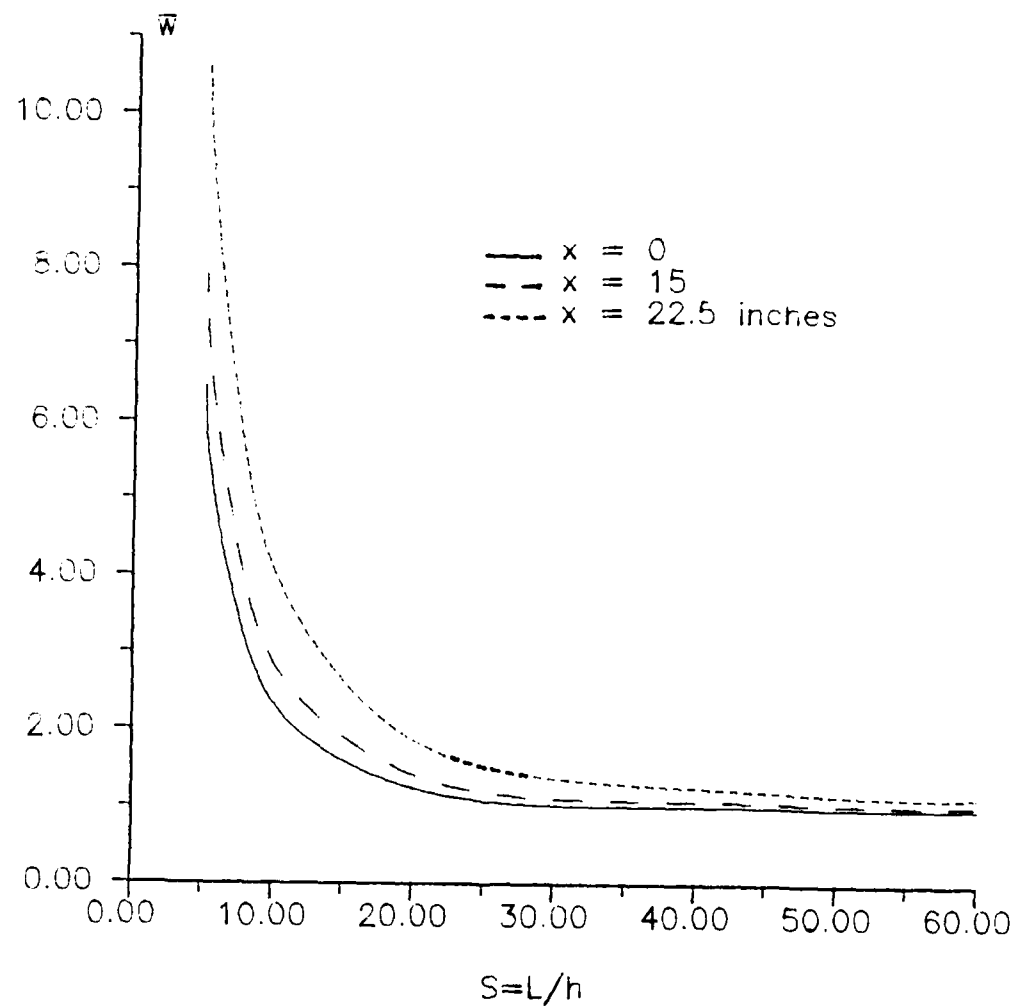
FIGURE 5.23. [0] Pressure Vessel, Transverse Displacement.

191
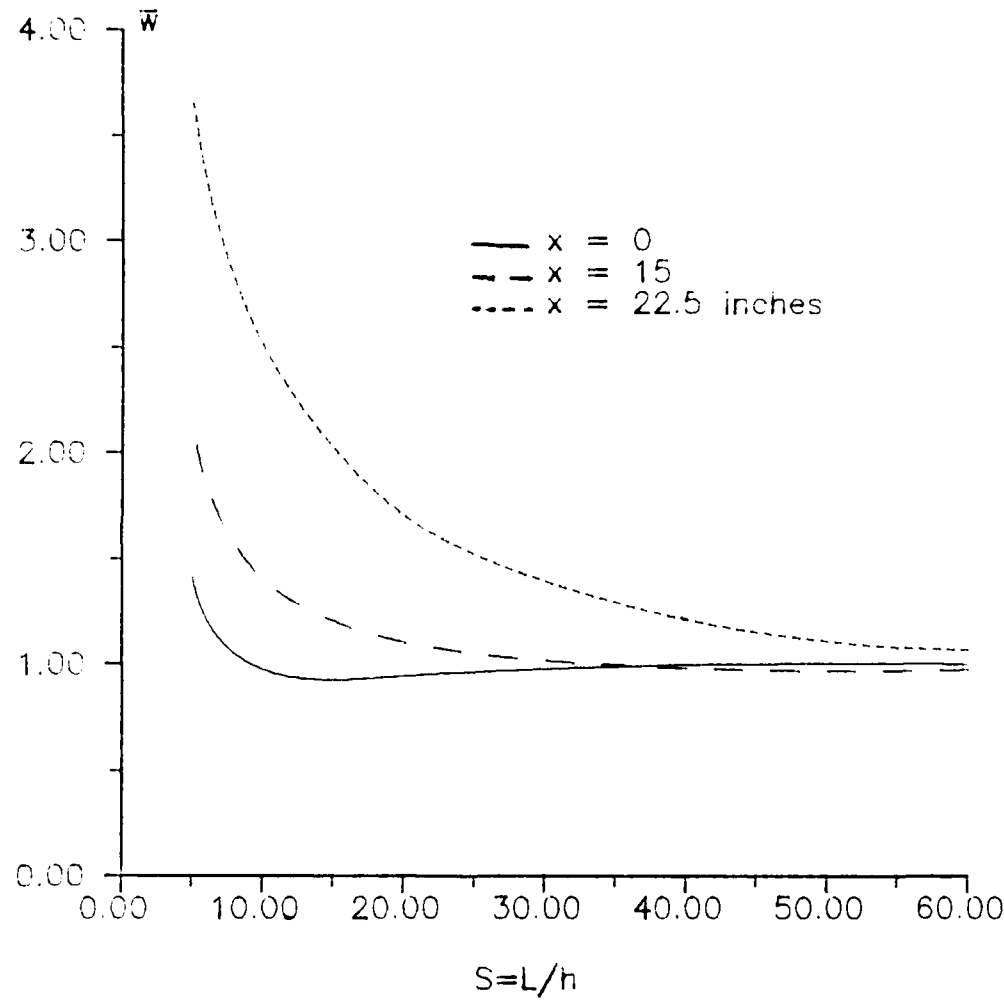
FIGURE 5.24. [0/90/0] Pressure Vessel, Transverse Displacement.

192
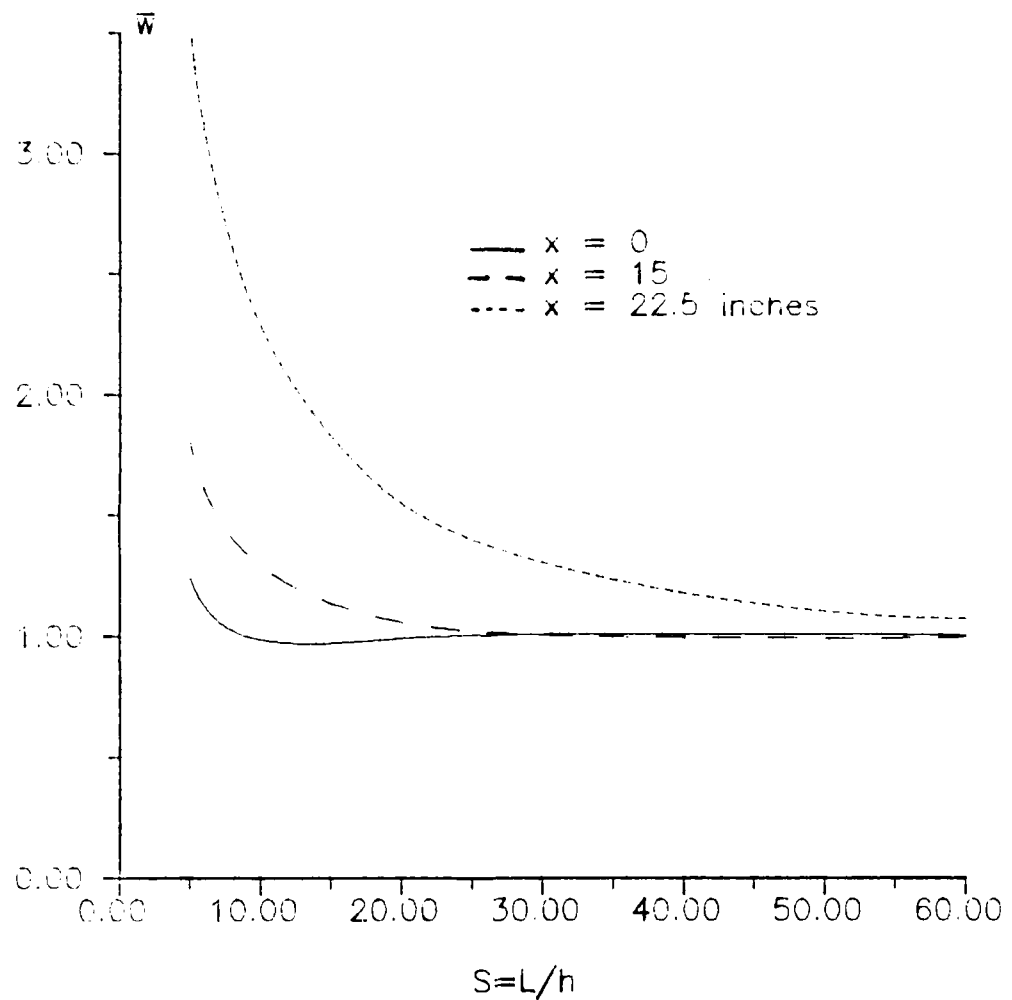
FIGURE 5.25. [-60/0/60]$_s$ Pressure Vessel, Transverse Displacement.

193
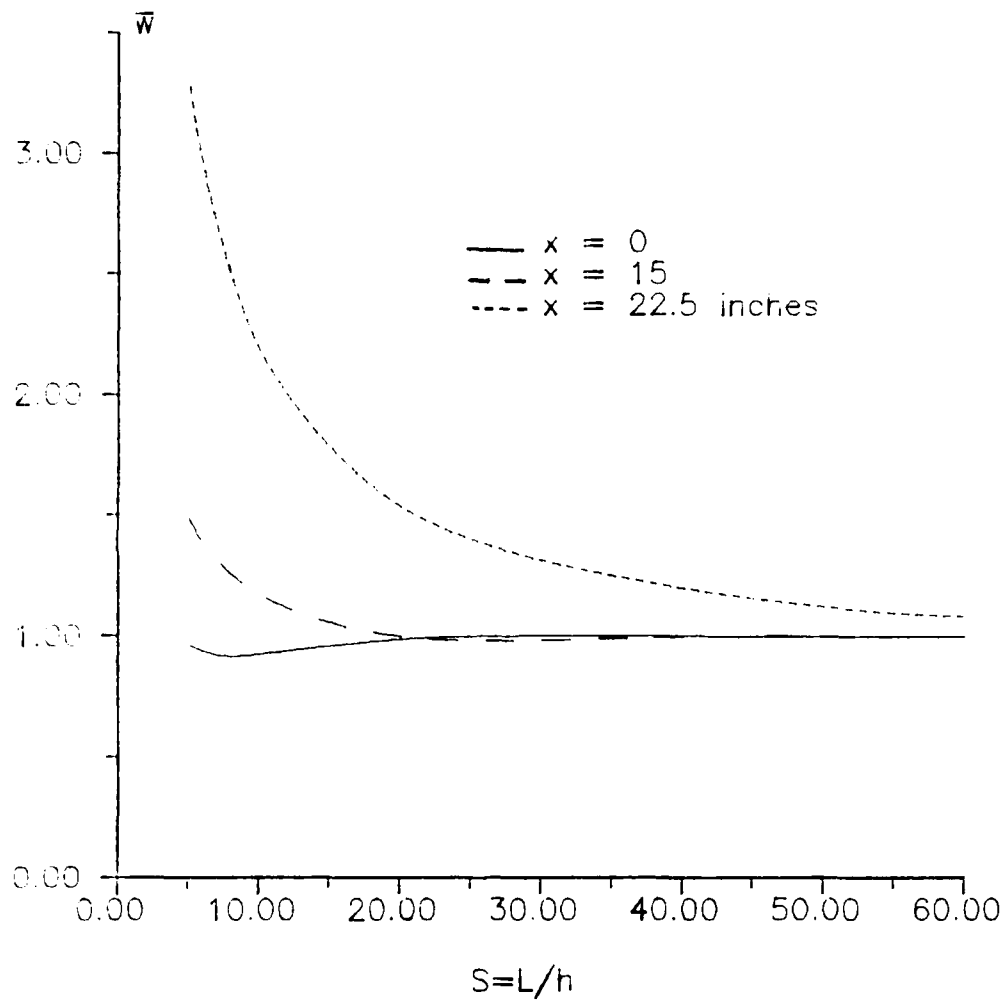
FIGURE 5.26. [90/0/90] Pressure Vessel, Transverse Displacement.

194
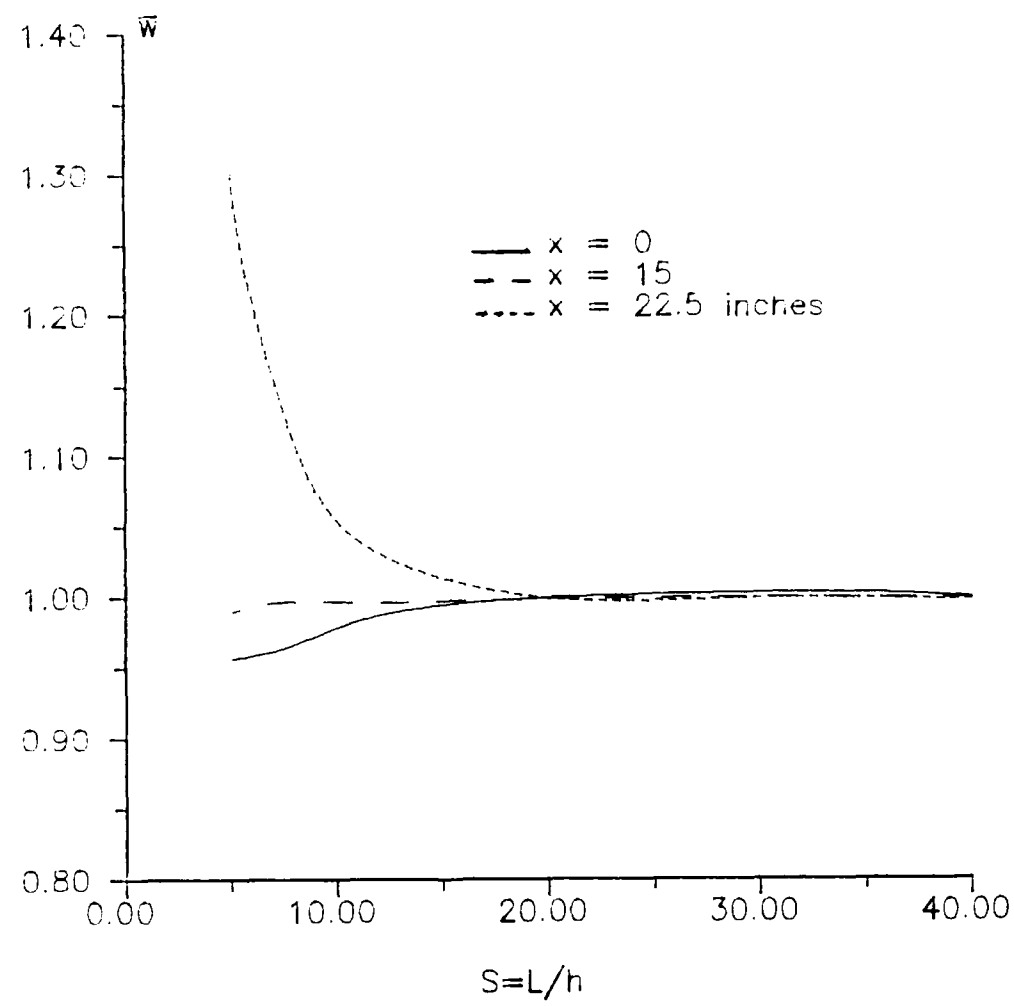
FIGURE 5.27. [90] Pressure Vessel, Transverse Displacement.
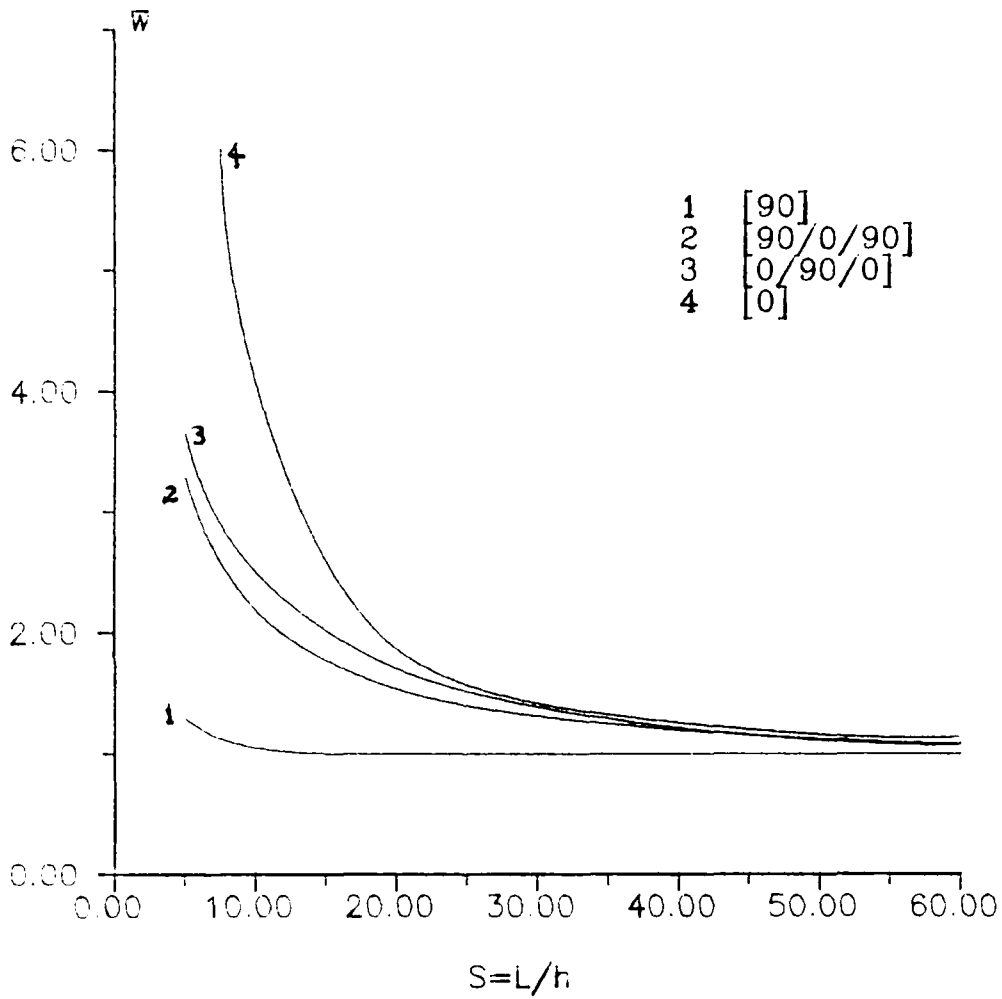
FIGURE 5.28. Laminate Pressure Vessel at x=22.5 in.

196
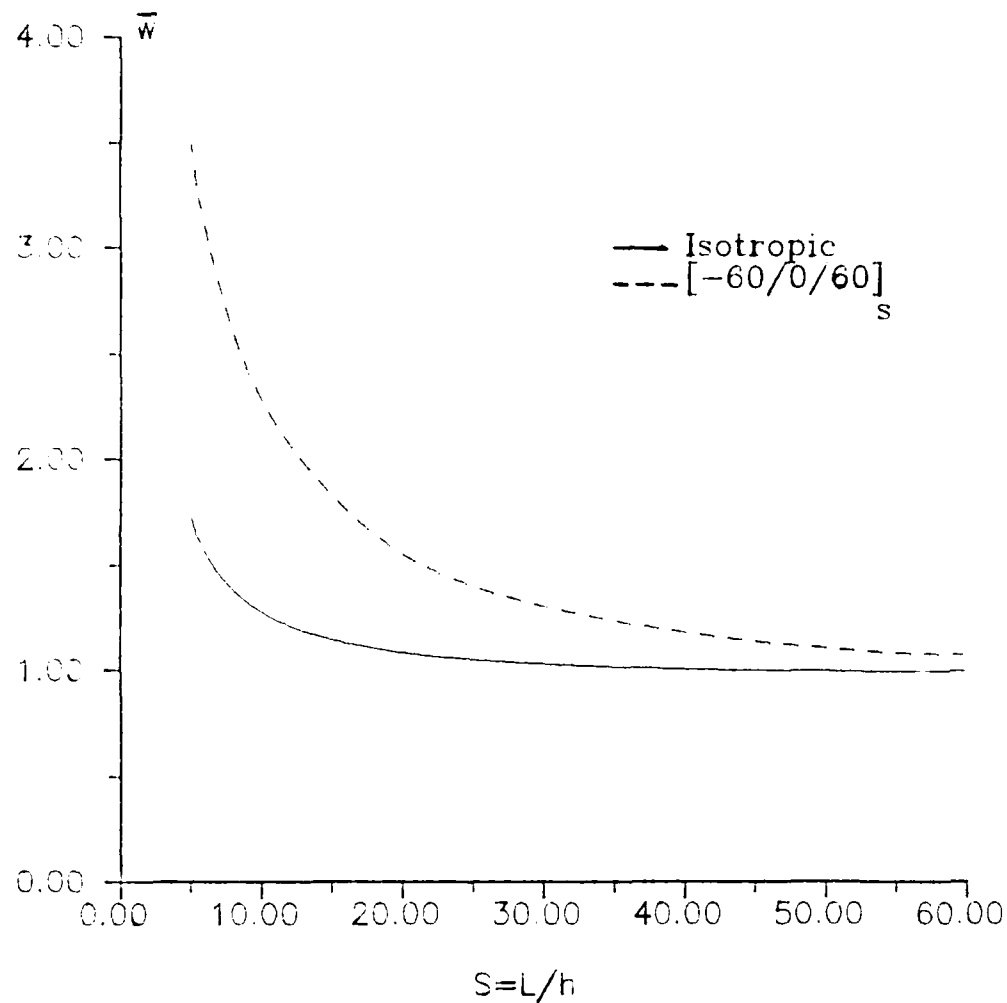
FIGURE 5.29. Isotropic and Quasi-Isotropic Pressure Vessels at x=22.5 in.

Based on the foregoing discussions of flat plate and cylindrical shell analyses, the following conclusions are drawn. The linear algorithms are valid; published results have been duplicated. The 28 dof element should only be used for flat plate cases. Neither the 28 or 36 dof element shows any evidence of shear locking. The simple support boundary condition of zero normal moment cannot be explicitly satisfied. Stresses are generally represented well within the continuum. Refinements near the boundaries are required for accurate stress calculation there. Transverse shear deformation gives a more flexible structure for a pinched cylinder and cylindrical pressure vessel, as in the flat plate, when bending is significant. Pressure vessel laminates are generally influenced to a greater degree by transverse shear than is the isotropic vessel.

Linear Bifurcation Analysis

As mentioned in the previous chapter, the primary purpose of the linear bifurcation study is that it represents a simple, inexpensive validation test of the nonlinear matrix, N_1. Bifurcation, as given by Eqn (4.40), then can be thought of as validation of only a subset of the nonlinear terms and therefore, an intermediate step between the linear, Eqn (4.35) and nonlinear analyses, Eqn (4.33). All of the linear bifurcation analyses performed in the present research use the fully linearized method. Comparisons are usually made with published results derived from the classical buckling approach. The distinction between the two bifurcation approaches can be found by examining Eqn (4.40) where in the present, we use N_1; the classical buckling approach uses K_σ, the initial stress matrix. As discussed in Ref (130), critical loads calculated by both methods can be significantly different. Furthermore, although the fully linearized is mathematically more complete in that more of the nonlinear terms are retained, it does not necessarily give the more accurate answers (130).

Results are presented in the following considering the von Karman plate and Donnell shallow shell strain displacement relations as well as new contributions resulting from the elemental formulation that allows large displacements and rotations. Typically, published results

199

are based on the former equations which are valid only for the so called intermediate nonlinearity (12). Intermediate nonlinearity restricts the magnitude of rotation that differential elements can undergo. When von Karman assumptions are discussed in this dissertation, it is the intermediate nonlinearity aspect of those assumptions that is being referred to. Therefore, for flat plate results generated by the present theory, the theoretical differences between the von Karman and the large rotation/displacement equations are only in the degree of nonlinearity assumed since both still include parabolic transverse shear, for example. Some of the published results for flat plate buckling used for comparisons are based on 3-D elasticity (49,116). These 3-D solutions, however, only assume intermediate nonlinearity, i.e., the von Karman plate equations. That is, although 3-D flexibility is included, as evidenced by nonzero ε_3 for example, only the midsurface strains ε_1, ε_2, and ε_6 are characterized by nonlinear displacement terms, and furthermore, the nonlinear terms are functions only of the transverse displacement, w.

The following analysis provokes questions pertaining to the differences between the two theoretical buckling approaches of classical and fully linearized. This area of research, outside the scope of the present work, has apparently received little attention as evidenced by the lone reference that addresses it (130). Since we are

200

primarily interested in providing a partial check of some of the nonlinear terms before proceeding to the general nonlinear algorithm of Eqn (4.33), only a few flat plate examples are examined followed by a single cylindrical shell case. For one flat plate case, significant differences between the present and published classical results occur. Several possible explanations are proposed.

In the discussion of each specific example to follow, the finite element based upon the large displacement and rotation assumptions is sometimes referred to as the full nonlinear element. However, to avoid confusion with the similar sounding fully linearized buckling approach, the former is abbreviated to FNL. Thus, results based on the original assumptions of Chapter III are referred to as either the large rotation/displacement or the FNL results.

The algorithm can be first tested versus the very simple Euler column as shown in Figure 5.30. For boundary conditions clamped at the root and free at the load application end, the classical buckling solution for the nondimensionalized buckling parameter, λ_{cr}, is given by Eqn (5.21). Finite element results were generated based on a 10x1 mesh of 28 dof elements for several values of the thickness, h. The thickness was varied because it was unknown how 2-D plate elements would respond when used to model a beam, especially for the cases where the magnitude of the thickness approached the width, b. For the case

201

where h=b, the plate elements are certainly no longer thin. However, we can duplicate 1-D beam theory to some degree by setting Poisson's ratio to zero and thus reducing the influence of the 2-D nature of the plate elements. Table 16 gives the nondimensionalized critical loads, λ, for various values of S=L/h. Results are calculated for both the von Karman (λ_{VK}) and large displacement/rotation (λ_{FNL}) strain displacement assumptions.

E=10.e6 psi
ν=0.
L=10. in.
b=1. in.
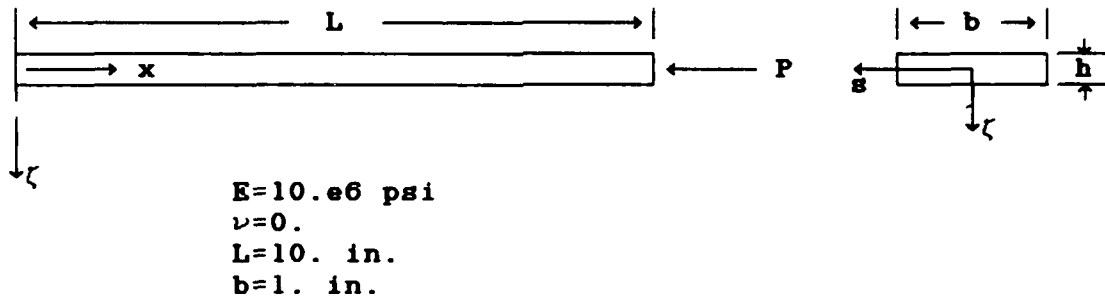
FIGURE 5.30. Clamped-Free Euler Column.

$$\lambda_{cr} = \frac{P_{cr} L^2}{\pi^2 EI} = .25 \qquad (5.21)$$

S=L/h	λ_{VK}	λ_{FNL}
400	.2505	.2505
200	.2506	.2506
100	.2506	.2506
50	.2504	.2504
20	.2501	.2498
10	.2491	.2476

TABLE 16. Euler Column Critical Loads for von Karman (λ_{VK}) and Large Displacement/Rotation, (λ_{FNL}) Elements.

With the exception of S=10, the λ_{VK} and λ_{FNL} compare very well with each other and with the classical result of Eqn (5.21). As shown in Table 16 for the thicker beam, S=10, the finite element results are slightly more flexible primarily due to the transverse shear deformation. The eigenvector is given for points along the x axis normalized by the tip displacement in Table 17 and compares exactly to 3 digits with the classical sinusoidal shape of Eqn (5.22) if a w dof is chosen as the prescribed dof such that the system of equations, Eqn (4.39), becomes determinant. However, if a u or v dof is prescribed, the calculated eigenvector is totally different and only gives nonzero components in either the x or s direction respectively. The shape of the eigenvector when v at the beam tip is prescribed equal to one is also shown in Table 17. For this case, all w components are zero and the shape of the eigenvector does not resemble the classical shape. Calculating the eigenvector proved troublesome throughout this analysis. This stems from the choice of the prescribed dof that must be made such that Eqn (4.39) can be solved. Except for one flat plate geometry to be examined later, if a dof in the 'correct' classical direction is prescribed, usually a w dof, then the 'correct' classical eigenvector is represented very accurately. On the other hand, if a dof is chosen that is not a component of the classical shape, then a totally different shape is attained. This anomaly makes

the eigenvector an unreliable source of information if it is used to compare solutions based upon the classical versus fully linearized approaches.

$$\frac{w(x)}{w_{tip}} = (1 - \cos \frac{\pi x}{2L})$$ (5.22)

x (in.)	$w(x)/w_{tip}$	$v(x)/v_{tip}$
0	0.000	0.000
1	.0122	.053
2	.0489	.16
3	.109	.26
4	.191	.37
5	.293	.47
6	.412	.58
7	.546	.68
8	.691	.79
9	.844	.90
10	1.000	1.00

TABLE 17. Clamped-Free Euler Column Eigenvectors for Either w_{tip} Prescribed or v_{tip} Prescribed.

We next consider an axially compressed simply supported square isotropic flat plate as shown in Figure 5.31, where P is an axial pressure quantity and a=8in. The boundary conditions are shown in Eqn (5.23). As can be seen, the symmetry conditions now include constraints on the inplane displacements, u and v. The classical buckling approaches do not have u and v dof, and hence, also do not require boundary conditions on them. However, to insure symmetry in the solutions for the present case where u and v are dof, symmetry conditions are included on them as well as on the

transverse dof. The isotropic material properties and the thickness used in the thin plate convergence study are shown in Eqn (5.24).
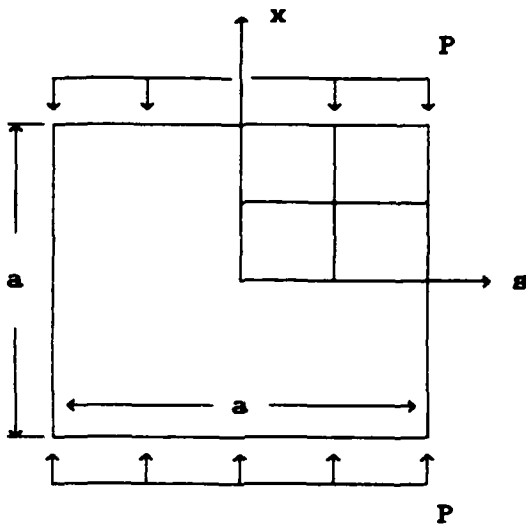
FIGURE 5.31. Flat Square Plate Under Axial Compression. Upper Quadrant 2x2 Discretization.

$\bullet x=a/2$: $w=\psi_2=0$

   $x=0$:   symmetry, $u=w,_1=\psi_1=0$

$\bullet s=a/2$: $w=\psi_1=0$ (5.23)

   $s=0$: $v=w,_2=\psi_2=0$

$$
\begin{aligned}
&E=10.e6 \text{ psi} \\
&\nu=.3 \\
&h=.08 \text{ in}
\end{aligned}
\qquad (5.24)
$$

Convergence to the classical buckling load, given by Eqn (5.25), is shown for the thin plate case in Table 18. Critical loads calculated for three mesh arrangements that represent one quarter of the plate are shown. Next, using the 8x8 mesh, the thickness of the plate is varied and

205

results are generated for both the von Karman (λ_{VK}) and the large displacement/rotation (λ_{FNL}) elements, see Table 19. Both can be compared to the published results of Reddy and Phan (54) (λ_{RP}) who use a Navier series classical buckling solution to the parabolic transverse shear theory and also to Stein (116) (λ_{3-D}) whose results are based on a series solution to the 3-D elasticity equations. Both published results are obtained through the intermediate von Karman nonlinearity.

$$\lambda_{cr} = \frac{P_{cr} h \, a^2}{\pi^2 \, D} = 4.00 \qquad\qquad (5.25)$$

Mesh	λ_{cr}
2x2	7.54
4x4	4.18
8x8	4.01

TABLE 18. Convergence of Buckling Load for Flat Isotropic Plate, 28 dof Elements.

S=a/h	λ_{VK}	λ_{RP}	λ_{3-D}	λ_{FNL}
400	4.159	*	4.00	4.159
200	4.043	*	4.00	4.042
100	4.012	3.9977	4.00	4.010
50	3.997	3.9909	*	3.991
20	3.947	3.9443	*	3.907
10	3.787	3.7865	3.75	3.650
5	3.264	3.2653	3.20	2.926

TABLE 19. Flat Isotropic Plate Buckling for Various Plate Thicknesses, 8x8 Mesh of 28 dof Elements. * not calculated.

As can be seen, the λ_{VK} compare very well with the Reddy and Phan results. Additionally, note that even for the very thick plate where the length of a side of the plate is only 5 times the thickness, the present λ_{VK} solution compares very well with the 3-D result. The FNL solution compares very closely with the von Karman results except for in the thicker plates where λ_{FNL} reflects a gradually more flexible structure. For S=5, λ_{FNL} is 10% less than λ_{VK}. Indeed, these results are more flexible than the 3-D elasticity results thus indicating that the addition of the inplane nonlinear displacement terms used in defining the strains for the FNL element have a greater influence at these thicknesses than does the inclusion of 3-D flexibility.

A final comment can be made in regard to the very thin plates, i.e., where S≥200. In these cases, the buckling load as calculated by the present formulation (λ_{VK} and λ_{FNL}) is indicative of a stiffer plate compared to the classical buckling result which asymptotically approaches 4.00. For plates that are very thin such as these, we would expect increased membrane influence over bending. In classical flat plate buckling, the inplane displacements are not considered in the solution as they are in the fully linearized approach. Therefore, the increased stiffness due to the more significant membrane behavior in the very thin plates is a reasonable result, whereas in the classical

approach, inextensibility is assumed.

Solutions are next presented for simply supported laminated flat plates. The material properties for these plates are given in Eqn (5.26). The published results of Phan and Reddy (58) are used for comparison. They solve for buckling loads, again, based on a classical buckling approach including parabolic transverse shear distribution except for this example, solve via a displacement finite element model. For the first case, a $[0/\pm45/90]_s$ laminate, the two sets of boundary conditions shown in Eqn (5.27) were tested based on discretization of one quarter of the plate geometry. The two sets of boundary conditions are identical except in the second, the normal inplane displacement along $s=\pm a/2$ is additionally restrained, see Figure 5.31. As a result of the boundary conditions used for the simply supported isotropic plate and the subsequent close correlation of those results with established results based upon classical buckling, those same boundary conditions were used to represent the simple supports for this case too. The additional boundary condition set places a constraint on the normal displacement v along $s=\pm a/2$ and therefore, will cause a compressive stress field throughout the plate in the s direction since free movement has been restrained at the boundary. The classical buckling approach assumes a constant compressive load in only the x direction for this case, and generally do not consider nonuniform prebuckled

stress fields. Similar to the linear plate case, nonzero D_{16} and D_{26} may give a nonsymmetric deformation pattern. However, Ref (58) apparently assumes biaxial symmetry by by modelling only a quarter plate.

$$
\begin{aligned}
E_1 &= 60.e6 \text{ psi} \\
E_2 &= 1.5e6 \text{ psi} \\
G_{12} &= G_{13} = .9e6 \text{ psi} \\
G_{23} &= .75e6 \text{ psi} \\
\nu_{12} &= .25
\end{aligned}
\tag{5.26}
$$

$$
\begin{aligned}
&\bullet x = a/2: && w = \psi_2 = 0 \\
& x = 0: && \text{symmetry, } u = w,_1 = \psi_1 \\
&\bullet s = a/2: && w = \psi_1 = 0 \quad \text{or} \quad v = w = \psi_1 = 0 \\
& s = 0: && \text{symmetry, } v = w,_2 = \psi_2 = 0
\end{aligned}
\tag{5.27}
$$

The convergence results for $S = a/h = 100$ are shown in Table 20 and compared to that found by Phan and Reddy (λ_{PR}). Also shown is the result due to fixing the normal displacement v along $s = \pm a/2$ edges. The classical solutions are reproduced well when this dof is free, as in the isotropic case. However, the biaxial stress field due to the additional compressive stresses in the s direction from the v boundary condition and the compressive applied loading in the x direction gives a buckling load that is significantly less than the classical. The additional compressive stresses due to the v boundary condition result in a more flexible structure as would be expected.

209

Mesh	λ_{VK}	λ_{PR}	λ_{VK} (v=0, s=a/2)
2x2	48.17		
4x4	43.16	42.819	32.72
8x8	42.72		

TABLE 20. Buckling Parameter for $[0/\pm45/90]_s$ laminate, 28 dof Elements, $\lambda = Pa^2/E_2h^2$.

The effect of transverse shear deformation is examined next by allowing the plate thickness to vary. Using the first set of boundary conditions of Eqn (5.27) and the 8x8 regular mesh, the buckling loads can be determined based upon both the von Karman (λ_{VK}) and the large displacement/rotation (λ_{FNL}) elements. These results are compared to those determined by Phan and Reddy in Table 21. The von Karman buckling loads match very well with the published results. The results based on the FNL element also compare very closely, where in the thicker plates a gradually more flexible result is given.

S=a/h	λ_{VK}	λ_{FNL}	λ_{PR}
100	42.72	42.68	42.819
50	42.05	41.94	41.877
20	37.17	36.68	37.115
10	26.82	26.05	26.799
4	9.308	8.923	9.3323

TABLE 21. Buckling Parameters for $[0/\pm45/90]_s$ Laminate for Various S=a/h, 8x8 Mesh of 28 dof Elements, $\lambda = Pa^2/E_2h^2$.

Excellent comparisons were also obtained for a

[0/90/90/0] laminate where in this case, the degree of material orthotropy was varied instead of the plate thickness. The first set of boundary conditions in Eqn (5.27) as well as the material properties of Eqn (5.26) still apply, except now vary E_1 keeping $S=a/h=10$ constant. The buckling results, as shown in Table 22, are compared to a series solution due to Phan and Reddy (λ_{PR}), the thin plate solution (λ_{CLPT}), and the result based on 3-D elasticity (λ_{3-D}). The latter is due to Noor (49) and based on a von Karman classical buckling approach.

E_1/E_2	λ_{VK}	λ_{FNL}	λ_{PR}	λ_{3-D}	λ_{CLPT}
3	5.404	5.153	5.1143	5.2944	5.7538
10	9.935	9.522	9.7740	9.7621	11.492
20	15.271	14.737	15.298	15.019	19.712
30	19.628	19.037	19.957	19.304	27.936
40	23.278	22.662	23.340	22.881	36.160

TABLE 22. Buckling Parameters for [0/90/90/0] Laminate for Various E_1/E_2, 8x8 Mesh of 28 dof Elements, $\lambda = Pa^2/E_2h^2$.

The first comment can be made comparing either of the present results, λ_{VK} or λ_{FNL}, with either λ_{PR} or λ_{3-D}. For all E_1/E_2 ratios, the comparisons are very good. Next, comparing the results from any of the values of the first four columns, i.e., those buckling loads resulting from theories that include transverse effects, with the results from the classical laminated plate theory (λ_{CLPT}), we see

211

that for increasing E_1/E_2, the buckling parameters diverge. Therefore, for laminates constructed of highly orthotropic materials, i.e., high ratios of E_1/E_2, the influence of transverse shear deformation becomes increasingly more pronounced as evidenced by the increasingly smaller buckling loads compared to the thin plate solution, λ_{CLPT}. A comparison of λ_{VK} and λ_{FNL} shows that the latter are, once again, indicative of a slightly more flexible structure. Comparing λ_{VK} and λ_{FNL} to the 3-D elasticity result, λ_{3-D}, we see that the former pair enclose the 3-D values for all values of E_1/E_2. This also occurred in the isotropic case, except for the very thin plate, see Table 19. Once again, the importance of the inplane nonlinear displacement terms resulting in λ_{FNL} is evident for these cases. As was also seen in the isotropic flat plate, the inclusion of the higher order displacement terms that define the FNL element apparently has a greater influence on the buckling load than just including 3-D flexibility to the intermediate nonlinearity that defines a von Karman plate.

The final flat plate linear bifurcation tests were performed on rectangular isotropic plates assuming the material properties of Eqn (5.24) and the boundary conditions of Eqn (5.23). As will be seen, the fully linearized buckling approach can give markedly different results for nonsquare plates than does the classical buckling approach. Consider the flat plates of Figure 5.32

212

where a/b=3 and a/b=.2.
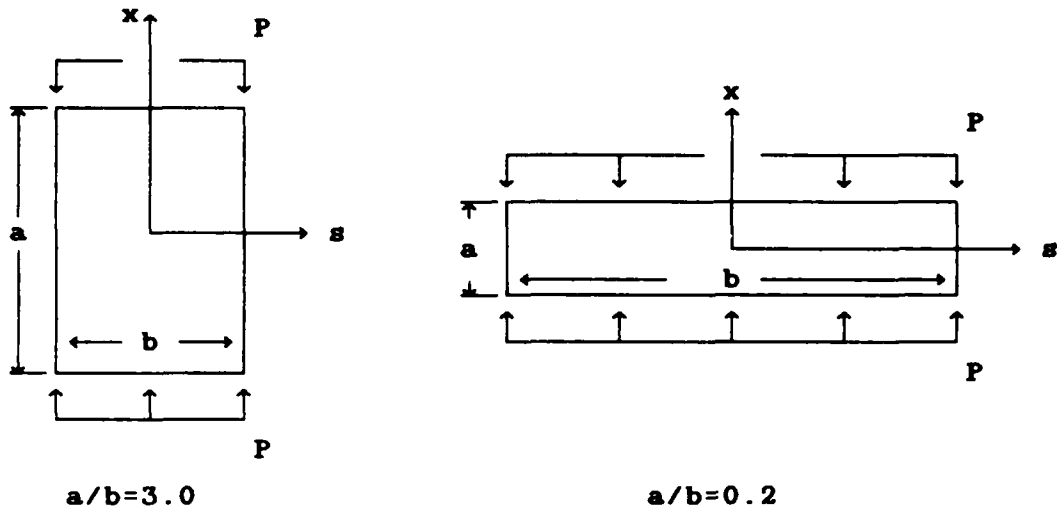
FIGURE 5.32. Isotropic Rectangular Axially Compressed Flat Plate Geometries.

Results based on a classical buckling approach and Navier series solution are again given by Phan and Reddy (58) for various S=a/h values. These are shown in Tables 23 and 24 ($\lambda = Pb^2/\pi^2 D$) for both plate geometries. Also shown are the solutions for the present theory resulting from both the von Karman and FNL assumptions, based on 8x8 meshes of the 28 dof element.

S=a/h	λ_{VK}	λ_{FNL}	λ_{PR}
400	4.806	4.804	*
100	4.047	4.032	3.998
50	*	3.890	3.991
10	*	2.064	3.787
5	1.070	0.705	3.265

TABLE 23. Isotropic Flat Plate, a/b=3. * not calculated.

S=a/h	λ_{VK}	λ_{FNL}	λ_{PR}
400	29.00	29.08	*
100	27.20	27.197	26.843
50	*	27.050	26.270
10	*	26.612	15.658
5	24.18	22.237	7.053

TABLE 24.   Isotropic Flat Plate, a/b=.2.   * not calculated.

The results of Tables 23 and 24 compare well with published results only for the thin plate case, i.e., S=100. For the thicker plates, the λ_{VK} is larger than λ_{FNL} consistent with previous results. For the very thin plates, i.e., S=400, λ_{FNL} and λ_{VK} are essentially equal, also consistent with previous results. However, very different buckling loads are predicted in the present approach for S=a/h values other than 100 compared to the Phan and Reddy solutions. When the plate resembles a column (a/b=3), the present solutions give a much more flexible structure than does the PR result. In contrast, for the plate with a/b=.2, the present case gives much stiffer results. Both plates show a gradual stiffening for the very thin plates compared to the classical buckling approach. This difference is due to the inclusion of the u and v dof which become increasingly more important for the thinner plates. This trend was seen in the square isotropic plate as well and was explained by similar reasoning.

A possible explanation for the large buckling loads given by the fully linearized approach for a/b=.2 and S≤100 is as follows. The classical approach assumes a uniform stress state in the x direction throughout the plate domain and zero stresses along the s direction and in shear. On the other hand, in the present approach, the compressive loading along x=±a/2 edges will develop tensile stresses along the s direction due to Poisson's ratio as well as inplane shearing stresses. These tensile stresses are greater for smaller a/b (12). The tension in the s direction results in a stiffer structure and therefore, larger values for buckling. Examination of these prebuckled stresses (σ_2 and σ_6) show them to be fairly small compared to σ_1, however. The tensile stress field is present for the plate where a/b=3 but it is a relatively much smaller effect. The results of Table 23 show that for S<100, the fully linearized approach gives buckling loads for a much more flexible plate. Examination of the eigenvectors for these cases shows a very erratic, undefinable shape where displacement components of adjacent nodes exhibit no clear pattern. However, for the plates with S≥100, the classical 3 half sine waves is very accurately represented. Based on this, the buckled modes for a/b=3 and S<100 may be totally different than that predicted by classical means. Since u, v, and w dof are always coupled, it is conceivable that these plates are buckling only inplane, or twisting out of

215

plane, or into some other shape.

Another possible explanation for the differences found in Tables 23 and 24 is in the boundary conditions. As discussed in the linear plate analysis, the zero moment force boundary condition cannot be identically satisfied. The effect of this is greater in plates that are not square since one pair of opposite boundaries are closer together.

Unfortunately, Ref (130) that studies the differences between the two buckling approaches and compares to collapse analyses, does not examine the axially loaded flat plate. The reason for this may be due to the fact that the 2-D plate theories cannot generate transverse displacements for axial loads in a general nonlinear collapse analysis as discussed in the previous chapter. At any rate, based on the excellent square plate comparisons and the study done by Ref (130) that shows dramatic differences resulting from the two buckling approaches, the author believes the algorithm is working correctly. This opinion is reinforced by the following shell example.

Keeping the original goal of the linear bifurcation analysis in mind, only one shell bifurcation solution is presented. This specific case was chosen since there exists a published result based on the fully linearized buckling approach in (130). Consider the isotropic clamped cylindrical shell subjected to uniform radial pressure studied previously in the linear analysis section, see

216

Figure 5.15. The fully linearized buckling load calculated by (130) is .285, whereas the classical approach gives a buckling load of .361. Interestingly, the nonlinear collapse analysis for this shell gives a response that is always stable, as will be seen in the next section. Therefore, the fully linearized and classical approaches are both wrong for this case, thus giving some indication of the value of bifurcation analysis.

The results for several mesh refinements are shown in Table 25 for both the Donnell and large displacement/rotation equations. Both the 28 dof element ($\dot{}$L$\dot{}$) and the 36 dof element ($\dot{}$Q$\dot{}$) were tested. The results show very good correlation with the published result, and therefore, validates the cylindrical shell N_1 matrix. The FNL element gives a slightly stiffer result compared to the Donnell element. Additionally, note that the 4x4 mesh results are not nearly as converged as they were for the linear clamped shell, see Table 10.

Mesh	q_o (Donnell)	q_o (FNL)
4x4L	.42	.42
4x4Q	.39	.39
8x8L	.294	.298
8x8Q	.286	.290

TABLE 25. Clamped Cylindrical Shell Buckling, in psi.

217

The preceding linear bifurcation analyses based on the fully linearized approach, confirm the N_1 formulation. The square plate examples correlate very well with the published results that are based on the classical approach. The many inplane plate nonlinear terms that are not included in a von Karman approach give bifurcation loads indicative of a more flexible structure even compared to 3-D formulations. Vastly different buckling loads are calculated for thick nonsquare plates in axial compression. Several explanations were proposed; primarily, the different buckling approaches is thought to be the reason for the disparity. The single cylindrical shell buckling case predicts the fully linearized load very accurately.

Nonlinear Analysis

The nonlinear analysis algorithm of Eqn (4.33) includes all of the features developed for this research effort. Both flat plate and cylindrical shell solutions can be generated based on the large displacement/rotation assumptions or on the simpler von Karman plate and Donnell shell assumptions. Additionally, equilibrium paths can be traced beyond critical points by incrementing components of displacement instead of load.

In the following, many problems are examined. The initial cases are for validation purposes and are typical test problems. For these problems, the von Karman plate or Donnell shell equations are invoked, at least at first, since the published solutions are usually based upon the same assumptions. Often, the element that can undergo large displacements and rotations will be applied to these cases as well, and near identical results are attained, thus reinforcing the validity and range of the simplified equations. The differences between the large displacement/rotation and Donnell equations become evident in deeper cylindrical panels and arches. For these cases, the displacements and rotations of differential elements begin to violate the intermediate nonlinearity assumptions of the Donnell shell equations. Unless otherwise stated, the finite element results presented are based upon the von Karman plate or the Donnell cylindrical shell solution

219

options.

The final problem examined is the axially compressed laminated cylindrical panel that has a large centered square cutout. The present solutions give a much more accurate nonlinear equilibrium path representation versus experimental data than previous finite element solutions.

We first examine isotropic flat plates subjected to uniform transverse pressure loading, q_o. Classical thin plate solutions were obtained by Levy (140) based on a Fourier series solution to von Karman plate equations. Consider the plate geometry of Figure 5.33 where $a=b=8$ in. and $h=.08$ in. The material properties are given in Eqn (5.28) and two sets of simple support boundary conditions in Eqns (5.29a) and (5.29b). Levy, in his closed form solution, applied inplane edge normal pressure distributions such that the inplane displacements normal to the edges remain zero throughout the transverse pressure loading history. Therefore, the boundary conditions of Eqn (5.29) constrain the normal inplane displacements along the plate edges. Since Levy does not discuss the inplane tangential edge displacements, both free conditions in Eqn (5.29a) and fixed conditions in Eqn (5.29b) are tested here. However, since he does not apply equivalent tangential inplane shear forces along the edges, the first case is probably better suited.

Transverse pressure and center displacement are

220

nondimensionalized as in Eqn (5.30). The linear results, i.e., based upon Eqn (4.35), are shown in Table 26, where both sets of the boundary conditions of Eqn (5.29) give identical solutions since the inplane and transverse dof are uncoupled. Since the 4x4 mesh is not quite converged, the 8x8 meshes were used in the nonlinear solution. Ten increments of nondimensionalized load, $\bar{q}=20$, resulted in the center plate displacements shown in Table 27.
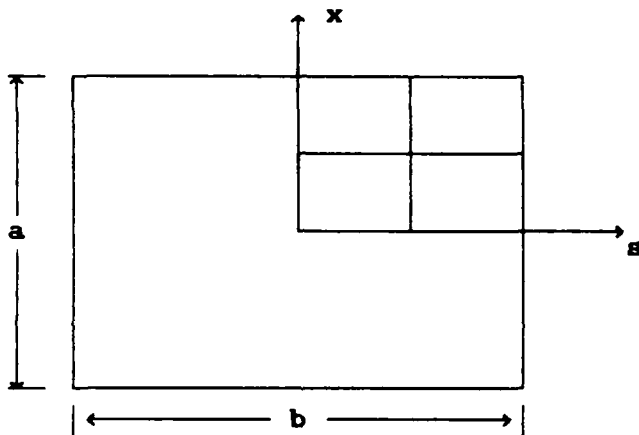
FIGURE 5.33. Flat Plate, One Quadrant Discretized Due To Symmetry.

$$E = 10.e6 \text{ psi}$$
$$\nu = .316 \tag{5.28}$$

$$\begin{aligned}
\bullet x=a/2: &\quad u=w=\psi_2=0 \\
x=0: &\quad \text{symmetry, } u=w,_2=\psi_2=0 \\
\bullet s=a/2: &\quad v=w=\psi_1=0 \\
s=0: &\quad \text{symmetry, } v=w,_1=\psi_1=0
\end{aligned} \tag{5.29a}$$

$\bullet x = a/2:$ $u = v = w = \psi_2 = 0$

$x = 0:$ symmetry, $u = w,_2 = \psi_2 = 0$ (5.29b)

$\bullet s = a/2:$ $u = v = w = \psi_1 = 0$

$s = 0:$ symmetry, $v = w,_1 = \psi_1 = 0$

$$\bar{q} = \frac{q_o a^4}{Eh^4}, \qquad \bar{w} = \frac{w(0,0)}{h} \qquad (5.30)$$

Mesh	$\bar{w}$
4x4	1.6845
8x8	1.7510

TABLE 26. Linear Results for Simply Supported Isotropic Plate for $\bar{q} = 40$.

$\bar{q}$	$\bar{w}$ (5.29a)	$\bar{w}$ (5.29b)
20	.5844	.5837
40	.8455	.8443
60	1.017	1.016
80	1.149	1.147
100	1.257	1.255
120	1.350	1.348
140	1.432	1.430
160	1.505	1.503
180	1.572	1.570
200	1.634	1.631

TABLE 27. Nonlinear $\bar{q}$ vs. $\bar{w}$ for both Boundary Condition Sets of Eqns (5.29a) and (5.29b).

As can be seen, there is very little difference between the two sets of data in Table 27. The results of Table 27

222

are plotted in Figure 5.34 versus the Levy results and the correlation is excellent. The plot shows that for this case, the linear theory compares well with the nonlinear theory only for center transverse displacements up to approximately one third the thickness. For larger displacements, the nonlinear results are indicative of a stiffer structure where we begin to see the effects of the plate's membrane resistance that is not included in a linear analysis.

Stresses are also calculated for $\bar{q}=100$ and 200. The nondimensionalization of stress is given in Eqn (5.31). Levy separately calculated the membrane and bending components of stress for two locations of the plate. Consequently, in the present case, the membrane quantities were taken to be the stress at the midplane, $\zeta=0$. This amount was then subtracted from the stresses given at the outer most fibers to get the maximum bending stresses. Tables 28 and 29 show the stresses calculated for both boundary conditions of Eqn (5.29) along with those reported by Levy. Table 28 shows that the bending stresses compare well with the Levy results for both sets of boundary conditions. However, as seen in Table 29, the membrane stresses compare only for the first boundary condition set where the tangential component of inplane displacement is free. It is concluded, therefore, that the first set of boundary conditions, i.e., that given by Eqn (5.29a), is the

correct set, as was originally believed.

$$(\bar{\sigma}_1, \bar{\sigma}_2, \bar{\sigma}_6) = (\sigma_1, \sigma_2, \sigma_6) \frac{a^2}{Eh^2} \qquad (5.31)$$

$\bar{q}$	$\bar{\sigma}_1, \bar{\sigma}_2$ $(x,s) = (0,0)$			$\bar{\sigma}_6$ $(x,s) = (4,4)$		
	(5.29a)	(5.29b)	Levy	(5.29a)	(5.29b)	Levy
100	7.186	7.164	7.3	6.772	6.849	6.5
200	8.864	8.839	9.5	9.692	9.832	9.2

TABLE 28. Bending Stresses for Plate Locations (x,s) Based on Boundary Conditions Eqns (5.29a) and (5.29b).

Pt.(x,s)	$\bar{q}$	$\bar{\sigma}_1, \bar{\sigma}_2$		
		(5.29a)	(5.29b)	Levy
(0,0)	100	4.934	4.956	4.9
	200	8.446	8.476	8.4
(4,4)	100	.730	.0014	0.6
	200	1.111	-.0045	1.0

TABLE 29. Membrane Stresses for Plate Locations (x,s) Based on Boundary Conditions Eqn (5.29a) and (5.29b).

224
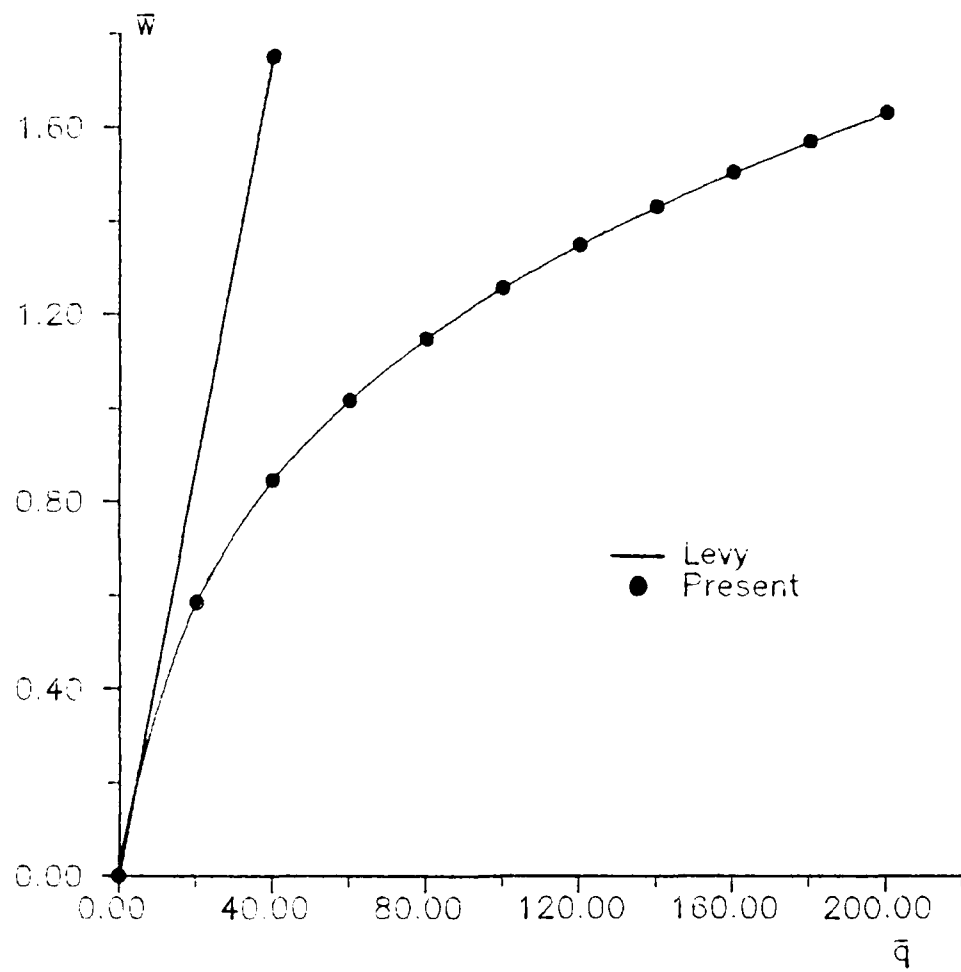
FIGURE 5.34. Nondimensionalized $\overline{w}$ vs $\overline{q}$ for Simply Supported Isotropic Flat Plate.

225

Results for a similar square isotropic clamped flat plate are also compared to a Levy series solution. The boundary conditions for this case are as shown in Eqn (5.32) where the tangential degrees of freedom are all unconstrained as stated by Levy (141). The identical symmetry conditions of Eqn (5.29) apply here also. Eight load increments of $\bar{q}=50$ give the nondimensionalized center plate displacement, $\bar{w}$, shown in Table 30 and plotted versus Levy in Figure 5.35. The transverse displacement profile along x for $\bar{q}=400$ normalized by the center value is shown in Figure 5.36 with the Levy results. Once again, transverse displacement results compare very well with the Levy solution.

$$\bullet x=a/2: \quad u=w=w,_1=\psi_1=0$$

$$\bullet s=a/2: \quad v=w=w,_2=\psi_2=0$$

(5.32)

$\bar{q}$	$\bar{w}$	$\bar{w}$ (Linear)
50	.5731	
100	.9228	
150	1.162	2.019
200	1.346	
250	1.497	
300	1.626	
350	1.739	
400	1.841	

TABLE 30. Clamped Isotropic Plate, 8x8 Mesh of 28 dof Elements.

226
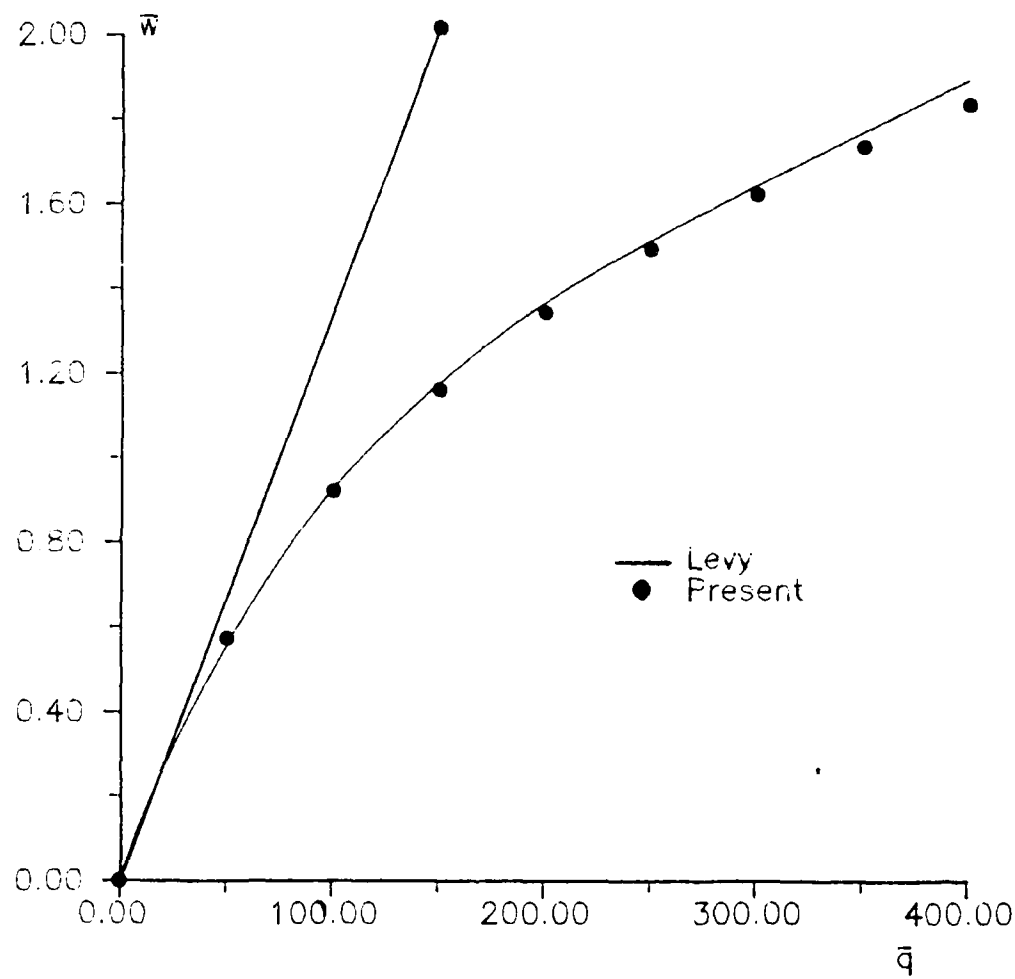
FIGURE 5.35. Nondimensionalized $\bar{w}$ vs $\bar{q}$ for Clamped Isotropic Flat Plate.

227
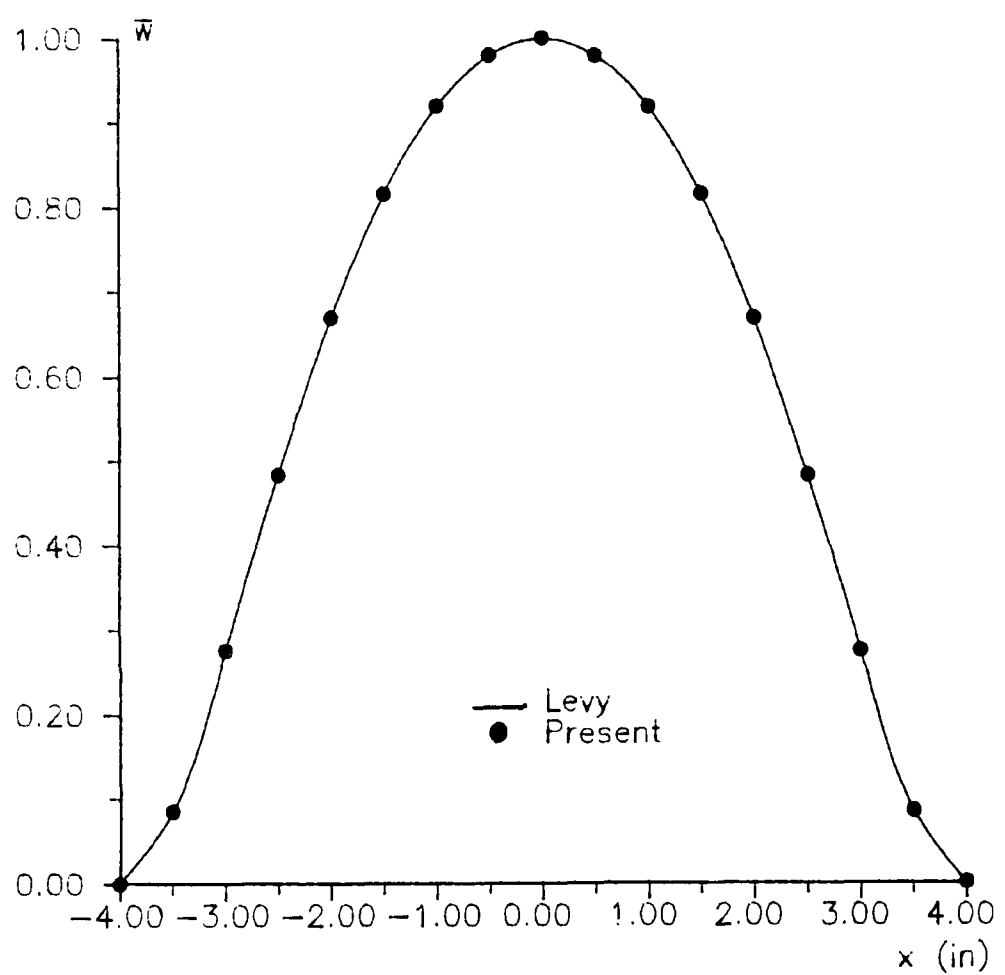
FIGURE 5.36. Transverse Displacement Profile Along x, Normalized by w(0,0), (s=0).

Membrane and bending stresses are calculated for both the center of the clamped plate, $(x,s)=(0,0)$, and at the middle edge, $(x,s)=(a/2,0)$ or $(0,a/2)$. These are compared to the Levy results in Tables 31 and 32. The stress results at the center of the plate compare reasonably well to the Levy values. However, near the plate boundary, the comparison is less accurate. This disagreement is probably due to the coarseness of the mesh. Near the boundary, the mesh is effectively coarser than in the plate center since the clamped conditions constrain so many degrees of freedom.

Generally, the results from the isotropic flat plates are in excellent agreement with the Levy results. Once this was confirmed, the simply supported plate was reanalyzed using the large displacement/rotation element and essentially identical results were attained versus the von Karman element. This is an expected result since the center displacement, for example, is less than twice the thickness at its maximum, see Figure 5.34.

$\overline{q}$	Membrane			Bending	
	$\overline{\sigma}_1,\overline{\sigma}_2$	Levy		$\overline{\sigma}_1,\overline{\sigma}_2$	Levy
100	2.710	2.5		8.460	9.0
200	5.743	6.0		11.21	11.5
300	8.371	8.0		12.70	14.0
400	10.73	10.0		13.72	15.0

TABLE 31. Stress Calculated at Plate Center, $(x,s)=(0,0)$.

	Membrane		Bending	
$\bar{q}$	$\bar{\sigma}_1, \bar{\sigma}_2$	Levy	$\bar{\sigma}_1, \bar{\sigma}_2$	Levy
100	1.533	2.0	18.21	24.0
200	3.171	5.0	29.23	40.5
300	4.490	8.0	37.65	53.0
400	5.587	9.5	44.67	66.0

TABLE 32. Stress Calculated at Middle Edge of Plate, $(x,s)=(a/2,0)$ or $(0,a/2)$.

An additional isotropic flat plate case can be examined in an effort to confirm the displacement control nonlinear equation solution procedure. The algorithm for the displacement incrementation scheme is a simplified version of those described in the literature (101-103) where components of displacement are prescribed and the equilibrium forces at these dof become the unknowns. The algorithm is tested on a clamped plate subjected to a center point load. The problem is solved in two ways. First, the point load is stepped and the displacements are calculated in the traditional Newton-Raphson approach; then, the center transverse displacement is stepped and the center point load and the other displacements are calculated.

Assume the plate geometry of Figure 5.33 with a=b=16 in. and h=.08 in. Fully clamped boundary conditions are assumed, i.e., all seven nodal dof are fixed along the boundaries. The material properties are given in Eqn (5.33), and nondimensionalized center plate transverse

displacement and load are defined in Eqn (5.34), where D is the plate flexural rigidity.

$$E = 10.e6 \text{ psi}$$
$$\nu = .3 \tag{5.33}$$

$$\bar{p} = \frac{p(0,0) \, a^2}{Dh} \quad , \quad \bar{w} = \frac{w(0,0)}{h} \tag{5.34}$$

The displacements are calculated based on load increments of $\bar{p}$=400, see Table 33. Due to symmetry, only 1/4 of the point load shown is applied to the plate model. The point loads are calculated in the second solution based on displacement increments of $\bar{w}$=.5, also shown in Table 33. Both sets of results are plotted in Figure 5.37 along with the results taken from Adotte (142). Adotte solves this problem via a finite difference scheme using von Karman and Kirchhoff plate assumptions.

From Figure 5.37, we see that the displacement and load incrementation schemes give the same equilibrium path, as would be expected. Also, the present results compare very well with Adotte's solution.

231

load incrementation algorithm		disp incrementation algorithm	
$\overline{p}$	$\overline{w}$	$\overline{w}$	$\overline{p}$
		1.0	67.818
800	1.8062		
		2.0	248.13
1600	2.4769		
2400	2.9405		
		3.0	629.83
3200	3.3070		
4000	3.6150		
4800	3.8834		
		4.0	1294.8

TABLE 33.   Center Point Loaded Plate Results for   Both   Load
and Displacement Incrementation.
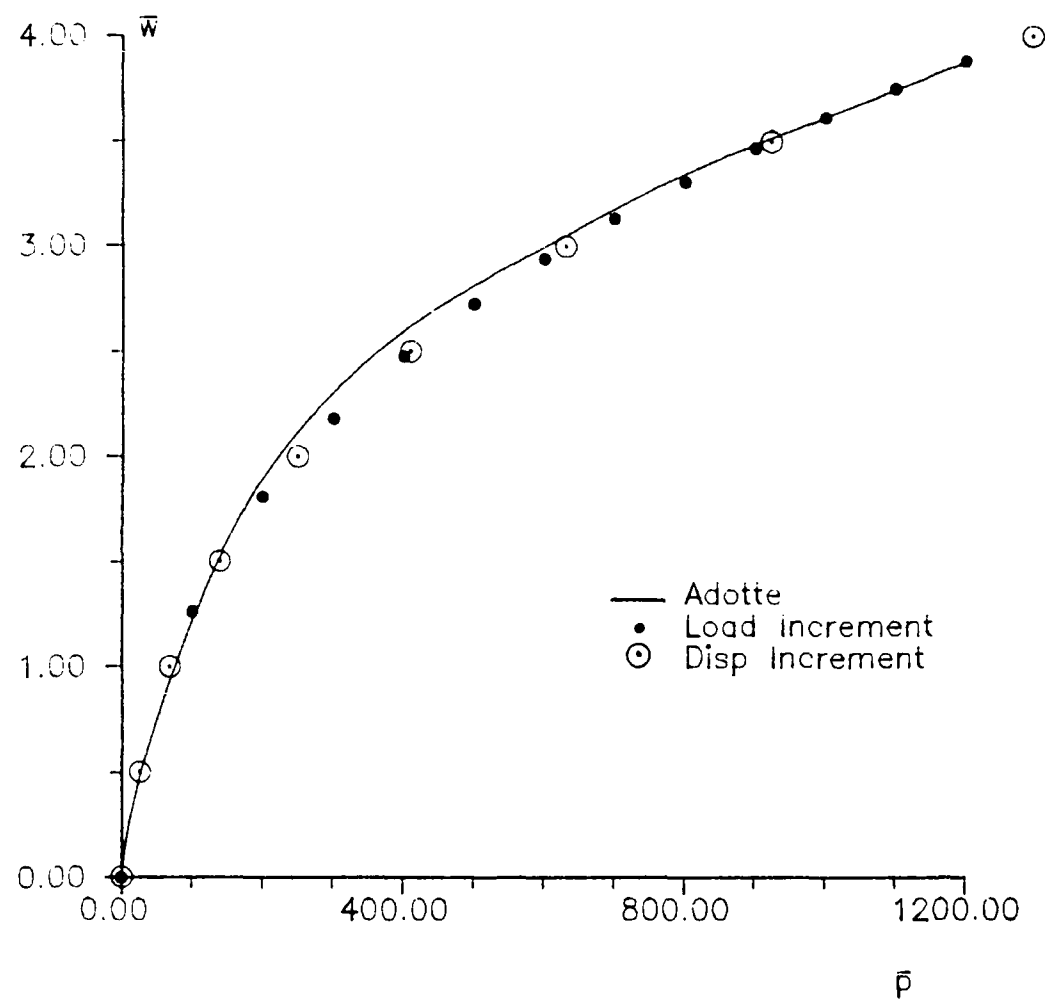
FIGURE 5.37. Nondimensionalized $\bar{w}$ vs $\bar{p}$ for Point Loaded Flat Plate.

233

Solutions to two transversely loaded laminated flat plates are next presented and compared to results obtained by Chia (143) and Putcha and Reddy (95). The first considers a clamped, see Eqn (5.35), unidirectional laminate with material properties as in Eqn (5.36). Thin plates with aspect ratios, 1.0 (a=b=8in.) and .75 (a=8, b=6in.), plate thickness of .08 in., are subjected to uniform transverse pressure q_o, see Figure 5.33. The nondimensionalized load and center transverse displacement, defined in Eqn (5.37), are shown in Table 34 and plotted versus the results of Chia in Figure 5.38. Chia's solution is derived using von Karman thin plate equations via a perturbation technique. Once again, the comparisons are excellent.

●x=a/2: $u=w=w,_1=\psi_1=0$

●s=b/2: $v=w=w,_2=\psi_2=0$ (5.35)

●x=s=0: symmetry

$$E_1 = 4.5e6 \text{ psi}$$
$$E_2 = 1.5e6 \text{ psi}$$
$$G_{12} = G_{13} = .75e6 \text{ psi}$$
$$G_{23} = .3e6 \text{ psi}$$
$$\nu_{12} = .25$$

(5.36)

$$\bar{q} = \frac{(1-\nu_{12}\nu_{21})\, q_o a^4}{E_2\, h^4} \quad , \quad \bar{w} = \frac{w(0,0)}{h} \qquad (5.37)$$

234

$\overline{q}$	$\overline{w}$ (b/a=1.)	$\overline{w}$ (b/a=.75)
5	.5214	.9114
10	.8521	1.332
15	1.080	1.609
20	1.255	1.822
25	1.399	*

TABLE 34. Unidirectional Flat Plate Laminate Results for b/a=1.0 and .75. * not calculated.

Next, consider a quasi-isotropic $[0/\pm45/90]_s$ square laminate subjected to uniform pressure, q_o. Both simple and clamped supports are assumed at the boundary and these are given in Eqn (5.38). The material properties are shown in Eqn (5.39). For this plate, let h=1.6in. and a=b=16in., therefore since S=a/h=10, significant transverse shear deformation is expected. Nondimensionalize the pressure and center transverse displacement as in Eqn (5.40). Table 35 shows the results for both sets of boundary conditions and Figure 5.39 show the plotted data versus the Putcha and Reddy solutions. The latter use a mixed finite element solution to solve the von Karman plate equations that also allow parabolic transverse shear distributions. The present and published approaches for this case are very similar and the results agree closely as expected.

Simple

● $x = \pm a/2$: $v=w=\psi_2=0$

● $s = \pm a/2$: $u=w=\psi_1=0$

Clamped

● $x = \pm a/2$: $u=w=w,_1=\psi_1=0$

● $s = \pm a/2$: $v=w=w,_2=\psi_2=0$

$$(5.38)$$

$$E_1 = 60.e6 \text{ psi}$$
$$E_2 = 1.5e6 \text{ psi}$$
$$G_{12} = G_{13} = .9e6 \text{ psi} \qquad\qquad (5.39)$$
$$G_{23} = .75e6 \text{ psi}$$
$$\nu_{12} = .25$$

$$\bar{q} = \frac{q_o a^4}{E_2 h^4} \quad , \quad \bar{w} = \frac{w(0,0)}{h} \qquad\qquad (5.40)$$

$\bar{q}$	$\bar{w}$ (Simple)	$\bar{w}$ (Clamped)
50	.2759	.1395
100	.4873	.2595
150	.6473	.3573
200	.7753	.4377
250	.8825	.5055

TABLE 35.   Thick Quasi-Isotropic Laminate Results.

The preceding flat plate nonlinear solutions confirm the applicability of the present algorithms to predict isotropic and laminated, thin and thick plate responses. Both transverse displacements and stresses are calculated accurately. Additionally, solutions can be determined by incrementing components of displacement as well as load.
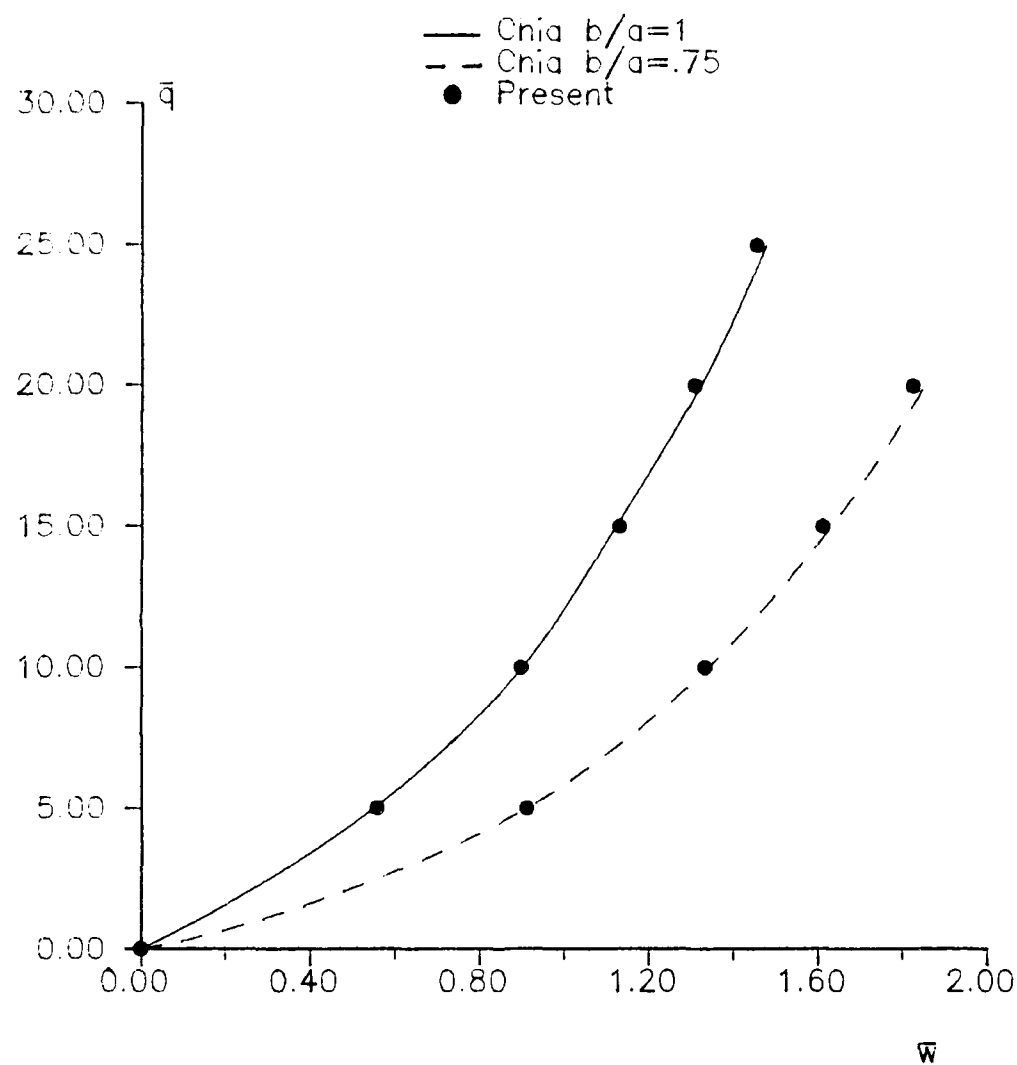
FIGURE 5.38. Nondimensionalized $\bar{w}$ vs $\bar{q}$ for Unidirectional Flat Plate Laminate.

237
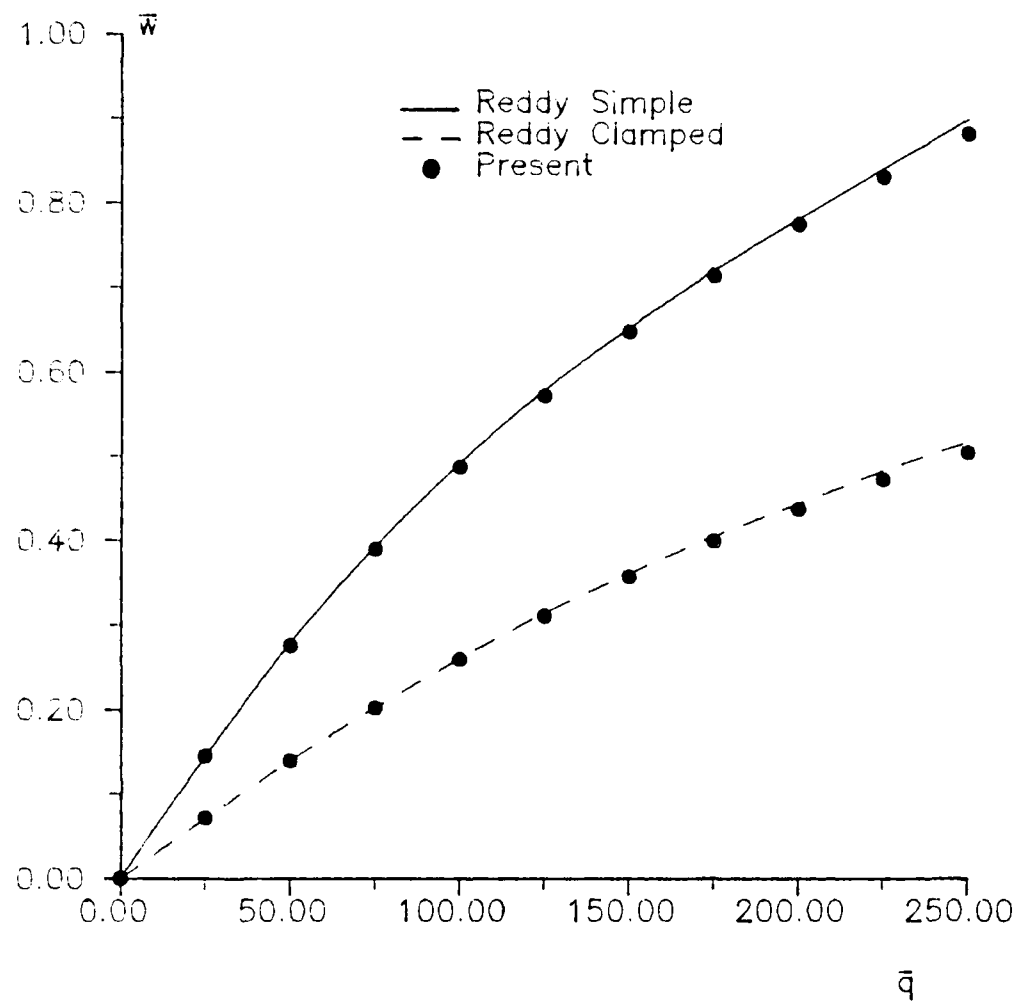
FIGURE 5.39. Nondimensionalized $\bar{w}$ vs $\bar{q}$ for $[0/\pm 45/90]_s$ Laminated Plate.

238

The first nonlinear cylindrical shell examined is the isotropic clamped panel under transverse pressure. This case was tested both in the linear and linear bifurcation analysis, see Figure 5.15 and Eqn (5.14) for geometry, boundary conditions, etc. Published results for the nonlinear response are available from several sources. Sabir and Lock (144) use an assumed strain function finite element approach and show that the solution given by Brebbia and Connor (136) is not fully converged. Brebbia and Connor use a Love/Donnell approach in a finite element formulation with assumed displacements similar to the present 28 dof element's u, v, w, $w,_1$, and $w,_2$ approximations. Recall that the present formulation also has the two additional dof, ψ_1 and ψ_2, at each node of the 28 dof element.

Pressure loads are incremented in steps of $q_o = .01$ psi and center transverse displacement solutions are shown in Table 36 for several mesh arrangements. The Table shows that as the load is increased, the various meshes give center displacements that begin to diverge. That is, although the initial loads indicate consistent responses for all meshes, they begin to differ increasingly as more load is applied, implying that convergence must be examined for the higher loads. The 8x8 28 dof element mesh (8x8L) gives results very similar to the 8x8 36 dof element mesh (8x8Q). This is consistent with the previous observation that the behavior of this shell is governed primarily by bending.

239

For this reason, the higher order approximations for u and v in the 36 dof element do not alter the solution significantly.

q_o psi	4x4L	8x8L	4x4Q	4x6Q	8x8Q
.04	11.941	12.016	12.259	12.105	12.113
.08	25.178	25.687	25.935	25.708	25.943
.12	40.093	41.882	41.491	41.416	42.437
.16	57.262	62.570	59.671	60.367	63.858
.20	77.599	94.164	81.776	85.122	98.637
.24	102.60	169.97	110.31	123.31	198.75
.28	134.54	254.14	150.33	193.38	277.43
.32	175.13	303.90	206.51	259.95	323.06
.36	220.15	340.23	263.44	304.52	356.87
.40	261.19	369.44	307.23	338.00	384.31

TABLE 36. Clamped Isotropic Panel Transverse Displacement w (in.) Results for Various Meshes.

The results of the 8x8Q mesh are plotted in Figure 5.40 versus results from Sabir and Lock. Note that for this Figure, the solid line indicates the present results and the discrete points represent the published results. This is the reverse of what has been presented in previous comparisons due to difficulty in reading the published graphs. The Figure also shows the linear bifurcation predictions based on both the fully linearized and classical approaches. The nonlinear response, however, does not indicate an instability as was mentioned earlier in the linear bifurcation discussion.
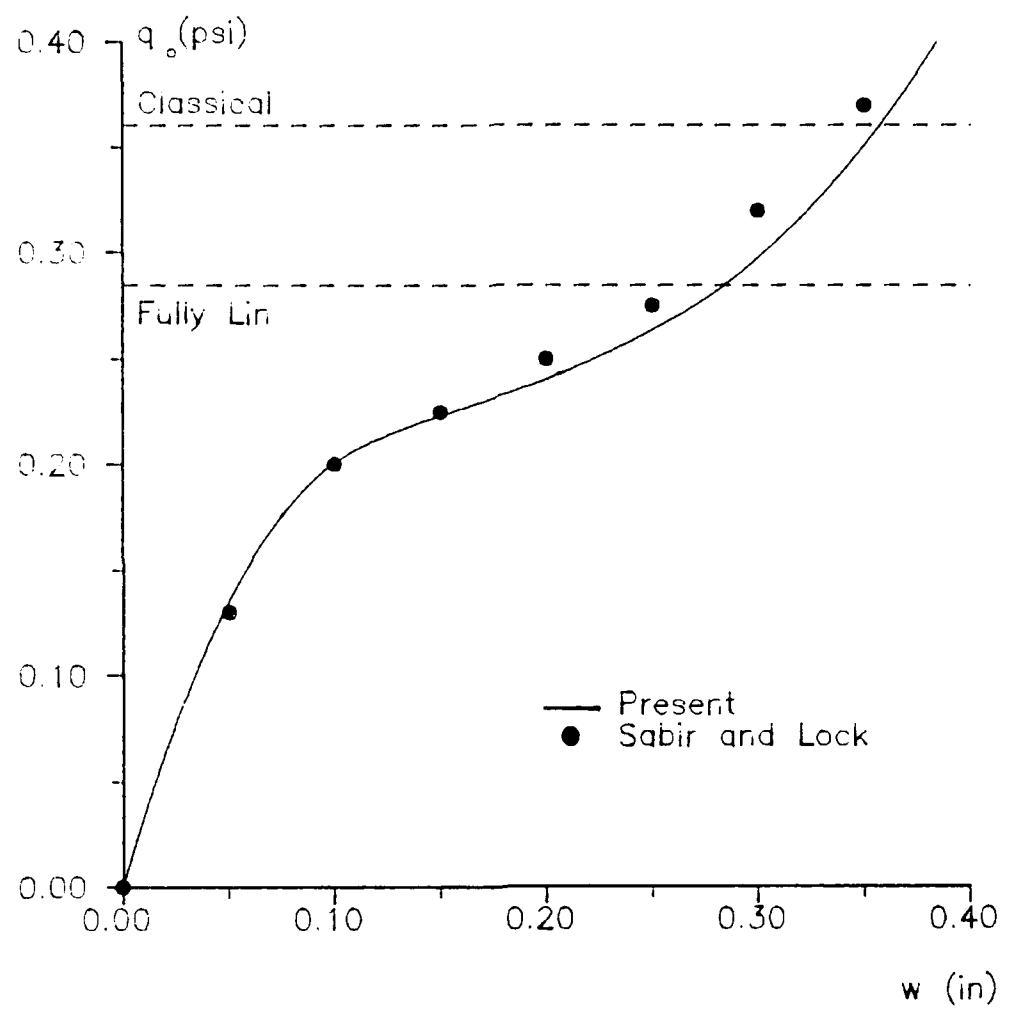
FIGURE 5.40. Clamped Cylindrical Shell Nonlinear Response and Bifurcation Loads.

241

The present nonlinear results appear to give a slightly more flexible response compared to Sabir and Lock. This difference could easily be due to the aforementioned transcribing errors. Another possibility is that the results are not fully converged. Although the present results are slightly more flexible than the published, this is the shell testcase that gave nonmonotonic convergence in the linear results, see Table 10. That is, it is possible that a further mesh refinement will give stiffer results, based on the results of Table 10. A final explanation is based on the additional dof in the present formulation, i.e., transverse shear deformation.

In the absence of closed form solutions based upon the classical assumptions where the transverse stresses are neglected, a valid nondimensionalization is required such that the effects of transverse shear deformation can be studied. Alternatively, finite element results based upon classical assumptions could be used for comparisons. Unfortunately, the present formulation does not allow classical solutions, i.e., the parabolic transverse shear stress distribution is always included. Hence, a nondimensionalization procedure is determined relying on similar problems that have closed form solutions.

The closed form series solution for the center transverse displacement of an isotropic clamped transversely pressure loaded square flat plate of length, L, is of the

242

form of Eqn (5.41a) and suggests the nondimensionalization of Eqn (5.41b). Additionally, the exact solution for a clamped cylindrical pressure vessel is of the form of Eqn (5.42a) and suggests the nondimensionalization of Eqn (5.42b). The Batdorf parameter, Z, as defined in Eqn (5.43), is often used in cylindrical shell geometric parametric studies. An additional parameter, M, also defined in Eqn (5.43), is used similarly for cylindrical panels (14). From Eqns (5.41)-(5.43), a nondimensionalization is defined as follows. If we allow the thickness of the shell, h, and the shell radius, R, to vary such that Rh is kept constant, and keeping the shell length, L, constant, then the nondimensionalizations of Eqn (5.41b) and Eqn (5.42b) are equivalent. In this way, the L/h ratio of the shell can be varied and results can be compared using either nondimensionalization and at the same time, the shell geometry parameters Z and M remain constant.

$$w(0,0) = \text{constant} \cdot \frac{q_o \, L^4}{E \, h^3} \qquad (5.41a)$$

$$\frac{w(0,0)}{h} \text{ versus } \frac{q_o \, L^4}{E \, h^4} \qquad (5.41b)$$

$$w(x,s) = f(x) \, \frac{q_o \, R^2}{E \, h} \qquad (5.42a)$$

$$\frac{w(0,0)}{h} \text{ versus } \frac{q_o \, R^2}{E \, h^2} \qquad (5.42b)$$

$$Z = \frac{L^2}{Rh} \left[1-\nu^2 \right]^{1/2}, \qquad M = \frac{(2R\theta)^2}{Rh} \left[3(1-\nu^2) \right]^{1/2} \frac{1}{\pi^2} \qquad (5.43)$$

where $2R\theta$ = arclength = L, see Figure 5.15.

Three shell geometries are tested with the thicknesses and radii given by the values in Table 37. The middle entry represents the original geometry. Therefore, changes in R and h give a shell geometry that has L/h 50% less and greater than the original. Note that the ratio R/h increases as L/h increases. Both are indicative of a thinner shell, that is, one that is influenced to a lesser degree by transverse shear deformation.

The finite element results for the three equilibrium paths are plotted in Figure 5.41 where $\bar{w}$ and $\bar{q}$ are defined by the quantities of Eqn (5.41b). Also shown are nondimensionalized Sabir and Lock data. The loading is not shown for $\bar{q} \leq 240$ since all cases give nearly identical results. This is a good indication that the nondimensionalization is valid since the original shell geometry compared well with the Sabir and Lock data for these values of loading. For loading $\bar{q} > 240$, the trend in the finite element results shows movement toward the published results as L/h is increased. This indicates that transverse shear deformation at least partially explains the more flexible displacements the present formulation generates based upon the original geometry of Figure 5.15.

244

When L/h is increased, the shell response is stiffer, i.e., there is less transverse shear deformation. However, as L/h and R/h are further increased, more and more membrane action relative to bending, is anticipated since the shell becomes so thin. For this reason, asymptotic results for the limiting case where L/h and R/h approach infinity are not expected. Despite this, the author believes that the flexible response at the higher loads for the original geometry is due to transverse shear deformation.

R (in)	h (in)	L/h	R/h
50	.25	80	200
100	.125	160	800
200	.0833	240	1800

TABLE 37. Shell Geometries for Clamped Cylindrical Shell.
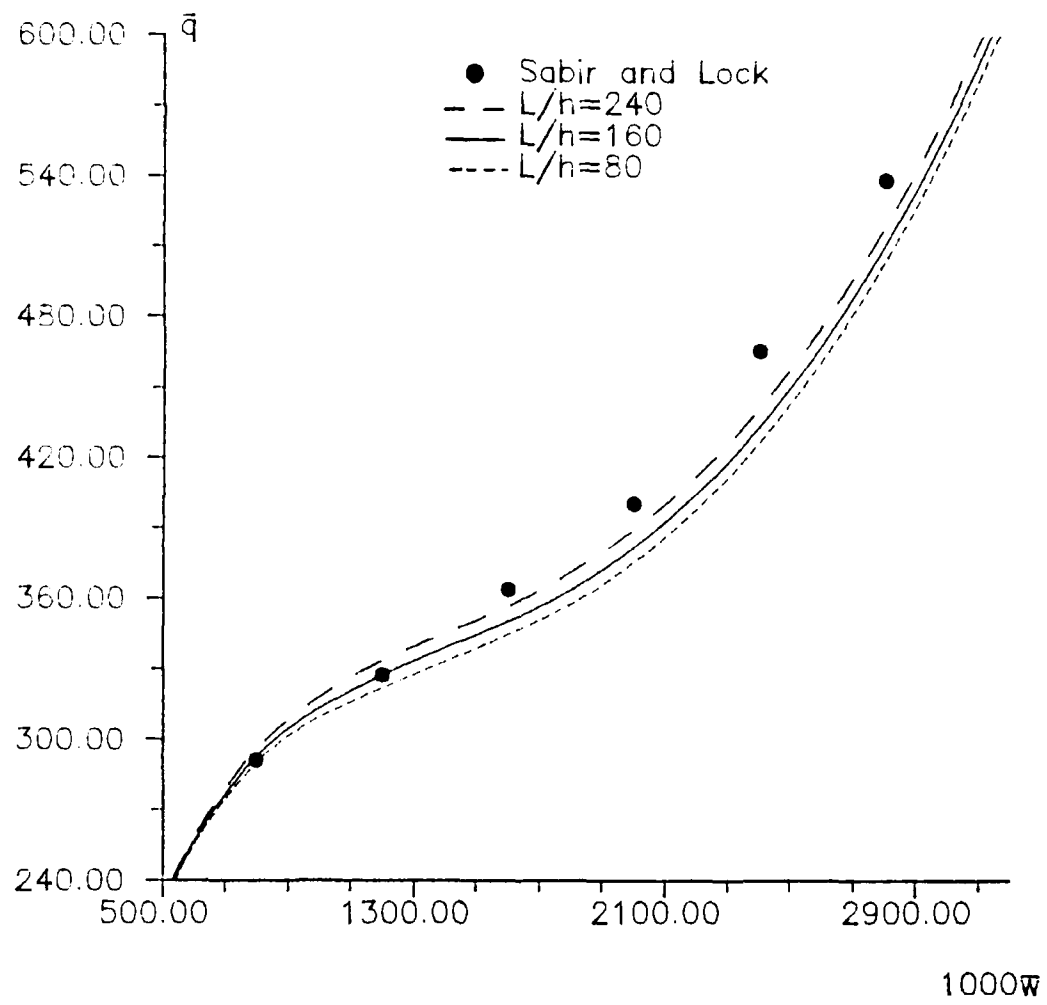
FIGURE 5.41. Nondimensionalized $\bar{q}$ vs $1000\bar{w}$ for Clamped Cylindrical Shell.

246

The second nonlinear shell testcase examined is the hinged-free point loaded cylindrical panel shown in Figure 5.42. This geometry is a popular validation problem since very different equilibrium paths result simply by varying the shell thickness. Once again, the results of Sabir and Lock (144) are used for comparison. For one shell thickness, a convergence study similar to that done in the previous shell example showed little differences between the 4x6Q and 8x8Q meshes and therefore results based on the former are presented for all cases. The boundary conditions are given in Eqn (5.44) for one quadrant of the shell of Figure 5.42. Because of expected snap through and snap back limit points in the load displacement response, the center transverse displacement was incremented instead of the point load. Figures 5.43-5.45 show the shell nonlinear response for three shell thicknesses. Superimposed on each Figure are the solutions taken from Sabir and Lock (144).

E = 4.5e6 psi
ν = .3
θ = .1 rad
R = 100 in.
h = 1.,.5,.25 in.
L = 20 in.
δ/b = .05
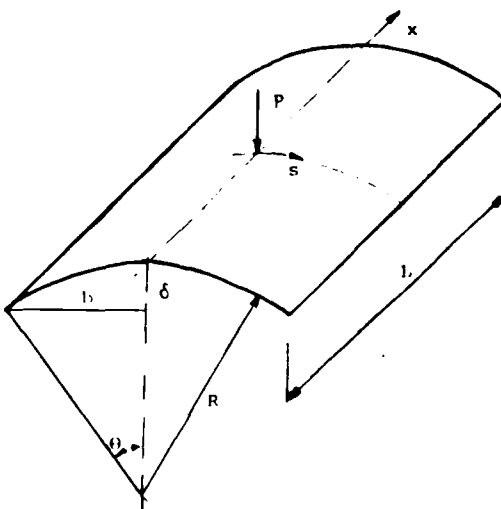
FIGURE 5.42. Hinged-Free Point Loaded Cylindrical Shell.

$\bullet x = 10$:   free

$\bullet s = 10$: $u = v = w = \psi_1 = 0$ (5.44)

$\bullet x, s = 0$:   symmetry

In Figure 5.43, the response is characterized by monotonically increasing load and displacement, i.e., the shell does not collapse. Initially, circumferential compression gives an increasingly more flexible response until an inflection occurs. At this point, the longitudinal tensile stresses dominate and the response is increasingly stiffer. In contrast, as seen in Figures 5.44 and 5.45, when the thickness is decreased, the response changes dramatically. Figure 5.44 shows the existence of a collapse point at A. For an increase in load beyond that at A, the shell will violently snap through to an inverted position where an increase in load will again result in an increase in displacement, as was discussed in Chapter IV. For this case, the free curved edges do not displace until the load at point A is reached. At this point, the free edges snap through to the inverted configuration. If the thickness of the shell is again halved, the response of Figure 5.45 results. For this case, a snap through point at A and a snap back point at B exist.

The finite element results for the present formulation compare very well with those of Sabir and Lock. The snap through points of Figures 5.44 and 5.45 are traversed easily

248

using the displacement control algorithm. The solution algorithm does not fail at the snap back point of Figure 5.45, but also cannot give any information on its existence. Sabir and Lock devised an algorithm where force and displacement control can be alternated automatically depending upon the characteristics of the equilibrium path, thereby representing both types of critical points.

This problem was reanalyzed using the 36 dof large displacement/rotation elements for thicknesses of .5 and .25 inches. The results were slightly more flexible than what the Donnell elements gave and are not shown. This is a reasonable result since only moderate rotations are experienced by the shell even after snap through when the shell is in an inverted configuration. Since the shell is shallow, these rotations are moderate at most.

The shallowness of a shell and its relation to post collapse angle of rotation can be explained by referencing Figure 5.46. The shell is considered shallow if the ratio δ/b is small. When the shell snaps through to the inverted position, i.e., the stable equilibrium position at point C of Figure 4.5, the rotations at the fixed end are expected to be near 2θ, see Figure 5.46 where the dashed line indicates the inverted configuration if no load were applied. This angle of rotation is small when δ/b is small. For the shell just analyzed, δ/b is only 0.05 and $2\theta \cong 11$ degrees. The calculated maximum rotations of points along

the hinged edge are about 10 degrees. Apparently, the Donnell equations, valid for moderate rotations, are adequate for this application.
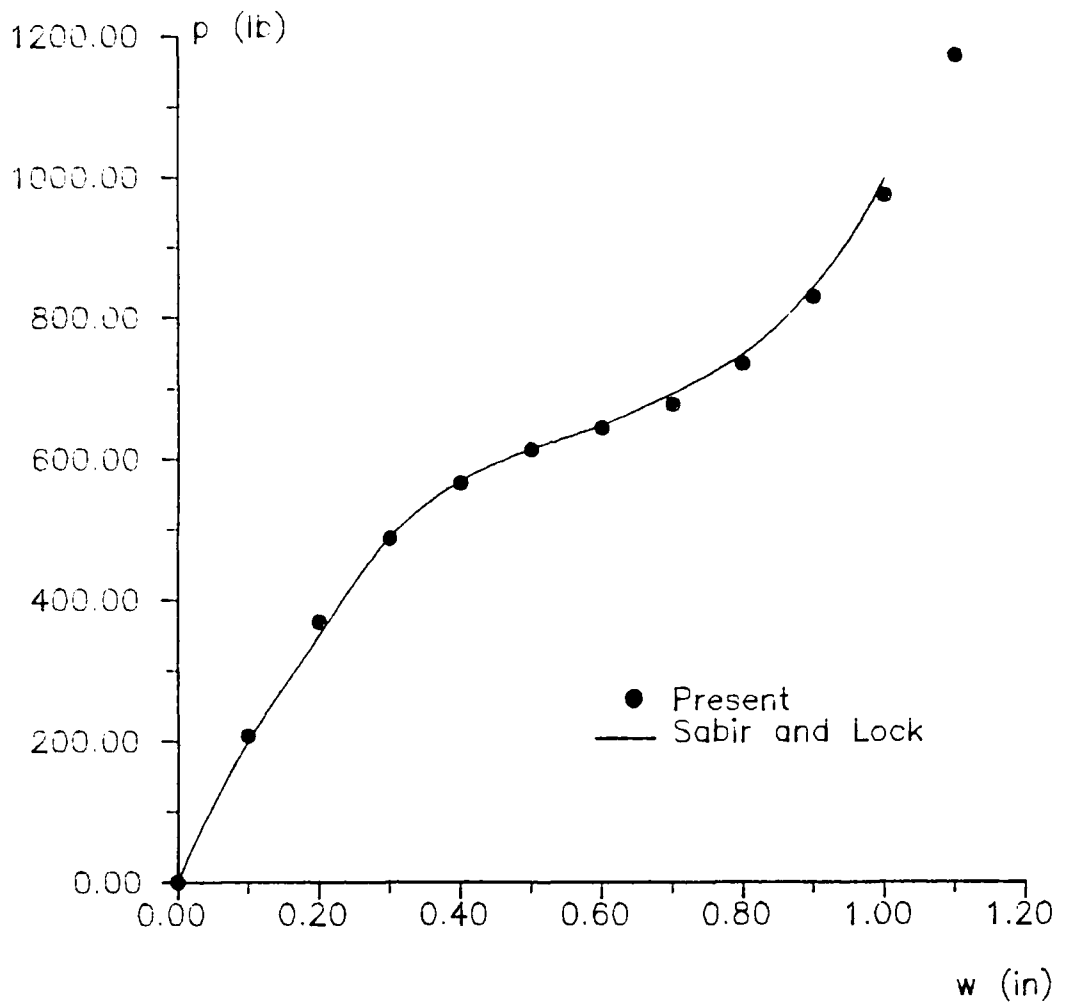
FIGURE 5.43. Point Loaded Cylindrical Shell Panel Response for h=1.0 in.
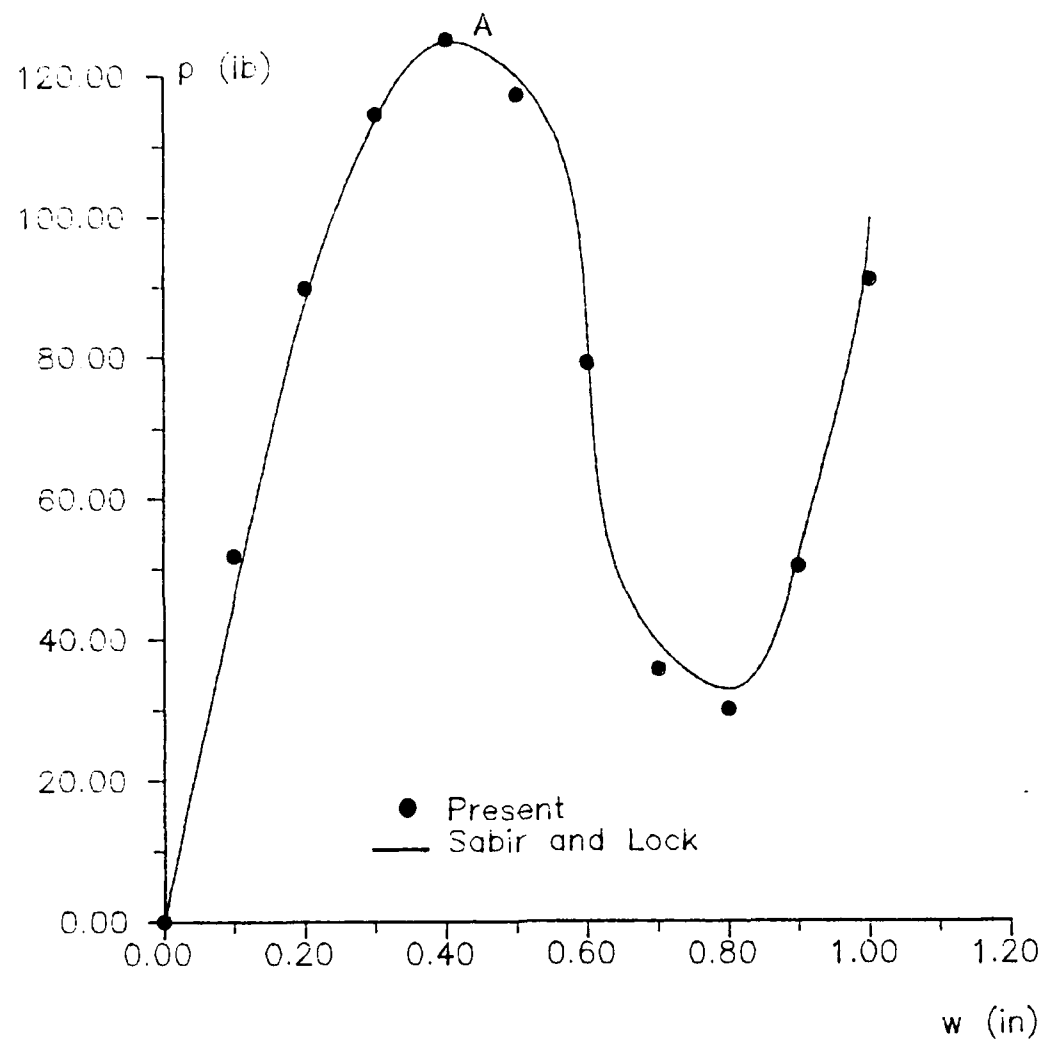
FIGURE 5.44. Point Loaded Cylindrical Shell Panel Response for h=.5 in.
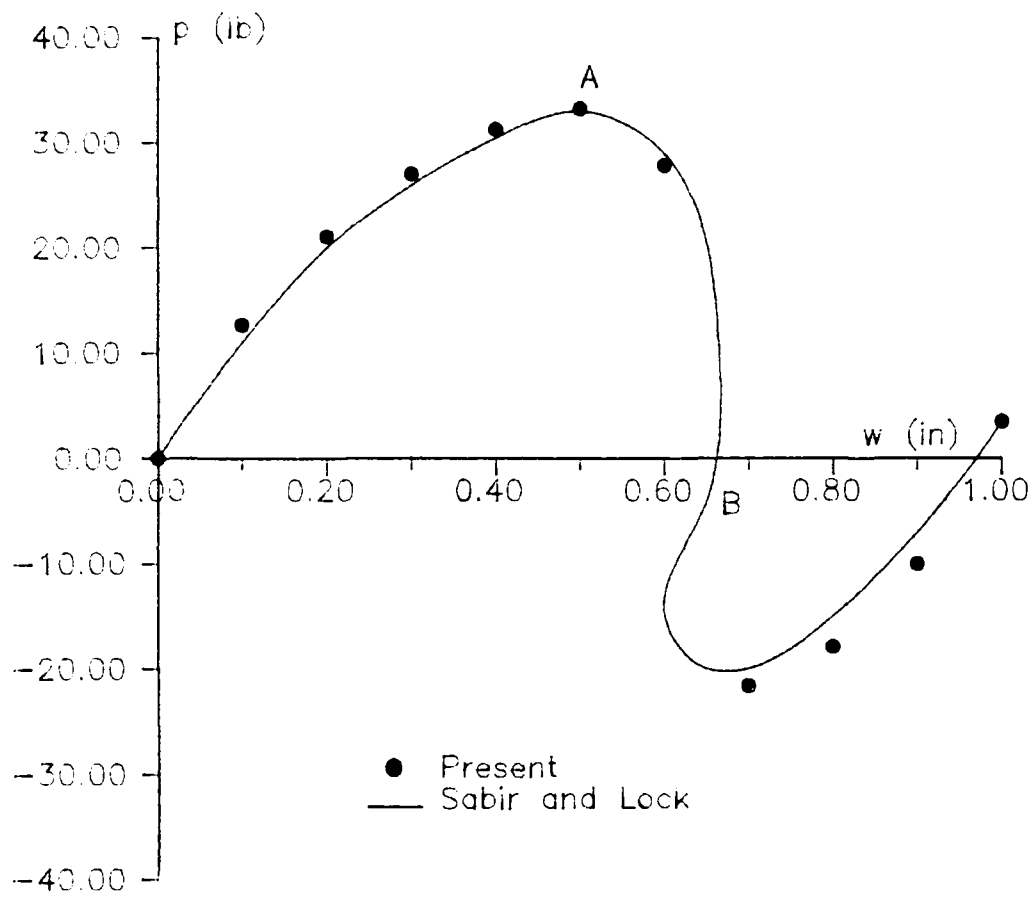
FIGURE 5.45.   Point Loaded Cylindrical Shell Panel   Response for h=.25 in.
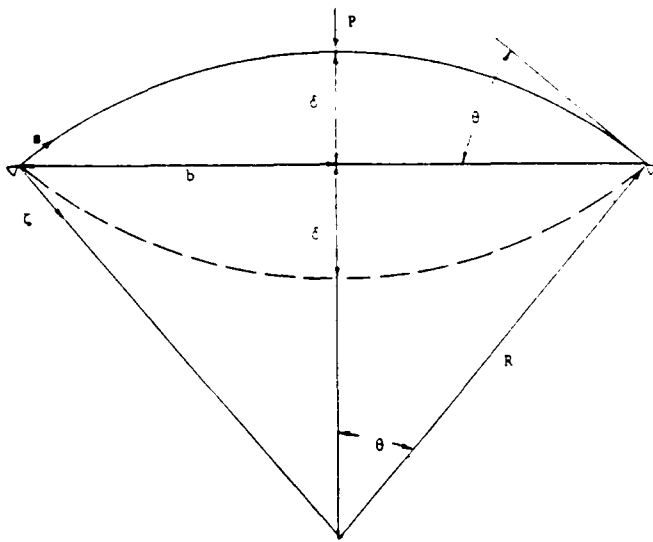
FIGURE 5.46.   Edge View of Shell Showing Shallowness.

We can next consider a similar deeper shell geometry where the quantities of Figure 5.46 are given in Eqn (5.45). This geometry was chosen in an effort to test the finite element code's ability to predict larger rotations.   The deeper shell will undergo greater edge rotations after snap through, i.e., at Point C of Figure 4.5.   For this case, the ratio δ/b is over twice the previous, and the inverted shape of the shell might have edge rotations of approximately $2\theta \cong$ 28.6 degrees, see Figure 5.46.

$$\begin{aligned} \theta &= .25 \text{ rad} = 14.3 \text{ degrees} \\ R &= 40. \text{ in.} \\ h &= .25 \\ \delta/b &= .1257 \end{aligned} \qquad (5.45)$$

Incrementing the displacement at the center of the panel as before gives the results shown in Table 38 for both Donnell and the large displacement/rotation assumptions.

253

For the initial displacement increments, the results of the two compare closely as would be expected since only small rotations have occurred. However, near the collapse point and beyond, the calculated equilibrium loads are, at times, very different. As the center displacement increases, maximum rotations, also given in Table 38, occur near the center of the panel, at first, then gradually move outward towards the edges. After the inverted configuration is attained, the maximum rotations will occur along the hinged edge.

	Donnell	FNL	Max Rotation
$w(0,0)$	$P(0,0)$	$P(0,0)$	(FNL, ψ_2)
0.3 in.	53.73	53.66 lbs	4.5 deg
0.6	89.52	89.01	8.2
0.9	133.50	131.94	11.0
1.2	101.16	94.01	13.5
1.5	54.48	45.79	15.4
1.8	2.683	-4.770	17.2
2.1	-72.95	-74.98	19.3
2.4	-57.06	-39.59	24.5
2.7	92.87	106.65	24.2

TABLE 38. Deep Hinged-Free Shell Results.

For rotations larger than approximately 11 degrees, the differences between the two approaches is evident in the Table. Although the rotations experienced by some points of the shell are quite large, the general response of the shell discretized with Donnell elements is very similar to the model that allows the large rotations as is seen in Figure

254

5.47 where the load displacement data of Table 38 is plotted. Note that at Point C, adjacent to the snap through Point A of Figure 5.47, w under the load is approximately 2.7 inches. This is slightly larger than $2\delta=2.49$ inches (see Figure 5.46) as would be expected. Additionally, note that the largest rotation in Table 38 is less than the predicted $2\theta=28.6$ degrees. This is also expected since after snap through, the shell is predominantly in tension. In this way, the shell is stretched and its curvature is less than that if there were no load. Therefore, because the load is still applied, the inverted configuration gives an angle of rotation that is smaller than $2\theta=28.6$ degrees.
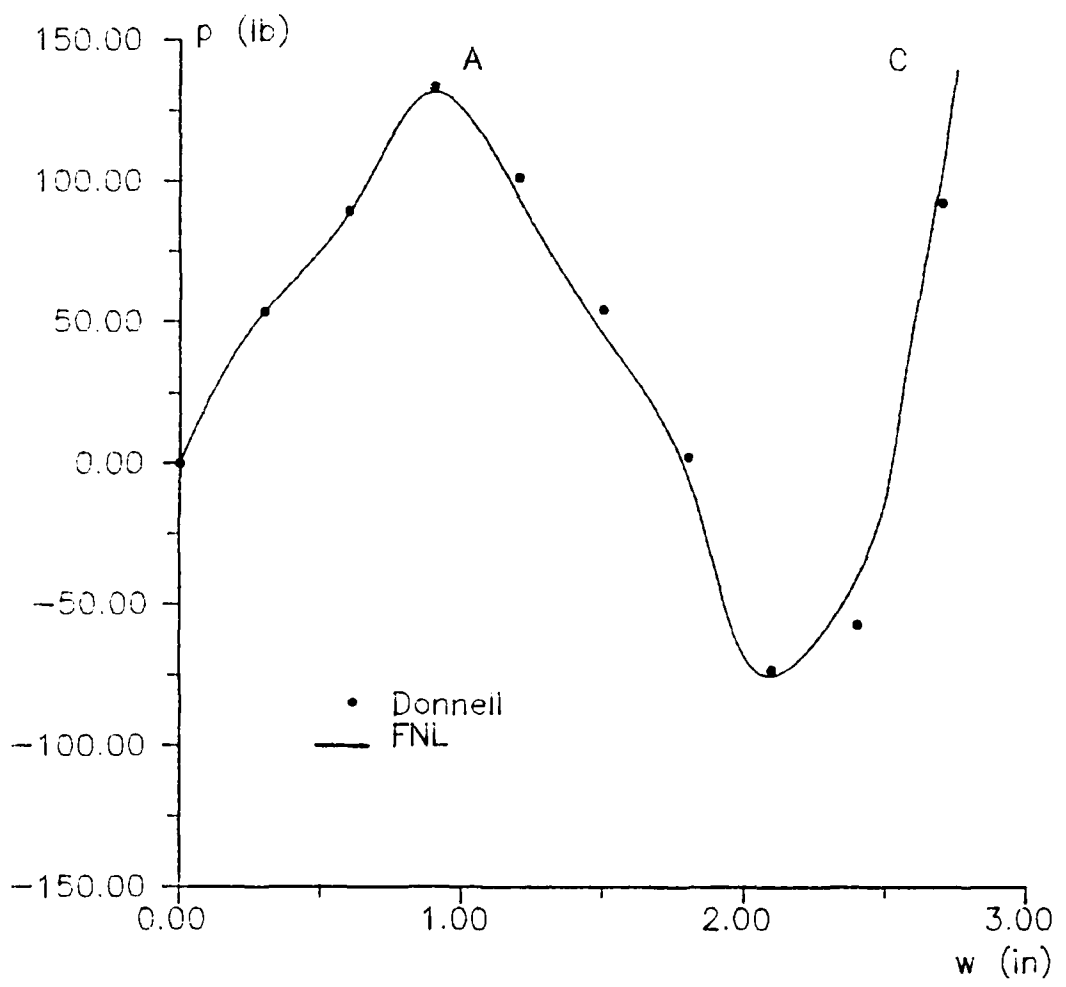
FIGURE 5.47. Deep Hinged-Free Cylindrical Shell, Donnell and FNL.

256

Larger displacements and rotations can be examined by studying deep circular arches. The simply supported arch subjected to a center point load is similar to the previous hinged-free cylindrical shell only simpler since the arch is effectively only a 1-D problem. A very shallow arch is first briefly examined to confirm that the modelling procedure is correct. Consider the arch shown in Figure 5.48 where the geometrical quantities are given in Eqn (5.46), and the simply supported boundary conditions in Eqn (5.47). The width of the arch, i.e., the dimension in the x coordinate direction, is assumed to be 1.0 and both of the circumferential edges, ●x=0 and 1.0, are completely free. As in the Euler column buckling problem, Poisson's ratio is set to zero in an attempt to better represent 1-D beam elements.

E = 10.e6 psi
ν = 0.0
I = area moment of inertia
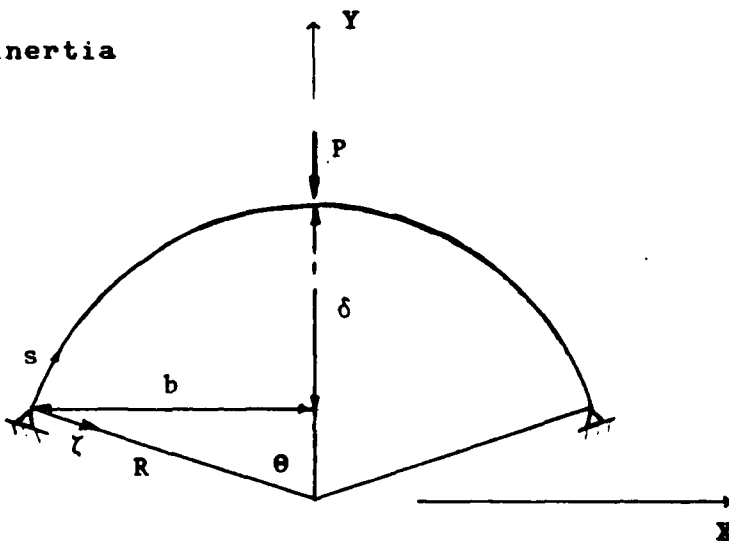
FIGURE 5.48. Circular Arch Geometry.

$$R = 100. \text{ in.}$$
$$h = .2 \text{ in.}$$
$$\Theta = 10 \text{ degrees} \qquad\qquad (5.46)$$
$$\delta/b = .0874$$

$$\bullet\; s = 0,\; 2R\Theta: \quad u=v=w=w,_1=\psi_1=0 \qquad (5.47)$$

For a 1x40Q mesh of elements, the nondimensionalized collapse loads are given for both Donnell and the FNL elements in Table 39. Also shown is the result taken from Walker (145) based on a finite element analysis. As can be seen, the results compare well and therefore confidence in the model is attained.

Donnell	FNL	Walker
75.936	75.378	76.21

TABLE 39. Shallow Circular Arch Collapse Loads, PR^2/EI.

Consider next a similar, but much deeper, arch where the geometrical quantities are shown in Eqn (5.48). For this case, δ/b and Θ are over five times larger than the shallow arch values. The boundary conditions and loading will result in a symmetric response where the arch crown displaces only radially. Results based on both Donnell and FNL assumptions are compared to the inextensible solution of Huddleston (146). Huddleston also provides closed form solutions for an arch with an extensible midsurface. He

258

defines the extensibility of the arch by a factor, c, as shown in Eqn (5.49); the inextensible solution is represented by c = 0 since the bending stiffness, EI, is very small compared to the axial stiffness, EA. The geometry of the arch for the present formulation gives an extensibility factor of c = 3.255e-6.

$$R = 100. \text{ in.}$$
$$h = 1.0 \text{ in.}$$
$$\theta = 53.13 \text{ deg.} \qquad (5.48)$$
$$\delta/b = .50$$

$$c = \frac{I}{A(2b)^2} \qquad (5.49)$$

where,

I=area moment of inertia
A=cross sectional area

Solutions are obtained by incrementing components of displacement and Figure 5.49 shows the center load displacement response of the arch compared to the Huddleston results for c=0 and .01. Table 40 also shows some of the present results for both the Donnell and FNL solutions. The collapse load for the Donnell arch is approximately 13% below the inextensible solution (c=0), yet is much larger than the published extensible solution (c=.01). The extensibility of the middle surface is seen to increase the deflection of the arch under load, as is expected since the arch is in compression. The parameter, c, for the present case is very small, and therefore, the results tend to

259

follow the c=0 results closely until near the peak load. The Donnell response falls between the two Huddleston curves in the post collapse regions and gives an expected response for the extensibility factor for the present arch geometry. The FNL collapse load is approximately 20% lower than the inextensible solution. Additionally, the post collapse response of the FNL model is different from the Donnell model and the inextensible results in that it does not fall between the c=0 and .01 curves. This is attributed to the higher order representation of the deformation of the midsurface of the arch. Recall the FNL formulation includes many nonlinear inplane displacement terms in the strain definitions that are not included in the Donnell equations. Therefore, one might expect a greater effect of extensibility in the FNL elements compared to the Donnell as the displacements become large, i.e., where the additional terms become more important. The transverse shear degrees of freedom will have a small effect but will also increase the displacement under load compared to the inextensible (147). Almroth and Brogan (124) saw a similar effect compared to the inextensible solution of a deep arch. The finite element formulation allows u and v displacements at the midplane and their results were consistently more flexible compared to the inextensible.
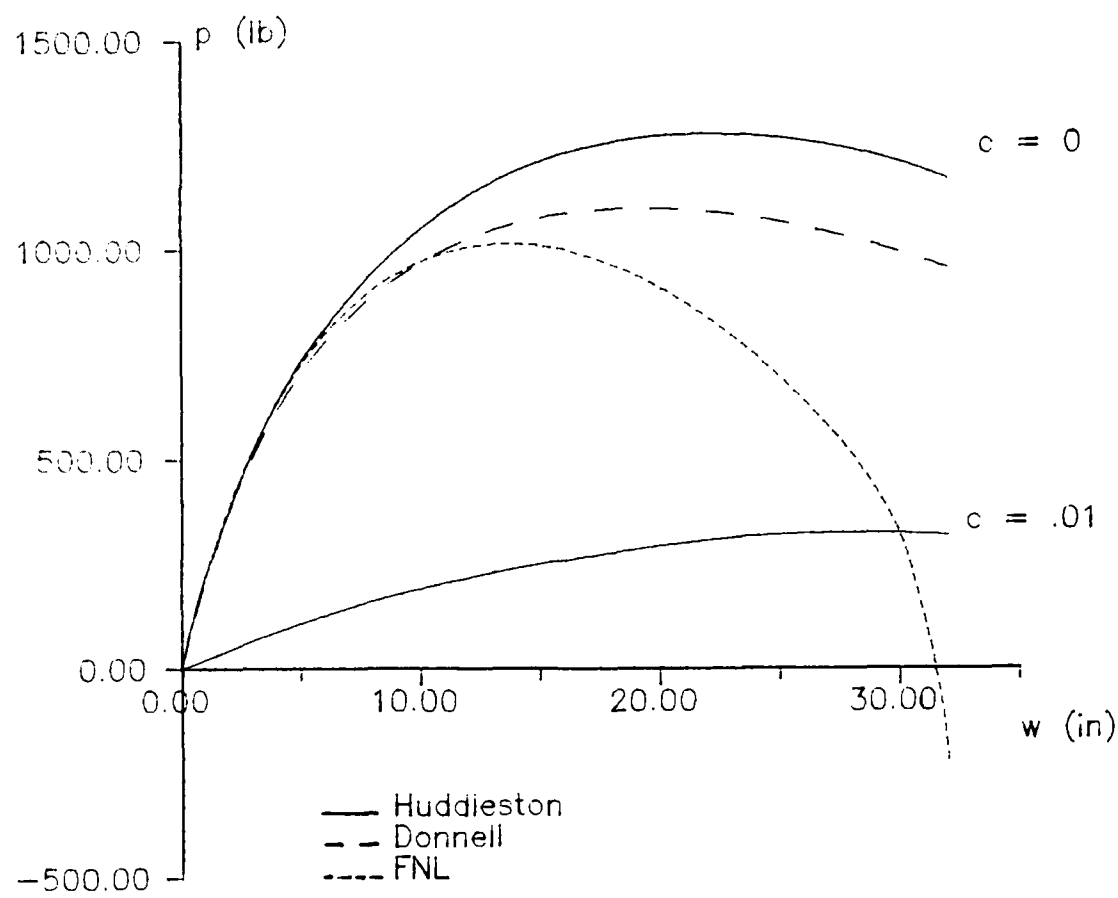
FIGURE 5.49. Deep Simple Supported Circular Arch Crown Displacement vs Load.

261

w (in)	Donnell (lbs)	FNL (lbs)
4.0	621.24	636.98
8.0	893.66	907.50
12.0	1028.2	1007.3
16.0	1088.3	998.80
20.0	1100.5	908.42
24.0	1078.4	748.04
28.0	1029.5	513.56
32.0	958.56	-219.98

TABLE 40.   Arch Crown Point Loads for Prescribed w.

The final circular arch problem is similar to Figure 5.48 only now the right support is fully clamped. These boundary conditions will give a nonsymmetric response where the crown will displace radially as well as circumferentially. The displacement of the crown can be represented easily by global horizontal and vertical components, i.e., by changes in the coordinates along X and Y of Figure 5.48. These are determined from displacements, w and v, as shown in Eqn (5.50). The geometrical quantities for this hinged-clamped arch are given in Eqn (5.51) and, once again, define a deep arch. Horizontal and vertical displacements of the crown resulting from the crown point load are shown in Table 41. Results are also compared to the inextensible solution of Dadeppo and Schmidt (148) in Figure (5.50). The quantities shown in Figure 5.50 are nondimensionalized load, $\bar{p}=pR^2/EI$ and vertical displacement of the crown under the load, $V=\Delta Y/R$.

$$\Delta Y = R \cos\left(\frac{s'}{R}\right) - (R-w)\cos\left(\frac{s'+v}{R}\right)$$

$$\Delta X = R \sin\left(\frac{s'}{R}\right) - (R-w)\sin\left(\frac{s'+v}{R}\right) \tag{5.50}$$

where s is the circumferential coordinate of a point on the undeformed arch, see Figure 5.48, and $s'=s+R\theta$.

$$
\begin{aligned}
R &= 100 \text{ in.} \\
h &= .25 \text{ in.} \\
\theta &= 50 \text{ degrees} \\
\delta/b &= .466
\end{aligned}
\tag{5.51}
$$

FNL			Donnell		
$\dfrac{PR^2}{EI}$	$-\dfrac{\Delta X}{R}$	$-\dfrac{\Delta Y}{R}$	$\dfrac{PR^2}{EI}$	$-\dfrac{\Delta X}{R}$	$-\dfrac{\Delta Y}{R}$
6.897	.00730	.02503	6.698	.00770	.02502
10.152	.01577	.05013	9.816	.01680	.05015
11.821	.02378	.07531	11.58	.02520	.07530
12.633	.03059	.1005	12.68	.03230	.1006
12.898	.03599	.1257	13.40	.03792	.1258
12.262	.04249	.1761	14.22	.04664	.2014
8.854	.04277	.2512	14.02	.04681	.2515
3.968	.03204	.3258	12.83	.04080	.3262

TABLE 41. Horizontal and Vertical Displacements of Arch Crown.

Results similar to the previous hinged-hinged deep arch are also exhibited here. The Donnell solution gives a collapse load 6% below the inextensible (148) and the FNL solution is 16% less than the inextensible. For a load approximately equal to the collapse load, the deformed shape of the arch is shown in Figure 5.51 where the maximum rotation of any point is 39 degrees and the maximum displacement is 85 times the thickness. The FNL formulation

results in greater extensibility than does the Donnell formulation. The FNL results indicate stretching of the midsurface of the elements near the crown up to approximately 5% greater than the Donnell.
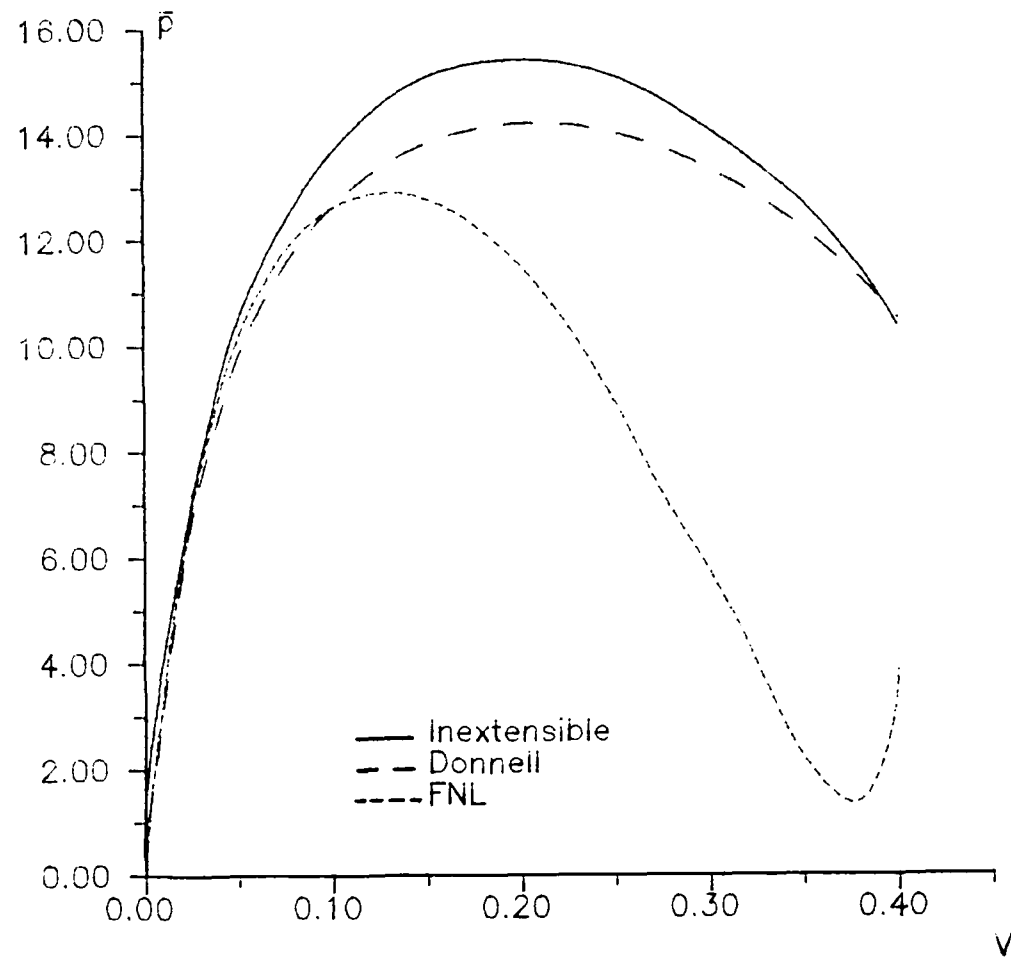
FIGURE 5.50. Deep Clamped-Hinged Arch Crown Vertical Displacement vs Load.
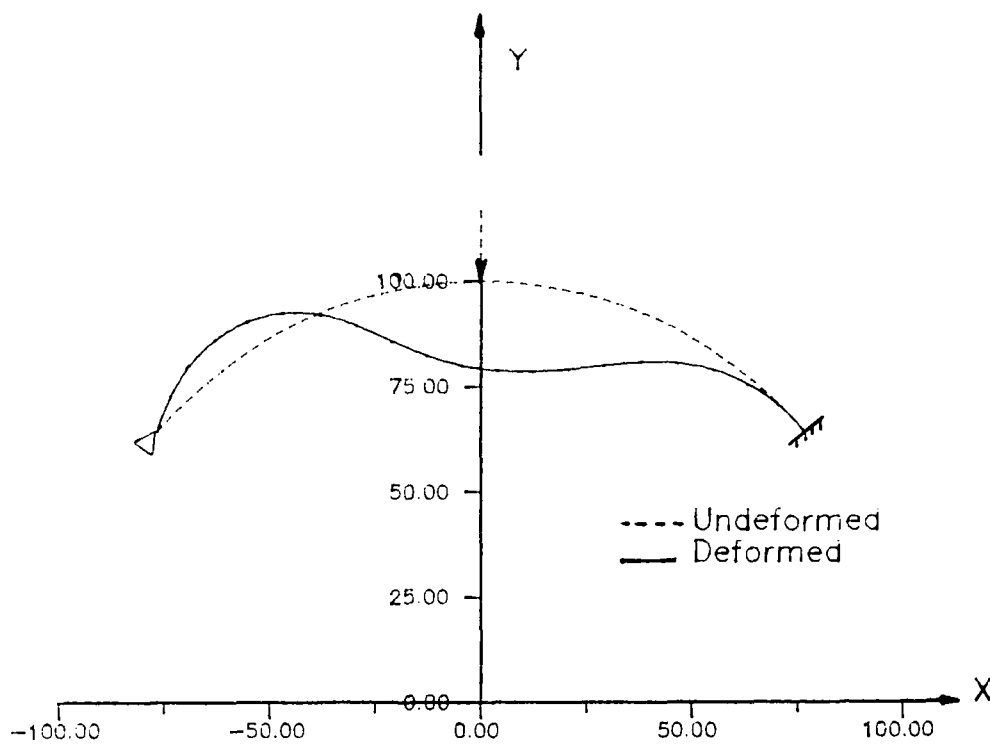
FIGURE 5.51.   Shape of Circular Arch Near Collapse Load.

265

The final problem of this research is to study the nonlinear behavior of axially compressed orthotropic cylindrical panels. Specifically, panels with square centered cutouts as shown in Figure 5.52 are of interest. This type of structure may be found on the fuselage of an aircraft, for example. Several investigators (1,149-154) here at AFIT have constructed and tested these types of panels while at the same time, have attempted to predict their response using the commercial nonlinear finite element analysis package, STAGS C-1. For the most part, their efforts have been successful for homogeneous panels, i.e., those without cutouts, and those with small cutouts. For the 12 x 12 in. panels, as in Figure 5.52, the comparisons between experimentally and analytically determined collapse loads have been favorable for square cutouts as large as 2 x 2 inches. Cutouts of this size represent less than 3% of the total panel area and are therefore considered small.

However, as studied by Tisler (1), the STAGS C-1 code was unable to give an accurate equilibrium path representation for quasi-isotropic panels with centered square 4 and 5 inch cutouts. These cutouts represent 11 and 17% of the total planform area, respectively, and are considered large. Furthermore, the displacement based formulation of that version of STAGS used by Tisler gave softer results compared to the experimental. This, of course, is the opposite of that expected. The finite

element model used by Tisler is comprised of flat elements that neglect transverse shear and normal stresses. Additionally, overly constrained boundary conditions were applied as well as those that more closely compare to the experimental apparatus. For these reasons, the analysis model should be stiffer than the actual panels. However, the experimental response was found to be above, or stiffer than that predicted by the finite element analysis. Not considered in the analysis model of Tisler were the residual stresses formed during panel fabrication and curing that were partially released when the panels were cut. As discussed by Tisler, the effect of this on the equilibrium paths of the panels with the cutouts is unknown, and could be a reason for the disparity in his results.

R = 12 in.
L = 12 in.
h = .039 or .045 in.

$[0/\pm45/90]_s$
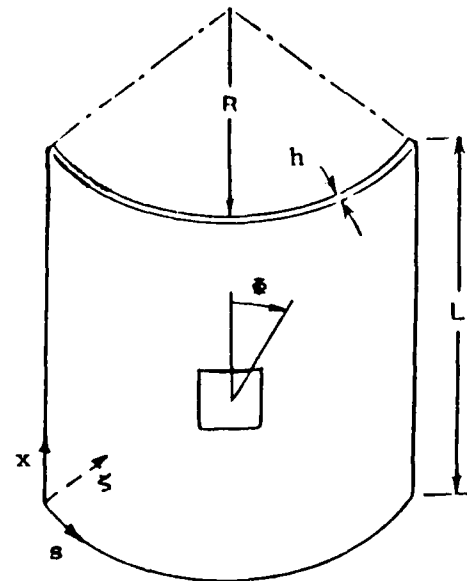
FIGURE 5.52. Panel Geometry Showing Square Cutout, Ply Orientation Angle, Φ.
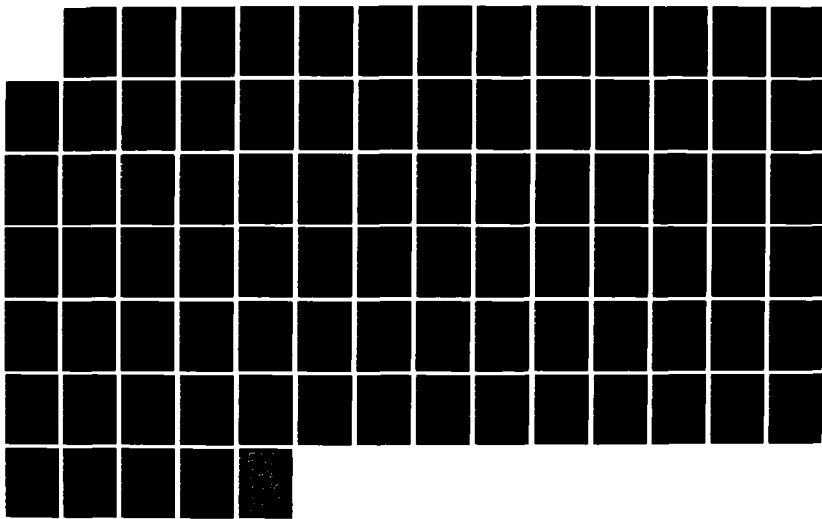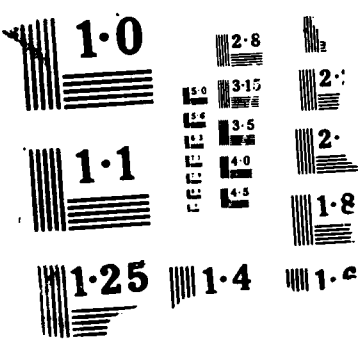
Deformed panel slope approximations derived from Linear Variable Differential Transducer (LVDT) measurements near the cutout indicated that some points of the panels with the large cutouts, i.e., the 4 and 5 inch, were experiencing moderate to large rotations of 5 to 10 degrees (1). Furthermore, numerical tests done by researchers at Lockheed (124) show that the flat shell elements used by Tisler in his finite element analysis can not accurately predict the response of a shell structure when rotations are of that size. This inability to undergo moderate to large rotations is more likely the cause of the disparity between the experimental and analytical results of Tisler. The Lockheed investigators, consequently, developed new nonlinear algorithms via a corotational formulation that should improve this deficiency (94).

Alternatively, the present formulation, with the curved shell elements that can generally undergo large displacements and rotations, is applied to this problem. Analytical results from panels with a 4 inch cutout and thicknesses h=.045 and .039 inches are compared to experimental data taken from Tisler. However, Tisler found cases of material failure in the thicker panels. For this reason, a limited analysis is presented for the .045 in. panels since plastic deformation is not considered in the present formulation. More extensive results were generated for the thinner panel since Tisler observed no evidence of

material failure in these panels.

The orthotropic material properties of the panels tested by Tisler are given in Eqn (5.52). The boundary conditions have the bottom edge, i.e., x=0, completely clamped, see Figure 5.52. The top edge is clamped as well, only the axial displacement, u, is prescribed since the analytical load is input by a uniform axial displacement along the top edge (x=L). As discussed by Tisler, the uniform displacement loading better resembles the actual test apparatus. He found that the distinction between uniform displacement and uniform loading along the top edge is very important for the panels with the large cutouts. The boundary conditions for the vertical edges are simple supports. However, post test inspection of the panels by Tisler showed evidence that the circumferential displacement, v, along these edges was not totally free as was originally thought. Therefore, the present analytical results will reflect two sets of boundary conditions for the vertical edges where the circumferential displacement, v, is free or fixed. The boundary conditions are shown in Eqn (5.53). Both boundary condition sets were also tested by Tisler, incidently, but the analytical results for both were still too flexible compared to the experiment.

$$E_1 = 18.844e6 \text{ psi}$$
$$E_2 = 1.468e6 \text{ psi}$$
$$G_{12} = G_{13} = .91e6 \text{ psi} \qquad (5.52)$$
$$G_{23} = .45e6 \text{ psi}$$
$$\nu_{12} = .28$$

$$\bullet x=0: \quad u=v=w=w,_1=w,_2=\psi_1=\psi_2=0$$
$$x=12: \quad v=w=w,_1=w,_2=\psi_1=\psi_2=0$$
$$\bullet s=0,12: \quad v=w=w,_2=\psi_2=0 \qquad (5.53)$$
$$\text{or} \quad w=w,_2=\psi_2=0$$

Initial model validation was based on linear analyses of several mesh arrangements of the 36 dof element both with and without the cutout. Figures 5.53-5.55 show three mesh arrangements for the shell midsurface planform where elements within the center square have been deleted to represent a panel with a 4 x 4 inch cutout. The user of the code can specify any elements he wishes to delete; the automatic mesh generation subroutine is used as always but no stiffness is calculated for the elements that represent the cutout, i.e., those deleted. Additionally, the nodes of those elements within the cutout not on the cutout border must be constrained. When the actual panels were cut, care was taken to ensure that the corners were rounded. In this way, large stress concentrations would not form at the corners as the panels were experimentally loaded. Therefore, although the cutout corners of the analytical model are sharp, mesh refinement is not as severe as

required for a singularity. By keeping the mesh refinement
relatively coarse, an analytical stress singularity can not
develop, hence representing the actual panels more
accurately.

The mesh arrangements shown in Figures 5.53-5.55 are
progressively more refined. The previous AFIT investigators
have shown that the 20x20 mesh of Figure 5.55 with half inch
square elements near the cutout generally gives converged
results for the STAGS elements that they used. The
nonlinear analyses to be presented here will show that the
20x20 mesh is probably not totally converged when used to
model the panel with the 4° cutout. A further refinement
was not tested because the 20x20 mesh already resulted in a
very large nonlinear problem. This mesh proved to be too
large for the Vax computer systems if double precision
arithmetic is used. This was less a result of the
theoretical formulation than the finite element coding since
writing code that worked was generally considered more
important than storage or time efficiency. Consequently, a
Cyber 845 with virtual memory was used only for the 20x20
mesh models. Because of the expensive nature of the Cyber
calculations, only a limited number of 20x20 analyses were
tried.

The results of the linear analysis for a prescribed
compressive axial displacement along the top edge of u=-10
mils (-.01 inches) are shown in Table 42 for panels with and

271

without the 4° cutout. For each mesh, the total top edge axial force, P_t, is shown. Note that the cutout gives a significantly more flexible panel. Additionally, the linear results show that the panel with a cutout converges more slowly than the one without. Generally, the coarser meshes give very good results compared to the 20x20 mesh in the linear tests.

Mesh	P_t (lbs)	
	no cutout	4° cutout
8x8	3440.6	2515.4
12x12	3427.3	2443.3
20x20	3427.1	2428.8

TABLE 42. Total Top Edge Compressive Force from Linear Analysis. Circumferential Displacement, v, Fixed Along Vertical Edges, h = .045 in.
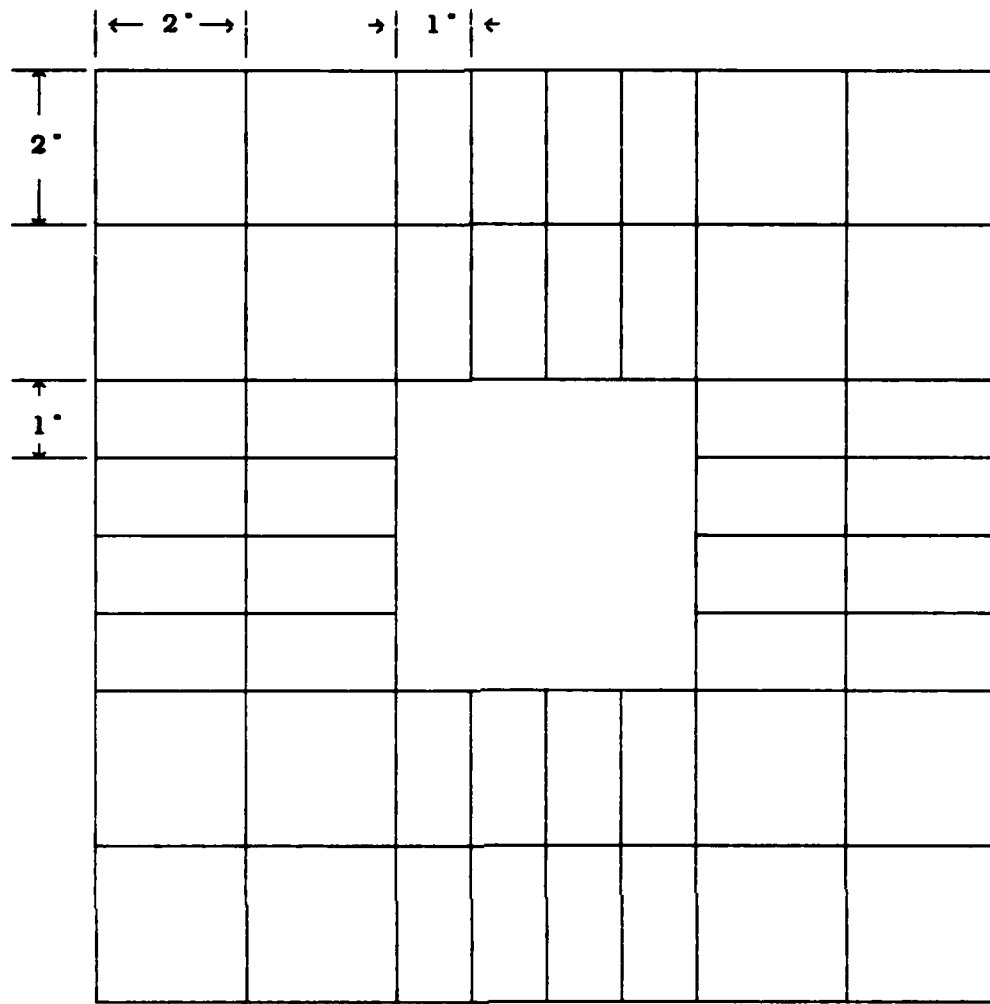
FIGURE 5.53.   8x8Q Mesh for Cylindrical Panel With 4° Cutout.
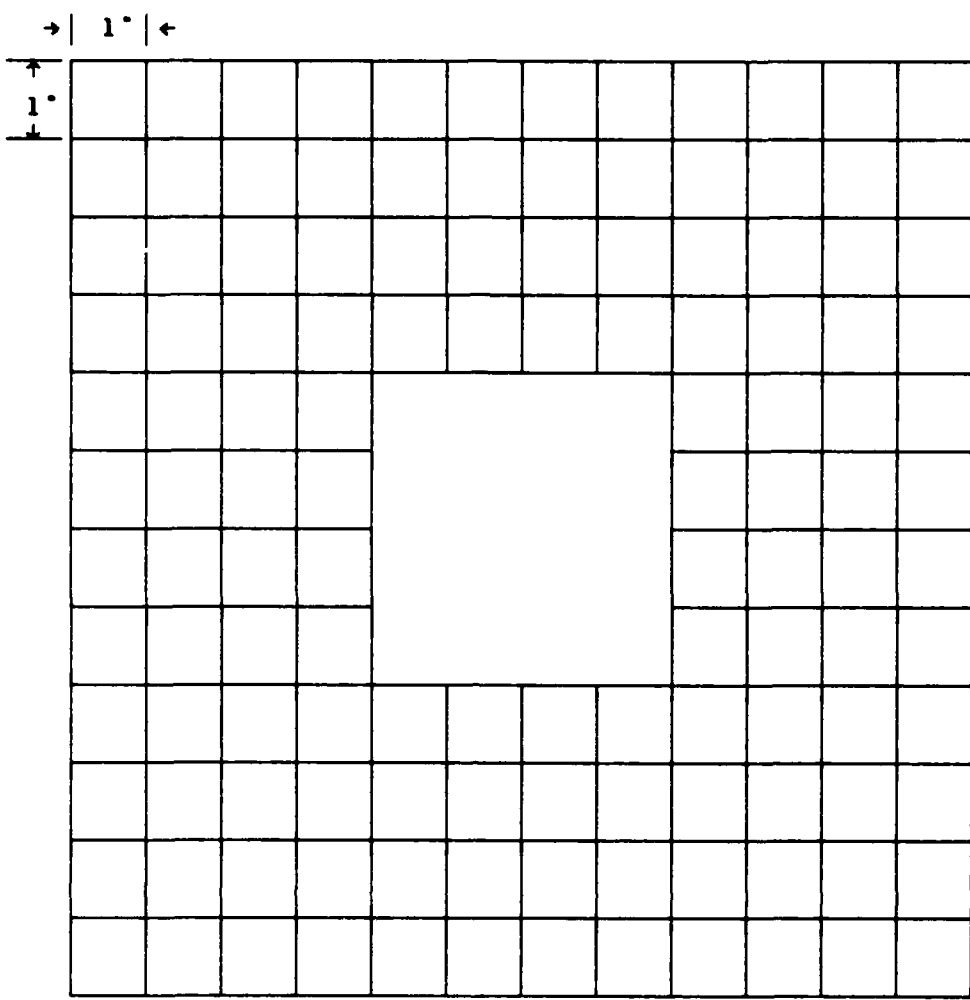
FIGURE 5.54.   12x12Q Mesh for Cylindrical Panel With 4°
Cutout.
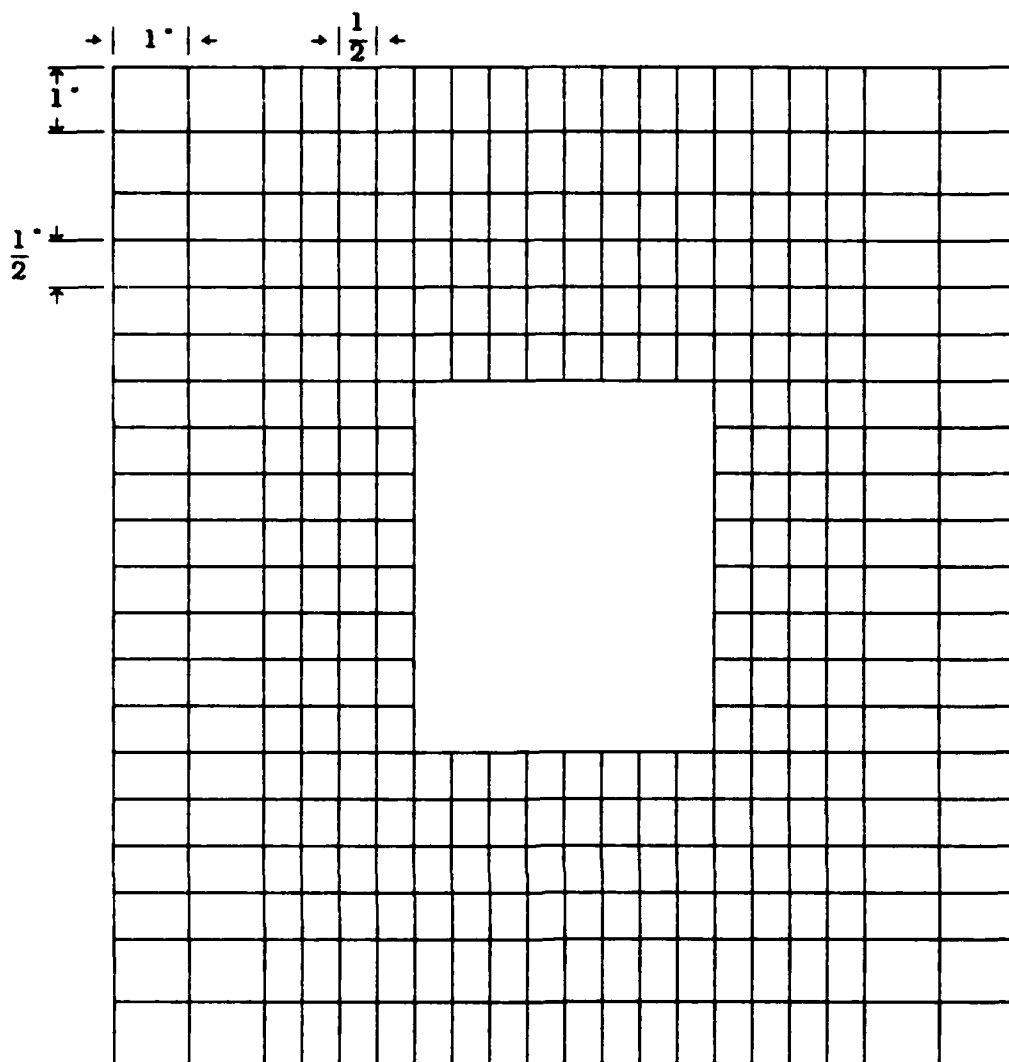
FIGURE 5.55.   20x20Q Mesh for Cylindrical Panel With 4˚ Cutout.

The same panel, i.e., h=.045 inches with v fixed along
the vertical edges, was next examined in a nonlinear
analysis. Figure 5.56 shows the nonlinear equilibrium path
results, i.e., compressive displacement (inches) versus
compressive load (pounds), for the homogeneous panel (no
cutout). The 4x4 mesh indicated was not shown earlier and
is a regular mesh used only in this case.   As the Figure

shows, the response is very linear until collapse occurs and the only significant difference between the meshes is the collapse load, see also Table 43. The 12x12 mesh gives a collapse load of 10796 lbs. This value is approximately 50% higher than results reported by Janisse (150) and Wilder (154). However, their panels were approximately 10% thinner and included more flexible boundary conditions.

More importantly, a geometric imperfection is not required in the present formulation to 'trigger' the nonlinear response. Apparently, the STAGS elemental formulation does not have adequate displacement coupling between the inplane and transverse displacements and therefore, to achieve collapse in panels that are axially compressed, a numerical imperfection with a small transverse amplitude must be assumed (16). To measure its effect in this analysis, a small transverse point load was applied at the panel center of the 12x12 mesh such that a small amplitude imperfection resulted throughout the panel. This had a negligible effect on the results.

The results of Figure 5.56 and Table 43 were generated from models consisting of the large displacement/rotation element. For the homogeneous panel, the rotations are small throughout the panel and virtually the same results were obtained using the Donnell elements (not shown), as would be expected.

276
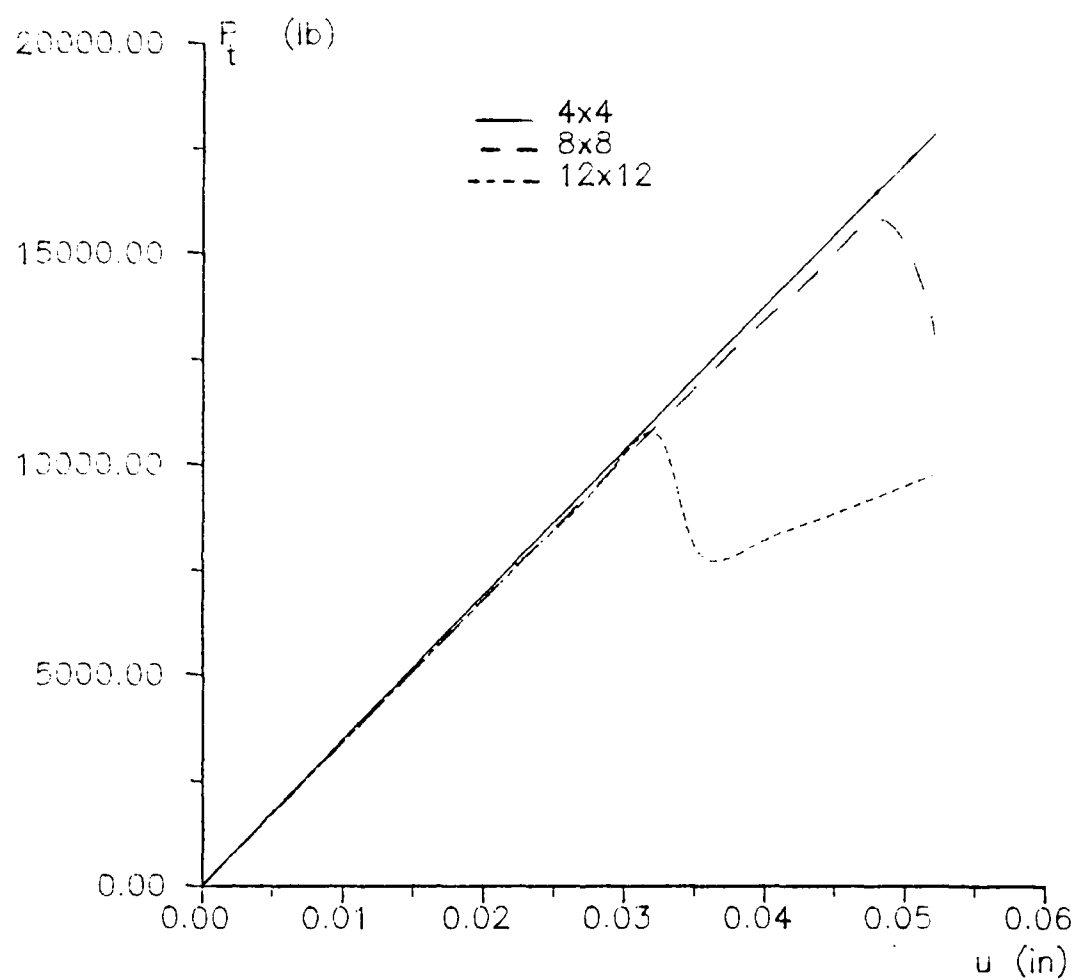
FIGURE 5.56. Homogeneous Panel Nonlinear Analysis, h=.045, v Fixed.

u (in.)	P_t (lbs)		
	4x4 Mesh	8x8 Mesh	12x12 Mesh
.008	2785.6	2745.3	2734.0
.012	4174.4	4112.2	4094.6
.016	5560.5	5474.8	5450.4
.020	6943.8	6832.7	6800.6
.024	8324.4	8185.2	8144.0
.028	9702.3	9531.0	9478.6
.032	11077.	10868.	10796.
.036	12450.	12192.	7751.0
.040	13819.	13492.	8244.7
.044	15186.	14727.	8756.1
.048	16550.	15875.	9277.6
.052	17911.	13118.	9804.1

TABLE 43. Top Edge Axial Compressive Displacement versus Compressive Load for Homogeneous Panel.

A panel with the same geometry and boundary conditions only now with a 4˚ cutout was next axially compressed and the total axial top edge force calculated. These results are shown in Figure 5.57 for the 8x8 and 12x12 meshes. The collapse load shown for the 12x12 mesh is 7473 lbs and is approximately 66% higher than the experimental result reported by Tisler. However, Tisler found that these panels collapsed due to material failure and therefore a close comparison can not be expected. Additionally, the results of Figure 5.57 are due to the stiffer boundary conditions of Eqn (5.53). The 20x20 mesh should give results that are more converged but was not evaluated for this panel thickness because of the high computer expense.

Instead, the thinner h=.039 in. panels were examined.

These panels showed no evidence of material failure during testing. Again, the global nonlinear response of the panel is indicated by the equilibrium path of top edge displacement versus load. The results for the three meshes of Figures 5.53-5.55 are shown in Figures 5.58 and 5.59. Additionally, the numerical data is tabulated in Tables 44 and 45. Figures 5.58 and 5.59 are those results obtained when the circumferential displacement is fixed and free, respectively. In Figure 5.58, the 12x12 collapse load is 6477 lbs. The 20x20 result had not yet collapsed for the largest axial compressive displacement shown. However, the results show that it should collapse for a P_t less than approximately 5000 lbs based on a crude extrapolation and the 12x12 results. In Figure 5.59, the 12x12 mesh collapses at a load of 3428 lbs. The load then starts to increase again resulting in a second collapse at a load of 3771 lbs. The two humped behavior of the 12x12 mesh in Figure 5.59 has been similarly reported by Knight and Starnes (2) in a study of the collapse of cylindrical panels with circular cutouts. The 20x20 mesh shows a collapse load of 3057 lbs. Figures 5.58 and 5.59 show that the circumferential displacement boundary condition has a fairly significant influence on the collapse load.
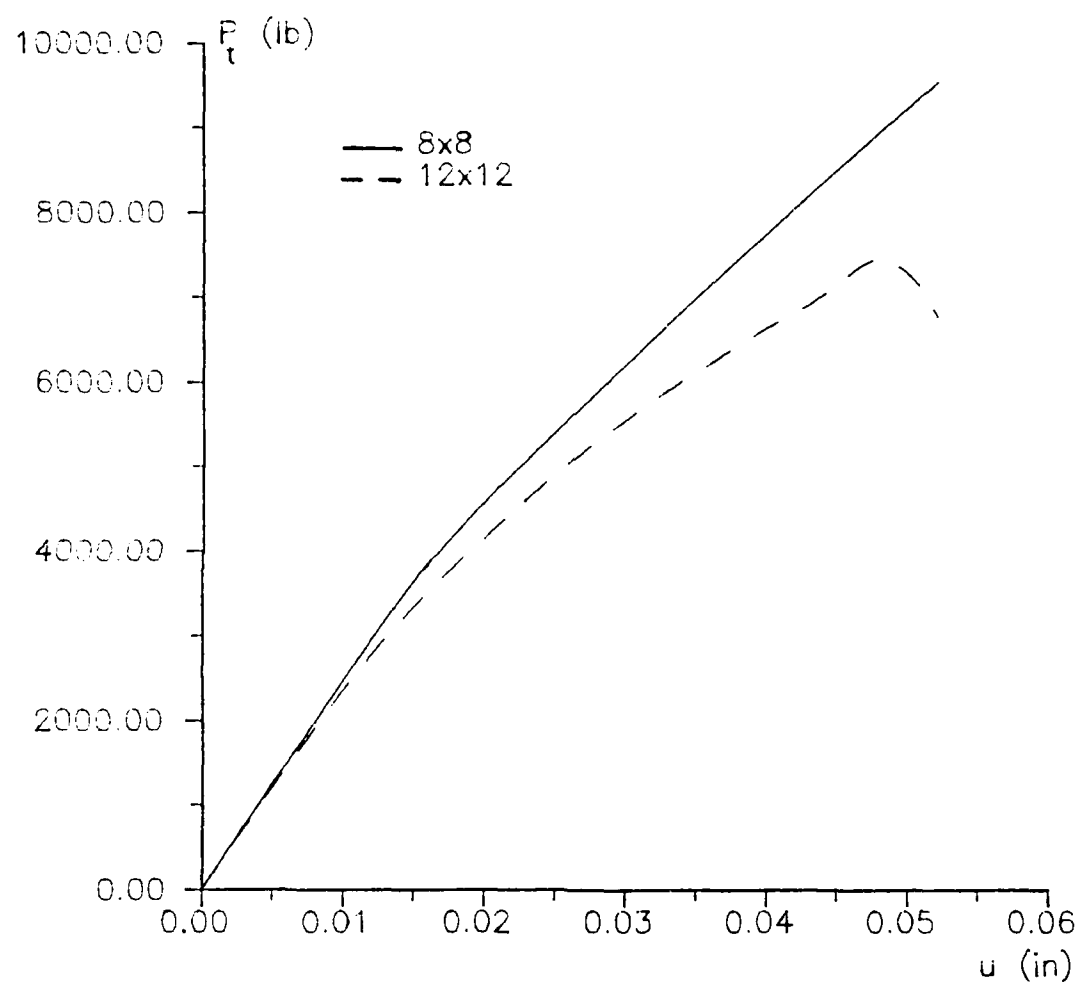
FIGURE 5.57. 4° Cutout Panel Nonlinear Analysis, h=.045, v Fixed.
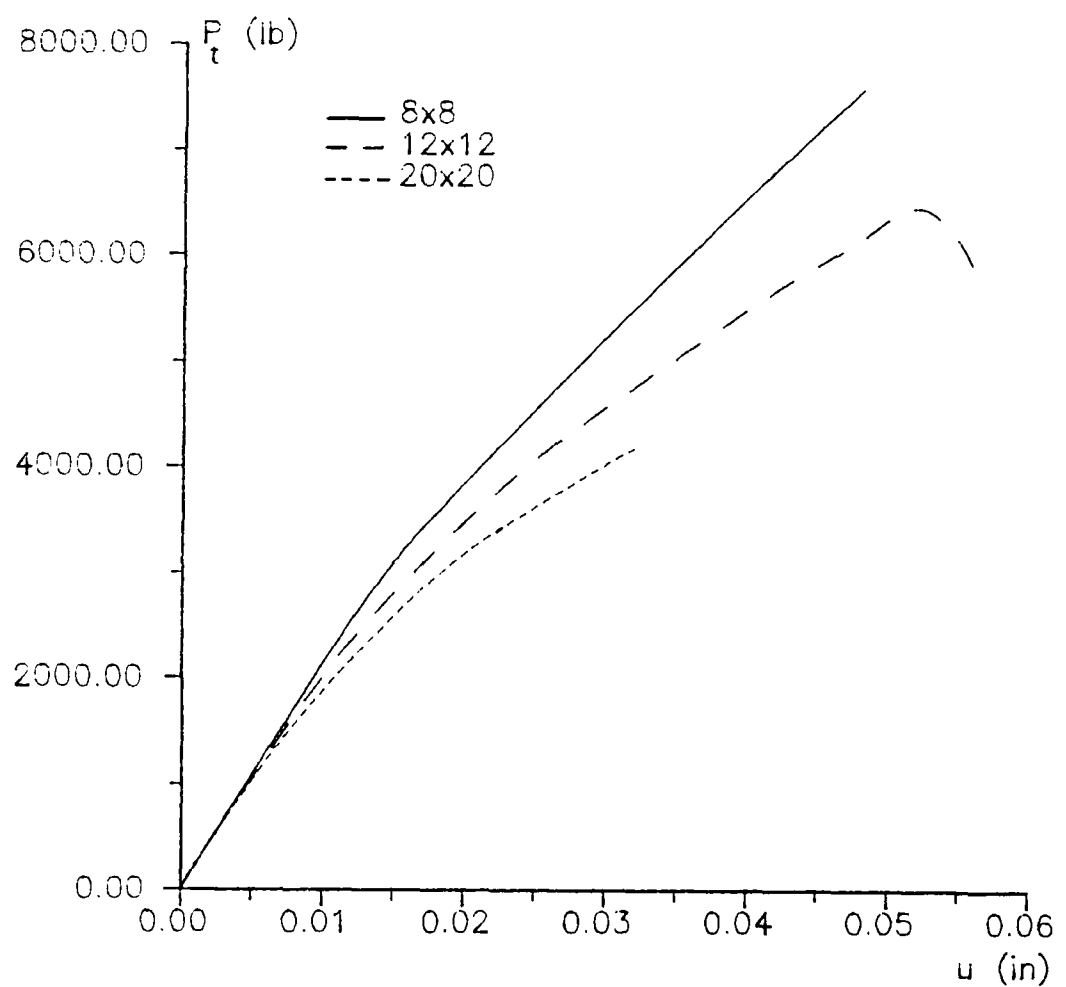
FIGURE 5.58. 4" Cutout Panel Nonlinear Analysis, h=.039, v Fixed.
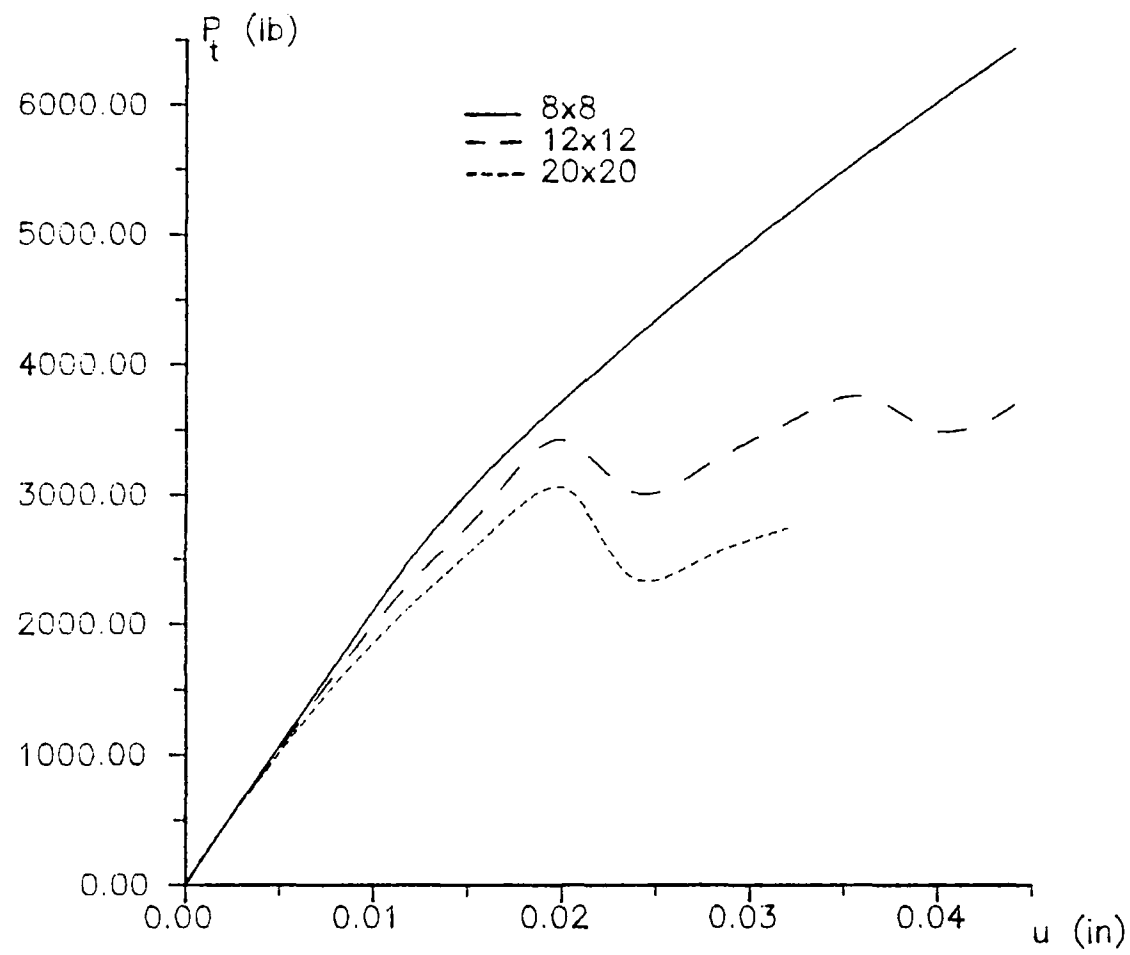
FIGURE 5.59. 4° Cutout Panel Nonlinear Analysis, h=.039, v Free.

282

u (in.)	P_t (lbs)		
	8x8	12x12	20x20
.008	1724.4	1650.0	1565.8
.012	2556.3	2362.0	2175.0
.016	3276.1	2955.5	2720.2
.020	3860.8	3492.6	3186.3
.024	4423.2	3974.9	3547.4
.028	4977.6	4396.5	*
.032	5522.2	4775.4	4193.7
.036	6058.2	5147.5	*
.040	6583.4	5515.9	*
.044	7097.3	5866.0	*
.048	7599.9	6186.5	*
.052	*	6477.3	*

TABLE 44.   4° Cutout Panel   Nonlinear   Analysis,   h=.039,   v
Fixed.   * not calculated.

u (in.)	P_t (lbs)		
	8x8	12x12	20x20
.008	1704.3	1637.7	1551.8
.012	2517.7	2339.5	2152.6
.016	3183.9	2924.3	2682.5
.020	3727.6	3428.1	3056.7
.024	4236.2	3017.3	2353.5
.028	4721.0	3267.7	2554.9
.032	5182.0	3567.7	2756.2
.036	5622.9	3771.7	*
.040	6043.7	3502.6	*
.044	6447.1	3703.0	*

TABLE 45.   4° Cutout Panel   Nonlinear   Analysis,   h=.039,   v
Free.   * not calculated.

A final comparison is made with the   .039   inch   panels
between Tisler experimental data and the present   analytical
results from the 20x20 mesh.   The experimental results shown

in the Figures represent the actual unmanipulated data and are taken from two panel tests. Figure 5.60 gives the global panel response of top edge axial displacement versus total load. This Figure shows an unusual experimental equilibrium path for axial loads less than 800 lbs. For these loads, the LVDT that measured the panel axial compression as the load was applied was reading tension. Wilder (154), who used the same test apparatus in a study of panel delaminations, discovered that this anomaly was due to an improper attachment of the panel to the loading structure. For loads above 800 lbs, for this data, the panel is properly seated and the data is valid. Wilder discusses a uniform bias that can be applied to the data from this LVDT. For the data shown in Figure 5.60, the bias is very small and not included. The experimental data shown in the Figure is exactly what the LVDT measured.

Also plotted in Figure 5.60 are the analytical results from the present formulation. As can be seen, the experimental panel collapse values of approximately 3500 lbs fall between the two analytical predictions. The panel with v free along the vertical edges predicts a smaller collapse load than the experimental and when v is fixed, the collapse is higher than the experimental. This would indicate that the actual panels were neither fully restrained nor fully free during loading and therefore some movement was permitted. This is consistent with the experimental

observations made by Tisler.

Analytical and experimental results for the local behavior of the panel are also compared in Figures 5.61 and 5.62. Load displacement curves are given for the radial displacement at two points near the cutout edge, see Figures. In these Figures, the comparisons for small values of axial load is poor. However, the comparisons for loads above approximately 800 lbs are quite good considering that we are examining very localized panel behavior. Except for an initial shift in the experimental data in both Figures, both of the analytical curves match the experimental trends. This shift in the data may be related to the panel seating problem discussed earlier.

Unfortunately, the expense of the 20x20 models prohibited a complete study of the comparisons between the large displacement/rotation and Donnell elements for this problem. The results from the 12x12 models, however, indicate that the Donnell elements give collapse loads that are approximately 10% higher than the higher order element. If this is an indication of the converged results as well, then the Donnell element might be better suited for this problem solely from a cost efficiency standpoint.

On the other hand, the maximum rotation that points of the panel undergo is approximately 12 degrees and this compares with the experimental results reported by Tisler. Rotations of this size may not fit the definition of

intermediate nonlinearity where Donnell equations are valid
and some evidence of this is seen in the 12x12 results where
the Donnell elements give increasingly stiffer results.
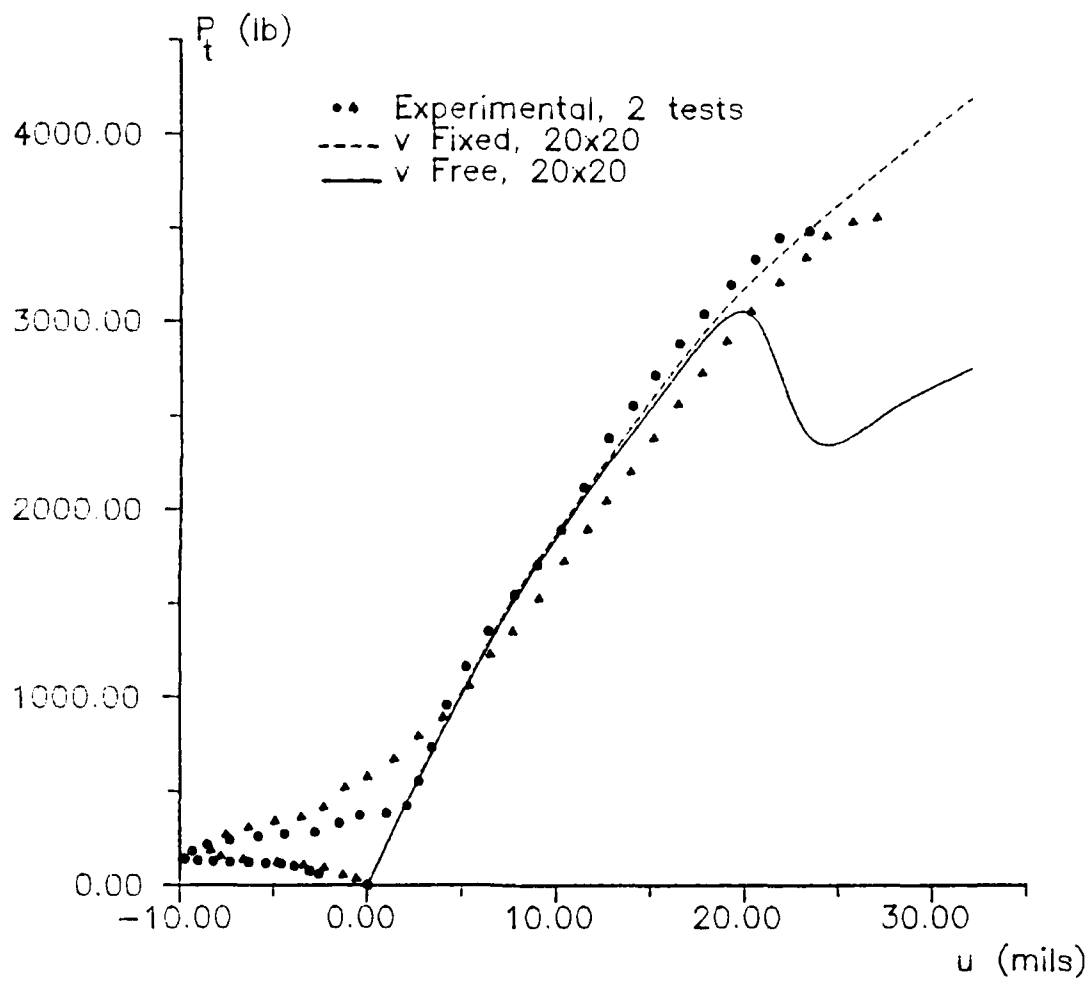
FIGURE 5.60. Global Panel Response, Compressive u vs Compressive P_t, 4˚ Cutout, h=.039.
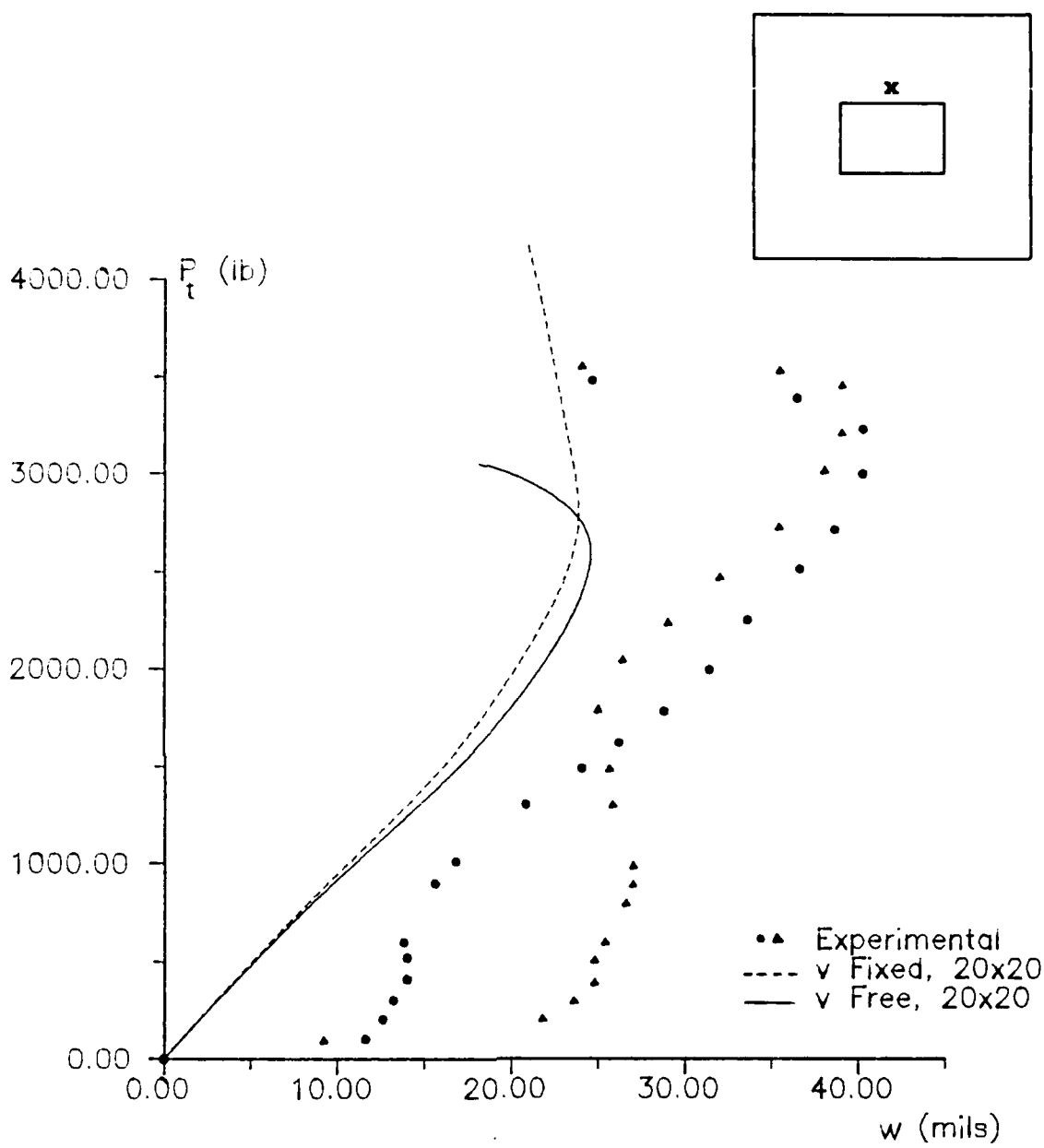
FIGURE 5.61. Local Panel Response, Radial Displacement, w, vs Compressive P_t for Point Shown.
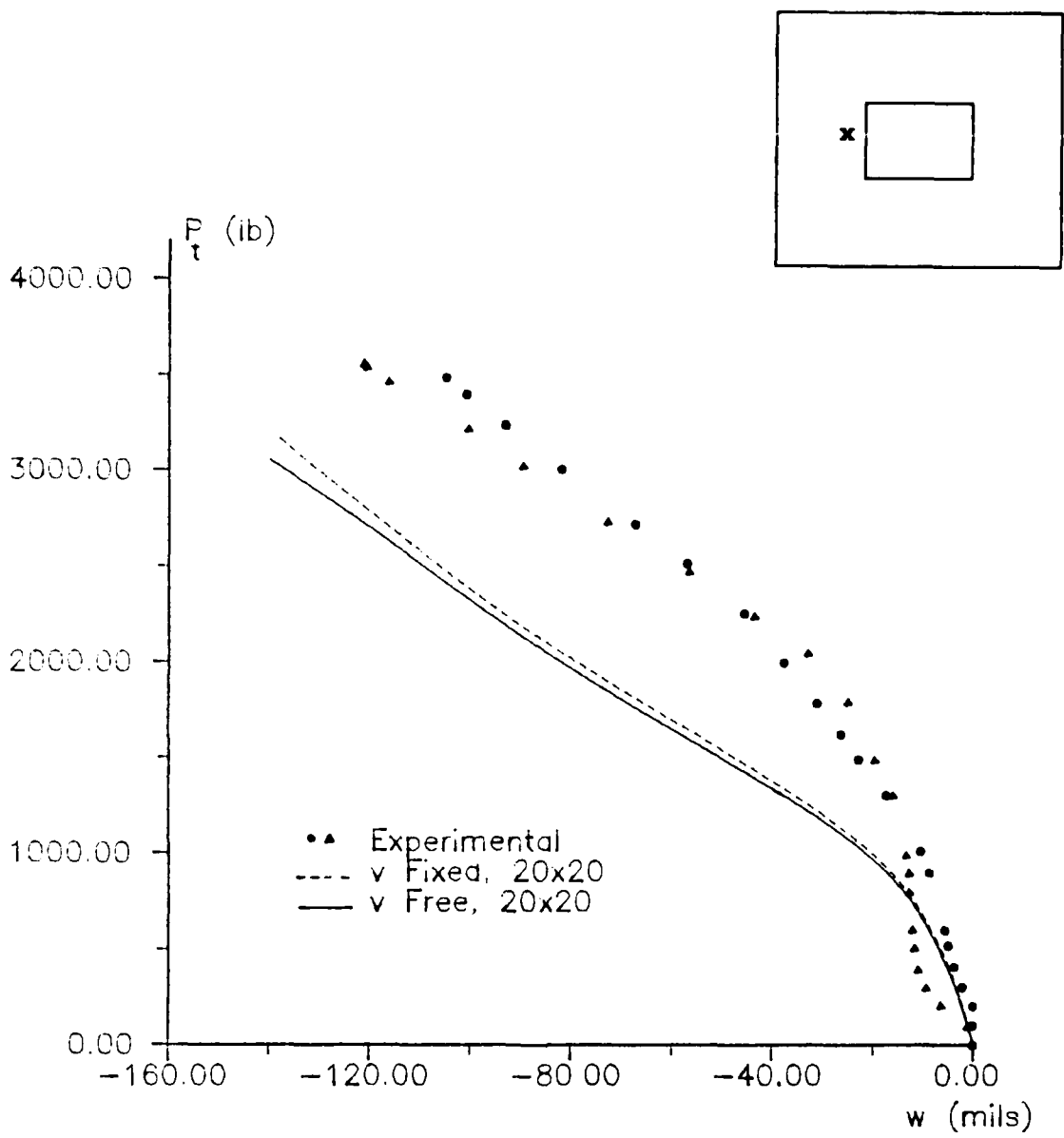
FIGURE 5.62. Local Panel Response, Radial Displacement, **w**, vs Compressive P_t for Point Shown.

288

VI. <u>Conclusions</u>

A two dimensional shell theory applicable to arbitrary geometries that can be described by orthogonal curvilinear coordinates has been developed. This theory encompasses large displacement and rotational geometric nonlinearity for small strain situations. Additionally, the theory includes a parabolic transverse shear stress and strain distribution through the shell thickness. The middle surface strain displacement definitions retain all of the nonlinear terms of Green's strain representation. The transverse strain displacement relations, on the other hand, are defined by only the linear displacement terms for simplicity.

The theory is next specialized to cylindrically shaped shells and then written in a finite element casting for numerical solutions. Two curved elements are defined, where a flat plate is described by setting the curvature to zero. The finite element program includes algorithms for linear, 'fully linearized' linear bifurcation, and nonlinear analyses. A displacement incrementation scheme for the solution of the resulting nonlinear equations from the nonlinear algorithm easily traverses limit points. Options are available for the simpler von Karman plate and Donnell cylindrical shell solutions in addition to the elements that can undergo the larger displacements and rotations.

Based on the above, many results are presented, both validation and unique contributions. From these results,

many conclusions have been made and are discussed below.

Several linear flat plate problems were analyzed for validation purposes. The 28 degree of freedom element includes only linear interpolation for the inplane displacements, u and v, since these displacements do not enter the solution for linear transversely loaded flat isotropic or symmetrically laminated plates. The element performs very well for both displacement and stress calculations. The formulation was first tested versus several classical thin plate solutions and the results indicate that the mesh does not shear lock based upon exact elemental integrations. Shear locking is a typical characteristic of the lower order transverse shear theories and its avoidance is a primary reason why the higher order parabolic distributions were assumed in the present study. Because of the nonconforming interpolations assumed for the transverse displacement, w, the solutions do not converge monotonically. Additionally, the convergence is not always from above, i.e., from a solution that is too stiff.

The plate elements were applied to cylindrical bending problems and compared to solutions based upon the three dimensional equations of elasticity. Even for the very thick plate strips where the plate length is only four times the thickness, the transverse and through the thickness axial displacement results are in excellent agreement with the 3-D solutions. Consistent with previous studies, the

effects of transverse shear become more and more pronounced giving increasingly more flexible results as the plate becomes thicker. The stress results for the unidirectional laminate are also in excellent agreement with the published results. However, the formulation could not give as accurate transverse stress results for the bidirectional laminate strips since equilibrium is not satisfied in the transverse direction at the ply interfaces. Consequently, the transverse stress is discontinuous at those points.

Similar conclusions are found for the rectangular plate bending solutions. That is, the displacement calculations are very accurate compared to published results based upon similar theories and 3-D solutions. The stress is calculated very accurately for isotropic and symmetrically laminated plates. Stress near the plate boundary is found best when refinements are made to the mesh. This is a direct consequence of the present formulation's inability to identically satisfy the zero normal moment simple support boundary condition. Only geometric boundary conditions can be identically satisfied.

The linear shell validation problems showed that the 36 degree of freedom element with the quadratic interpolations for the inplane displacements is generally required over the simpler 28 dof element. The 28 dof element gives results that are significantly stiffer than the published answers for the cases where membrane deformation is not small.

291

Accurate displacement results were determined for a variety of standard testcases.

Two of these cases were the subject of extended studies that examined both transverse shear deformation and inextensibility of the middle surface leading to unique results. The present formulation generally can not duplicate solutions that have been based on assumptions of inextensible middle surface since the middle surface displacements, u and v, are always coupled into the solution. This first became evident when the thin pinched cylinder results were compared to the inextensible solution of Timoshenko. When the pinched cylinder became very thin, the membrane deformation becomes significant compared to bending, and consequently, the displacements are smaller than that predicted by the inextensible solution that neglects them due to tension at the midsurface. Additionally, the Timoshenko solution does not consider transverse shear deformation. As the cylinder becomes thicker, the transverse effects become more pronounced giving greater displacements than the Timoshenko solution.

Transverse shear deformation was found to be significant for cylindrical pressure vessels as well. The radial displacement for the pressure vessel is greater relative to the classical solution that neglects transverse shear for the thicker geometries. This is especially true near the rigid end plates where bending is severe. The

292

quasi-isotropic pressure vessel is influenced by transverse shear deformation to a greater degree than is the isotropic construction. Pressure vessels with greater longitudinal stiffness than circumferential, i.e., for unidirectional or laminated contructions, experience greater transverse shear deformation especially near the clamped edge where there is significant bending deformation. For the pressure vessels where the circumferential stiffness is less than the longitudinal, a countershear point exists along the longitudinal axis resulting in smaller transverse displacements compared to the classical solution in the center regions of the vessel.

A "fully linearized" linear bifurcation approach validated the nonlinear N_4 matrix. This approach couples the inplane and transverse degrees of freedom both in the pre- and postbuckling regimes. The classical approach, in contrast, assumes inextensibility of the middle surface, and consequently, the inplane displacements are not included in the solution. Except for one plate case, excellent results were attainable using the fully linearized method with von Karman nonlinearity. The fully linearized linear bifurcation algorithm does not predict buckling mode shapes reliably since u,v,w are coupled in the solution. Different shapes result depending upon the dof that is prescribed in solving the n-1 equations for the eigenvector. For nonsquare axially loaded flat plates, except for the

classical thin geometry, very different buckling loads resulted via the fully linearized approach compared to the classical. The differences are mainly attributed to the different approaches where inextensibility is assumed in classical but not in the fully linearized.

The element that can undergo the large displacements and rotations was applied to the square flat plate bifurcation case as well giving unique results. Solutions for thicker plates gave critical buckling loads up to 10% less than the published 3-D solutions that allow only a von Karman nonlinearity. This may be an indication that the higher order nonlinear terms have a greater impact on the critical load than does 3-D flexibility for these geometries.

The lone cylindrical shell bifurcation case examined resulted in very good critical load comparison to the published result, also based on a fully linearized approach. Interestingly, this shell geometry actually does not buckle as the nonlinear result showed. This one instance indicates that bifurcation is not always an accurate measure of the loss of stability. Based upon all of the linear bifurcation problems, the nonlinear matrix N_1 was considered correctly formulated.

The flat plate nonlinear cases examined gave very good displacement and stress results based upon either von Karman or the large displacement and rotational formulation. The

large rotational formulation gave very similar results to the von Karman results thus indicating the validity and range of the simpler assumptions of the latter for the magnitudes of displacement and rotation examined.

The nonlinear shell formulation gives excellent comparisons to published results for those cases that allow an extensible middle surface. On the other hand, the circular arch solutions based on the present theory gave responses consistently more flexible than the published results that are based on an inextensible middle surface. However, the present solutions do resemble published closed form and finite element results that have a middle surface that can deform inplane.

The accuracy of the present formulation in following larger displacements and rotations is indicated by several deep shells or arch geometries. Approximate expected rotations of points near the simple supports and displacements of the crown can be calculated based on simple geometry for the stable post snap through region of the equilibrium path. The present formulation, in all cases, predicted results similar to these values. The large displacement and rotational formulation predicted rotations up to 24 degrees for points along the boundary of the hinged-free shell. Additionally, this shell experienced a crown displacement of 11 times its thickness. The Donnell shell element was applied to this problem also. Somewhat

surprisingly, the results show the same overall trends as the large displacement/rotation element. However, the equilibrium load for a given deformed shell configuration is significantly different once the rotations exceed about 11 degrees. A deep circular arch with nonsymmetric boundary conditions experienced a maximum angle of rotation of 39 degrees and displacements up to 85 times the arch thickness.

The present formulation was applied to axially compressed quasi-isotropic cylindrical panels that have centered cutouts. This geometry has been studied very successfully by several AFIT investigators except for the case where the cutouts represent more than about 10% of the panel's planform. For these cases, the local rotations of points near the cutout exceed the limitations of the intermediate nonlinearity of the analytical formulations that were used to predict the panel response. The present formulation accurately predicts the global axial load versus axial top edge displacement compared to experimental results. Additionally, the finite element results for two points near the cutout edge indicate an ability to capture panel behavior that is very localized.

In a related study, the present formulation predicts collapse for axially loaded perfect cylindrical panels, i.e., ones without cutouts. Other formulations typically require an imperfection to 'trigger' the nonlinear response. However, the present formulation includes a degree of

296

displacement coupling not usually assumed and therefore, the numerical imperfection is not required. Along the same lines, the present formulation does not include displacement coupling such that an axially loaded flat plate will collapse in an nonlinear analysis. For this case, the numerical imperfection is required.

Bibliography

1. Tisler, T.W. _Collapse Analysis of Cylindrical Composite Panels with Large Cutouts Under an Axial Load_, M.S. Thesis GA/MS/86D-1. School of Engineering, Air Force Institute of Technology (AU), Wright-Patterson AFB, OH, 1986.

2. Knight, N.F. and J.H. Starnes. "Postbuckling Behavior of Axially Compressed Graphite Epoxy Cylindrical Panels with Circular Holes," in _Collapse Analysis of Structures_, ed. by L.H. Sobel, ASME, PVP Vol. 84, 1984.

3. Ericksen, J.L. and P.M. Naghdi. "Exact Theory of Stress and Strain in Rods and Shells," _Archive of Rational Mechanics_, 1, 1957.

4. Green, A.E., P.M. Naghdi, and W.L. Wainwright. "A General Theory of a Cosserat Surface," _Archive of Rational Mechanics_, 20, 1965.

5. Cohen, H. and C.N. DeSilva. "Nonlinear Theory of Elastic Directed Surfaces," _Jour of Math Physics_, 7, 1966.

6. Saada, A.S. _Elasticity Theory and Applications_, Pergamon Press, 1974.

7. Marlowe, M.B. and W. Flugge. _Some New Developments in the Foundations of Shell Theory_, LSMC-6-78-68-13, 1968.

8. Mollman, H. _Introduction to the Theory of Thin Shells_, John Wiley and Sons, 1981.

9. Kraus, H. _Thin Elastic Shells_, John Wiley and Sons, Inc., 1967.

10. Niordson, F.I. _Introduction To Shell Theory_, Technical University of Denmark, 1980.

11. Shames, I.H. and C.L. Dym. _Energy and Finite Element Methods in Structural Mechanics_, McGraw Hill, 1985.

12. Brush, D.O. and B.O. Almroth. _Buckling of Bars, Plates, and Shells_, McGraw Hill, 1975.

13. Bauld, N.R. and K. Satyamurthy. _Collapse Load Analysis for Plates and Shells_, AFFDL-TR-79-3038, 1979.

14. Sobel, L.H., T. Weller, and B.L. Agarwal. "Buckling of Cylindrical Panels Under Axial Compression," _Comp and Struct_, 6, 1976.

15. Brogan, F. and B.O. Almroth. "Buckling of Cylinders With Cutouts Experiment and Analysis," Int J Solids Struct, 8, 1970.

16. Becker, M.L., A.N. Palazotto, and N.S. Khot. "Instability of Composite Panels," J of Aircraft, 18,1981.

17. Khot, N.S. Effect of Fiber Orientation on Initial Postbuckling Behavior and Imperfection Sensitivity of Composite Cylindrical Shells, AFFDL-TR-70-125, Wright-Patterson AFB Oh, 45433, 1970.

18. Bushnell, D. "Static Collapse: A Study of Methods and Modes of Behavior," Finite Elements in Analysis and Design, 1, 1985.

19. Librescu, L. "Refined Geometrically Nonlinear Theories of Anisotropic Laminated Shells", Quart Appl Math, 45, 1987.

20. Sanders, J.L. "Nonlinear Theories for Thin Shells," Appl Math., XXI(1), 1962.

21. Sanders, J.L. An Improved First Aproximation Theory for Thin Shells, NASA TR R-24, 1959.

22. Koiter, W.T. "A Consistent First Approximation in the General Theory of Thin Elastic Shells," Proc Sym on Theory of Thin Elastic Shells, Amsterdam, North Holland, 1960.

23. Koiter, W.T. "Foundations and Basic Equations of Shell Theory-A Survey of Recent Progress,", IUTAM Symposium, Copenhagen, 1967, in Theory of Thin Shells, ed. by F.I. Niordson.

24. Novozhilov, V.V. The Theory of Thin Shells, P. Noordhoff Ltd, 1959.

25. Vlasov, V.Z. General Theory of Shells and its Application in Engineering, NASA-TT-F99, 1964.

26. Donnell, L.H. Stability of Thin Walled Tubes Under Torsion, NACA 479, 1933.

27. Morley, L.S.D. "An Improvement of Donnell's Approximation for Thin-Walled Circular Cylinders," Quart Journ Mech and Applied Math, 12, 1959.

28. Cheng, S. and F.B. He. "Theory of Orthotropic and Composite Cylindrical Shells, Accurate and Simple Fourth Order Governing Equations," Journ of Applied Mech, 51, 1984.

29. Cheng, S. "On An Accurate Theory for Circular Cylindrical Shells," Journ of Applied Mech, 1973.

30. John, F. "Estimates for the Derivatives of the Stresses in a Thin Shell and Interior Shell Equations," Communications on Pure and Appl Math, Vol XVIII, 1965.

31. Reddy, J.N. Energy and Variational Methods in Applied Mechanics, John Wiley and Sons, 1984.

32. Hildebrand, F.B., E. Reissner, and G.B. Thomas. Notes on the Foundations of the Theory of Small Displacements of Orthotropic Shells, NACA-TN-1833, 1949.

33. Naghdi, P.M. "On the Theory of Thin Elastic Shells," Quart Appl Math, 14, 1957.

34. Reissner, E. "The Effect of Transverse Shear Deformation on the Bending of Elastic Plates," Journ of Applied Mech, 1945.

35. Reissner, E. Small Bending and Stretching of Sandwich Type Shells, NACA-TN-1832, 1949.

36. Mindlin, R.D. "Influence of Rotatory Inertia and Shear on Flexural Motions of Isotropic Elastic Plates," Journ of Applied Mech, 18, 1951.

37. Levinson, M. "An Accurate Simple Theory of the Statics and Dynamics of Elastic Plates," Mech Research Comm, 7, 1980.

38. Murthy, M.V.V. An Improved Transverse Shear Deformation Theory for Laminated Anisotropic Plates, NASA-TP-1903, 1981.

39. Bhimaraddi, A. "A Higher Order Theory for Free Vibration Analysis of Circular Cylindrical Shells," Int J Solids Struct, 20, 7, 1984.

40. Ambartsumyan, S.A. Theory of Anisotropic Shells, NASA-TT-F-118, 1964.

41. Vinson, J.R. and R.L. Sierakowski. The Behavior of Structures Composed of Composite Materials, M. Nijhoff, 1986.

42. Jones, R.J. Mechanics of Composite Materials, McGraw Hill, 1975.

43. Ashton, J.E. and J.M. Whitney. Theory of Laminated Plates, Technomic, 1970.

44. Dong, S.B., K.S. Pister, and R.L. Taylor. "On the Theory of Laminated Anisotropic Shells and Plates," Journ of Aero Sci, 29, 1962.

45.   Bert, C.W. "Structural Theory for Laminated Anisotropic Elastic Shells," J Composite Matls, 1, 1967.

46.   Yang, Norris, and Stavsky. "Elastic Wave Propagation in Heterogeneous Plates," Int J Solids Struct, 2, 1966.

47.   Whitney, J.M. and N.J. Pagano. "Shear Deformation in Heterogeneous Plates," Journ of Applied Mech, 1970.

48.   Reddy, J.N. "Exact Solutions of Moderately Thick Laminated Shells," J Eng Mech, ASCE 110, 5, 1984.

49.   Noor, A.K. "Stability of Multilayered Composite Plates," Fibre Science and Tech, 8, 1975.

50.   Hirano, Y. "Buckling of Angle Ply Laminated Circular Cylindrical Shells," Journ of Appl Mech, 46, Mar 1979.

51.   Stavsky, Y. and S. Friedland. "Stability of Heterogeneous Orthotropic Cylindrical Shells in Axial Compression," Israel J of Tech, 7, 1, 2, 1967.

52.   Greenberg, J.B. and Y. Stavsky. "Buckling and Vibration of Orthotropic Composite Cylindrical Shells," Acta Mechanica, 36, 1980.

53.   Reddy, J.N. and W.C. Chao. "A Comparison of Closed Form and Finite Element Solution of Thick Laminated Anisotropic Rectangular Plates," Nuclear Engineering and Design, 64, 1981.

54.   Reddy, J.N. and N.D. Phan. "Stability and Vibration of Isotropic, Orthotropic, and Laminated Plates According to a Higher Order Shear Deformation Theory," J Sound Vibration, 98(2), 1985.

55.   Soldatos, K.P. "Stability and Vibration of Thickness Shear Deformable Cross-Ply Laminated Non-Circular Cylindrical Shells," PVP, 115, ASME, 1986.

56.   Soldatos, K.P. "Buckling of Axially Compressed Antisymmetric Angle Ply Laminated Circular Cylindrical Panels According to a Refined Shear Deformable Shell Theory," to be published in ASME PVP conference proceedings, 1987.

57.   Reddy, J.N. "A Simple Higher Order Theory for Laminated Composite Plates," Journ of Applied Mech, 51, 1984.

58.   Phan, N.D. and J.N. Reddy. "Analysis of Laminated Composite Plates Using a Higher Order Shear Deformation Theory," IJNME, 21, 1985.

59.   Soldatos, K.P. and G.J Tzivanidis. 'Buckling and Vibration of Cross Ply Laminated Circular Cylindrical Panels,' J of Appl Math and Physics (ZAMP), 33 Mar, 1982.

60. Soldatos, K.P. and G.J. Tzivanidis. 'Buckling and Vibration of Cross Ply Laminated Noncircular Cylindrical Panels,' J Sound Vib, 82(3), 1982.

61. Reddy, J.N. and C.F. Liu. 'A Higher Order Shear Deformation Theory of Laminated Elastic Shells,' Int J Eng Sci, 23,3, 1985.

62. Pagano, N.J. 'Exact Solutions for Composite Laminates in Cylindrical Bending,' J Composite Matls, 3, 1969.

63.   Pagano, N.J. 'Influence of Shear Coupling in Cylindrical Bending of Anisotropic Laminates,' J Composite Matls, 4, 1970.

64.   Pagano, N.J. 'Exact Solutions for Rectangular Bidirectional Composites and Sandwich Plates,' J Composite Matls, 4, 1970.

65. Pagano, N.J. 'Further Study of Composite Laminates Under Cylindrical Bending,' J Composite Matls, 5, 1971.

66. Srinivas, S. and A.K. Rao. 'Bending, Vibration, and Buckling of Simply Supported Thick Orthotropic Rectangular Plates and Laminates,' Int J Solid Struct, 6, 1970.

67. Ren, J.G. 'Exact Solutions for Laminated Cylindrical Shells in Cylindrical Bending', Composites Sci Tech, 29, 1987.

68. Reddy, J.N. and K. Chandrashekhara. 'Nonlinear Analysis of Laminated Shells Including Transverse Shear Strains,' AIAA, 23, 3, 1985.

69.   Figueiras, J.A. and D.R.J. Owen. 'Analysis of Elasto-Plastic and Geometrically Nonlinear Anisotropic Plates and Shells,' Finite Element Software for Plates and Shells, edited by Hinton and Owen, Pineridge Press, 1984.

70. Zienkiewicz, O.C. The Finite Element Method, McGraw Hill, 1977.

71. Bogner, F.K., R.L. Fox, and L.A. Schmit. 'A Cylindrical Shell Discrete Element,' AIAA, 5, 4, 1967.

72. Yang, T.Y. 'High Order Rectangular Shallow Shell Finite Element,' J of Eng Mech Div, ASCE EM1, 1973.

73.   Idelsohn, "On the Use of Deep Shallow or Flat Shell
Finite Elements for Analysis of Thin Shell Structures," Comp
Meth in Appl Mech and Eng, 26, 1981.

74.   Ahmad, S., B. Irons, and O.C. Zienkiewicz. "Analysis of
Thick and Thin Shell Structures by Curved Finite Elements,"
IJNME, 2, 1970.

75.   Zienkiewicz, O.C., R.D. Taylor, and J.M. Too. "Reduced
Integration Technique in General Analysis of Plates and
Shells," IJNME, 3, 1971.

76.   Parisch, H. "A Critical Survey of the 9-Mode
Degenerated Shell Element with Special Emphasis on Thin
Shell Application and Reduced Integration," Comp Meth in
Appl Mech and Eng, 20, 1979.

77.   Kui, L.X., G.Q. Liu, and O.C. Zienkiewicz. "A
Generalized Method for the Finite Element Analysis of Thin
Shells," IJNME, 21, 1985.

78.   Wempner, G. A. "Finite Elements, Finite Rotations, and
Small Strains of Flexible Shells," Int J Solids Struct, 5,
1969.

79.   Brockman, R.A. A Penalty Function Approach for the
Nonlinear Finite Element Analysis of Thin Shells, PhD
Dissertation, Univ of Dayton, 1979.

80.   Park, K.C. and G.M. Stanley. "A Curved C$^{\circ}$ Shell Element
Based on Assumed Natural Coordinate Strains," Journ of
Applied Mech, 53, 1986.

81.   Pryor, C.W. and R.M. Barker. "A Finite Element Analysis
Including Transverse Shear Effects for Applications to
Laminated Plates," AIAA, 9, 5, 1971.

82.   Hinrichsen, R.L. and A.N. Palazotto. "Nonlinear Finite
Element Analysis of Thick Composite Plates Using a Cubic
Spline Function," AIAA, 24, 11, 1986.

83.   Palazotto, A.N. and W.P. Witt. "Formulation of a
Nonlinear Compatible Finite Element or Analysis of Laminated
Composites," Comp and Struct, 21, 6, 1985.

84.   Noor, A. and M.D. Mathers.   Shear Flexible Finite
Element Models of Laminated Composite Plates and Shells,
NASA TN D8044, 1975.

85.   Reddy, J.N. "Geometrically Nonlinear Transient Analysis
of Laminate Composite Plates," AIAA, 21,4 Apr 1983.

86. Reddy, J.N. 'Finite Element Modelling of Layered Anisotropic Composite Plates and Shells--A Review of Recent Research,' Shock Vibration Digest, 13, 12, 1981.

87. Schmit, L.A. and B.R. Monforton. 'Finite Deflection Discrete Element Analysis of Sandwich Plates and Cylindrical Shells with Laminated Faces,' AIAA, 8, 8, 1970.

88. Leissa, A.W. Buckling of Laminated Composite Plates and Shell Panels, AFWAL-TR-85-3069, Wright-Patterson AFB, Oh. 45433.

89. Stolarski, H., T.Belyschtco, N. Carpenter, and J. Kennedy. 'A Simple Triangular Curved Shell Element for Collapse Analysis,' in Collapse Analysis of Structures, ed by L.H. Sobel and K Thomas, PVP, 84, ASME, 1984.

90. Noor, A. and J. Peters. 'Nonlinear Analysis of Anisotropic Panels,' AIAA, 24, 9, 1986.

91. Meroueh, K.A. 'On a Formulation of a Nonlinear Theoy of Plates and Shells with Applications,' Comp and Struct, 24, 5, 1986.

92. Surana, K.S. 'Geometrically Nonlinear Formulation for Curved Shell Elements,' IJNME, 19, 1983.

93. Surana, K.S. 'A Generalized Geometrically Nonlinear Formulation with Large Rotations for Finite Elements with Rotational Degrees of Freedom,' Comp and Struct, 24, 1986.

94. Rankin, C.C., P. Stehlin, and F.A. Brogran. Enhancements to the STAGS Computer Code, NASA CR 4000, 1986.

95. Putcha, N.S. and J.N. Reddy. 'A Refined Mixed Shear Flexible Finite Element for the Nonlinear Analysis of Laminated Plates,' Comp and Struct, 22, 4, 1986.

96. Stricklin, J.A. and W.E. Haisler. 'Formulations and Solution Procedures for Nonlinear Structural Analysis', Comp and Struct, 7, 1977.

97. Bathe, K.J. and A.P. Cimento. 'Some Practical Procedures for the Solution of Nonlinear Finite Element Equations', Comp Mtds in Appl Mech and Eng, 22, 1980.

98. Riks, E. 'Progress in Collapse Analyses', Journ of Press Vessel Tech, 109, 1987.

99. Waszczyszyn, Z. "Numerical Problems of Nonlinear Stability Analysis of Elastic Structures", Comp and Struct, 17, 1, 1983.

100. Bergan, P.G. "Automated Incremental-Iterative Solution Methods in Structural Mechanics", in Recent Advances in Nonlinear Computational Mechanics, eds Hinton, Owen, and Taylor, Pineridge Press 1982.

101. Ramm, E. "The Riks/Wempner Approach-An Extension of the Displacement Control Method in Nonlinear Analyses", in Recent Advances in Nonlinear Computational Mechanics, eds Hinton, Owen, and Taylor, Pineridge Press 1982.

102. Batoz J.L. and G. Dhatt. "Incremental Displacement Algorithms for Nonlinear Problems", IJNME, 14, 1979.

103. Zienkiewicz, O.C. "Incremental Displacement in Nonlinear Analysis", IJNME, 3, 1971.

104. Riks, E. "An Incremental Approach to the Solution of Snapping and Buckling Problems", Int J Solids Struct, 15, 1979.

105. Riks, E. "The Application of Newton's Method to the Problem of Elastic Stability", Journ of Appl Mech, 1972.

106. Wempner, G.A. "Discrete Approximations Related to Nonlinear Theories of Solids", Int J Solids Struct, 7, 1971.

107. Crisfield, M.A. "A Fast Incremental/Iterative Solution Procedure That Handles Snap-Through", Comp and Struct, 13, 1981.

108. Crisfield, M.A. "Solution Procedures for Nonlinear Structural Problems", in Recent Advances in Nonlinear Computational Mechanics, eds Hinton, Owen, and Taylor, 1982.

109. Crisfield, M.A. "An Arc Length Method Including Line Searches and Accelerations", IJNME, 19, 1983.

110. Padovan J. and R. Moscarello. "Locally Bound Constrained Newton Raphson Solution Algorithms," Comp and Struct, 23, 1986.

111. Vanderplaats, Optimization Techniques for Nonlinear Engineering Design with Applications, McGraw Hill, 1984.

112. Mathies, H. and G. Strang. "The Solution of Nonlinear Finite Element Equations", IJNME, 14, 1979.

113. Novozhilov, V.V. Foundations of the Nonlinear Theory of Elasticity, Graylock Press, 1953.

114. Washizu, K. _Variational Methods in Elasticity and Plasticity_, Pergamon Press, 1982.

115. Bathe, K.J. _Finite Element Procedures in Engineering Analysis_, Prentice Hall, 1982.

116. Stein, M. "Nonlinear Theory for Plates and Shells Including the Effects of Transverse Shearing," _AIAA_, 24, 9, 1986.

117. Tsai, S.W. _Composite Design_, Think Composites, 1987.

118. Kwon, Y.W. and J.E. Akin. "Analysis of Layered Composite Plates using a Higher Order Deformation Theory," _Comp and Struct_, 27,5 1987.

119. Lo K.H., R.M. Christensen, E.M. Wu. "A High Order Theory of Plate Deformation", _Journ Appl Mech_, 44, Dec 1977.

120. Rajasekaran, S. and D.W. Murray. "Incremental Finite Element Matrices", _J of Struct Div_, ASCE, 1973.

121. Cook, R.D. _Concepts and Applications of Finite Element Analysis_, John Wiley and Sons, 1981.

122. Gallagher, R.H. _Finite Element Analysis Fundamentals_, Prentice Hall, 1975.

123. Walz, J.E, R.E. Fulton, and N.J. Cyrus. _Accuracy and Convergence of Finite Element Approximations_, AFFDL-TR-68-150, 1968.

124. Almroth, B.O. and F.A. Brogan. _Numerical Procedures for Analysis of Structural Shells_, AFWAL-TR-80-3129, Wright-Patterson AFB, Oh. 1980.

125. Fraeijis De Veubeke, B. "A Conforming Finite Element for Plate Bending," _Int J Solids Struct_, 4, 1968.

126. Pian, T.H.H. and P. Tong. "Basis of Finite Element Methods for Solid Continua," _IJNME_, 1, 1969.

127. Tong, P. "New Displacement Hybird Finite Element Models for Solid Continua," _IJNME_, 2, 1970.

128. Reissner, E. "Formulation of Variational Theorems in Geometrically Nonlinear Elasticity," _J Eng Mech_, 110,9 1984.

129. Reddy, J.N. _An Introduction to the Finite Element Method_, McGraw Hill, 1984.

130. Chang S.C. and J.J. Chen. "Effectiveness of Linear Bifurcation Analysis for Predicting the Nonlinear Stability Limits of Structure," IJNME, 23, 1986.

131. Wood R.D. and B.Schrefler, "Geometrically Nonlinear Analysis a Correlation of Finite Element Notations," IJNME, 12, 1978.

132. Thompson, J.M.T. and G.W. Hunt. A General Theory of Elastic Stability, John Wiley and Sons, 1973.

133. Szilard, R. Theory and Analysis of Plates-Classical and Numerical Methods, Prentice Hall, 1974.

134. Noor, A.K, M.D. Mathers, and M.S. Anderson. "Exploiting Symmetries for Efficient Postbuckling Analysis of Composite Plates," AIAA, 15,1 1977.

135. Reddy, J.N. "A Note on Symmetry Conditions in Transient Response of Unsymmetrically Laminated Anisotropic Plates," IJNME, 20, 1, 1984.

136. Brebbia, C. and J. Connor. "Geometrically Nonlinear Finite Element Analysis," J of Eng Mech Div, ASCE, 1969.

137. Scordelis, A.C. and K.S. Lo. "Computer Analysis of Cylindrical Shells," American Concrete Institute, 1964.

138. Timoshenko, S.P. and Woinowsky-Krieger. Theory of Plates and Shells, McGraw Hill, 1959.

139. Timoshenko, S.P. and J.N. Goodier. Theory of Elasticity, McGraw Hill, 1970.

140. Levy, S. Bending of Rectangular Plates with Large Deflections, NACA TN 846, 1942.

141. Levy, S. Square Plate with Clamped Edges Under Normal Pressure Producing Large Deflections, NACA TN 847, 1942.

142. Adotte, G. "Second Order Theory in Orthotropic Plates," J of Struct Div, ASCE 1967.

143. Chia, C.Y. "Large Deflection of Rectangular Orthotropic Plates," J of Eng Mech Div, ASCE, 1972.

144. Sabir, A.B. and A.C. Lock. "The Application of Finite Elements to the Large Deflection Geometrically Nonlinear Behaviour of Cylindrical Shells," Variational Methods in Engineering, ed C.A.Brebbia and H. Tottenham, Southhampton Press, 1972.

307

145. Walker, A.C. "A Nonlinear Finite Element Analysis of Shallow Circular Arches," Int J Solids Struct, 5, 1969.

146. Huddleston J.V. "Finite Deflections and Snap Through of High Circular Arches," Journ of Appl Mech, Dec 1968.

147. Schmidt, R. and D.A. Dadeppo. "A Survey of Literature on Large Defections of Non Shallow Arches," J Industrial Math Soc, 21, 1971.

148. Dadeppo D.A. and R. Schmidt. "Instability of Clamped Hinged Circular Arches Subjected to a Point Load," Journ of Appl Mech, 42, 1975.

149. Hebert, J.S. and A.N. Palazotto. "Comparison Between Experimental and Numerical Buckling of Curved Cylindrical Composite Panels," Proceed of 12 Southeastern Conf on Theoretical and Appl Mech, 1984.

150. Janisse T.C. and A.N. Palazotto. "Collapse Analysis of Composite Cylindrical Panels with Small Cutouts," J Aircraft, 21,9, 1984.

151. Lee C.E. and A.N. Palazotto. "Collapse Analysis of Composite Cylindrical Panels with Small Cutouts," J Composite Struct, 4, 1985.

152. Hermsen, M.F. and A.N. Palazotto. "The Effects of Cutout Location and Material Degradation on the Collapse of Composite Cylindrical Panels," Nonlinear Analysis and NDE of Composite Material Vessels and Components, ed D.Hui, J.Duke, H.Chung, PVP, 115,ASME, 1986.

153. Horban B.A. and A.N. Palazotto. "The Experimental Buckling of Cylindrical Composite Panels with Eccentrically Located Circular Delaminations," AIAA paper no. 86-0882, 1986.

154. Wilder, B.L. A Study of Damage Tolerance in Curved Composite Panels, M.S. Thesis, AFIT/GA/AA/88M-2, Wright Patterson, Oh, 1988.

Vita

Scott T. Dennis was born September 8, 1957 in Borne, Massachusetts. He received a Bachelor of Science in Engineering Mechanics from the U.S. Air Force Academy in May 1979. After spending over two years in the Air Force Flight Dynamics Laboratory working in aircraft survivability, he attended graduate school at the Massachusetts Institute of Technology, earning a Master of Science degree in Aeronautics and Astronautics (Structures) in February 1983. From there, he worked as a structural engineer at the Air Force Weapons Laboratory. He entered the School of Engineering, Air Force Institute of Technology, in July 1985.

Permanent Address: 43 Victoria Circle
                    Dover, De 19901

Appendix A: Strain Displacement for Arbitrary Shell Geometry

I. $\underline{\varepsilon}_i^{\,\circ}$ and $\varkappa_j^I$ from Eqn (3.47).

$$\underline{\varepsilon}_1^{\,\circ} = \left[\frac{u,_1}{\alpha_1} + \frac{h_{1,2}}{h_1 \alpha_2} v + \frac{h_{1,3}}{h_1} w\right] + \frac{u,_1^2}{2\alpha_1^2} + \frac{1}{2h_1^2}\left[p_{21}^2 + w,_1^2\right]$$

$$+ \frac{h_{1,2}^2}{2h_1^2\alpha_2^2} v^2 + \frac{h_{1,2}^2}{2h_2^2\alpha_1^2} u^2 + \frac{h_{1,3}^2}{2h_1^2} w^2 + \frac{h_{1,3}^2}{2\alpha_1^2} u^2 + \frac{h_{1,2}h_{1,3}}{h_1^2 \alpha_2} wv$$

$$+ \frac{h_{1,2}}{\alpha_2\alpha_1 h_1}\left[u,_1 v - uv,_1\right] + \frac{h_{1,3}}{\alpha_1 h_1}\left[u,_1 w - uw,_1\right] \tag{A.1}$$

$$\underline{\varepsilon}_2^{\,\circ} = \left[\frac{v,_2}{\alpha_2} + \frac{h_{2,1}}{h_2 \alpha_1} u + \frac{h_{2,3}}{h_2} w\right] + \frac{v,_2^2}{2\alpha_2^2} + \frac{1}{2h_2^2}\left[p_{12}^2 + w,_2^2\right]$$

$$+ \frac{h_{2,1}^2}{2h_2^2\alpha_1^2} u^2 + \frac{h_{2,1}^2}{2h_1^2\alpha_2^2} v^2 + \frac{h_{2,3}^2}{2h_2^2} w^2 + \frac{h_{2,3}^2}{2\alpha_2^2} v^2 + \frac{h_{2,1}h_{2,3}}{h_2^2 \alpha_1} wu$$

$$+ \frac{h_{2,1}}{\alpha_2\alpha_1 h_2}\left[v,_2 u - vu,_2\right] + \frac{h_{2,3}}{\alpha_2 h_2}\left[v,_2 w - vw,_2\right] \tag{A.2}$$

$$\underline{\varepsilon}_6^{\,\circ} = \left[\frac{p_{12}}{h_2} + \frac{p_{21}}{h_1} - \frac{h_{2,1}}{\alpha_2 h_1} v - \frac{h_{1,2}}{\alpha_1 h_2} u\right] + \frac{p_{12}}{\alpha_1 h_2} u,_1 + \frac{p_{21}}{\alpha_2 h_1} v,_2$$

$$+ \frac{h_{1,2}}{\alpha_1 \alpha_2 h_2}\left[vu,_2 - uv,_2\right] + \frac{h_{2,1}}{\alpha_1 \alpha_2 h_1}\left[uv,_1 - u,_1 v\right] + \frac{w,_1 w,_2}{h_1 h_2}$$

$$+ \frac{h_{2,3}}{\alpha_2 h_1}\left[v,_1 w - vw,_1\right] - \frac{h_{2,1}h_{1,2}}{\alpha_2^2 h_1^2} v^2 - \frac{h_{2,1}h_{1,2}}{\alpha_1^2 h_2^2} u^2$$

$$+ \frac{h_{1,3}h_{2,3}}{\alpha_1 \alpha_2} uv - \frac{h_{1,3}h_{2,1}}{h_1^2 \alpha_2} wv - \frac{h_{2,3}h_{1,2}}{\alpha_1 h_2^2} uw \tag{A.3}$$

$$\varkappa_1^1 = \left(\frac{l_{11}}{h_1} + \frac{h_{1,2}}{h_1 h_2} \psi_2 \right) + \frac{l_{11}}{h_1 \alpha_1} u_{,1} + \frac{l_{21} P_{21}}{h_1^2} + \frac{h_{1,2}^2}{h_1^2 h_2 \alpha_2} v \psi_2$$

$$+ \frac{h_{1,2}^2}{h_1 h_2^2 \alpha_1} u \psi_1 + \frac{h_{1,3}^2}{h_1 \alpha_1} u \psi_1 + \frac{h_{1,2}}{h_1^2 \alpha_2} \left[l_{11} v - \psi_1 v_{,1} \right]$$

$$+ \frac{h_{1,3}}{h_1^2} \left[w l_{11} - \psi_1 w_{,1} \right] + \frac{h_{1,2} h_{1,3}}{h_1^2 h_2} \psi_2 w + \frac{h_{1,2}}{h_1 h_2 \alpha_1} \left[\psi_2 u_{,1} - l_{21} u \right]$$

<div style="text-align:right">(A.4)</div>

$$\varkappa_2^2 = \left(\frac{l_{22}}{h_2} + \frac{h_{2,1}}{h_1 h_2} \psi_1 \right) + \frac{l_{22}}{h_2 \alpha_2} v_{,2} + \frac{l_{12} P_{12}}{h_2^2} + \frac{h_{2,1}^2}{h_2^2 h_1 \alpha_1} u \psi_1$$

$$+ \frac{h_{2,1}^2}{h_2 h_1^2 \alpha_2} v \psi_2 + \frac{h_{2,3}^2}{h_2 \alpha_2} v \psi_2 + \frac{h_{2,1}}{h_2^2 \alpha_1} \left[l_{22} u - \psi_2 u_{,2} \right]$$

$$+ \frac{h_{2,3}}{h_2^2} \left[w l_{22} - \psi_2 w_{,2} \right] + \frac{h_{2,1} h_{2,3}}{h_2^2 h_1} \psi_1 w + \frac{h_{2,1}}{h_1 h_2 \alpha_2} \left[\psi_1 v_{,2} - l_{12} v \right]$$

<div style="text-align:right">(A.5)</div>

$$\varkappa_6^1 = \left(\frac{l_{12}}{h_2} + \frac{l_{21}}{h_1} - \frac{h_{2,1}}{h_1 h_2}\psi_2 - \frac{h_{1,2}}{h_1 h_2}\psi_1 \right) + \frac{l_{12}u_{,1}}{\alpha_1 h_2} + \frac{l_{11}u_{,2}}{\alpha_1 h_2}$$

$$+ \frac{h_{1,2}}{\alpha_2 h_1 h_2}\left(vl_{12} - \psi_1 v_{,2} \right) + \frac{h_{1,2}}{\alpha_1 h_2^2}\left(\psi_2 u_{,2} - l_{22}u \right) + \frac{l_{22}v_{,1}}{\alpha_2 h_1}$$

$$+ \frac{h_{2,1}}{\alpha_1 h_1 h_2}\left(ul_{21} - \psi_2 u_{,1} \right) + \frac{h_{2,1}}{\alpha_2 h_1^2}\left(\psi_1 v_{,1} - l_{11}v \right) + \frac{l_{21}v_{,2}}{\alpha_2 h_1}$$

$$+ \frac{h_{1,3}}{h_1 h_2}\left(wl_{12} - w_{,2}\psi_1 \right) + \frac{h_{2,3}}{h_1 h_2}\left(wl_{21} - w_{,1}\psi_2 \right)$$

$$- \frac{h_{2,1}h_{1,2}}{\alpha_2 h_1^2 h_2} 2\psi_2 v - \frac{h_{2,1}h_{1,2}}{\alpha_1 h_2^2 h_1} 2\psi_1 u - \frac{h_{1,3}h_{2,1}}{h_1^2 h_2}\psi_2 w$$

$$- \frac{h_{2,3}h_{1,2}}{h_2^2 h_1}\psi_1 w + \frac{h_{1,3}h_{2,3}}{\alpha_1 h_2} u\psi_2 + \frac{h_{2,3}h_{1,3}}{\alpha_2 h_1} v\psi_1$$

$$+ \frac{h_{2,1}}{\alpha_1 h_1 h_2}\left(l_{21}u - \psi_2 u_{,1} \right) + \frac{h_{2,1}}{h_1^2 \alpha_2}\left(\psi_1 v_{,1} - l_{11}v \right) \tag{A.6}$$

$$\varkappa_1^2 = \frac{1}{2h_1^2}\left(l_{11}^2 + l_{21}^2 \right) + \frac{h_{1,2}^2}{2h_1^2 h_2^2}\left(\psi_1^2 + \psi_2^2 \right)$$

$$+ \frac{h_{1,2}}{h_2 h_1^2}\left(\psi_2 l_{11} - \psi_1 l_{21} \right) + \frac{h_{1,3}^2}{2h_1^2}\psi_1^2 \tag{A.7}$$

$$\varkappa_2^2 = \frac{1}{2h_2^2}\left(l_{22}^2 + l_{12}^2 \right) + \frac{h_{2,1}^2}{2h_1^2 h_2^2}\left(\psi_1^2 + \psi_2^2 \right)$$

$$+ \frac{h_{2,1}}{h_1 h_2^2}\left(\psi_1 l_{22} - \psi_2 l_{12} \right) + \frac{h_{2,3}^2}{2h_2^2}\psi_2^2 \tag{A.8}$$

312

$$\kappa_6^2 = \frac{1}{h_1 h_2}\Big[l_{11}l_{12} + l_{21}l_{22}\Big] - \frac{h_{2,1}h_{1,2}}{h_1^2 h_2^2}\psi_1^2 - \frac{h_{2,1}h_{1,2}}{h_1^2 h_2^2}\psi_2^2$$

$$+ \frac{h_{1,2}}{h_1 h_2^2}\Big[l_{12}\psi_2 - l_{22}\psi_1\Big] + \frac{h_{2,1}}{h_2 h_1^2}\Big[l_{21}\psi_1 - l_{11}\psi_2\Big]$$

$$+ \frac{h_{1,3}h_{2,3}}{h_1 \, h_2}\psi_1\psi_2$$

$$\text{(A.9)}$$

$$\kappa_1^3 = \frac{m_{1,1}}{h_2} + \frac{h_{1,2}}{h_1 h_2}m_2 + \frac{m_{1,1}}{\alpha_1 h_1}u_{,1} + \frac{p_{21}m_{2,1}}{h_1^2} + \frac{h_{1,2}^2 m_2}{\alpha_2 h_2 h_1^2}v$$

$$+ \frac{h_{1,2}^2}{h_2^2 \alpha_1 h_1}um_1 + \frac{h_{1,3}^2}{\alpha_1 h_1}um_1 + \frac{h_{1,2}}{\alpha_2 h_1^2}\Big[m_{1,1}v - m_1 v_{,1}\Big]$$

$$+ \frac{h_{1,2}}{\alpha_1 h_1 h_2}\Big[m_2 u_{,1} - m_{2,1}u\Big] + \frac{h_{1,3}}{h_1^2}\Big[m_{1,1}w - m_1 w_{,1}\Big]$$

$$+ \frac{h_{1,2}h_{1,3}}{h_1^2 \, h_2}m_2 w$$

$$\text{(A.10)}$$

$$\kappa_2^3 = \frac{m_{2,2}}{h_2} + \frac{h_{2,1}}{h_1 h_2}m_1 + \frac{m_{2,2}}{\alpha_2 h_2}v_{,2} + \frac{p_{12}m_{1,2}}{h_2^2} + \frac{h_{2,1}^2 m_1}{\alpha_1 h_1 h_2^2}u$$

$$+ \frac{h_{2,1}^2}{h_1^2 \alpha_2 h_2}vm_2 + \frac{h_{2,3}^2}{\alpha_2 h_2}vm_2 + \frac{h_{2,1}}{\alpha_1 h_2^2}\Big[m_{2,2}u - m_2 u_{,2}\Big]$$

$$+ \frac{h_{2,1}}{\alpha_2 h_1 h_2}\Big[m_1 v_{,2} - m_{1,2}v\Big] + \frac{h_{2,3}}{h_2^2}\Big[m_{2,2}w - m_2 w_{,2}\Big]$$

$$+ \frac{h_{2,1}h_{2,3}}{h_2^2 \, h_1}m_1 w$$

$$\text{(A.11)}$$

$$\varkappa_6^3 = \frac{m_{1,2}}{h_2} + \frac{m_{2,1}}{h_1} - \frac{h_{2,1}}{h_1 h_2} m_2 - \frac{h_{1,2}}{h_1 h_2} m_1 + \frac{m_{1,2}}{\alpha_1 h_2} u_{,1} + \frac{m_{1,1}}{\alpha_1 h_2} u_{,2}$$

$$+ \frac{m_{2,1}}{\alpha_2 h_1} v_{,2} + \frac{h_{1,3}}{h_1 h_2}\left(m_{1,2}w - m_1 w_{,2}\right) + \frac{h_{2,3}}{h_1 h_2}\left(m_{2,1}w - m_2 w_{,1}\right)$$

$$+ \frac{h_{1,2}}{\alpha_2 h_1 h_2}\left(v m_{1,2} - m_1 v_{,2}\right) + \frac{h_{1,2}}{\alpha_1 h_2^2}\left(m_2 u_{,2} - m_{2,2}u\right)$$

$$+ \frac{h_{2,1}}{\alpha_1 h_2 h_1}\left(u m_{2,1} - m_2 u_{,1}\right) + \frac{h_{2,1}}{\alpha_2 h_1^2}\left(m_1 v_{,1} - m_{1,1}v\right)$$

$$- 2\frac{h_{2,1}h_{1,2}}{\alpha_2 h_1^2 h_2} v m_2 - 2\frac{h_{2,1}h_{1,2}}{\alpha_1 h_2^2 h_1} u m_1 - \frac{h_{1,3}h_{2,1}}{h_1^2 h_2} m_2 w$$

$$- \frac{h_{2,3}h_{1,2}}{h_2^2 h_1} m_1 w + \frac{h_{1,3}h_{2,3}}{\alpha_1 h_2} u m_2 + \frac{h_{2,3}h_{1,3}}{\alpha_2 h_1} v m_1 + \frac{m_{2,2}}{\alpha_2 h_1} v_{,1}$$

$$\text{(A.12)}$$

$$\varkappa_1^4 = \frac{l_{11}m_{1,1}}{h_1^2} + \frac{l_{21}m_{2,1}}{h_1^2} + \frac{h_{1,2}^2}{h_2^2 h_1^2}\left(\psi_2 m_2 + \psi_1 m_1\right) + \frac{h_{1,3}^2}{h_1^2}\psi_1 m_1$$

$$+ \frac{h_{1,2}}{h_1^2 h_2}\left(\psi_2 m_{1,1} + m_2 l_{11} - m_{2,1}\psi_1 - m_1 l_{21}\right)$$

$$\text{(A.13)}$$

$$\varkappa_2^4 = \frac{l_{22}m_{2,2}}{h_2^2} + \frac{l_{12}m_{1,2}}{h_2^2} + \frac{h_{2,1}^2}{h_2^2 h_1^2}\left(\psi_2 m_2 + \psi_1 m_1\right) + \frac{h_{2,3}^2}{h_2^2}\psi_2 m_2$$

$$+ \frac{h_{2,1}}{h_2^2 h_1}\left(\psi_1 m_{2,2} + m_1 l_{22} - m_{1,2}\psi_2 - m_2 l_{12}\right)$$

$$\text{(A.14)}$$

314

$$\kappa_6^4 = \frac{1}{h_1 h_2}\left[l_{11}m_{1,2} + m_{1,1}l_{12} + l_{21}m_{2,2} + m_{2,1}l_{22}\right]$$

$$+ \frac{h_{1,2}}{h_1 h_2^2}\left[\psi_2 m_{1,2} + l_{12}m_2 - m_{2,2}\psi_1 - l_{22}\,m_1\right]$$

$$+ \frac{h_{2,1}}{h_2 h_1^2}\left[\psi_1 m_{2,1} + l_{21}m_1 - m_{1,1}\psi_2 - l_{11}\,m_2\right]$$

$$+ \frac{h_{1,3}h_{2,3}}{h_1 h_2}\left[\psi_1 m_2 + \psi_2 m_1\right] - 2\frac{h_{2,1}h_{1,2}}{h_1^2 h_2^2}\left[\psi_2 m_2 + \psi_1 m_1\right]$$

$$\text{(A.15)}$$

$$\kappa_1^6 = \frac{1}{2h_1^2}\left[m_{1,1}^2 + m_{2,1}^2\right] + \frac{h_{1,2}^2}{h_1^2 h_2^2}\left[m_2^2 + m_1^2\right] + \frac{h_{1,3}^2}{2h_1^2}\,m_1^2$$

$$+ \frac{h_{1,2}}{h_2 h_1^2}\left[m_{1,1}m_2 - m_1 m_{2,1}\right]$$

$$\text{(A.16)}$$

$$\kappa_2^6 = \frac{1}{2h_2^2}\left[m_{2,2}^2 + m_{1,2}^2\right] + \frac{h_{2,1}^2}{2h_1^2 h_2^2}\left[m_2^2 + m_1^2\right] + \frac{h_{2,3}^2}{2h_2^2}\,m_2^2$$

$$+ \frac{h_{2,1}}{h_1 h_2^2}\left[m_{2,2}m_1 - m_2 m_{1,2}\right]$$

$$\text{(A.17)}$$

$$\kappa_6^6 = \frac{1}{h_1 h_2}\Big(m_{1,1}m_{1,2} + m_{2,1}m_{2,2}\Big) + \frac{h_{1,2}}{h_2^2 h_1}\Big(m_2 m_{1,2} - m_1 m_{2,2}\Big)$$

$$+ \frac{h_{2,1}}{h_1^2 h_2}\Big(m_1 m_{2,1} - m_2 m_{1,1}\Big) - \frac{h_{2,1}h_{1,2}}{h_1^2 \, h_2^2}\Big(m_1^2 + m_2^2\Big)$$

$$+ \frac{h_{1,3}h_{2,3}}{h_1 h_2} \, m_1 m_2 \hspace{3cm} (A.18)$$

where,

$$p_1 = u(1-\zeta/R_1) \hspace{2cm} m_1 = k\Big(\frac{w_{,1}}{\alpha_1} + \psi_1\Big)$$

$$p_2 = v(1-\zeta/R_2)$$

$$\hspace{5cm} m_2 = k\Big(\frac{w_{,2}}{\alpha_2} + \psi_2\Big)$$

$$p_{11} = u_{,1}(1-\zeta/R_1)$$

$$p_{12} = u_{,2}(1-\zeta/R_1) \hspace{2cm} h_1 = \alpha_1(1-\zeta/R_1)$$

$$p_{21} = v_{,1}(1-\zeta/R_2) \hspace{2cm} h_2 = \alpha_2(1-\zeta/R_2)$$

$$p_{22} = v_{,2}(1-\zeta/R_2)$$

$$l_{11} = \frac{R_{1,1}u}{R_1^2} + \psi_{1,1} \hspace{2cm} l_{12} = \frac{R_{1,2}u}{R_1^2} + \psi_{1,2}$$

$$l_{22} = \frac{R_{2,2}v}{R_2^2} + \psi_{2,2} \hspace{2cm} l_{21} = \frac{R_{2,1}v}{R_2^2} + \psi_{2,1}$$

II. Approximations of the scale factor terms that appear in Eqns (A.1-A.18) similar to those of Eqn (3.48). Terms f_I and g_I are defined.

1. $\dfrac{h_{1,2}}{h_1} \cong \dfrac{\alpha_{1,2}}{\alpha_1} + \zeta\dfrac{R_{1,2}}{R_1^2} = f_1 + \zeta g_1$

2. $\dfrac{h_{1,3}}{h_1} \cong \dfrac{-1}{R_1} - \zeta\dfrac{1}{R_1^2} = f_2 + \zeta g_2$

3. $\dfrac{1}{h_1^2} \cong \dfrac{1}{\alpha_1^2} + \zeta \dfrac{2}{\alpha_1^2 R_1} = f_3 + \zeta g_3$

4. $\dfrac{h_{1,2}^2}{h_1^2} \cong \dfrac{\alpha_{1,2}^2}{\alpha_1^2} + 2\zeta \dfrac{\alpha_{1,2} R_{1,2}}{\alpha_1 R_1^2} = f_4 + \zeta g_4$

5. $\dfrac{h_{1,2}^2}{h_2^2} \cong \dfrac{\alpha_{1,2}^2}{\alpha_2^2} + 2\zeta \left[-\dfrac{\alpha_{1,2}^2}{\alpha_2^2 R_1} + \dfrac{\alpha_1 \alpha_{1,2} R_{1,2}}{\alpha_2^2 R_1^2} + \dfrac{\alpha_{1,2}^2}{\alpha_2^2 R_2} \right] = f_5 + \zeta g_5$

6. $\dfrac{h_{1,3}^2}{h_1^2} \cong \dfrac{1}{R_1^2} + \zeta \dfrac{2}{R_1^3} = f_6 + \zeta g_6$

7. $h_{1,3}^2 = \dfrac{\alpha_1^2}{R_1^2} = f_7$

8. $\dfrac{h_{1,2} h_{1,3}}{h_1^2} \cong -\dfrac{\alpha_{1,2}}{\alpha_1 R_1} - \zeta \left(\dfrac{\alpha_{1,2}}{\alpha_1 R_1^2} + \dfrac{R_{1,2}}{R_1^3} \right) = f_8 + \zeta g_8$

9. $\dfrac{h_{2,3}}{h_2} \cong -\dfrac{1}{R_2} - \zeta \dfrac{1}{R_2^2} = f_9 + \zeta g_9$

10. $\dfrac{h_{2,1}}{h_2} \cong \dfrac{\alpha_{2,1}}{\alpha_2} + \zeta \dfrac{R_{2,1}}{R_2^2} = f_{10} + \zeta g_{10}$

11. $\dfrac{1}{h_2^2} \cong \dfrac{1}{\alpha_2^2} + \zeta \dfrac{2}{\alpha_2^2 R_2} = f_{11} + \zeta g_{11}$

12. $\dfrac{h_{2,1}^2}{h_2^2} \cong \dfrac{\alpha_{2,1}^2}{\alpha_2^2} + 2\zeta \dfrac{\alpha_{2,1} R_{2,1}}{\alpha_2 R_2^2} = f_{12} + \zeta g_{12}$

13. $\dfrac{h_{2,1}^2}{h_1^2} \cong \dfrac{\alpha_{2,1}^2}{\alpha_1^2} + 2\zeta \left[\dfrac{-\alpha_{2,1}^2}{\alpha_1^2 R_2} + \dfrac{\alpha_2 R_{2,1} \alpha_{2,1}^2}{\alpha_1^2 R_2^2} + \dfrac{\alpha_{2,1}^2}{\alpha_1^2 R_1} \right] = f_{13} + \zeta g_{13}$

14. $\dfrac{h_{2,3}^2}{h_2^2} \cong \dfrac{1}{R_2^2} + \zeta \dfrac{2}{R_2^3} = f_{14} + \zeta g_{14}$

317

15. $h_{2,3}^2 = \dfrac{\alpha_2^2}{R_2^2} = f_{15}$

16. $\dfrac{h_{2,3}h_{2,1}}{h_2^2} \cong -\dfrac{\alpha_{2,1}}{R_2\alpha_2} - \zeta\left(\dfrac{R_{2,1}}{R_2^3} + \dfrac{\alpha_{2,1}}{R_2^2\alpha_2}\right) = f_{16} + \zeta g_{16}$

17. $\dfrac{1}{h_2} \cong \dfrac{1}{\alpha_2} + \zeta\dfrac{1}{\alpha_2 R_2} = f_{17} + \zeta g_{17}$

18. $\dfrac{1}{h_1} \cong \dfrac{1}{\alpha_1} + \zeta\dfrac{1}{\alpha_1 R_1} = f_{18} + \zeta g_{18}$

19. $\dfrac{h_{2,1}}{h_1} \cong \dfrac{\alpha_{2,1}}{\alpha_1} + \zeta\left(\dfrac{R_{2,1}\alpha_2}{\alpha_1 R_2^2} - \dfrac{\alpha_{2,1}}{\alpha_1 R_2} + \dfrac{\alpha_{2,1}}{\alpha_1 R_1}\right) = f_{19} + \zeta g_{19}$

20. $\dfrac{h_{1,2}}{h_2} \cong \dfrac{\alpha_{1,2}}{\alpha_2} + \zeta\left(\dfrac{R_{1,2}\alpha_1}{\alpha_2 R_1^2} - \dfrac{\alpha_{1,2}}{\alpha_2 R_1} + \dfrac{\alpha_{1,2}}{\alpha_2 R_2}\right) = f_{20} + \zeta g_{20}$

21. $\dfrac{1}{h_1 h_2} \cong \dfrac{1}{\alpha_1\alpha_2} + \zeta\,\dfrac{1}{\alpha_1\alpha_2}\left(\dfrac{1}{R_1} + \dfrac{1}{R_2}\right) = f_{21} + \zeta g_{21}$

22. $\dfrac{h_{1,3}}{h_2} \cong -\dfrac{\alpha_1}{R_1\alpha_2} - \zeta\dfrac{\alpha_1}{R_1 R_2\alpha_2} = f_{22} + \zeta g_{22}$

23. $\dfrac{h_{2,3}}{h_1} \cong -\dfrac{\alpha_2}{R_2\alpha_1} - \zeta\dfrac{\alpha_2}{R_1 R_2\alpha_1} = f_{23} + \zeta g_{23}$

24. $\dfrac{h_{2,1}h_{1,2}}{h_1^2} \cong \dfrac{\alpha_{1,2}\alpha_{2,1}}{\alpha_1^2} + \zeta\left(\dfrac{R_{1,2}\alpha_{2,1}}{\alpha_1 R_1^2} + \dfrac{\alpha_{1,2}\alpha_{1,2}}{\alpha_1^2 R_1} - \dfrac{\alpha_{2,1}\alpha_{1,2}}{R_2\alpha_1^2}\right.$

$\left. + \dfrac{R_{2,1}\alpha_2\alpha_{1,2}}{R_2^2\alpha_1^2}\right) = f_{24} + \zeta g_{24}$

25. $$\frac{h_{2,1}h_{1,2}}{h_2^2} \cong \frac{\alpha_{1,2}\alpha_{2,1}}{\alpha_2^2} + \zeta\left[\frac{R_{2,1}\alpha_{1,2}}{\alpha_2 R_2^2} + \frac{\alpha_{1,2}\alpha_{1,2}}{\alpha_2^2 R_2} - \frac{\alpha_{2,1}\alpha_{1,2}}{R_1\alpha_2^2}\right.$$

$$\left. + \frac{R_{1,2}\alpha_1\alpha_{2,1}}{R_1^2\alpha_2^2}\right] = f_{25} + \zeta g_{25}$$

26. $$h_{1,3}h_{2,3} \cong \frac{\alpha_1\alpha_2}{R_1 R_2} = f_{26}$$

27. $$\frac{h_{1,3}h_{2,1}}{h_1^2} \cong -\frac{\alpha_{2,1}}{R_1\alpha_1} + \zeta\left[-\frac{R_{2,1}\alpha_2}{R_1\alpha_1 R_2^2} + \frac{\alpha_{2,1}}{R_2 R_1\alpha_1} - 2\frac{\alpha_{2,1}}{R_1^2\alpha_1}\right]$$

$$= f_{27} + \zeta g_{27}$$

28. $$\frac{h_{2,3}h_{1,2}}{h_2^2} \cong -\frac{\alpha_{1,2}}{R_2\alpha_2} + \zeta\left[-\frac{R_{1,2}\alpha_1}{R_2\alpha_2 R_1^2} + \frac{\alpha_{1,2}}{R_1 R_2\alpha_2} - 2\frac{\alpha_{1,2}}{R_2^2\alpha_2}\right]$$

$$= f_{28} + \zeta g_{28}$$

29. $$\frac{h_{1,2}}{h_1 h_2} \cong \frac{\alpha_{1,2}}{\alpha_1\alpha_2} + \zeta\left[\frac{\alpha_{1,2}}{\alpha_1\alpha_2 R_2} + \frac{R_{1,2}}{\alpha_2 R_1^2}\right] = f_{29} + \zeta g_{29}$$

30. $$\frac{h_{1,2}^2}{h_1^2 h_2} \cong \frac{\alpha_{1,2}^2}{\alpha_2\alpha_1^2} + \zeta\left[\frac{2\alpha_{1,2}R_{1,2}}{\alpha_1\alpha_2 R_1^2} + \frac{\alpha_{1,2}^2}{\alpha_2\alpha_1^2 R_2}\right] = f_{30} + \zeta g_{30}$$

31. $$\frac{h_{2,1}^2}{h_2^2 h_1} \cong \frac{\alpha_{2,1}^2}{\alpha_1\alpha_2^2} + \zeta\left[\frac{2\alpha_{1,2}R_{1,2}}{\alpha_2^2 R_1^2} - \frac{\alpha_{1,2}^2}{\alpha_1\alpha_2^2 R_1} + 2\frac{\alpha_{1,2}^2}{\alpha_1\alpha_2^2 R_2}\right] = f_{31} + \zeta g_{31}$$

32. $$\frac{h_{1,3}^2}{h_1} \cong \frac{\alpha_1}{R_1^2} + \zeta\frac{\alpha_1}{R_1^3} = f_{32} + \zeta g_{32}$$

33. $\dfrac{h_{1,2}}{h_1^2} \cong \dfrac{\alpha_{1,2}}{\alpha_1^2} + \zeta\left(\dfrac{R_{1,2}}{\alpha_1 R_1^2} + \dfrac{\alpha_{1,2}}{\alpha_1^2 R_1}\right) = f_{33} + \zeta g_{33}$

34. $\dfrac{h_{1,3}}{h_1^2} \cong \dfrac{-1}{\alpha_1 R_1} - \zeta\dfrac{2}{\alpha_1 R_1^2} = f_{34} + \zeta g_{34}$

35. $\dfrac{h_{1,2}h_{1,3}}{h_1^2 h_2} \cong -\dfrac{\alpha_{1,2}}{\alpha_1\alpha_2 R_1} - \zeta\left(\dfrac{\alpha_{1,2}}{\alpha_1\alpha_2 R_1^2} + \dfrac{R_{1,2}}{\alpha_2 R_1^3} + \dfrac{\alpha_{1,2}}{\alpha_1\alpha_2 R_1 R_2}\right)$

$\qquad = f_{35} + \zeta g_{35}$

36. $\dfrac{h_{2,1}}{h_1 h_2} \cong \dfrac{\alpha_{2,1}}{\alpha_1\alpha_2} + \zeta\left(\dfrac{\alpha_{2,1}}{\alpha_1\alpha_2 R_1} + \dfrac{R_{2,1}}{\alpha_1 R_2^2}\right) = f_{36} + \zeta g_{36}$

37. $\dfrac{h_{2,1}^2}{h_1 h_2^2} \cong \dfrac{\alpha_{2,1}^2}{\alpha_2^2\alpha_1} + \zeta\left(\dfrac{2\alpha_{2,1}R_{2,1}}{\alpha_1\alpha_2 R_2^2} + \dfrac{\alpha_{2,1}^2}{\alpha_2^2\alpha_1 R_1}\right) = f_{37} + \zeta g_{37}$

38. $\dfrac{h_{2,1}^2}{h_2 h_1^2} \cong \dfrac{\alpha_{2,1}^2}{\alpha_1^2\alpha_2} + \zeta\left(\dfrac{2\alpha_{2,1}R_{2,1}}{\alpha_1^2 R_2^2} + 2\dfrac{\alpha_{2,1}^2}{\alpha_1^2\alpha_2 R_1} - \dfrac{\alpha_{2,1}^2}{\alpha_1^2 R_2^2\alpha_2}\right)$

$\qquad = f_{38} + \zeta g_{38}$

39. $\dfrac{h_{2,3}^2}{h_2} \cong \dfrac{\alpha_2}{R_2^2} + \zeta\dfrac{\alpha_2}{R_2^3} = f_{39} + \zeta g_{39}$

40. $\dfrac{h_{2,1}}{h_2^2} \cong \dfrac{\alpha_{2,1}}{\alpha_2^2} + \zeta\left(\dfrac{R_{2,1}}{\alpha_2 R_2^2} + \dfrac{\alpha_{2,1}}{\alpha_2^2 R_2}\right) = f_{40} + \zeta g_{40}$

41. $\dfrac{h_{2,3}h_{2,1}}{h_1 h_2^2} \cong \dfrac{-\alpha_{2,1}}{R_2\alpha_1\alpha_2} + \zeta\left(-\dfrac{R_{2,1}}{\alpha_1 R_2^3} - \dfrac{\alpha_{2,1}}{\alpha_1\alpha_2 R_2^2} - \dfrac{\alpha_{2,1}}{R_1 R_2\alpha_1\alpha_2}\right)$

$\qquad = f_{41} + \zeta g_{41}$

42. $\dfrac{h_{2,3}}{h_2^2} \cong -\dfrac{1}{\alpha_2 R_2} - \zeta\dfrac{2}{\alpha_2 R_2^2} = f_{42} + \zeta g_{42}$

43. $\dfrac{h_{1,2}}{h_2^2} \cong \dfrac{\alpha_{1,2}}{\alpha_2^2} + \zeta \left(\dfrac{\alpha_1 R_{1,2}}{R_1^2 \alpha_2^2} - \dfrac{\alpha_{1,2}}{R_1 \alpha_2^2} + \dfrac{2\alpha_{1,2}}{\alpha_2^2 R_2} \right) = f_{43} + \zeta g_{43}$

44. $\dfrac{h_{2,1}^-}{h_1^2} \cong \dfrac{\alpha_{2,1}}{\alpha_1^2} + \zeta \left(\dfrac{\alpha_2 R_{2,1}}{R_2^2 \alpha_1^2} - \dfrac{\alpha_{2,1}}{R_2 \alpha_1^2} + \dfrac{2\alpha_{2,1}}{\alpha_1^2 R_1} \right) = f_{44} + \zeta g_{44}$

45. $\dfrac{h_{1,3}}{h_1 h_2} \cong \dfrac{-1}{R_1 \alpha_2} + \zeta \left(\dfrac{-1}{R_1 R_2 \alpha_2} - \dfrac{1}{R_1^2 \alpha_2} \right) = f_{45} + \zeta g_{45}$

46. $\dfrac{h_{2,3}}{h_1 h_2} \cong \dfrac{-1}{R_2 \alpha_1} + \zeta \left(\dfrac{-1}{R_1 R_2 \alpha_1} - \dfrac{1}{R_2^2 \alpha_1} \right) = f_{46} + \zeta g_{46}$

47. $\dfrac{h_{2,1} h_{1,2}}{h_1^2 h_2} \cong \dfrac{\alpha_{1,2} \alpha_{2,1}}{\alpha_2 \alpha_1^2} + \zeta \left(\dfrac{R_{1,2} \alpha_{2,1}}{\alpha_1 \alpha_2 R_1^2} + \dfrac{\alpha_{1,2} \alpha_{2,1}}{\alpha_2 \alpha_1^2 R_1} + \right.$

$\left. + \dfrac{R_{2,1} \alpha_{1,2}}{R_2^2 \alpha_1^2} \right) = f_{47} + \zeta g_{47}$

48. $\dfrac{h_{1,2} h_{2,1}}{h_2^2 h_1} \cong \dfrac{\alpha_{1,2} \alpha_{2,1}}{\alpha_1 \alpha_2^2} + \zeta \left(\dfrac{R_{2,1} \alpha_{1,2}}{\alpha_2 \alpha_1 R_2^2} + \dfrac{\alpha_{2,1} \alpha_{1,2}}{\alpha_1 \alpha_2^2 R_2} + \right.$

$\left. + \dfrac{R_{1,2} \alpha_{2,1}}{R_1^2 \alpha_2^2} \right) = f_{48} + \zeta g_{48}$

49. $\dfrac{h_{1,3} h_{2,1}}{h_1^2 h_2} \cong \dfrac{-\alpha_{2,1}}{R_1 \alpha_1 \alpha_2} + \zeta \left(\dfrac{-R_{2,1}}{R_1 \alpha_1 R_2^2} - \dfrac{2\alpha_{2,1}}{R_1^2 \alpha_1 \alpha_2} \right) = f_{49} + \zeta g_{49}$

50. $\dfrac{h_{2,3} h_{1,2}}{h_2^2 h_1} \cong \dfrac{-\alpha_{1,2}}{R_2 \alpha_2 \alpha_1} + \zeta \left(\dfrac{-R_{1,2}}{R_2 R_1^2 \alpha_2} - \dfrac{2\alpha_{1,2}}{R_2^2 \alpha_1 \alpha_2} \right) = f_{50} + \zeta g_{50}$

51. $\dfrac{h_{1,3} h_{2,3}}{h_2} \cong \dfrac{\alpha_1}{R_1 R_2} + \zeta \dfrac{\alpha_1}{R_1 R_2^2} = f_{51} + \zeta g_{51}$

52. $\dfrac{h_{1,3}h_{2,3}}{h_1} \cong \dfrac{\alpha_2}{R_1 R_2} + \zeta \dfrac{\alpha_2}{R_2 R_1^2} = f_{52} + \zeta g_{52}$

53. $\dfrac{h_{1,2}^2}{h_1^2 h_2^2} \cong \dfrac{\alpha_{1,2}^2}{\alpha_1^2 \alpha_2^2} + \zeta \left(\dfrac{\alpha_{1,2}^2}{\alpha_1^2 \alpha_2^2 R_2} + \dfrac{R_{1,2}\alpha_{1,2}}{\alpha_2^2 R_1^2 \alpha_1} \right) = f_{53} + \zeta g_{53}$

54. $\dfrac{h_{1,2}}{h_1^2 h_2} \cong \dfrac{\alpha_{1,2}}{\alpha_1^2 \alpha_2} + \zeta \left(\dfrac{\alpha_{1,2}}{\alpha_1^2 \alpha_2 R_2} + \dfrac{R_{1,2}}{\alpha_2 R_1^2 \alpha_1} + \dfrac{\alpha_{1,2}}{\alpha_1^2 \alpha_2 R_1} \right) = f_{54} + \zeta g_{54}$

55. $\dfrac{h_{2,1}^2}{h_1^2 h_2^2} \cong \dfrac{\alpha_{2,1}^2}{\alpha_1^2 \alpha_2^2} + 2\zeta \left(\dfrac{\alpha_{2,1}^2}{\alpha_1^2 \alpha_2^2 R_1} + \dfrac{R_{2,1}\alpha_{2,1}}{\alpha_1^2 R_2^2 \alpha_2} \right) = f_{55} + \zeta g_{55}$

56. $\dfrac{h_{2,1}}{h_2^2 h_1} \cong \dfrac{\alpha_{2,1}}{\alpha_2^2 \alpha_1} + \zeta \left(\dfrac{\alpha_{2,1}}{\alpha_1 \alpha_2^2 R_1} + \dfrac{R_{2,1}}{\alpha_1 R_2^2 \alpha_2} + \dfrac{\alpha_{2,1}}{\alpha_2^2 \alpha_1 R_2} \right) = f_{56} + \zeta g_{56}$

57. $\dfrac{h_{1,2}}{h_1 h_2^2} \cong \dfrac{\alpha_{1,2}}{\alpha_1 \alpha_2^2} + \zeta \left(2\dfrac{\alpha_{1,2}}{\alpha_1 \alpha_2^2 R_2} + \dfrac{R_{1,2}}{\alpha_2^2 R_1^2} \right) = f_{57} + \zeta g_{57}$

58. $\dfrac{h_{2,1}}{h_2 h_1^2} \cong \dfrac{\alpha_{2,1}}{\alpha_2 \alpha_1^2} + \zeta \left(2\dfrac{\alpha_{2,1}}{\alpha_2 \alpha_1^2 R_1} + \dfrac{R_{2,1}}{\alpha_1^2 R_2^2} \right) = f_{58} + \zeta g_{58}$

59. $\dfrac{h_{2,1}h_{1,2}}{h_1^2 \; h_2^2} \cong \dfrac{\alpha_{2,1}\alpha_{1,2}}{\alpha_1^2 \; \alpha_2^2} + \zeta \left(\dfrac{R_{1,2}\alpha_{2,1}}{\alpha_2^2 \alpha_1 R_1^2} + \dfrac{\alpha_{1,2}\alpha_{2,1}}{\alpha_1^2 \; \alpha_2^2} \left(\dfrac{1}{R_1} + \dfrac{1}{R_2} \right) \right.$

$\left. + \dfrac{R_{2,1}\alpha_{1,2}}{R_2^2 \alpha_1^2 \alpha_2} \right) = f_{59} + \zeta g_{59}$

60. $\dfrac{h_{1,3}h_{2,3}}{h_1 h_2} \cong \dfrac{1}{R_1 R_2} + \zeta \dfrac{1}{R_1 R_2} \left(\dfrac{1}{R_1} + \dfrac{1}{R_2} \right) = f_{60} + \zeta g_{60}$

III. ε_i° and $\varkappa_{ip}$ from Eqn (3.49).

$$\varepsilon_1^\circ = u_{,1}/\alpha_1 + f_1 v/\alpha_2 + f_2 w + u_{,1}^2/2\alpha_1^2 + f_3 w_{,1}^2/2 + f_3 v_{,1}^2/2$$

$$+ f_4 v^2/2\alpha_2^2 + f_5 u^2/2\alpha_1^2 + f_6 w^2/2 + f_7 u^2/2\alpha_1^2 + f_8 wv/\alpha_2$$

$$+ f_1(u_{,1}v - uv_{,1})/\alpha_1\alpha_2 + f_2(u_{,1}w - uw_{,1})/\alpha_1$$

$$\varepsilon_2^\circ = v_{,2}/\alpha_2 + f_9 w + f_{10} u/\alpha_1 + v_{,2}^2/2\alpha_2^2 + f_{11} w_{,2}^2/2 + f_{11} u_{,2}^2/2$$

$$+ f_{12} u^2/2 + f_{13} v^2/2\alpha_2^2 + f_{14} w^2/2 + f_{15} v^2/2\alpha_2^2 + f_{16} uw/\alpha_1$$

$$+ f_{10}(uv_{,2} - vu_{,2})/\alpha_1\alpha_2 + f_9(v_{,2}w - vw_{,2})/\alpha_2$$

$$\varepsilon_6^\circ = f_{17} u_{,2} + f_{18} v_{,1} - f_{19} v/\alpha_2 - f_{20} u/\alpha_1 + u_{,1} u_{,2} f_{17}/\alpha_1$$

$$+ v_{,2} v_{,1} f_{18}/\alpha_2 + f_{21} w_{,1} w_{,2} + f_{20}(vu_{,2} - uv_{,2})/\alpha_1\alpha_2$$

$$+ f_{19}(uv_{,1} - u_{,1}v)/\alpha_1\alpha_2 + f_{22}(u_{,2}w - uw_{,2})/\alpha_1 - f_{24} v^2/\alpha_2^2$$

$$+ f_{23}(v_{,1}w - vw_{,1})/\alpha_2 - f_{25} u^2/\alpha_1^2$$

$$+ f_{26} uv/\alpha_1\alpha_2 - f_{28} uw/\alpha_1 - f_{27} wv/\alpha_2$$

$$\varkappa_{11} = g_1 v/\alpha_2 + g_2 w + g_3 w_{,1}^2/2 + v_{,1}^2(g_3 - 2f_3/R_2)/2 + g_4 v^2/2\alpha_2^2$$

$$+ g_5 u^2/2\alpha_1^2 + g_6 w^2/2 + g_1(u_{,1}v - uv_{,1})/\alpha_1\alpha_2 + g_8 wv/\alpha_2$$

$$+ g_2(u_{,1}w - uw_{,1})/\alpha_1 + f_{18} l_{11} + f_{29}\psi_2 + f_{18} l_{11} u_{,1}/\alpha_1$$

$$+ f_3 l_{21} v_{,1} + f_{30} v\psi_2/\alpha_2 + f_{31} u\psi_1/\alpha_1 + f_{32} u\psi_1/\alpha_1 + f_{35}\psi_2 w$$

$$+ f_{33}(l_{11}v - \psi_1 v_{,1})/\alpha_2 + f_{29}(\psi_2 u_{,1} - l_{21}u)/\alpha_1$$

$$+ f_{34}(wl_{11} - \psi_1 w_{,1})$$

323

$$\omega_{21} = g_9 w + g_{10} u/\alpha_1 + u_{,2}^2 (g_{11} - 2f_{11}/R_1)/2 + g_{11} w_{,2}^2/2 +$$

$$+ g_{12} u^2/2\alpha_1^2 + g_{13} v^2/2\alpha_2^2 + g_{14} w^2/2 + g_{10}(uv_{,2} - vu_{,2})/\alpha_1\alpha_2$$

$$+ g_9(v_{,2} w - vw_{,2})/\alpha_2 + g_{16} uw/\alpha_1 + f_{17} l_{22} + f_{36}\psi_1$$

$$+ f_{17} v_{,2} l_{22}/\alpha_2 + l_{12} u_{,2} f_{11} + f_{37} u\psi_1/\alpha_1 + f_{38} v\psi_2/\alpha_2$$

$$+ f_{39} v\psi_2/\alpha_2 + f_{40}(l_{22} u - \psi_2 u_{,2})/\alpha_1$$

$$+ f_{36}(\psi_1 v_{,2} - l_{12} v)/\alpha_2 + f_{42}(l_{22} w - \psi_2 w_{,2}) + f_{41}\psi_1 w$$

$$\varkappa_{61} = u_{,2}(g_{17} - f_{17}/R_1) + v_{,1}(g_{18} - f_{18}/R_2) - g_{19} v/\alpha_2$$

$$- g_{20} u/\alpha_1 + u_{,1} u_{,2}(g_{17} - f_{17}/R_1)/\alpha_1 + g_{21} w_{,1} w_{,2}$$

$$+ v_{,1} v_{,2}(g_{18} - f_{18}/R_2)/\alpha_2 + g_{20}(vu_{,2} - uv_{,2})/\alpha_1\alpha_2$$

$$+ g_{19}(uv_{,1} - u_{,1} v)/\alpha_1\alpha_2 + g_{22}(u_{,2} w - uw_{,2})/\alpha_1$$

$$+ g_{23}(v_{,1} w - vw_{,1})/\alpha_2 - g_{24} v^2/\alpha_2^2 - g_{25} u^2/\alpha_1^2 + g_{26} uv/\alpha_1\alpha_2$$

$$- g_{27} wv/\alpha_2 - g_{28} uw/\alpha_2 + f_{17} l_{12} + f_{18} l_{21} - f_{36}\psi_{21} - f_{29}\psi_1$$

$$+ f_{17} l_{12} u_{,1}/\alpha_1 + f_{17} l_{11} u_{,2}/\alpha_1 + f_{18} l_{22} v_{,1}/\alpha_2$$

$$+ f_{18} l_{21} v_{,2}/\alpha_2 + f_{29}(vl_{12} - \psi_1 v_{,2})/\alpha_2 + f_{52} v\psi_1/\alpha_2$$

$$+ f_{43}(\psi_2 u_{,2} - l_{22} u)/\alpha_1 + f_{36}(l_{21} u - \psi_2 u_{,1})/\alpha_1 + f_{51} u\psi_2/\alpha_1$$

$$+ f_{44}(\psi_1 v_{,1} - l_{11} v)/\alpha_2 + f_{45}(wl_{12} - w_{,2}\psi_1) - f_{50}\psi_1 w$$

$$+ f_{46}(wl_{21} - w_{,1}\psi_2) - 2f_{47}\psi_2 v/\alpha_2 - 2f_{48} u\psi_1/\alpha_1 - f_{49}\psi_2 w$$

$$\varkappa_{12} = v_{,1}^2(-2g_3/R_2 + f_3/R_2^2)/2 + l_{21}v_{,1}(g_3 - f_3/R_2) + g_{18}l_{11}$$

$$+ g_{29}\psi_2 + g_{18}l_{11}u_{,1}/\alpha_1 + g_{30}v\psi_2/\alpha_1 + g_{32}u\psi_1/\alpha_1 + f_6\psi_1^2/2$$

$$+ \bar{g}_{33}(l_{11}v - \psi_1 v_{,1})/\alpha_2 + g_{29}(\psi_2 u_{,1} - l_{21}u)/\alpha_1$$

$$+ g_{34}(wl_{11} - \psi_1 w_{,1}) + g_{35}\psi_2 w + f_3(l_{11}^2 + l_{21}^2)/2$$

$$+ f_{53}(\psi_1^2 + \psi_2^2)/2 + f_{54}(\psi_2 l_{11} - \psi_1 l_{21}) + g_{31}u\psi_1/\alpha_1$$

$$\varkappa_{22} = u_{,2}^2(2g_{11}/R_1 + f_{11}/R_1^2)/2 + l_{12}u_{,2}(g_{11} - f_{11}/R_1)$$

$$+ g_{17}l_{22} + g_{36}\psi_1 + g_{17}l_{22}v_{,2}/\alpha_2 + g_{37}u\psi_1/\alpha_1 + g_{38}v\psi_2/\alpha_2$$

$$+ g_{39}v\psi_2/\alpha_2 + g_{40}(l_{22}u - \psi_2 u_{,2})/\alpha_1 + g_{36}(\psi_1 v_{,2} - l_{12}v)/\alpha_2$$

$$+ g_{42}(l_{22}w - \psi_2 w_{,2}) + g_{41}\psi_1 w + f_{11}(l_{22}^2 + l_{12}^2)/2$$

$$+ f_{55}(\psi_1^2 + \psi_2^2)/2 + f_{56}(\psi_1 l_{22} - \psi_2 l_{12}) + f_{14}\psi_2^2/2$$

$$\varkappa_{62} = -u_{,2}g_{17}/R_1 - v_{,1}g_{18}/R_2 - u_{,1}u_{,2}g_{17}/\alpha_1 R_1 + g_{17}l_{12}$$

$$- v_{,2}v_{,1}g_{18}/\alpha_2 R_2 + g_{18}l_{21} + g_{17}(l_{12}u_{,1}+l_{11}u_{,2})/\alpha_1$$

$$- g_{36}\psi_2 - g_{29}\psi_1 + g_{18}(l_{22}v_{,1}+l_{21}v_{,2})/\alpha_2 + f_{60}\psi_1\psi_2$$

$$+ g_{29}(vl_{12}-\psi_1 v_{,2})/\alpha_2 + g_{43}(\psi_2 u_{,2} - l_{22}u)/\alpha_1 - f_{59}\psi_1^2$$

$$+ g_{36}(l_{21}u - \psi_2 u_{,1})/\alpha_1 + g_{44}(\psi_1 v_{,1} - l_{11}v)/\alpha_2 - f_{59}\psi_2^2$$

$$+ g_{45}(wl_{12} - w_{,2}\psi_1) + g_{46}(wl_{21} - w_{,1}\psi_2) - 2g_{47}v\psi_2/\alpha_2$$

$$- 2g_{48}u\psi_1/\alpha_1 - g_{49}w\psi_2 - g_{50}w\psi_1 + g_{51}u\psi_2/\alpha_1 + g_{52}v\psi_1/\alpha_2$$

$$+ f_{21}(l_{11}l_{12} + l_{21}l_{22}) + f_{37}(l_{12}\psi_2 - l_{22}\psi_1)$$

$$+ f_{38}(l_{21}\psi_1 - l_{11}\psi_2)$$

$$\kappa_{13} = v_{,1}^2 g_3/2R_2^2 - 1_{21}v_{,1}g_3/R_2 + g_3(1_{11}^2+1_{21}^2)/2 + g_{53}(\psi_1^2+\psi_2^2)/2$$

$$+ g_{54}(\psi_2 1_{11} - \psi_1 1_{21}) + g_6\psi_1^2/2 + f_{18}m_{1,1} + f_{29}m_2 + f_{35}m_2w$$

$$+ f_{18}m_{1,1}u_{,1} + f_{30}m_2v/\alpha_2 + f_{31}um_1/\alpha_1 + f_{32}um_1/\alpha_1$$

$$+ f_{33}(m_{1,1}v - m_1v_{,1})/\alpha_2 + f_{29}(m_2u_{,1} - m_{2,1}u)/\alpha_1$$

$$+ f_{34}(m_{1,1}w - m_1w_{,1}) + f_3m_{2,1}v_{,1}$$

$$\kappa_{23} = u_{,2}^2 g_{11}/2R_1^2 - 1_{12}u_{,2}g_{11}/R_1 + g_{11}(1_{22}^2+1_{12}^2)/2 + f_{41}m_1w$$

$$+ g_{55}(\psi_1^2 + \psi_2^2)/2 + g_{56}(\psi_1 1_{22} - \psi_2 1_{12}) + g_{14}\psi_2^2/2 + f_{17}m_{2,2}$$

$$+ f_{36}m_1 + f_{17}v_{,2}m_{2,2}/\alpha_2 + f_{11}m_{1,2}u_{,2} + f_{37}um_1/\alpha_1$$

$$+ f_{38}vm_2/\alpha_2 + f_{39}m_2v/\alpha_2 + f_{40}(um_{2,2} - m_2u_{,2})/\alpha_1$$

$$+ f_{36}(v_{,2}m_1 - m_{1,2}v)/\alpha_2 + f_{42}(m_{2,2}w - m_2w_{,2})$$

$$\kappa_{63} = g_{21}(1_{11}1_{12} + 1_{21}1_{22}) + g_{57}(1_{12}\psi_2 - 1_{22}\psi_1) + f_{52}m_1v/\alpha_2$$

$$+ g_{58}(1_{21}\psi_1 - 1_{11}\psi_2) - g_{59}\psi_2^2 - g_{59}\psi_1^2 + g_{60}\psi_1\psi_2 + f_{17}m_{1,2}$$

$$+ f_{18}m_{2,1} - f_{36}m_2 - f_{29}m_1 + f_{17}m_{1,1}u_{,2}/\alpha_1 + f_{17}m_{1,2}u_{,1}/\alpha_1$$

$$+ f_{18}v_{,1}m_{2,2}/\alpha_2 + f_{18}m_{2,1}v_{,2}/\alpha_2 + f_{45}(m_{1,2}w - m_1w_{,2})$$

$$+ f_{46}(m_{2,1}w - m_2w_{,1}) - 2f_{47}vm_2/\alpha_2 - 2f_{48}um_1/\alpha_1$$

$$+ f_{51}um_2/\alpha_1 + f_{29}(vm_{1,2} - m_1v_{,2})/\alpha_2 + f_{43}(m_2u_{,2}-m_{2,2}u)/\alpha_1$$

$$+ f_{36}(m_{2,1}u - m_2u_{,1})/\alpha_1 + f_{44}(m_1v_{,1} - m_{1,1}v)/\alpha_2 - f_{49}m_2w$$

$$- f_{50}m_1w$$

$$x_{14} = m_{2,1}v_{,1}(g_3 - g_3/R_2) + g_{18}m_{1,1} + g_{29}m_2 + g_{18}u_{,1}m_{1,1}/\alpha_1$$

$$+ g_{30}m_2 v/\alpha_2 + g_{31}um_1/\alpha_1 + g_{32}um_1/\alpha_1 + f_6\psi_1 m_1$$

$$+ g_{33}(m_{1,1}v - m_1 v_{,1})/\alpha_2 + g_{29}(m_2 u_{,1} - m_{2,1}u)/\alpha_1 + g_{35}m_2 w$$

$$+ g_{34}(m_{1,1}w - m_1 w_{,1}) + f_3 l_{11}m_{1,1} + f_3 l_{21}m_{2,1}$$

$$+ f_{54}(\psi_2 m_{1,1} + m_2 l_{11} - m_{2,1}\psi_1 - m_1 l_{21}) + f_{53}(\psi_2 m_2 + \psi_1 m_1)$$

$$x_{24} = m_{1,2}u_{,2}(g_{11} - f_{11}/R_1) + g_{17}m_{2,2} + g_{36}m_1 + g_{17}m_{2,2}v_{,2}/\alpha_2$$

$$+ g_{37}um_1/\alpha_1 + g_{38}vm_2/\alpha_2 + g_{39}m_2 v/\alpha_2 + f_{14}\psi_2 m_2$$

$$+ g_{40}(um_{2,2} - m_2 u_{,2})/\alpha_1 + g_{36}(v_{,2}m_1 - m_{1,2}v)/\alpha_2$$

$$+ g_{42}(m_{2,2}w - m_2 w_{,2}) + g_{41}m_1 w + f_{11}(l_{22}m_{2,2} + l_{12}m_{1,2})$$

$$+ f_{55}(\psi_1 m_1 + \psi_2 m_2) + f_{56}(\psi_1 m_{2,2} + m_1 l_{22} - m_{1,2}\psi_2 - m_2 l_{12})$$

$$x_{64} = g_{17}m_{1,2} + g_{18}m_{2,1} - g_{36}m_2 - g_{29}m_1 + g_{17}m_{1,2}u_{,1}/\alpha_1$$

$$+ g_{18}v_{,1}m_{2,2}/\alpha_2 + g_{18}m_{2,1}v_{,2}/\alpha_2 + g_{43}(m_{1,2}w - m_1 w_{,2})$$

$$+ g_{46}(m_{2,1}w - m_2 w_{,1}) - 2g_{47}vm_2/\alpha_2 - 2g_{48}um_1/\alpha_1$$

$$+ g_{29}(vm_{1,2} - m_1 v_{,2})/\alpha_2 + g_{43}(m_2 u_{,2} - m_{2,2}u)/\alpha_1 - g_{49}m_2 w$$

$$+ g_{36}(m_{2,1}u - m_2 u_{,1})/\alpha_1 + g_{44}(m_1 v_{,1} - m_{1,1}v)/\alpha_2 - g_{50}m_1 w$$

$$+ g_{51}um_2/\alpha_1 + g_{52}m_1 v/\alpha_2 + f_{60}(\psi_1 m_2 + \psi_2 m_1)$$

$$+ f_{21}(l_{11}m_{1,2} + m_{1,1}l_{12} + l_{21}m_{2,2} + m_{2,1}l_{22}) - 2f_{59}(\psi_2 m_2 + \psi_1 m_1)$$

$$+ f_{57}(\psi_2 m_{1,2} + l_{12}m_2 - m_{2,2}\psi_1 - l_{22}m_1) + g_{17}m_{1,1}u_{,2}/\alpha_1$$

$$+ f_{59}(\psi_1 m_{2,1} + l_{21}m_1 - m_{1,1}\psi_2 - l_{11}m_2)$$

$$\varkappa_{15} = -m_{2,1}v_{\cdot,1}g_3/R_2 + g_3(l_{11}m_{1,1}+l_{21}m_{2,1}) + g_6\psi_1m_1$$

$$+ g_{53}(\psi_2m_2 + \psi_1m_1) + g_{54}(\psi_2m_{1,1}+m_2l_{11}-m_{2,1}\psi_1-m_1l_{21})$$

$$\varkappa_{25} = -m_{1,2}u_{\cdot,2}g_{11}R_1 + g_{11}(l_{22}m_{2,2}+l_{12}m_{1,2}) + g_{14}\psi_2m_2$$

$$+ g_{55}(\psi_1m_1 + \psi_2m_2) + g_{56}(\psi_1m_{2,2}+m_1l_{22}-m_{1,2}\psi_2-m_2l_{12})$$

$$\varkappa_{65} = g_{21}(l_{11}m_{1,2} + m_{1,1}l_{12} + l_{21}m_{2,2} + m_{2,1}l_{22})$$

$$+ g_{60}(\psi_1m_2 + \psi_2m_1) - 2g_{59}(\psi_2m_2 + \psi_1m_1)$$

$$+ g_{57}(\psi_2m_{1,2} + l_{12}m_2 - m_{2,2}\psi_1 - l_{22}m_1)$$

$$+ g_{58}(\psi_1m_{2,1} + l_{21}m_1 - m_{1,1}\psi_2 - l_{11}m_2)$$

$$\varkappa_{16} = f_3(m_{1,1}^2 + m_{2,1}^2)/2 + f_{53}(m_2^2 + m_1^2)/2 + f_6m_1^2/2$$

$$+ f_{54}(m_{1,1}m_2 - m_1m_{2,1})$$

$$\varkappa_{26} = f_{11}(m_{2,2}^2 + m_{1,2}^2)/2 + f_{55}(m_1^2 + m_2^2)/2 + f_{14}m_2^2/2$$

$$+ f_{56}(m_{2,2}m_1 - m_2m_{1,2})$$

$$\varkappa_{66} = f_{21}(m_{1,1}m_{1,2} + m_{2,1}m_{2,2}) + f_{57}(m_2m_{1,2} - m_1m_{2,2})$$

$$+ f_{58}(m_1m_{2,1} - m_2m_{1,1}) - f_{59}(m_1^2 + m_2^2) + f_{60}m_1m_2$$

$$\varkappa_{17} = g_3(m_{1,1}^2 + m_{2,1}^2)/2 + g_{53}(m_2^2 + m_1^2)/2 + g_6m_1^2/2$$

$$+ g_{54}(m_{1,1}m_2 - m_1m_{2,1})$$

$$\varkappa_{27} = g_{11}(m_{2,2}^2 + m_{1,2}^2)/2 + g_{55}(m_1^2 + m_2^2)/2 + g_{14}m_2^2/2$$

$$+ g_{56}(m_{2,2}m_1 - m_2m_{1,2})$$

$$\varkappa_{67} = g_{21}(m_{1,1}m_{1,2} + m_{2,1}m_{2,2}) + g_{57}(m_2m_{1,2} - m_1m_{2,2})$$

$$+ g_{58}(m_1m_{2,1} - m_2m_{1,1}) - g_{59}(m_1^2 + m_2^2) + g_{60}m_1m_2$$

Appendix B: von Karman Plate and Donnell Shell Strain Displacement Relations

I. von Karman Flat Plate

The von Karman plate strain displacement relations are shown in Eqn (B.1).

$$\varepsilon_1 = u_{1,1} + \frac{1}{2} w^2_{,1}$$

$$\varepsilon_2 = u_{2,2} + \frac{1}{2} w^2_{,2} \tag{B.1}$$

$$\varepsilon_6 = u_{1,2} + u_{2,1} + w_{,1}w_{,2}$$

where u_1, u_2 are given by the kinematics of Eqn (3.44) with $R_\gamma = 0$ and $\alpha_\gamma = 1$. Using Eqn (3.44) in Eqn (B.1) then gives,

$$\varepsilon_1 = u_{,1} + \zeta\psi_{1,1} + \zeta^3 k(w_{,11} + \psi_{1,1}) + \frac{1}{2} w^2_{,1}$$

$$\varepsilon_2 = v_{,2} + \zeta\psi_{2,2} + \zeta^3 k(w_{,22} + \psi_{2,2}) + \frac{1}{2} w^2_{,2} \tag{B.2}$$

$$\varepsilon_6 = u_{,2} + v_{,1} + \zeta(\psi_{1,2} + \psi_{2,1}) + \zeta^3 k(2w_{,12} + \psi_{1,2} + \psi_{2,1})$$
$$+ w_{,1}w_{,2}$$

where $k = -4/3h^2$

From Eqn (B.2), the nonlinear terms are only in the transverse displacement, w, and are not functions of the transverse coordinate ζ. The strain energy terms are found via Eqn (3.62) where the strain components of Eqn (3.49) are given from Eqn (B.2) by Eqn (B.3-B.5).

$$\varepsilon_1 = \varepsilon_1^\circ + \zeta^P \varkappa_{1p}$$

where,

$$\varepsilon_1^\circ = u_{,1} + \frac{1}{2} w_{,1}^2 \qquad (B.3)$$

$$\varkappa_{11} = \psi_{1,1}$$

$$\varkappa_{13} = k(w_{,11} + \psi_{1,1})$$

$$\varkappa_{1p}(p=2,4,5,6,7) = 0$$

$$\varepsilon_2 = \varepsilon_2^\circ + \zeta^P \varkappa_{2p}$$

where,

$$\varepsilon_2^\circ = v_{,2} + \frac{1}{2} w_{,2}^2 \qquad (B.4)$$

$$\varkappa_{21} = \psi_{2,2}$$

$$\varkappa_{23} = k(w_{,22} + \psi_{2,2})$$

$$\varkappa_{2p}(p=2,4,5,6,7) = 0$$

$$\varepsilon_6 = \varepsilon_6^\circ + \zeta^P \varkappa_{6p}$$

where,

$$\varepsilon_6^\circ = u_{,2} + v_{,1} + w_{,1}w_{,2} \qquad (B.5)$$

$$\varkappa_{61} = \psi_{1,2} + \psi_{2,1}$$

$$\varkappa_{63} = k(2w_{,12} + \psi_{1,2} + \psi_{2,1})$$

$$\varkappa_{6p}(p=2,4,5,6,7) = 0$$

Referencing Eqn (3.62), energy expressions that are cubic or quartic in displacement result from Eqn (3.62a,b). The quartic terms result from Eqn (3.62a) and are A_{ij} energy terms only. The cubic terms result from Eqn (3.62b) and are B_{ij} and E_{ij} terms only. For symmetrically arranged laminates or isotropic constructions, $B_{ij}=E_{ij}=0$ for all i,j.

Therefore, since only the cubic and quartic displacement energy terms result in nonlinear terms in the equilibrium equations ($\delta\Pi_p=0$), the only nonlinear terms are A_{ij} terms.

II. Donnell Cylindrical Shell

The Donnell cylindrical shell strain displacement relations are shown in Eqn (B.6).

$$\varepsilon_1 = u_{1,1} + \frac{1}{2} w_{,1}^2$$

$$\varepsilon_2 = u_{2,2} - w/R + \frac{1}{2} w_{,2}^2$$

$$\varepsilon_6 = u_{1,2} + u_{2,1} + w_{,1}w_{,2}$$

(B.6)

where u_1 and u_2 are given by the kinematics of Eqn (3.44) with $R_1=0$, $R_2=R$, and $\alpha_\gamma=1$. Using Eqn (3.44) in Eqn (B.6) then gives,

$$\varepsilon_1 = u_{,1} + \zeta\psi_{1,1} + \zeta^3 k(w_{,11} + \psi_{1,1}) + \frac{1}{2} w_{,1}^2$$

$$\varepsilon_2 = v_{,2} - w/R + \zeta(-v_{,2}/R + \psi_{2,2})$$

$$+ \zeta^3 k(w_{,22} + \psi_{2,2}) + \frac{1}{2} w_{,2}^2$$

(B.7)

$$\varepsilon_6 = u_{,2} + v_{,1} + \zeta(\psi_{1,2} + \psi_{2,1} - v_{,1}/R)$$

$$+ \zeta^3 k(2w_{,12} + \psi_{1,2} + \psi_{2,1}) + w_{,1}w_{,2}$$

where $k=-4/3h^2$

The strain energy terms are found via Eqn (3.62) where the strain components of Eqn (3.49) are given from Eqn (B.7) by Eqns (B.8-B.10).

$$\varepsilon_1 = \varepsilon_1^\circ + \zeta^P \varkappa_{1p}$$

where,

$$\varepsilon_1^\circ = u,_1 + \frac{1}{2} w,_1^2$$

$$\varkappa_{11} = \psi_{1,1}$$

$$\varkappa_{13} = k(w,_{11} + \psi_{1,1})$$

$$\varkappa_{1p}(p=2,4,5,6,7) = 0$$

(B.8)

$$\varepsilon_2 = \varepsilon_2^\circ + \zeta^P \varkappa_{2p}$$

where,

$$\varepsilon_2^\circ = v,_2 - w/R + \frac{1}{2} w,_2^2$$

$$\varkappa_{21} = \psi_{2,2} - v,_2/R$$

$$\varkappa_{23} = k(w,_{22} + \psi_{2,2})$$

$$\varkappa_{2p}(p=2,4,5,6,7) = 0$$

(B.9)

$$\varepsilon_6 = \varepsilon_6^\circ + \zeta^P \varkappa_{6p}$$

where,

$$\varepsilon_6^\circ = u,_2 + v,_1 + w,_1 w,_2$$

$$\varkappa_{61} = \psi_{1,2} + \psi_{2,1} - v,_1/R$$

$$\varkappa_{63} = k(2w,_{12} + \psi_{1,2} + \psi_{2,1})$$

$$\varkappa_{6p}(p=2,4,5,6,7) = 0$$

(B.10)

For the same reasons as given for the von Karman plate expressions, only A_{ij} nonlinear terms will result in the equilibrium equations for isotropic or symmetrically arranged constructions. For both cases above, the transverse shear strain displacement relations are given by Eqn (3.56). These terms will result in linear displacement terms in the equilibrium equations.

Appendix C: Finite Element Strain Definition Arrays

The following are the nonzero entries in the 15 $_jL_I$, 24 $_jH_I$, and 4 $_jS_I$ of Eqn (4.7) and (4.16) for cylindrical coordinates. Only the nonzero terms of the diagonal and upper diagonal are shown for the symmetric $_jH_I$.

I. $_jL_I$

$_0L_1(2) = 1$

$_0L_2(6) = 1$, $_0L_2(7) = -1/R$

$_0L_6(3) = {_0L_6}(5) = 1$

$_1L_1(14) = 1$

$_1L_2(7) = -1/R^2$, $_1L_2(18) = 1$

$_1L_6(3) = -{_1L_6}(5) = -1/R$, $_1L_6(15) = {_1L_6}(17) = 1$

$_2L_2(18) = 1/R$

$_2L_6(15) = 1/R$

$_3L_1(10) = {_3L_1}(18) = k$ (C.1)

$_3L_2(11) = {_3L_2}(18) = k$

$_3L_6(12) = 2k$, $_3L_6(15) = {_3L_6}(17) = k$

$_4L_2(11) = {_4L_2}(18) = k/R$

$_4L_6(12) = {_4L_6}(15) = k/R$

II. $_jH_I$

$_0H_1$: $(2,2) = (5,5) = (8,8) = 1$

$_0H_2$: $(3,3) = (6,6) = (9,9) = 1$

   $(4,4) = (7,7) = 1/R^2$ (C.2)

   $(6,7) = -(4,9) = 1/R$

333

$_0H_\sigma$: $(2,3) = (5,6) = (8,9) = 1$

$(5,7) = -(4,8) = -1/R$

$_1H_1$: $(5,5) = -2/R,\ (2,14) = (5,17) = 1$

$_1H_2$: $(3,3) = (9,9) = 2/R,\ (7,7) = 2/R^3$

$(6,7) = -(4,9) = -(4,16) = 1/R^2$

$(3,15) = (6,18) = 1$

$(9,16) = -(7,18) = 1/R$

$_1H_\sigma$: $(2,3) = -(5,6) = (4,8) = (8,9) = 1/R$

$(8,16) = -(7,17) = 1/R,\ (3,14) = (2,15) = 1$

$(5,18) = (6,17) = 1$

$_2H_1$: $(5,5) = 1/R^2,\ (5,17) = -1/R,\ (14,14) = (17,17) = 1$

$_2H_2$: $(15,15) = (18,18) = 1,\ (16,16) = 1/R^2,\ (3,15) = 2/R$

$(4,16) = 1/R^3,\ (7,18) = -(9,16) = -2/R^2$

$(6,18) = 1/R$

$_2H_\sigma$: $(2,15) = (3,14) = 1/R,\ (7,17) = -(8,16) = 1/R^2$

$(14,15) = (17,18) = 1$

$_3H_1$: $(2,10) = (2,14) = (5,12) = (5,17) = k$

$_3H_2$: $(3,12) = (3,15) = (6,11) = (6,18) = k$

$(4,9) = (4,16) = k/R^2,$

$(7,11) = (7,18) = -(9,16) = -k/R,\ (9,9) = 2k/R$

$(15,15) = (18,18) = 2/R,\ (16,16) = 2/R^3$

$_3H_\sigma$: $(2,12) = (2,15) = (3,10) = (3,14) = k$

$(5,11) = (5,18) = (6,12) = (6,17) = k$

$(7,12) = (7,17) = -(8,9) = -(8,16) = k/R$

$(14,15) = (17,18) = 1/R$

$_4H_1$: $(5,12) = (5,17) = -k/R,\ (10,14) = (12,17) = k$

$$(14,14) = (17,17) = 2k$$

$_4H_2$: $\quad (3,12) = (3,15) = 2k/R, \quad (4,9) = (4,16) = k/R^3$

$\quad\quad (6,11) = (6,18) = k/R,$

$\quad\quad (7,11) = (7,18) = -(16,16) = -2k/R^2$

$\quad\quad (9,9) = 4k/R^2, \quad (9,16) = 3k/R^2$

$\quad\quad (11,18) = (12,15) = k$

$\quad\quad (15,15) = (18,18) = 2k$

$_4H_6$: $\quad (2,12) = (2,15) = (3,10) = (3,14) = k/R$

$\quad\quad (8,9) = (8,16) = -(7,12) = -(7,17) = k/R^2$

$\quad\quad (10,15) = (11,17) = (12,14) = (12,18) = k$

$\quad\quad (14,15) = (17,18) = 2k$

$_5H_2$: $\quad (9,16) = 2k/R^3, \quad (11,18) = (12,15) = 2k/R$

$\quad\quad (15,15) = (18,18) = 4k/R, \quad (16,16) = 4k/R^3$

$_5H_6$: $\quad (10,15) = (11,17) = (12,14) = (12,18) = k/R$

$\quad\quad (14,15) = (17,18) = 2k/R$

$_6H_1$: $\quad (10,10) = (10,14) = (12,12) = (12,17) = k^2$

$\quad\quad (14,14) = (17,17) = k^2$

$_6H_2$: $\quad (9,9) = (9,16) = (16,16) = k^2/R^2$

$\quad\quad (11,11) = (11,18) = (12,12) = (12,15) = k^2$

$\quad\quad (15,15) = (18,18) = k^2$

$_6H_6$: $\quad (10,12) = (10,15) = (11,12) = (11,17) = k^2$

$\quad\quad (12,14) = (12,18) = (14,15) = (17,18) = k^2$

$_7H_2$: $\quad (9,9) = (9,16) = (16,16) = 2k^2/R^3$

$\quad\quad (11,11) = (11,18) = (12,12) = (12,15) = 2k^2/R$

$\quad\quad (15,15) = (18,18) = k^2/R$

$_7H_6$: $\quad (10,12) = (10,15) = (11,12) = (11,17) = k^2/R$

$$(12,14) = (12,18) = (14,15) = (17,18) = k^2/R$$

III. $_JS_I$

$$_0S_4(9) = {_0S_4(16)} = 1$$

$$_0S_5(8) = {_0S_5(13)} = 1$$

$$_2S_4(9) = {_2S_4(16)} = 3k \tag{C.3}$$

$$_2S_5(8) = {_2S_5(13)} = 3k$$

Appendix D: MACSYMA Decks for $\hat{K}$, $\hat{N}_1$, and $\hat{N}_2$

The following MACSYMA commands were used to generate FORTRAN code for the elements of $\hat{K}$, $\hat{N}_1$, and $\hat{N}_2$ of Eqn (4.15). The first two decks shown generate the $_JL_I$ of Eqn (4.7) $,_JS_I$ of Eqn (4.16) and the $_JH_I$ of Eqn (4.7). The third deck generates the elements of $\hat{N}_1$. That deck shown actually only gives the A_{ij}, D_{ij}, and F_{ij} terms; however, the logic for the remaining terms is shown within the MACSYMA comment cards `/*  */` at the end. The elements of $\hat{N}_1$ were determined individually for each set of the elasticity arrays A_{ij} to T_{ij}. That is, a separate MACSYMA run generated only the A_{ij} terms, etc. The final deck attached generates the terms of $\hat{N}_2$ for a symmetrically stacked laminate. The terms were calculated individually for each elasticity array as in the $\hat{N}_1$ calculations. The decks for $\hat{K}$ were lost but are very similar to the $\hat{N}_1$ and $\hat{N}_2$ logic and are based upon Eqn (4.7) and (4.16). The important parts of those decks are attached at the end. The elements of the elasticity arrays A_{ij} to T_{ij} were formed interactively and saved in the file `ELASFOR.SV`.

```
/*   LMAT   */
/*   SET UP MATRICES L0-L4 AND S0,S2   */
WRITEFILE("LMATWF");
L0:EMATRIX(18,3,1,2,1)+EMATRIX(18,3,1,6,2)+EMATRIX(18,3,-1/R,7,2)+
    EMATRIX(18,3,1,3,3)+EMATRIX(18,3,1,5,3);
L1:EMATRIX(18,3,1,14,1)+EMATRIX(18,3,-1/R^2,7,2)+EMATRIX(18,3,1,18,2)+
    EMATRIX(18,3,1/R,3,3)+EMATRIX(18,3,-1/R,5,3)+EMATRIX(18,3,1,15,3)+
    EMATRIX(18,3,1,17,3);
L2:EMATRIX(18,3,1/R,18,2)+EMATRIX(18,3,1/R,15,3);
L3:EMATRIX(18,3,K1,10,1)+EMATRIX(18,3,K1,14,1)+EMATRIX(18,3,K1,11,2)+
    EMATRIX(18,3,K1,18,2)+EMATRIX(18,3,2*K1,12,3)+EMATRIX(18,3,K1,15,3)+
    EMATRIX(18,3,K1,17,3);
L4:EMATRIX(18,3,K1/R,11,2)+EMATRIX(18,3,K1/R,18,2)+EMATRIX(18,3,K1/R,12,3)+
    EMATRIX(18,3,K1/R,15,3);
S0:EMATRIX(18,2,1,9,1)+EMATRIX(18,2,1,16,1)+EMATRIX(18,2,1,8,2)+
    EMATRIX(18,2,1,13,2);
S2:EMATRIX(18,2,3*K1,9,1)+EMATRIX(18,2,3*K1,16,1)+EMATRIX(18,2,3*K1,9,2)+
    EMATRIX(18,2,3*K1,13,2);
L0T:TRANSPOSE(L0);
L1T:TRANSPOSE(L1);
L2T:TRANSPOSE(L2);
L3T:TRANSPOSE(L3);
L4T:TRANSPOSE(L4);
S0T:TRANSPOSE(S0);
S2T:TRANSPOSE(S2);
CLOSEFILE();
SAVE("LMATRIX.SV",L0,L1,L2,L3,L4,L0T,L1T,L2T,L3T,L4T,S0,S2,S0T,S2T);
```

338

```
/* HMAT */
/* SET MATRICES HO - H7 */
WRITEFILE("HMATWF");
MO:EMATRIX(18,54,1,2,2)+EMATRIX(18,54,1,5,5)+
   EMATRIX(18,54,1,8,8)+EMATRIX(18,54,1,3,21)+
   EMATRIX(18,54,1/R^2,4,22)+EMATRIX(18,54,1,6,24)+
   EMATRIX(18,54,1/R^2,7,25)+EMATRIX(18,54,1,9,27)+
   EMATRIX(18,54,1/R,9,22)+EMATRIX(18,54,1/R,4,27)+
   EMATRIX(18,54,-1/R,7,24)+EMATRIX(18,54,-1/R,6,25)+
   EMATRIX(18,54,1,3,38)+EMATRIX(18,54,1,2,39)+
   EMATRIX(18,54,1,5,42)+EMATRIX(18,54,1,6,41)+
   EMATRIX(18,54,1/R,8,40)+EMATRIX(18,54,1/R,4,44)+
   EMATRIX(18,54,-1/R,7,41)+EMATRIX(18,54,-1/R,5,43)+
   EMATRIX(18,54,1,8,45)+EMATRIX(18,54,1,9,44);
/*
*/
H1:EMATRIX(18,54,-2/R,5,5)+EMATRIX(18,54,1,14,2)+
   EMATRIX(18,54,1,2,14)+EMATRIX(18,54,1,17,5)+
   EMATRIX(18,54,1,5,17)+EMATRIX(18,54,2/R,3,21)+
   EMATRIX(18,54,2/R^3,7,25)+EMATRIX(18,54,2/R,9,27)+
   EMATRIX(18,54,-1/R^2,6,25)+EMATRIX(18,34,-1/R^2,7,24)+
   EMATRIX(18,54,1/R^2,9,22)+EMATRIX(18,54,1/R^2,4,27)+
   EMATRIX(18,54,1,15,21)+EMATRIX(18,54,1,3,33)+
   EMATRIX(18,54,1/R^2,16,22)+EMATRIX(18,54,1/R^2,4,34)+
   EMATRIX(18,54,1/R,16,27)+EMATRIX(18,54,1/R,9,34)+
   EMATRIX(18,54,1,18,24)+EMATRIX(18,54,1,6,36)+
   EMATRIX(18,54,-1/R,18,25)+EMATRIX(18,54,-1/R,7,36)+
   EMATRIX(18,54,1/R,3,38)+EMATRIX(18,54,1/R,2,39)+
   EMATRIX(18,54,1,15,38)+EMATRIX(18,54,1,2,51)+
   EMATRIX(18,54,1,14,39)+EMATRIX(18,54,1,3,50)+
   EMATRIX(18,54,1/R,8,40)+EMATRIX(18,54,1,5,54)+
   EMATRIX(18,54,-1/R,5,42)+EMATRIX(18,54,-1/R,6,41)+
   EMATRIX(18,54,1,18,41)+EMATRIX(18,54,1/R,4,44)+
   EMATRIX(18,54,1,17,42)+EMATRIX(18,54,1,6,53)+
   EMATRIX(18,54,-1/R,17,43)+EMATRIX(18,54,-1/R,7,53)+
   EMATRIX(18,54,1/R,8,45)+EMATRIX(18,54,1/R,9,44)+
   EMATRIX(18,54,1/R,16,44)+EMATRIX(18,54,1/R,8,52);
/*
*/
H2:EMATRIX(18,54,1/R^2,5,5)+EMATRIX(18,54,-1/R,5,17)+
   EMATRIX(18,54,-1/R,17,5)+EMATRIX(18,54,1,14,14)+
   EMATRIX(18,54,1,17,17)+EMATRIX(18,54,2/R,3,33)+
   EMATRIX(18,54,2/R,15,21)+EMATRIX(18,54,1/R^3,4,34)+
   EMATRIX(18,54,1/R^3,16,22)+EMATRIX(18,54,1/R,18,24)+
   EMATRIX(18,54,1/R,6,36)+EMATRIX(18,54,-2/R^2,18,25)+
   EMATRIX(18,54,-2/R^2,7,36)+EMATRIX(18,54,2/R^2,9,34)+
   EMATRIX(18,54,2/R^2,16,27)+EMATRIX(18,54,1,15,33)+
   EMATRIX(18,54,1/R^2,16,34)+EMATRIX(18,54,1,18,36)+
   EMATRIX(18,54,1/R,2,51)+EMATRIX(18,54,1/R,15,38)+
   EMATRIX(18,54,1/R,3,50)+EMATRIX(18,54,1/R,14,39)+
   EMATRIX(18,54,-1/R^2,17,43)+EMATRIX(18,54,-1/R^2,7,53)+
   EMATRIX(18,54,1/R^2,16,44)+EMATRIX(18,54,1/R^2,8,52)+
   EMATRIX(18,54,1,15,50)+EMATRIX(18,54,1,18,53)+
   EMATRIX(18,54,1,17,54)+EMATRIX(18,54,1,14,51);
/*
*/
H3:EMATRIX(18,54,K1,2,10)+EMATRIX(18,54,K1,10,2)+
   EMATRIX(18,54,K1,2,14)+EMATRIX(18,54,K1,5,12)+
   EMATRIX(18,54,K1,12,5)+EMATRIX(18,54,K1,17,5)+
   EMATRIX(18,54,K1,5,17)+EMATRIX(18,54,K1,14,2)+
```

```
                 EMATRIX(18,54,K1,3,30)+EMATRIX(18,54,K1,12,21)+
                 EMATRIX(18,54,K1,3,33)+EMATRIX(18,54,K1,15,21)+
                 EMATRIX(18,54,K1/R^2,4,27)+EMATRIX(18,54,K1/R^2,9,22)+
                _EMATRIX(18,54,K1,11,24)+EMATRIX(18,54,K1,6,29)+
                 EMATRIX(18,54,K1,18,24)+EMATRIX(18,54,K1,6,36)+
                 EMATRIX(18,54,-K1/R,7,29)+EMATRIX(18,54,-K1/R,11,25)+
                 EMATRIX(18,54,-K1/R,18,25)+EMATRIX(18,54,-K1/R,7,36)+
                 EMATRIX(18,54,2*K1/R,9,27)+EMATRIX(18,54,K1/R,16,27)+
                 EMATRIX(18,54,K1/R,9,34)+EMATRIX(18,54,2/R,15,33)+
                 EMATRIX(18,54,2/R^3,16,34)+EMATRIX(18,54,2/R,18,36)+
                 EMATRIX(18,54,K1,2,48)+EMATRIX(18,54,K1,12,38)+
                 EMATRIX(18,54,K1,15,38)+EMATRIX(18,54,K1,2,51)+
                 EMATRIX(18,54,K1,3,46)+EMATRIX(18,54,K1,10,39)+
                 EMATRIX(18,54,K1/R^2,16,22)+EMATRIX(18,54,K1,14,39)+
                 EMATRIX(18,54,K1,3,50)+EMATRIX(18,54,K1,5,47)+
                 EMATRIX(18,54,K1,11,41)+EMATRIX(18,54,K1,6,53)+
                 EMATRIX(18,54,K1,17,42)+EMATRIX(18,54,-K1/R,12,43)+
                 EMATRIX(18,54,-K1/R,7,48)+EMATRIX(18,54,-K1/R,17,43)+
                 EMATRIX(18,54,-K1/R,7,53)+EMATRIX(18,54,K1/R,9,44)+
                 EMATRIX(18,54,K1/R,8,45)+EMATRIX(18,54,K1/R,8,52)+
                 EMATRIX(18,54,K1/R,16,44)+EMATRIX(18,54,1/R,14,51)+
                 EMATRIX(18,54,1/R,15,50)+EMATRIX(18,54,1/R,18,53)+
                 EMATRIX(18,54,1/R,17,54)+EMATRIX(18,54,K1/R^2,4,34)+
                 EMATRIX(18,54,K1,18,41)+EMATRIX(18,54,K1,6,48)+
                 EMATRIX(18,54,K1,5,54)+EMATRIX(18,54,K1,12,42);
         /*
         */
         H4:EMATRIX(18,54,-K1/R,5,12)+EMATRIX(18,54,-K1/R,12,5)+
                 EMATRIX(18,54,-K1/R,5,17)+EMATRIX(18,54,-K1/R,17,5)+
                 EMATRIX(18,54,K1,10,14)+EMATRIX(18,54,K1,14,10)+
                 EMATRIX(18,54,K1,17,12)+EMATRIX(18,54,K1,12,17)+
                 EMATRIX(18,54,2*K1,14,14)+EMATRIX(18,54,2*K1,17,17)+
                 EMATRIX(18,54,2*K1/R,3,30)+EMATRIX(18,54,2*K1/R,12,21)+
                 EMATRIX(18,54,2*K1/R,3,33)+EMATRIX(18,54,2*K1/R,15,21)+
                 EMATRIX(18,54,K1/R^3,4,27)+EMATRIX(18,54,K1/R^3,9,22)+
                 EMATRIX(18,54,K1/R^3,4,34)+EMATRIX(18,54,K1/R^3,16,22)+
                 EMATRIX(18,54,K1/R,11,24)+EMATRIX(18,54,K1/R,6,29)+
                 EMATRIX(18,54,K1/R,18,24)+EMATRIX(18,54,-2*K1/R^2,7,29)+
                 EMATRIX(18,54,-2*K1/R^2,11,25)+EMATRIX(18,54,-2*K1/R^2,18,25)+
                 EMATRIX(18,54,-2*K1/R^2,7,36)+EMATRIX(18,54,4*K1/R^2,9,27)+
                 EMATRIX(18,54,3*K1/R^2,9,34)+EMATRIX(18,54,3*K1/R^2,16,27)+
                 EMATRIX(18,54,K1,18,29)+EMATRIX(18,54,K1,11,36)+
                 EMATRIX(18,54,K1,15,30)+EMATRIX(18,54,K1,12,33)+
                 EMATRIX(18,54,2*K1,15,33)+EMATRIX(18,54,2*K1/R^2,16,34)+
                 EMATRIX(18,54,2*K1,18,36)+EMATRIX(18,54,K1/R,2,48)+
                 EMATRIX(18,54,K1/R,12,38)+EMATRIX(18,54,K1/R,2,51)+
                 EMATRIX(18,54,K1/R,15,38)+EMATRIX(18,54,K1/R,3,46)+
                 EMATRIX(18,54,K1/R,10,39)+EMATRIX(18,54,K1/R,3,50)+
                 EMATRIX(18,54,K1/R,14,39)+EMATRIX(18,54,-K1/R^2,7,48)+
                 EMATRIX(18,54,-K1/R^2,12,43)+EMATRIX(18,54,-K1/R^2,7,53)+
                 EMATRIX(18,54,-K1/R^2,17,43)+EMATRIX(18,54,K1/R^2,9,44)+
                 EMATRIX(18,54,K1/R^2,8,45)+EMATRIX(18,54,K1/R^2,8,52)+
                 EMATRIX(18,54,K1/R^2,16,44)+EMATRIX(18,54,K1,15,46)+
                 EMATRIX(18,54,K1,10,51)+EMATRIX(18,54,K1,17,47)+
                 EMATRIX(18,54,K1,11,53)+EMATRIX(18,54,K1,12,50)+
                 EMATRIX(18,54,K1,14,48)+EMATRIX(18,54,K1,18,48)+
                 EMATRIX(18,54,K1,12,54)+EMATRIX(18,54,2*K1,15,50)+
                 EMATRIX(18,54,2*K1,14,51)+EMATRIX(18,54,2*K1,18,53)+
                 EMATRIX(18,54,2*K1,17,54)+EMATRIX(18,54,K1/R,6,36);
         /*
```

```
*/
M5:EMATRIX(18,54,2*K1/R^3,16,27)+EMATRIX(18,54,2*K1/R^3,9,34)+
    EMATRIX(18,54,2*K1/R,18,29)+EMATRIX(18,54,2*K1/R,11,36)+
    -EMATRIX(18,54,2*K1/R,12,33)+EMATRIX(18,54,2*K1/R,15,30)+
    EMATRIX(18,54,4*K1/R,15,33)+EMATRIX(18,54,4*K1/R^3,16,34)+
    EMATRIX(18,54,4*K1/R,18,36)+EMATRIX(18,54,K1/R,15,46)+
    EMATRIX(18,54,K1/R,10,51)+EMATRIX(18,54,K1/R,17,47)+
    EMATRIX(18,54,K1/R,11,53)+EMATRIX(18,54,K1/R,12,50)+
    EMATRIX(18,54,K1/R,14,48)+EMATRIX(18,54,K1/R,18,48)+
    EMATRIX(18,54,K1/R,12,54)+EMATRIX(18,54,2*K1/R,14,51)+
    EMATRIX(18,54,2*K1/R,15,50)+EMATRIX(18,54,2*K1/R,18,53)+
    EMATRIX(18,54,2*K1/R,17,54);
/*
*/
M6:EMATRIX(18,54,K1^2,10,10)+EMATRIX(18,54,K1^2,10,14)+
    EMATRIX(18,54,K1^2,14,10)+EMATRIX(18,54,K1^2,12,12)+
    EMATRIX(18,54,K1^2,17,12)+EMATRIX(18,54,K1^2,12,17)+
    EMATRIX(18,54,K1^2,14,14)+EMATRIX(18,54,K1^2,17,17)+
    EMATRIX(18,54,K1^2/R^2,9,27)+EMATRIX(18,54,K1^2,11,29)+
    EMATRIX(18,54,K1^2,12,30)+EMATRIX(18,54,K1^2,15,33)+
    EMATRIX(18,54,K1^2/R^2,16,34)+EMATRIX(18,54,K1^2,18,36)+
    EMATRIX(18,54,K1^2/R^2,16,27)+EMATRIX(18,54,K1^2/R^2,9,34)+
    EMATRIX(18,54,K1^2,18,29)+EMATRIX(18,54,K1^2,11,36)+
    EMATRIX(18,54,K1^2,12,33)+
    EMATRIX(18,54,K1^2,12,46)+EMATRIX(18,54,K1^2,10,48)+
    EMATRIX(18,54,K1^2,15,46)+EMATRIX(18,54,K1^2,10,51)+
    EMATRIX(18,54,K1^2,11,48)+EMATRIX(18,54,K1^2,12,47)+
    EMATRIX(18,54,K1^2,11,53)+EMATRIX(18,54,K1^2,17,47)+
    EMATRIX(18,54,K1^2,14,48)+EMATRIX(18,54,K1^2,12,50)+
    EMATRIX(18,54,K1^2,18,48)+EMATRIX(18,54,K1^2,12,54)+
    EMATRIX(18,54,K1^2,15,50)+EMATRIX(18,54,K1^2,14,51)+
    EMATRIX(18,54,K1^2,18,53)+EMATRIX(18,54,K1^2,17,54)+
    EMATRIX(18,54,K1^2,15,30);
/*
*/
H7:EMATRIX(18,54,2*K1^2/R^3,9,27)+EMATRIX(18,54,2*K1^2/R,11,29)+
    EMATRIX(18,54,2*K1^2/R,12,30)+EMATRIX(18,54,2*K1^2/R,15,33)+
    EMATRIX(18,54,2*K1^2/R^3,16,34)+EMATRIX(18,54,2*K1^2/R,18,36)+
    EMATRIX(18,54,2*K1^2/R^3,16,27)+EMATRIX(18,54,2*K1^2/R^3,9,34)+
    EMATRIX(18,54,2*K1^2/R,18,29)+EMATRIX(18,54,2*K1^2/R,11,36)+
    EMATRIX(18,54,2*K1^2/R,12,33)+EMATRIX(18,54,2*K1^2/R,15,30)+
    EMATRIX(18,54,K1^2/R,10,48)+EMATRIX(18,54,K1^2/R,12,46)+
    EMATRIX(18,54,K1^2/R,10,51)+EMATRIX(18,54,K1^2/R,15,46)+
    EMATRIX(18,54,K1^2/R,11,48)+EMATRIX(18,54,K1^2/R,12,47)+
    EMATRIX(18,54,K1^2/R,17,47)+EMATRIX(18,54,K1^2/R,11,53)+
    EMATRIX(18,54,K1^2/R,12,50)+EMATRIX(18,54,K1^2/R,14,48)+
    EMATRIX(18,54,K1^2/R,12,54)+EMATRIX(18,54,K1^2/R,18,48)+
    EMATRIX(18,54,K1^2/R,14,51)+EMATRIX(18,54,K1^2/R,15,50)+
    EMATRIX(18,54,K1^2/R,18,53)+EMATRIX(18,54,K1^2/R,17,54);
CLOSEFILE();
SAVE("HMATRIX.SV",H0,H1,H2,H3,H4,H5,H6,H7);
```

```
/*   N1MAT  */
/*   ASSEMBLE MATRIX N1  */
DYNAMALLOC:TRUE;
WRITEFILE("N1");
LOADFILE("HMATP.SV");
LOADFILE("ELASFOR.SV");
KILL(A,B,DD,E,F,G,H,I,J,K,L,P,R,S,T,AS,DS,FS);
LOADFILE("LMATP.SV");
N1:ZEROMATRIX(18,18)$
  FOR II:1 THRU 3 DO
 FOR JJ:1 THRU 3 DO
  (I1:3*(-9*II^2+33*II-12),
   J2:3*(9*JJ^2-39*JJ+48),
   I2:3*(9*II^2-39*II+48),
   J1:3*(-9*JJ^2+33*JJ-12),
/*  */
SUBIO:SUBMATRIX(HO,I1,I1-1,I1-2,I1-3,I1-4,I1-5,I1-6,I1-7,
     I1-8,I1-9,I1-10,I1-11,I1-12,I1-13,I1-14,I1-15,I1-16,
     I1-17,I2,I2-1,I2-2,I2-3,I2-4,I2-5,I2-6,I2-7,I2-8,I2-9,I2-10,
     I2-11,I2-12,I2-13,I2-14,I2-15,I2-16,I2-17),
SUBJO:SUBMATRIX(HO,J1,J1-1,J1-2,J1-3,J1-4,J1-5,J1-6,J1-7,
     J1-8,J1-9,J1-10,J1-11,J1-12,J1-13,J1-14,J1-15,J1-16,
     J1-17,J2,J2-1,J2-2,J2-3,J2-4,J2-5,J2-6,J2-7,J2-8,J2-9,J2-10,
     J2-11,J2-12,J2-13,J2-14,J2-15,J2-16,J2-17),
   PRINT("1",II,JJ),
/*  */
SUBI1:SUBMATRIX(H1,I1,I1-1,I1-2,I1-3,I1-4,I1-5,I1-6,I1-7,
     I1-8,I1-9,I1-10,I1-11,I1-12,I1-13,I1-14,I1-15,I1-16,
     I1-17,I2,I2-1,I2-2,I2-3,I2-4,I2-5,I2-6,I2-7,I2-8,I2-9,I2-10,
     I2-11,I2-12,I2-13,I2-14,I2-15,I2-16,I2-17),
SUBJ1:SUBMATRIX(H1,J1,J1-1,J1-2,J1-3,J1-4,J1-5,J1-6,J1-7,
     J1-8,J1-9,J1-10,J1-11,J1-12,J1-13,J1-14,J1-15,J1-16,
     J1-17,J2,J2-1,J2-2,J2-3,J2-4,J2-5,J2-6,J2-7,J2-8,J2-9,J2-10,
     J2-11,J2-12,J2-13,J2-14,J2-15,J2-16,J2-17),
PRINT("2",II,JJ),
/*  */
SUBI2:SUBMATRIX(H2,I1,I1-1,I1-2,I1-3,I1-4,I1-5,I1-6,I1-7,
     I1-8,I1-9,I1-10,I1-11,I1-12,I1-13,I1-14,I1-15,I1-16,
     I1-17,I2,I2-1,I2-2,I2-3,I2-4,I2-5,I2-6,I2-7,I2-8,I2-9,I2-10,
     I2-11,I2-12,I2-13,I2-14,I2-15,I2-16,I2-17),
SUBJ2:SUBMATRIX(H2,J1,J1-1,J1-2,J1-3,J1-4,J1-5,J1-6,J1-7,
     J1-8,J1-9,J1-10,J1-11,J1-12,J1-13,J1-14,J1-15,J1-16,
     J1-17,J2,J2-1,J2-2,J2-3,J2-4,J2-5,J2-6,J2-7,J2-8,J2-9,J2-10,
     J2-11,J2-12,J2-13,J2-14,J2-15,J2-16,J2-17),
PRINT("3",II,JJ),
/*  */
SUBI3:SUBMATRIX(H3,I1,I1-1,I1-2,I1-3,I1-4,I1-5,I1-6,I1-7,
     I1-8,I1-9,I1-10,I1-11,I1-12,I1-13,I1-14,I1-15,I1-16,
     I1-17,I2,I2-1,I2-2,I2-3,I2-4,I2-5,I2-6,I2-7,I2-8,I2-9,I2-10,
     I2-11,I2-12,I2-13,I2-14,I2-15,I2-16,I2-17),
SUBJ3:SUBMATRIX(H3,J1,J1-1,J1-2,J1-3,J1-4,J1-5,J1-6,J1-7,
     J1-8,J1-9,J1-10,J1-11,J1-12,J1-13,J1-14,J1-15,J1-16,
     J1-17,J2,J2-1,J2-2,J2-3,J2-4,J2-5,J2-6,J2-7,J2-8,J2-9,J2-10,
     J2-11,J2-12,J2-13,J2-14,J2-15,J2-16,J2-17),
PRINT("4",II,JJ),
/*  */
SUBI4:SUBMATRIX(H4,I1,I1-1,I1-2,I1-3,I1-4,I1-5,I1-6,I1-7,
     I1-8,I1-9,I1-10,I1-11,I1-12,I1-13,I1-14,I1-15,I1-16,
     I1-17,I2,I2-1,I2-2,I2-3,I2-4,I2-5,I2-6,I2-7,I2-8,I2-9,I2-10,
     I2-11,I2-12,I2-13,I2-14,I2-15,I2-16,I2-17),
```

```
SUBJ4:SUBMATRIX(H4,J1,J1-1,J1-2,J1-3,J1-4,J1-5,J1-6,J1-7,
     J1-8,J1-9,J1-10,J1-11,J1-12,J1-13,J1-14,J1-15,J1-16,
     J1-17,J2,J2-1,J2-2,J2-3,J2-4,J2-5,J2-6,J2-7,J2-8,J2-9,J2-10,
     -J2-11,J2-12,J2-13,J2-14,J2-15,J2-16,J2-17),
PRINT("5",II,JJ),
/*  */   /*
SUBI5:SUBMATRIX(H5,I1,I1-1,I1-2,I1-3,I1-4,I1-5,I1-6,I1-7,
     I1-8,I1-9,I1-10,I1-11,I1-12,I1-13,I1-14,I1-15,I1-16,
     I1-17,I2,I2-1,I2-2,I2-3,I2-4,I2-5,I2-6,I2-7,I2-8,I2-9,I2-10,
     I2-11,I2-12,I2-13,I2-14,I2-15,I2-16,I2-17),
SUBJ5:SUBMATRIX(H5,J1,J1-1,J1-2,J1-3,J1-4,J1-5,J1-6,J1-7,
     J1-8,J1-9,J1-10,J1-11,J1-12,J1-13,J1-14,J1-15,J1-16,
     J1-17,J2,J2-1,J2-2,J2-3,J2-4,J2-5,J2-6,J2-7,J2-8,J2-9,J2-10,
     J2-11,J2-12,J2-13,J2-14,J2-15,J2-16,J2-17),
PRINT("6",II,JJ),
/*  */
SUBI6:SUBMATRIX(H6,I1,I1-1,I1-2,I1-3,I1-4,I1-5,I1-6,I1-7,
     I1-8,I1-9,I1-10,I1-11,I1-12,I1-13,I1-14,I1-15,I1-16,
     I1-17,I2,I2-1,I2-2,I2-3,I2-4,I2-5,I2-6,I2-7,I2-8,I2-9,I2-10,
     I2-11,I2-12,I2-13,I2-14,I2-15,I2-16,I2-17),
SUBJ6:SUBMATRIX(H6,J1,J1-1,J1-2,J1-3,J1-4,J1-5,J1-6,J1-7,
     J1-8,J1-9,J1-10,J1-11,J1-12,J1-13,J1-14,J1-15,J1-16,
     J1-17,J2,J2-1,J2-2,J2-3,J2-4,J2-5,J2-6,J2-7,J2-8,J2-9,J2-10,
     J2-11,J2-12,J2-13,J2-14,J2-15,J2-16,J2-17),
PRINT("7",II,JJ),
/*  */
SUBI7:SUBMATRIX(H7,I1,I1-1,I1-2,I1-3,I1-4,I1-5,I1-6,I1-7,
     I1-8,I1-9,I1-10,I1-11,I1-12,I1-13,I1-14,I1-15,I1-16,
     I1-17,I2,I2-1,I2-2,I2-3,I2-4,I2-5,I2-6,I2-7,I2-8,I2-9,I2-10,
     I2-11,I2-12,I2-13,I2-14,I2-15,I2-16,I2-17),
SUBJ7:SUBMATRIX(H7,J1,J1-1,J1-2,J1-3,J1-4,J1-5,J1-6,J1-7,
     J1-8,J1-9,J1-10,J1-11,J1-12,J1-13,J1-14,J1-15,J1-16,
     J1-17,J2,J2-1,J2-2,J2-3,J2-4,J2-5,J2-6,J2-7,J2-8,J2-9,J2-10,
     J2-11,J2-12,J2-13,J2-14,J2-15,J2-16,J2-17),
PRINT("8",II,JJ),
/*  */
     N1:N1+A[II,JJ]*(COL(L0,II).TQ.SUBJ0+(TQ.COL(L0,II))*SUBJ0
          +SUBI0.Q.ROW(L0T,JJ))+
        DD[II,JJ]*(COL(L0,II).TQ.SUBJ2+(TC.COL(L0,II))*SUBJ2
          +SUBI2.Q.ROW(L0T,JJ)+
           COL(L2,II).TQ.SUBJ0+(TQ.COL(L2,II))*SUBJ0
          +SUBI0.Q.ROW(L2T,JJ)+
           COL(L1,II).TQ.SUBJ1+(TQ.COL(L1,II))*SUBJ1
          +SUBI1.Q.ROW(L1T,JJ)),
PRINT("9",II,JJ),
  N1:N1+F[II,JJ]*(COL(L0,II).TQ.SUBJ4+(TQ.COL(L0,II))*SUBJ4
          +SUBI4.Q.ROW(L0T,JJ)+
           COL(L4,II).TQ.SUBJ0+(TQ.COL(L4,II))*SUBJ0
          +SUBI0.Q.ROW(L4T,JJ)+
           COL(L1,II).TQ.SUBJ3+(TQ.COL(L1,II))*SUBJ3
          +SUBI3.Q.ROW(L1T,JJ)+
           COL(L3,II).TQ.SUBJ1+(TQ.COL(L3,II))*SUBJ1
          +SUBI1.Q.ROW(L3T,JJ)+
           COL(L2,II).TQ.SUBJ2+(TQ.COL(L2,II))*SUBJ2
          +SUBI2.Q.ROW(L2T,JJ)),
KILL(SUBJ0,SUBJ1,SUBJ2,SUBJ3,SUBJ4,SUBJ5,SUBJ6,SUBJ7),
KILL(SUBI0,SUBI1,SUBI2,SUBI3,SUBI4,SUBI5,SUBI6,SUBI7),
PRINT("10",II,JJ)):
/*  */
KILL(Q,TG):
```

```
KILL(LO,LOT,L1,L1T,L2,L2T,L3,L3T,L4,L4T);
KILL(HO,H1,H2,H3,H4,H5,H6,H7);
/*   -*/
N1S:ZEROMATRIX(18,18)$
FOR II:1 THRU 18 DO
 FOR JJ:II THRU 18 DO
  N1S[II,JJ]:N1[II,JJ];
KILL(N1);
/*      */
N1:ZEROMATRIX(18,18)$
  FOR II:1 THRU 18 DO
  FOR JJ:II THRU 18 DO
(PRINT("FOR",II,JJ),
 N1[II,JJ]:FACTOROUT(N1S[II,JJ],Q(1),Q(2),Q(3),Q(4),Q(5),Q(6),
 Q(7),Q(8),Q(9),C(10),Q(11),C(12),Q(13),Q(14),Q(15),Q(16),
 Q(17),Q(18)))$
SAVE("N1.SV",N1);
FORTRAN(STN1=N1);
 CLOSEFILE();
/*    N1:N1+H[II,JJ]*(COL(LO,II).TQ.SUBJ6+(TQ.COL(LO,II))*SUBJ6
                +SUBI6.Q.ROW(LOT,JJ)+
                  COL(L1,II).TQ.SUBJ5+(TQ.COL(L1,II))*SUBJ5
                +SUBI5.Q.ROW(L1T,JJ)+
                  COL(L2,II).TC.SUBJ4+(TQ.COL(L2,II))*SUBJ4
                +SUBI4.Q.ROW(L2T,JJ)+
                  COL(L3,II).TQ.SUBJ3+(TQ.COL(L3,II))*SUBJ3
                +SUBI3.Q.ROW(L3T,JJ)+
                COL(L4,II).TQ.SUBJ2+(TQ.COL(L4,II))*SUBJ2
                +SUBI2.Q.ROW(L4T,JJ)),
PRINT("11",II,JJ),
 N1:N1+J[II,JJ]*(COL(L1,II).TQ.SUBJ7+(TQ.COL(L1,II))*SUBJ7
                +SUBI7.Q.ROW(L1T,JJ)+
                  COL(L2,II).TQ.SUBJ6+(TQ.COL(L2,II))*SUBJ6
                +SUBI6.Q.ROW(L2T,JJ)+
                  COL(L3,II).TQ.SUBJ5+(TQ.COL(L3,II))*SUBJ5
                +SUBI5.Q.ROW(L3T,JJ)+
                  COL(L4,II).TQ.SUBJ4+(TQ.COL(L4,II))*SUBJ4
                +SUBI4.Q.ROW(L4T,JJ)),
PRINT("12",II,JJ),
 N1:N1+L[II,JJ]*(COL(L3,II).TQ.SUBJ7+(TQ.COL(L3,II))*SUBJ7
                +SUBI7.Q.ROW(L3T,JJ)+
                  COL(L4,II).TC.SUBJ6+(TQ.COL(L4,II))*SUBJ6
                +SUBI6.Q.ROW(L4T,JJ)),  */
/*      B[II,JJ]*(COL(LO,II).TQ.SUBJ1+(TQ.COL(LO,II))*SUBJ1
                +SUBI1.Q.ROW(LOT,JJ)+
                  COL(L1,II).TQ.SUBJO+(TQ.COL(L1,II))*SUBJO
                +SUBIO.Q.ROW(L1T,JJ))+
            E[II,JJ]*(COL(LO,II).TQ.SUBJ3+(TQ.COL(LO,II))*SUBJ3
                +SUBI3.Q.ROW(LOT,JJ)+
                  COL(L3,II).TQ.SUBJO+(TQ.COL(L3,II))*SUBJO
                +SUBIO.Q.ROW(L3T,JJ)+
                  COL(L1,II).TQ.SUBJ2+(TQ.COL(L1,II))*SUBJ2
                +SUBI2.Q.ROW(L1T,JJ)+
                  COL(L2,II).TC.SUBJ1+(TQ.COL(L2,II))*SUBJ1
                +SUBI1.Q.ROW(L2T,JJ))+
            G[II,JJ]*(COL(LO,II).TQ.SUBJ5+(TQ.COL(LO,II))*SUBJ5
                +SUBI5.Q.ROW(LOT,JJ)+
                  COL(L2,II).TQ.SUBJ3+(TQ.COL(L2,II))*SUBJ3
                +SUBI3.Q.ROW(L2T,JJ)+
                  COL(L1,II).TC.SUBJ4+(TQ.COL(L1,II))*SUBJ4
```

```
        +SUBI4.Q.ROW(L1T,JJ)+
         COL(L4,II).TC.SUBJ1+(TQ.COL(L4,II))*SUBJ1
        +SUBI1.Q.ROW(L4T,JJ)+
         COL(L3,II).TQ.SUBJ2+(TQ.COL(L3,II))*SUBJ2
        +SUBI2.Q.ROW(L3T,JJ))+
   I[II,JJ]*(COL(L0,II).TQ.SUBJ7+(TQ.COL(L0,I))*SUBJ7
        +SUBI7.Q.ROW(L0T,JJ)+
         COL(L1,II).TQ.SUBJ6+(TQ.COL(L1,II))*SUBJ6
        +SUBI6.Q.ROW(L1T,JJ)+
         COL(L2,II).TC.SUBJ5+(TQ.COL(L2,II))*SUBJ5
        +SUBI5.Q.ROW(L2T,JJ)+
         COL(L3,II).TQ.SUBJ4+(TQ.COL(L3,II))*SUBJ4
        +SUBI4.Q.ROW(L3T,JJ)+
         COL(L4,II).TC.SUBJ3+(TQ.COL(L4,II))*SUBJ3
        +SUBI3.Q.ROW(L4T,JJ))+
   K[II,JJ]*(COL(L2,II).TQ.SUBJ7+(TQ.COL(L2,II))*SUBJ7
        +SUBI7.Q.ROW(L2T,JJ)+
         COL(L3,II).TQ.SUBJ6+(TQ.COL(L3,II))*SUBJ6
        +SUBI6.Q.ROW(L3T,JJ)+
         COL(L4,II).TC.SUBJ5+(TQ.COL(L4,II))*SUBJ5
        +SUBI5.Q.ROW(L4T,JJ))+
   P[II,JJ]*(COL(L4,II).TQ.SUBJ7+(TQ.COL(L4,II))*SUBJ7
        +SUBI7.Q.ROW(L4T,JJ))):    */
```

```
/*   N2MAT  */
/*   ASSEMBLE MATRIX N2  */
DYNAM_LOC:TRUE;
WRITEFILE("N2J");
LOADFILE("HMATP.SV");
LOADFILE("ELASFOR.SV");
KILL(A,B,DD,E,F,G,H,I,K,L,P,R,S,T);
N2J:ZEROMATRIX(18,18)$
FOR II:1 THRU 3 DO
 FOR JJ:1 THRU 3 DO
   (I1:3*(-9*II^2+33*II-12),
    J2:3*(9*JJ^2-39*JJ+48),
    I2:3*(9*II^2-39*II+48),
    J1:3*(-9*JJ^2+33*JJ-12),
 /*   */
SUBI0:SUBMATRIX(H0,I1,I1-1,I1-2,I1-3,I1-4,I1-5,I1-6,I1-7,
      I1-8,I1-9,I1-10,I1-11,I1-12,I1-13,I1-14,I1-15,I1-16,
      I1-17,I2,I2-1,I2-2,I2-3,I2-4,I2-5,I2-6,I2-7,I2-8,I2-9,I2-10,
      I2-11,I2-12,I2-13,I2-14,I2-15,I2-16,I2-17),
SUBJ0:SUBMATRIX(H0,J1,J1-1,J1-2,J1-3,J1-4,J1-5,J1-6,J1-7,
      J1-8,J1-9,J1-10,J1-11,J1-12,J1-13,J1-14,J1-15,J1-16,
      J1-17,J2,J2-1,J2-2,J2-3,J2-4,J2-5,J2-6,J2-7,J2-8,J2-9,J2-10,
      J2-11,J2-12,J2-13,J2-14,J2-15,J2-16,J2-17),
PRINT("1",II,JJ),
 /*   */
SUBI1:SUBMATRIX(H1,I1,I1-1,I1-2,I1-3,I1-4,I1-5,I1-6,I1-7,
      I1-8,I1-9,I1-10,I1-11,I1-12,I1-13,I1-14,I1-15,I1-16,
      I1-17,I2,I2-1,I2-2,I2-3,I2-4,I2-5,I2-6,I2-7,I2-8,I2-9,I2-10,
      I2-11,I2-12,I2-13,I2-14,I2-15,I2-16,I2-17),
SUBJ1:SUBMATRIX(H1,J1,J1-1,J1-2,J1-3,J1-4,J1-5,J1-6,J1-7,
      J1-8,J1-9,J1-10,J1-11,J1-12,J1-13,J1-14,J1-15,J1-16,
      J1-17,J2,J2-1,J2-2,J2-3,J2-4,J2-5,J2-6,J2-7,J2-8,J2-9,J2-10,
      J2-11,J2-12,J2-13,J2-14,J2-15,J2-16,J2-17),
PRINT("2",II,JJ),
 /*   */
SUBI2:SUBMATRIX(H2,I1,I1-1,I1-2,I1-3,I1-4,I1-5,I1-6,I1-7,
      I1-8,I1-9,I1-10,I1-11,I1-12,I1-13,I1-14,I1-15,I1-16,
      I1-17,I2,I2-1,I2-2,I2-3,I2-4,I2-5,I2-6,I2-7,I2-8,I2-9,I2-10,
      I2-11,I2-12,I2-13,I2-14,I2-15,I2-16,I2-17),
SUBJ2:SUBMATRIX(H2,J1,J1-1,J1-2,J1-3,J1-4,J1-5,J1-6,J1-7,
      J1-8,J1-9,J1-10,J1-11,J1-12,J1-13,J1-14,J1-15,J1-16,
      J1-17,J2,J2-1,J2-2,J2-3,J2-4,J2-5,J2-6,J2-7,J2-8,J2-9,J2-10,
      J2-11,J2-12,J2-13,J2-14,J2-15,J2-16,J2-17),
PRINT("3",II,JJ),
 /*   */
SUBI3:SUBMATRIX(H3,I1,I1-1,I1-2,I1-3,I1-4,I1-5,I1-6,I1-7,
      I1-8,I1-9,I1-10,I1-11,I1-12,I1-13,I1-14,I1-15,I1-16,
      I1-17,I2,I2-1,I2-2,I2-3,I2-4,I2-5,I2-6,I2-7,I2-8,I2-9,I2-10,
      I2-11,I2-12,I2-13,I2-14,I2-15,I2-16,I2-17),
SUBJ3:SUBMATRIX(H3,J1,J1-1,J1-2,J1-3,J1-4,J1-5,J1-6,J1-7,
      J1-8,J1-9,J1-10,J1-11,J1-12,J1-13,J1-14,J1-15,J1-16,
      J1-17,J2,J2-1,J2-2,J2-3,J2-4,J2-5,J2-6,J2-7,J2-8,J2-9,J2-10,
      J2-11,J2-12,J2-13,J2-14,J2-15,J2-16,J2-17),
PRINT("4",II,JJ),
 /*   */
SUBI4:SUBMATRIX(H4,I1,I1-1,I1-2,I1-3,I1-4,I1-5,I1-6,I1-7,
      I1-8,I1-9,I1-10,I1-11,I1-12,I1-13,I1-14,I1-15,I1-16,
      I1-17,I2,I2-1,I2-2,I2-3,I2-4,I2-5,I2-6,I2-7,I2-8,I2-9,I2-10,
      I2-11,I2-12,I2-13,I2-14,I2-15,I2-16,I2-17),
SUBJ4:SUBMATRIX(H4,J1,J1-1,J1-2,J1-3,J1-4,J1-5,J1-6,J1-7,
```

```
                    J1-8,J1-9,J1-10,J1-11,J1-12,J1-13,J1-14,J1-15,J1-16,
                    J1-17,J2,J2-1,J2-2,J2-3,J2-4,J2-5,J2-6,J2-7,J2-8,J2-9,J2-10,
                    J2-11,J2-12,J2-13,J2-14,J2-15,J2-16,J2-17),
      PRINT("5",II,JJ),
      /* */    /*
      SUBI5:SUBMATRIX(H5,I1,I1-1,I1-2,I1-3,I1-4,I1-5,I1-6,I1-7,
            I1-8,I1-9,I1-10,I1-11,I1-12,I1-13,I1-14,I1-15,I1-16,
            I1-17,I2,I2-1,I2-2,I2-3,I2-4,I2-5,I2-6,I2-7,I2-8,I2-9,I2-10,
            I2-11,I2-12,I2-13,I2-14,I2-15,I2-16,I2-17),
      SUBJ5:SUBMATRIX(H5,J1,J1-1,J1-2,J1-3,J1-4,J1-5,J1-6,J1-7,
            J1-8,J1-9,J1-10,J1-11,J1-12,J1-13,J1-14,J1-15,J1-16,
            J1-17,J2,J2-1,J2-2,J2-3,J2-4,J2-5,J2-6,J2-7,J2-8,J2-9,J2-10,
            J2-11,J2-12,J2-13,J2-14,J2-15,J2-16,J2-17),
      PRINT("6",II,JJ),
      /* */
      SUBI6:SUBMATRIX(H6,I1,I1-1,I1-2,I1-3,I1-4,I1-5,I1-6,I1-7,
            I1-8,I1-9,I1-10,I1-11,I1-12,I1-13,I1-14,I1-15,I1-16,
            I1-17,I2,I2-1,I2-2,I2-3,I2-4,I2-5,I2-6,I2-7,I2-8,I2-9,I2-10,
            I2-11,I2-12,I2-13,I2-14,I2-15,I2-16,I2-17),
      SUBJ6:SUBMATRIX(H6,J1,J1-1,J1-2,J1-3,J1-4,J1-5,J1-6,J1-7,
            J1-8,J1-9,J1-10,J1-11,J1-12,J1-13,J1-14,J1-15,J1-16,
            J1-17,J2,J2-1,J2-2,J2-3,J2-4,J2-5,J2-6,J2-7,J2-8,J2-9,J2-10,
            J2-11,J2-12,J2-13,J2-14,J2-15,J2-16,J2-17),
      PRINT("7",II,JJ),
      /* */
      SUBI7:SUBMATRIX(H7,I1,I1-1,I1-2,I1-3,I1-4,I1-5,I1-6,I1-7,
            I1-8,I1-9,I1-10,I1-11,I1-12,I1-13,I1-14,I1-15,I1-16,
            I1-17,I2,I2-1,I2-2,I2-3,I2-4,I2-5,I2-6,I2-7,I2-8,I2-9,I2-10,
            I2-11,I2-12,I2-13,I2-14,I2-15,I2-16,I2-17),
      SUBJ7:SUBMATRIX(H7,J1,J1-1,J1-2,J1-3,J1-4,J1-5,J1-6,J1-7,
            J1-8,J1-9,J1-10,J1-11,J1-12,J1-13,J1-14,J1-15,J1-16,
            J1-17,J2,J2-1,J2-2,J2-3,J2-4,J2-5,J2-6,J2-7,J2-8,J2-9,J2-10,
            J2-11,J2-12,J2-13,J2-14,J2-15,J2-16,J2-17),    */
      PRINT("8",II,JJ),
      /* */
      C:1/3,
         N2:N2+A[II,JJ]*(SUBI0.Q.TQ.SUBJ0+.5*(TQ.SUBJ0.Q)*SUBI0)+
               DD[II,JJ]*(C*(SUBI0.Q.TQ.SUBJ2+.5*(TC.SUBI0.Q)*SUBJ2+
                        SUBI2.Q.TQ.SUBJ0+.5*(TQ.SUBI2.Q)*SUBJ0)+
                        SUBI1.G.TQ.SUBJ1+.5*(TQ.SUBJ1.Q)*SUBI1),
      PRINT("9",II,JJ),
         N2:N2+F[II,JJ]*(C*(SUBI0.Q.TQ.SUBJ4+.5*(TQ.SUBI0.Q)*SUBJ4+
                        SUBI4.Q.TQ.SUBJ0+.5*(TQ.SUBI4.Q)*SUBJ0+
                        2*(SUBI1.Q.TQ.SUBJ3+.5*(TQ.SUBI1.Q)*SUBJ3+
                        SUBI3.Q.TQ.SUBJ1+.5*(TQ.SUBI3.Q)*SUBJ1))+
                        SUBI2.Q.TQ.SUBJ2+.5*(TQ.SUBJ2.Q)*SUBI2),
      PRINT("10",II,JJ)):
      /*     N2:N2+H[II,JJ]*(C*(SUBI0.C.TQ.SUBJ6+.5*(TQ.SUBI0.Q)*SUBJ6+
                        SUBI6.Q.TQ.SUBJ0+.5*(TQ.SUBI6.Q)*SUBJ0+
                        2*(SUBI1.G.TQ.SUBJ5+.5*(TQ.SUBI1.Q)*SUBJ5+
                        SUBI5.Q.TQ.SUBJ1+.5*(TQ.SUBI5.Q)*SUBJ1)+
                        2*(SUBI2.Q.TQ.SUBJ4+.5*(TQ.SUBI2.Q)*SUBJ4+
                        SUBI4.G.TQ.SUBJ2+.5*(TQ.SUBI4.Q)*SUBJ2))+
                        SUBI3.Q.TQ.SUBJ3+.5*(TQ.SUBJ3.Q)*SUBI3),
      PRINT("11",II,JJ),
         N2:N2+J[II,JJ]*(SUBI4.C.TQ.SUBJ4+.5*(TQ.SUBJ4.C)*SUBI4+
                        C*(2*(SUBI1.Q.TQ.SUBJ7+.5*(TQ.SUBI1.Q)*SUBJ7+
                        SUBI7.Q.TQ.SUBJ1+.5*(TQ.SUBI7.Q)*SUBJ1)+
                        2*(SUBI2.Q.TQ.SUBJ6+.5*(TQ.SUBI2.Q)*SUBJ6+
                        SUBI6.Q.TQ.SUBJ2+.5*(TQ.SUBI6.Q)*SUBJ2)+
```

347

```
                2*(SUBI3.Q.TQ.SUBJ5+.5*(TQ.SUBI3.Q)*SUBJ5+
                    SUBI5.Q.TQ.SUBJ3+.5*(TQ.SUBI5.Q)*SUBJ3))),
        PRINT("12",II,JJ),
            N2:N2+L[II,JJ]*(SUBI5.Q.TQ.SUBJ5+.5*(TQ.SUBJ5.Q)*SUBI5+
                    C*(2*(SUBI3.Q.TQ.SUBJ7+.5*(TQ.SUBI3.Q)*SUBJ7+
                    SUBI7.Q.TQ.SUBJ3+.5*(TQ.SUBI7.Q)*SUBJ3)+
                    2*(SUBI4.Q.TQ.SUBJ6+.5*(TQ.SUBI4.Q)*SUBJ6+
                    SUBI6.Q.TQ.SUBJ4+.5*(TQ.SUBI6.Q)*SUBJ4))),
        PRINT("13",II,JJ),
            N2:N2+R[II,JJ]*(SUBI6.Q.TQ.SUBJ6+.5*(TQ.SUBJ6.Q)*SUBI6+
                    C*(2*(SUBI5.Q.TQ.SUBJ7+.5*(TQ.SUBI5.Q)*SUBJ7+
                    SUBI7.Q.TQ.SUBJ5+.5*(TQ.SUBI7.Q)*SUBJ5)))+
                TEII,JJ]*(SUBI7.Q.TQ.SUBJ7+.5*(TQ.SUBJ7.Q)*SUBI7)),
        KILL(SUBI0,SUBI1,SUBI2,SUBI3,SUBI4,SUBI5,SUBI6,SUBI7),
        KILL(SUBJ0,SUBJ1,SUSJ2,SUBJ3,SUBJ4,SUBJ5,SUBJ6,SUBJ7),
        PRINT("10",II,JJ)):
/*   */
KILL(Q,TQ);
N2S:ZEROMATRIX(18,18)$
FOR II:1 THRU 18 DO
  FOR JJ:II THRU 18 DO
   N2S[II,JJ]:N2[II,JJ]);
FOR II:1 THRU 18 DO
 FOR JJ:II THRU 18 DO
  (PRINT("FOR",II,JJ),
  N2[II,JJ]:FACTOROUT(N2S[II,JJ],Q(1),Q(2),Q(3),Q(4),Q(5),Q(6),Q(7),
  Q(8),Q(9),Q(10),Q(11),Q(12),Q(13),Q(14),Q(15),Q(16),Q(17),Q(18))):
SAVE("N2.SV",N2):
FORTRAN(STN2=N2):
CLOSEFILE():
/* N2:N2+B[II,JJ]*C*(SUBI0.Q.TQ.SUBJ1+.5*(TQ.SUBI0.Q)*SUBJ1+
                    SUBI1.Q.TQ.SUBJ0+.5*(TQ.SUBI1.Q)*SUBJ0),
        PRINT(II,JJ),
            N2:N2+E[II,JJ]*C*(SUBI0.Q.TQ.SUBJ3+.5*(TQ.SUBI0.Q)*SUBJ3+
                    SUBI3.Q.TQ.SUBJ0+.5*(TQ.SUBI3.Q)*SUBJ0+
                    2*(SUBI1.Q.TQ.SUBJ2+.5*(TQ.SUBI1.Q)*SUBJ2+
                    SUBI2.Q.TQ.SUBJ1+.5*(TQ.SUBI2.Q)*SUBJ1)),
        PRINT(II,JJ),
            N2:N2+G[II,JJ]*C*(SUBI0.Q.TQ.SUBJ5+.5*(TQ.SUBI0.Q)*SUBJ5+
                    SUBI5.Q.TQ.SUBJ0+.5*(TQ.SUBI5.Q)*SUBJ0+
                    2*(SUBI1.Q.TQ.SUBJ4+.5*(TQ.SUBI1.Q)*SUBJ4+
                    SUBI4.Q.TQ.SUBJ1+.5*(TQ.SUBI4.Q)*SUBJ1)+
                    2*(SUBI2.Q.TQ.SUBJ3+.5*(TQ.SUBI2.Q)*SUBJ3+
                    SUBI3.Q.TQ.SUBJ2+.5*(TQ.SUBI3.Q)*SUBJ2)),
        PRINT(II,JJ),
            N2:N2+I[II,JJ]*C*(SUBI0.Q.TQ.SUBJ7+.5*(TQ.SUBI0.Q)*SUBJ7+
                    SUBI7.Q.TQ.SUBJ0+.5*(TQ.SUBI7.Q)*SUBJ0+
                    2*(SUBI1.Q.TQ.SUBJ6+.5*(TQ.SUBI1.Q)*SUBJ6+
                    SUBI6.Q.TQ.SUBJ1+.5*(TQ.SUBI6.Q)*SUBJ1)+
                    2*(SUBI2.Q.TQ.SUBJ5+.5*(TQ.SUBI2.Q)*SUBJ5+
                    SUBI5.Q.TQ.SUBJ2+.5*(TQ.SUBI5.Q)*SUBJ2)+
                    2*(SUBI3.Q.TQ.SUBJ4+.5*(TQ.SUBI3.Q)*SUBJ4+
                    SUBI4.Q.TQ.SUBJ3+.5*(TQ.SUBI4.Q)*SUBJ3)),
        PRINT(II,JJ),
            N2:N2+K[II,JJ]*C*(2*(SUBI2.Q.TQ.SUBJ7+.5*(TQ.SUBI2.Q)*SUBJ7+
                    SUBI7.Q.TQ.SUBJ2+.5*(TQ.SUBI7.Q)*SUBJ2)+
                    2*(SUBI3.Q.TQ.SUBJ6+.5*(TQ.SUBI3.Q)*SUBJ6+
                    SUBI6.Q.TQ.SUBJ3+.5*(TQ.SUBI6.Q)*SUBJ3)+
                    2*(SUBI4.Q.TQ.SUBJ5+.5*(TQ.SUBI4.Q)*SUBJ5+
                    SUBI5.Q.TQ.SUBJ4+.5*(TQ.SUBI5.Q)*SUBJ4)),
```

```
                    PRINT(II,JJ),
                       N2:N2+P[III,JJ]*C*(2*(SUBI4.Q.TQ.SUBJ7+.5*(TQ.SUBI4.Q)*SUBJ7+
                                    SUBI7.Q.TQ.SUBJ4+.5*(TQ.SUBI7.Q)*SUBJ4)+
                                  2*(SUBI5.Q.TQ.SUBJ6+.5*(TQ.SUBI5.Q)*SUBJ6+
                                    SUBI6.Q.TQ.SUBJ5+.5*(TQ.SUBI6.Q)*SUBJ5)),
                    PRINT(II,JJ),
                       N2:N2+S[II,JJ]*2*C*(SUBI6.Q.TQ.SUBJ7+.5*(TQ.SUBI6.Q)*SUBJ7+
                                    SUBI7.Q.TQ.SUBJ6+.5*(TQ.SUBI7.Q)*SUBJ6)); */




(C5)  K:ZEROMATRIX(18,18)$

(C6)  KS:ZEROMATRIX(18,18)$

(C7)  FOR II:1 THRU 3 DO
       FOR JJ:1 THRU 3 DO
      (PRINT(II,JJ),
       K:K+A[II,JJ]*(COL(L0,II).ROW(L0T,JJ))+
          DD[II,JJ]*(COL(L1,II).ROW(L1T,JJ)+
                  COL(L0,II).ROW(L2T,JJ)+COL(L2,II).ROW(L0T,JJ))+
            F[II,JJ]*(COL(L2,II).ROW(L2T,JJ)+
                  COL(L1,II).ROW(L3T,JJ)+COL(L3,II).ROW(L1T,JJ)+
                  COL(L0,II).ROW(L4T,JJ)+COL(L4,II).ROW(L0T,JJ)));




(C5)  K:ZEROMATRIX(18,18)$

(C6)  FOR II:1 THRU 3 DO
       FOR JJ:1 THRU 3 DO
      (PRINT(II,JJ),
       K:K+H[II,JJ]*(COL(L3,II).ROW(L3T,JJ)+
                  COL(L2,II).ROW(L4T,JJ)+COL(L4,II).ROW(L2T,JJ))+
            J[II,JJ]*(COL(L4,II).ROW(L4T,JJ)));




(C8)  FOR II:1 THRU 2 DO
       FOR JJ:1 THRU 2 DO
      (KS:KS+AS[II,JJ]*(COL(S0,II).ROW(S0T,JJ))+
          DS[II,JJ]*(COL(S0,II).ROW(S2T,JJ)+COL(S2,II).ROW(S0T,JJ))+
            FS[II,JJ]*(COL(S2,II).ROW(S2T,JJ)),
        PRINT(II,JJ)));
```

349

Appendix E: Shear Locking

This approach explains, to some degree, why the elements formulated in Chapter IV do not suffer from shear locking. First, ideas are taken from Ref (121) explaining why the Reissner-Mindlin (RM) elements do shear lock.

Consider the simply supported beam of length 2a as shown in Figure E.1 that is subjected to a linear moment distribution, $M(x) = M_o x/a$. The moment is integrated twice to give a cubic transverse displacement, $w(x)$, where $w(-a)=w(0)=w(a)=0$. Under this loading, the deflected shape of the beam resembles that shown in Figure E.2 where the ends have rotated an angle θ_B due to M_o and all sections also rotate an additional angle θ_S due to the transverse shear, $Q_x = dM/dx = M_o/a$.
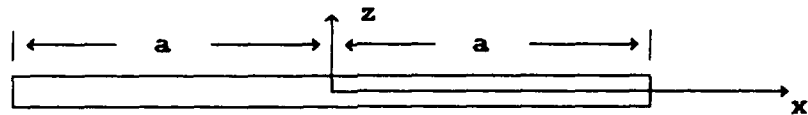

FIGURE E.1. Simply Supported Beam.

FIGURE E.2. Deflected Shape of Beam Under Linear Moment Distribution.

Next, consider the beam of Figures E.1 and E.2 discretized using a single RM beam element. The element has degrees of freedom w and θ at the nodes and the continuum displacements are either linearly or quadratically interpolated. The transverse displacement and the rotations are independent due to the characteristics of the potential energy expression. Impose a rotation $\theta_B + \theta_S$ at each of the end nodes, and for the quadratic element also impose $-\theta_S + \theta_B/2$ at the center node. For these elements, w must equal zero for all x since it vanishes at the simple supports and we have assumed linear and quadratic interpolations, see Figure E.3. Therefore, $\gamma_{zx} = w,_x - \theta = -\theta$ for all x. The actual beam will have $\theta \gg \gamma_{xz}$ and too much energy is stored for the transverse shear. References (75,76) explain how reduced or selective integration alleviates shear locking.
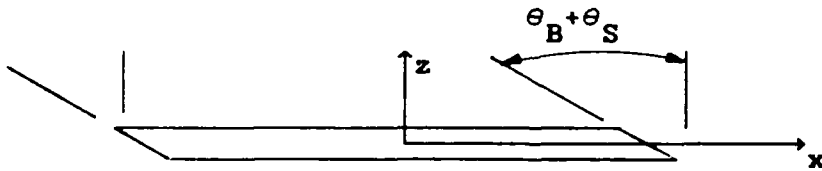

FIGURE E.3. RM Element Deformed Shape for Linear Moment Distribution.

In the present case, each node would have w, $w,_x$, and θ as degrees of freedom. Since a cubic w is assumed within the beam domain, $w,_x$ equals zero only at a finite number of points as it should. For this case, $\gamma_{zx} = w,_x - \theta$ correctly.

351

REPORT DOCUMENTATION PAGE

1a. REPORT SECURITY CLASSIFICATION	1b. RESTRICTIVE MARKINGS
Unclassified	

2a. SECURITY CLASSIFICATION AUTHORITY	3. DISTRIBUTION/AVAILABILITY OF REPORT
	Approved for public release;
2b. DECLASSIFICATION/DOWNGRADING SCHEDULE	distribution unlimited.

4. PERFORMING ORGANIZATION REPORT NUMBER(S)	5. MONITORING ORGANIZATION REPORT NUMBER(S)
AFIT/DS/AA/88-1	

6a. NAME OF PERFORMING ORGANIZATION	6b. OFFICE SYMBOL (If applicable)	7a. NAME OF MONITORING ORGANIZATION
Engineering	AFIT/ENY	

6c. ADDRESS (City, State, and ZIP Code)	7b. ADDRESS (City, State, and ZIP Code)
Air Force Institute of Technology Wright-Patterson AFB, Ohio 45433-6583	

8a. NAME OF FUNDING/SPONSORING ORGANIZATION	8b. OFFICE SYMBOL (If applicable)	9. PROCUREMENT INSTRUMENT IDENTIFICATION NUMBER

8c. ADDRESS (City, State, and ZIP Code)	10. SOURCE OF FUNDING NUMBERS			
	PROGRAM ELEMENT NO.	PROJECT NO.	TASK NO	WORK UNIT ACCESSION NO.

11. TITLE (Include Security Classification)

LARGE DISPLACEMENT AND ROTATIONAL FORMULATION FOR LAMINATED CYLINDRICAL SHELLS INCLUDING PARABOLIC TRANSVERSE SHEAR (Unclassified)

12. PERSONAL AUTHOR(S)
Scott T. Dennis, Captain, USAF

13a. TYPE OF REPORT	13b. TIME COVERED	14. DATE OF REPORT (Year, Month, Day)	15. PAGE COUNT
PhD Dissertation	FROM _____ TO _____	88 May	373

16. SUPPLEMENTARY NOTATION

17. COSATI CODES			18. SUBJECT TERMS (Continue on reverse if necessary and identify by block number)		
FIELD	GROUP	SUB-GROUP	Nonlinear	Transverse Shear	Collapse
11	04		Shell	Flat Plate	Finite Element
			Composite	Buckling	Large Rotation

19. ABSTRACT (Continue on reverse if necessary and identify by block number)

Dr. Anthony N. Palazotto

Approved for public release: IAW AFR 190-1.
LYNN E. WOLAVER
Dean for Research and Professional Development
Air Force Institute of Technology (AFSC)
Wright-Patterson AFB OH 45433

20. DISTRIBUTION/AVAILABILITY OF ABSTRACT	21. ABSTRACT SECURITY CLASSIFICATION
☒ UNCLASSIFIED/UNLIMITED ☐ SAME AS RPT ☐ DTIC USERS	Unclassified

22a. NAME OF RESPONSIBLE INDIVIDUAL	22b. TELEPHONE (Include Area Code)	22c. OFFICE SYMBOL
Dr Anthony N. Palazotto	513-255-2998	AFIT/ENY

DD Form 1473, JUN 86 — *Previous editions are obsolete.* —

19.

A two dimensional geometrically nonlinear shell theory applicable to arbitrary geometries that can be described by orthogonal curvilinear coordinates and encompassing large displacements and rotations for small strain situations has been developed. Additionally, the theory includes a parabolic transverse shear stress distribution through the thickness. Two curved 28 and 36 degree of freedom finite elements are defined based on specialization of the theory to cylindrical coordinates. The computer program includes algorithms for linear, "fully linearized" linear bifurcation, and nonlinear problems. Post collapse nonlinear solutions are found through a displacement incrementation scheme. The code provides solutions to the intermediate nonlinear von Karman flat plate and Donnell cylindrical shell equations in addition to the large displacement and rotational formulation.

Flat plate and cylindrical shell solutions do not shear lock based upon exact elemental integrations. Transverse shear deformation was found to be significant for linear thick pinched cylinders and clamped pressure vessels. Orthotropic pressure vessels where the longitudinal stiffness is greater than the circumferential experience much more transverse shear deformation than do those where the circumferential stiffness is greater than the longitudinal. Middle surface inextensibility is often assumed in the closed form solutions used for comparison with the present approach. The consequences of this assumption is examined for both linear and nonlinear problems. The present formulation is applied to axially compressed quasi-isotropic cylindrical panels. Due to the high degree of displacement coupling resulting from the large displacement/rotation assumptions, collapse loads are predicted without including numerical geometric imperfections that some formulations require to "trigger" the nonlinear response. Analytical results of axially compressed panels that have large (>10% of planform area) centered square cutouts were compared to experimental data. The present approach very accurately predicts both global and localized panel response.

END

DATED

FILM

8 — 88

DTIC